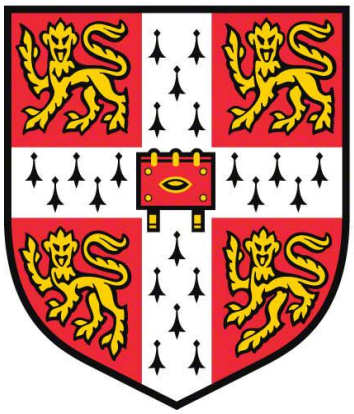
EXPLORING THE ROLE OF PROGRAMMED AXON DEATH GENES SARM1 AND NMNAT2 IN HUMAN DISEASE



Mirlinda ADEMI

Corpus Christi College

John van Geest Centre for Brain Repair

Department of Clinical Neurosciences

University of Cambridge

This thesis is submitted for the degree of

Doctor of Philosophy

January 2023

"Die wahre Motivation quer durch alle Wissenschaften ist, dass man wissen möchte."

Anton Zeilinger

Declaration

I hereby confirm that the content of this thesis is the result of my own work and includes nothing which is the outcome of work done in collaboration except as declared in the preface and specified in the text. It is not substantially the same as any work that has already been submitted before for any degree or other qualification except as declared in the preface and specified in the text. It does not exceed the prescribed word limit for the Clinical Medicine and Clinical Veterinary Medicine Degree Committee.

Abstract

Exploring the role of programmed axon death genes SARM1 and NMNAT2 in human disease

Programmed axon death (PAD) is an evolutionary-conserved path of axon destruction initiated by injury and disease. Two proteins are known to profoundly influence axonal health: the pro-death SARM1 and its upstream regulator, the pro-survival NMNAT2. Notably, complete removal of *SARM1* has been shown to rescue injured axons permanently in one case and delay axon loss in many others, alleviating animal models of Parkinson's disease, traumatic brain injury, glaucoma, and other disorders. While mechanistic studies of these two proteins have been the focus of recent years, human genetics of PAD had been studied to a much lesser extent, despite growing interest and investment from several pharmaceutical companies to target SARM1 therapeutically. Consequently, the aim of this thesis was to address this knowledge gap and investigate how human gene variants in *NMNAT2* and *SARM1* influence axon vulnerability. Chapter 3 of this thesis revolves around the role of naturally-occurring *SARM1* alleles in the human population many of which encode SARM1 loss-of-function (LoF) coding variants. They influence SARM1 enzymatic activity and axon survival functions, likely to reflect protective effects in disease. Importantly, two variants tested confer dominant LoF effects suggesting even stronger effects on disease risk. In chapter 4, biallelic NMNAT2 LoF alleles are described in two siblings affected by a severe polyneuropathy. In addition to the newly-identified patient variants, a small set of artificial and natural NMNAT2 missense variants is tested for pathogenic LoF of the protein. Thirdly, chapter 5 revolves around SARM1 missense variants found in the genomic cohorts UK Biobank and the 100,000 Genomes Project. Furthermore, it is investigated whether SARM1 LoF is underrepresented in disease cohorts, implying a protection against axonal insult. This is done by comparing frequencies of predicted and confirmed SARM1 LoF alleles between disease and control groups. Finally, I discuss how knowledge of these and other SARM1/NMNAT2 function-altering alleles will be useful for further establishing links between SARM1-dependent PAD and human pathologies that would be good candidates for the use of SARM1-blocking drugs in the future.

Mirlinda ADEMI

Acknowledgments

The past four years have significantly shaped my academic and personal growth and there are various people without whom the work in this thesis would not have been possible.

First and foremost, many thanks go to my supervisor Professor Michael Coleman for his relentless support and mentorship throughout these years. I am most thankful for his dedication to my scientific and professional development and his constant encouragement to resist academic fatigue in response to difficult peer review processes, which made the final months of experimental work during my PhD a lot less stressful. I also admire the fact that despite his senior role he has remained so humble and approachable, establishing a safe and enjoyable lab environment for everyone. I would also like to thank the MRC DTP Programme and the Pinsent Darwin Trust for recognising my academic potential and providing me with a full scholarship to fund this PhD.

Furthermore, profound gratitude goes to Dr. Jon Gilley. His wealth of knowledge, technical expertise and scientific advice never cease to impress me. Scientifically, his contribution has been most significant towards my work on SARM1 LoF variants in the human population, as well as the tedious publication process that followed. He has provided valuable comments concerning experimental design, data analysis, as well as scientific writing. I wish I could write half as skilfully as Jon writes his academic papers.

Thanks also go to the whole Coleman Group, past and present members, for the fun times in the lab and their support, especially Dr. Andrea Loreto who has not just shared his excitement for anything Wallerian degeneration-related but also contributed to many fruitful scientific discussions related to my projects. The most incredible people who have made my time in the lab all the more rewarding with their friendship are Christina, Maha, Olivia and Shaline. Christina and Maha in particular have been a huge source of motivation and immense support throughout my highs and lows in the lab. In addition, Denisa has been great company over many cups of coffee or homemade baked goods while sitting in the ugly open-plan PhD office of the BRC building.

Beyond the science accomplished, I'm so grateful for the people outside the lab I have shared my PhD journey in Cambridge with, all of whom have formed the most amazing support network I could go back to at different stages of this journey. Thanks go to Zeynep who

was bound to become a dear friend after the Loch Lomond axon degeneration conference in 2019 and with whom I share my fondest Cambridge memories. Her sisterhood is one of the best gifts my time in Cambridge has blessed me with. I am also thankful to Aleks and his great sense of humour, to Rohit & Tanvi for always making me laugh and for cooking some of my most favourite Paneer dishes, to Faraj for his care and love during our Sunday "dates", to Maysoon who is my favourite dancing partner and Kahwa barista, to Salman & Samuel for being good company and listeners, to Omar & Sondos (together with Samuel) for being so inclusive and adopting me into the Egyptian gang, to Hadil for her kind gestures and friendship. Aida and Saba were there for me during the very last stretch of my PhD and I also owe Sami for kindly debugging my latex file on a day of desperation. Finally, to Kasra whom I met at the very end, whose calm nature made me worry a little less and, most importantly, reminded me of what life is, can, should and should not be about.

I owe the greatest acknowledgment to my family for which this short paragraph doesn't do justice. My siblings have been the best companions throughout my life and the biggest source of mental support bridging our age gaps with their mature attitude and advice so perfectly well I would sometimes end up questioning my supposed wisdom as an elder sibling. My sister Zarije has kept me sane, answered 1 am phone calls anytime I felt the urge to pour my heart out and came up with the most comforting words when my research got scooped. It is through her I have come to understand what the word unconditional really means. Her support has very much been complemented by the witty comments of my brother Bekim, his stoic attitude and capability to listen to anything I have to share, independently of how serious or ridiculous it may be. Together the two have been the most cheerful and a perfectly complementary duo to be supported by; I could not do without one or the other. Last but not least, thanks go to Mami and Babi, and their constant effort and sacrifices to make our lives better and easier than theirs ever were. It is your shoulders I stand on.

Mirlinda
Cambridge, December 2022

Contents

Declaration iii

Abstract v

Acknowledgments vii

List of Figures xvii

List of Tables xx

Abbreviations xxi

1 Introduction 1

1.1 General background . . . 1

1.1.1 Why the study of axon death matters . . . 1

1.1.2 The burden of neurological diseases . . . 2

1.1.3 The importance of axonal homeostasis . . . 3

1.1.4 Axonopathy, the impairment of axons . . . 4

1.2 How the discovery of WLD^S mice changed the perception of how axons die 5

1.2.1 From Augustus Waller to now . . . 5

1.2.2 Detailed studies of the WLD^S mouse give mechanistic insights . . . 6

1.2.3 An axon-specific self-destruction mechanism . . . 7

1.2.4 The evolutionary importance of a distinct axon death pathway. . . . 8

1.3 Molecular players of programmed axon death . . . 9

1.3.1 NMNAT2, a pro-survival factor. . . . 9

1.3.2 SARM1, a pro-degenerative factor . . . 11

1.3.3 Stathmin-2 . . . 16

1.3.4 A mitogen-activated protein kinase cascade . . . 16

1.3.5 Axundead acts downstream of dSarm . . . 17

1.3.6 Mitochondria have a dual role in programmed axon death . . . 17

1.3.7 The roles of Calcium, Calpain and Calpastatin . . . 17

1.4 Slowing down programmed axon death in pre-clinical disease models . . . 19
1.4.1 WLD^S delays axon degeneration rates in disease models 19
1.4.2 *SARM1*-deficiency also efficiently delays axon degeneration in disease models 20
1.4.3 Manipulation of PAD rates in primary neuronal cultures 21
1.5 Bridging the gap between animal studies and human disease 22
1.6 Aims of this thesis 24

2 Materials and Methods 27
2.1 Generation of constructs 27
2.1.1 SARM1 and NMNAT2 variant selection strategy 27
2.1.2 Design and preparation of primers 27
2.1.3 Generation of constructs and site directed mutagenesis 28
2.1.4 DpnI digest and transformation 29
2.1.5 Restriction digest and gel electrophoresis 31
2.1.6 Mini-, Midi-, Maxipreps 31
2.2 Cell culture related work 32
2.2.1 Animals 32
2.2.2 HEK 293T cell culture and transfection 32
2.2.3 Primary neuronal cultures from dissociated SCGs 33
2.3 Metabolite measurements and NADase activity 34
2.3.1 In-cell NAD(P) quantification 34
2.3.2 In-cell ATP quantification 35
2.3.3 Purification of FLAG-tagged SARM1 and NMNAT2 35
2.3.4 NADase assays using recombinant SARM1 protein 36
2.3.5 NAD synthesis assays using recombinant NMNAT2 protein 37
2.4 Immunoblotting 38
2.5 Flow cytometric analysis 39
2.6 Immunostaining 39
2.7 Axon degeneration experiments 40
2.7.1 Microinjections 40
2.7.2 Axotomy assays 40
2.8 Model display 42
2.9 Database analysis 42
2.10 Statistical analysis 42
2.11 Figures and Illustrations 42

3 SARM1 natural variants cause both intrinsic & dominant LoF influencing axon survival 43

3.1 Chapter summary . . . 43
3.2 Introduction . . . 44
3.2.1 A model of how SARM1 is activated secondary to injury . . . 44
3.2.2 Programmed axon death in human disease . . . 45
3.2.3 Aims of this chapter . . . 46
3.3 Results . . . 47
3.3.1 Candidate selection of naturally-occurring variants in human SARM1 47
3.3.2 NAD levels in transfected HEK 293T cells are altered by naturally-occurring human SARM1 variants . . . 50
3.3.3 Investigation of human SARM1 variant expression levels in transfected HEK 293T cells . . . 51
3.3.4 Transfection efficiency of HEK 293T cells is consistent between different human SARM1 variants . . . 56
3.3.5 Several natural human SARM1 TIR domain variants lack constitutive (basal) NADase activity . . . 58
3.3.6 Human SARM1 TIR domain variants which display no basal NADase activity also lack NMN-induced NADase activity . . . 62
3.3.7 Most SARM1 TIR domain variants that lack NADase activity also fail to trigger neurite degeneration . . . 63
3.3.8 SARM1 LoF variants used for microinjection into SCG neurons are sufficiently expressed . . . 66
3.3.9 SARM1 LoF variants do not have cytotoxic effects on neuronal cell bodies . . . 69
3.3.10 GoF E399K SARM1 does not accelerate injury-induced neurite degeneration relative to WT SARM1 . . . 71
3.3.11 D594E and E686K SARM1 act as dominant negatives on axon degeneration . . . 75
3.4 Discussion . . . 79
3.4.1 Summary of findings . . . 79
3.4.2 SARM1 LoF may be underrepresented in disease groups . . . 81
3.4.3 SARM1 LoF frequency in the human population . . . 81
3.4.4 SARM1 LoF variants are located within the TIR domain . . . 82
3.4.5 Do compensatory mechanisms for SARM1 GoF exist? . . . 84

3.4.6 Limitations of the study . . . 84
3.4.7 Conclusion . . . 85

4 Functional characterisation of two patient & other rare NMNAT2 missense variants 87
4.1 Chapter summary . . . 87
4.2 Introduction . . . 88
4.2.1 Aims of this chapter . . . 90
4.3 Results . . . 90
4.3.1 Biallelic compound heterozygous NMNAT2 mutations in two siblings with a severe chronic neuropathy . . . 90
4.3.2 Clinical features of the patients with NMNAT2 variants . . . 91
4.3.3 Strategic candidate selection of other NMNAT2 variants within region 90-105 aa . . . 92
4.3.4 Metabolite analysis of NMNAT2 variants expressed in NRK1-HEK cells is not conclusive . . . 96
4.3.5 Several NMNAT2 variants within region 90-105 aa show reduced capacity to promote neurite survival . . . 99
4.3.6 NMNAT2 LoF variants used for microinjection into SCG neurons are sufficiently expressed . . . 103
4.3.7 Enzymatic activities in comparison: W92R, V98M and T95A NMNAT2 have reduced NAD synthesis capacities . . . 106
4.4 Discussion . . . 110
4.4.1 Summary of findings . . . 110
4.4.2 Technical limitations . . . 110
4.4.3 Adults carrying heterozygous NMNAT2 LoF mutations appear clinically healthy . . . 112
4.4.4 Biallelic NMNAT2 LoF associated to human axonopathies . . . 113
4.4.5 Importance of genomic databases & future directions . . . 113

5 Screening genomic databases for disease-associated coding variants in PAD genes 115
5.1 Chapter summary . . . 115
5.2 Introduction . . . 116
5.2.1 The axon vulnerability spectrum . . . 116
5.2.2 NMNAT2 & SARM1 variation associated with disease . . . 117
5.2.3 The potential of WGS in PAD research . . . 120

5.2.4 Aims and limitations of this chapter . . . 120
5.3 results . . . 122
5.3.1 The use of the UK Biobank cohort to screen for human SARM1 coding missense variants . . . 122
5.3.2 SARM1 coding missense variation present in neurological phenotypes of UK Biobank participants . . . 123
5.3.3 SARM1 LoF variant frequencies in axonopathy cohorts within the UK Biobank . . . 128
5.3.4 The use of the 100,000 Genomes Project to screen for human SARM1 coding missense variants . . . 130
5.3.5 SARM1 coding missense variation present in rare diseases within the 100,000 Genomes Project . . . 131
5.4 Discussion . . . 133
5.4.1 Limitations of this chapter . . . 133
5.4.2 Suggested future experimental work . . . 133
5.4.3 The role of SARM1 LoF in disease . . . 133

6 Discussion **135**
6.1 Summary of findings . . . 135
6.2 Future directions . . . 138
6.2.1 Proof-of-concept in humans or knock-in mice . . . 138
6.2.2 Expansion of patient databases is necessary . . . 138
6.2.3 Peripheral neuropathy: a promising PAD target . . . 139
6.2.4 How PAD could contribute to complex disease . . . 139
6.2.5 Rare peripheral neuropathies . . . 140
6.2.6 Insights from structural biology of SARM1 . . . 141
6.2.7 NAD and related supplements . . . 141
6.3 PAD-targeting therapies and their limitations . . . 142
6.4 Other outstanding questions . . . 142
6.5 Conclusion . . . 143

Bibliography **145**

List of Figures

1.1 Augustus Waller's and Ramon Cajal's hand drawn observations of Wallerian degeneration. . . . 6
1.2 NMNATs and components of the WLD^S chimeric protein. . . . 7
1.3 SARM1 domains, its crystal structure and activation mechanism. . . . 13
1.4 SARM1 and NMNAT2 are regulators of axon health. . . . 14

2.1 Structure of pLVX-ZsGreen1 and pCMV-Tag 4A plasmid constructs used in chapter 4 and chapter 3. . . . 30
2.2 Experimental setup for microinjection assays. . . . 41

3.1 A working model of how SARM1 is activated in injured axons. . . . 45
3.2 Naturally-occurring SARM1 coding variants assessed in this study. . . . 48
3.3 In-cell NAD levels are not depleted by several SARM1 TIR domain variants. 51
3.4 SARM1 variant expression levels in transfected HEK 293T cells. . . . 54
3.5 Moderate positive correlation between ZsGreen fluorescence and in-cell NAD values. . . . 55
3.6 HEK 293T transfection efficiency of different human SARM1 constructs is comparable. . . . 57
3.7 Schematic illustration of the *in vitro* NADase assay using purified bead-bound human SARM1. . . . 58
3.8 Immunopurification of recombinant SARM1 variants used in NADase assays. 59
3.9 Several SARM1 TIR domain variants are LoF for basal (constitutive) and NMN-induced NADase activity. . . . 61
3.10 NADase LoF SARM1 TIR domain variants fail to induce degeneration in response to physical injury. . . . 65
3.11 Expression levels of natural SARM1 variants expressed from pCMV-Tag4A backbones in microinjected *Sarm1*$^{-/-}$ SCG neurons. . . . 67
3.12 SARM1 variant expression levels from untagged pCMV-Tag4A backbones in transfected HEK 293T cells. . . . 68

3.13 Natural human SARM1 variants with a LoF phenotype do not have cytotoxic effects. . . . 70
3.14 A simplified model based on which it was hypothesised that NADase GoF E399K SARM1 variant would lead to accelerated degeneration relative to the WT protein. . . . 71
3.15 NADase GoF E399K SARM1 variant does not accelerate degeneration in response to physical axotomy. . . . 73
3.16 Transfection efficiency and cell death rates of cells transfected with E399K SARM1 GoF variant are similar to WT SARM1. . . . 74
3.17 D594E and E686K SARM1 have dominant LoF properties in axotomised wild-type SCG cultures. . . . 77
3.18 Co-expression of WT SARM1 together with D594E or E686K SARM1 results in a dominant SARM1 LoF. . . . 78
3.19 Locations of SARM1 missense variants that confer full LoF in the SARM1 TIR domain crystal structure. . . . 80

4.1 Rare compound heterozygous NMNAT2 variants in two siblings with chronic neuropathy. . . . 91
4.2 Selection strategy of NMNAT2 variants targeted for mutagenesis in the present study. . . . 94
4.3 Locations of characterised missense variation in the predicted NMNAT2 protein structure. . . . 95
4.4 NRK1-HEK cells are not a good model to indirectly screen for differences in NMNAT2 variant enzyme activity. . . . 98
4.5 Several NMNAT2 variants have reduced capacity to maintain neurite survival of axotomised primary neuronal cultures . . . 101
4.6 Generated NMNAT2 variants do not have cytotoxic effects on primary neuronal cultures. . . . 102
4.7 Steady-state expression of NMNAT2 variants from pCMV-Tag4-based constructs used for microinjection into SCG neurons. . . . 104
4.8 Expression levels of NMNAT2 variants expressed from pCMV-Tag4A backbones in microinjected WT SCG neurons. . . . 105
4.9 Immunopurification of recombinant NMNAT2 variants used in NAD synthesis assays. . . . 108
4.10 Comparison of NAD synthesis activity of recombinant NMNAT2 protein. . . 109

5.1 The emergence of an axon vulnerability spectrum. . . . 118

5.2 Pie chart of neurological disease sub groups analysed within 100,000 Genomes Project. 130

6.1 PhD results support the idea of an axon vulnerability spectrum. 137

List of Tables

2.1 SARM1-specific oligonucleotide primers used for site-directed mutagenesis. 29
2.2 NMNAT2-specific oligonucleotide primers used for site-directed mutagenesis. 29
2.3 Mutagenesis protocol for generating *SARM1* and *NMNAT2* expression constructs. . . . 31
2.4 Example reaction of a restriction digest. . . . 31
2.5 Protocol for up- or downscaling transfection of HEK 293T cells. . . . 33
2.6 Media preparations used for primary neuronal cultures. . . . 34
2.7 Details of antibodies used in the projects discussed in this thesis. . . . 39

3.1 Human SARM1 ARM, SAM and TIR domain coding variants in gnomAD and dbSNP. . . . 49
3.2 Summary of findings for natural SARM1 variants presented in this chapter. 80

4.1 Summary of clinical features in affected siblings. . . . 92
4.2 Human NMNAT2 natural and artificial coding variants analysed in this study. 93
4.3 Overview of changes caused by experimental manipulations employed in Figure 4.4C and D. . . . 97
4.4 Summary of findings from functional analyses of natural and artificial NMNAT2 variants presented in this chapter. . . . 111

5.1 SARM1 coding variants in Parkinson's disease patients from UK Biobank . 123
5.2 Single SARM1 coding variant found in both amyotrophic lateral sclerosis (ALS) and hereditary ataxia patients from UK Biobank . . . 123
5.3 SARM1 coding variants in Alzheimer's disease patients from UK Biobank. 123
5.4 SARM1 coding variants in patients with unspecified dementia from UK Biobank . . . 124
5.5 SARM1 coding variants in patients with vascular dementia from UK Biobank 124
5.6 SARM1 coding variants in patients with hereditary and idiopathic neuropathy from UK Biobank . . . 124
5.7 SARM1 coding variants in patients with mononeuropathy from UK Biobank 124

5.8 SARM1 coding variants in patients with a mononeuropathy of the upper limb from UK Biobank . . . 125
5.9 SARM1 coding variants in patients with a mononeuropathy of the lower limb from UK Biobank . . . 126
5.10 SARM1 coding variants in patients with facial nerve palsy from UK Biobank 126
5.11 SARM1 coding variants in patients with glaucoma from UK Biobank . . . 127
5.12 Occurrences of *SARM1* alleles encoding predicted and confirmed LoF variants in disease cohorts in the UK Biobank. . . . 129
5.13 100,000 Genomes selected for rare SARM1 coding variant analysis. . . . 131
5.14 SARM1 missense variants patients with EO and familial Parkinson's disease in the 100k Genomes database. . . . 131
5.15 SARM1 missense variants patients with hereditary ataxia in the 100k Genomes database. . . . 131
5.16 SARM1 missense variants patients with hereditary spastic paraplegia in the 100k Genomes database. . . . 132
5.17 SARM1 missense variants patients with Charcot-Marie-Tooth disease in the 100k Genomes database. . . . 132
5.18 SARM1 missense variants patients with early-onset dystonia in the 100k Genomes database. . . . 132
5.19 SARM1 missense variants patients with paediatric motor neuronopathies in the 100k Genomes database. . . . 132
5.20 SARM1 missense variants patients with ALS and other motor neuron disease in the 100k Genomes database. . . . 132
5.21 SARM1 missense variants patients with early-onset dementia in the 100k Genomes database. . . . 132

Abbreviations

Aa	Amino acid
AD	Alzheimer's disease
ADP	Adenosine diphosphate
ADPR	Adenosine-5'-O-diphosphoribose
ALS	Amyotrophic lateral sclerosis
ALS-FTD	ALS- frontotemporal dementia
ARM	Armadillo repeat motif
ASO	Antisense oligonucleotide
ATP	Adenosine triphosphate
BACK	BTB and C-terminal Kelch
BAK	BCL-2 homologous antagonist killer
BAX	BCL-2-associated X
BCA	Bicinchoninic acid assay
Bp	Base pair
BTB	Bric-à-brac, tramtrack, broad complex
cADPR	Cyclic adenosine-5'-O-diphosphoribose
CCCP	Carbonyl cyanide m-chlorophenyl hydrazone
CD38	Cluster of differentiation 38
CIPN	Chemotherapy-induced peripheral neuropathy
CMT	Chracot-Marie-Tooth
CNS	Central Nervous System
CZ-48	Sulfo-ara-F-NMN
DALY	Disability adjusted life years
DAPI	4,6-Diamidin-2-phenylindol
DIV	Days in vitro
DLK	Dual leucine zipper-bearing kinase
DMEM	Dulbecco's Modified Eagle Medium
dNMNAT	Homolog of NMNAT in Drosophila melanogaster
DPN	Diabetic peripheral neuropathy

DRG	Dorsal root ganglion cells
dSarm	Homologue of SARM1 in Drosophila melanogaster
DsRed	Discosoma red fluorescent protein
EAE	Experimental autoimmune encephalomyelitis
EO	Early-onset
Exac	Exome Aggregation Consortium
FACS	Fluorescence Activated Cell Sorting
FADS	Fetal akinesia deformation sequence
FBS	Fetal bovine serum
FDR	False discovery rate
FK866	N-[4-(1-benzoyl-4-piperidinyl)butyl]-3-(3-pyridinyl)-2Epropenamide
FTD	Frontotemporal dementia
GAPDH	Glyceraldehyde 3-phosphate dehydrogenase
gnomAD	Genome Aggregation Database
GoF	Gain of function
GWAS	Genome-wide association studies
h	Hour(s)
HEK 293T cells	Human Embryonic Kidney (HEK) 293
HFD	High-fat diet
hiPSC	Human induced pluripotent stem cells
HPV	Human papillomavirus
IL-17	Interleukin-17
ISTID2	Isoform-specific targeting and interaction domain 2
JNK	c-Jun N-terminal kinase
LB	Lysogeny broth
LoF	Loss of function
LAVC	La Crosse virus
LZK	Leucine zipper kinase
MAPK	Mitogen-activated protein kinase
MAP2K	Mitogen-activated protein kinase kinase
MAP3K	Mitogen-activated protein kinase kinase kinase
MAP4K	Mitogen-activated protein kinase kinase kinase kinase
MBP	Myelin basic protein
MLKL	Mixed lineage kinase domain like pseudokinase
MLS	Mitochondrial localisation sequence
MW	Molecular weight

MS	Multiple sclerosis
MTS	mitochondrial targeting signal
MYCBP2	MYC Binding Protein 2
MyD88	Myeloid differentiation primary response 88
NA	Nicotinic acid
NaAD	Nicotinic acid adenine dinucleotide
NAD	Nicotinamide adenine dinucleotide
NADH	Reduced nicotinamide adenine dinucleotide
NADP	Nicotinamide adenine dinucleotide phosphate
NADPH	Reduced nicotinamide adenine dinucleotide phosphate
NAM	Nicotinamide
NaMN	Nicotinic acid mononucleotide
NAMPT	Nicotinamide phosphoribosyltransferase
NCBI	National Centre for Biotechnology Information
NfL	Neurofilament light chain
NGF	Nerve growth factor
NMN	Nicotinamide mononucleotide
NMNAT1/2/3	Nicotinamide mononucleotide adenyltransferase 1/2/3
NMNd	NMN deamidase
NR	Nicotinamide riboside
NRK1	Nicotinamide riboside kinase 1
OMIM	Online Mendelian Inheritance in Man
ORF	Open reading frame
PAD	Programmed axon death
PBS	Phosphate buffered saline
PCR	Polymerase chain reaction
PD	Parkinson's disease
PDB	Protein Data Bank
PHR1	Pam/highwire/rpm-1 protein (also known as MYCBP2)
pLoF	Predicted loss of function
pmn	Progressive motor neuropathy
PNRR	Peripheral Neuropathy Research Registry
PNS	Peripheral nervous system
PO	Myelin protein zero
POZ	Pox virus and Zinc finger domain
RGC	Retinal ganglion cells

ROS	Reactive oxygen species
RT	Room temperature
RyR	Ryanadine receptor
SAM	Sterile alpha motif domain
SARM1	Sterile Alpha and TIR Motif Containing 1
SCG	Superior cervical ganglion cells
SCG10	Superior cervical ganglion 10
SDS-PAGE	Sodium dodecylsulfate polyacrylamide gel electrophoresis
SEM	Standard error of the mean
SIFT Score	Scale-invariant feature transform score
SIRTs	Sirtuins
SMA	Spinal muscular atrophy
SNP	Single nucleotide polymorphism
SOD1	Superoxide dismutase 1
SPF	Specific pathogen free
STING	Stimulator of interferon genes
STMN2	Stathmin-2
STZ	Streptozotocin
TBE	TRIS-Borate-EDTA-Buffer
TBS	Tris buffered saline
TBST	TBS with 0.05 % Tween 20
TDP-43	Transactive response DNA binding protein 43 kDa
TIR	Toll-Interleukin receptor
TLR	Toll-like receptor
TNF	Tumor necrosis factor
TRIF	TIR-domain-containing adapter-inducing interferon-β
UBE4b	Ubiquitination factor E4B
UPS	Ubiquitin–proteasome system
VAD	Vacor adenine dinucleotide
VSV	Vesicular stomatitis virus
WD	Wallerian degeneration
WGS	Whole-genome sequencing
WLDs	Wallerian degeneration-slow
Wnd	Wallenda
WT	Wild-type

1

Introduction

1.1 General background

1.1.1 Why the study of axon death matters

In the late 19th century Augustus Waller was the first to observe that frog cranial nerves disintegrate in response to axotomy [1]. Waller's observations were made at a time when even the existence of discrete neurons in the brain was highly controversial [2]. Nor did he know that axons existed in the first place, referring to them as "*the medulla of the nerve*" [1]. Little did he know a whole research field revolving around degenerating axons - the long, slender projections of neurons - would be named after him decades later [3]. His work was followed up by Santiago Ramón y Cajal who provided a detailed histological description of degenerating axons [4]. Waller's and Cajal's contributions have been expanded since resulting in the research of axon death, more commonly known as Wallerian degeneration or programmed axon death (PAD). The past three decades have majorly shaped this field of research [5]. Although the exact molecular and cellular signalling cascade by which axon degeneration is executed remains to be fully understood, we now know that injured axons actively execute their own death through an evolutionarily conserved signalling cascade. By definition, Wallerian degeneration is axon death secondary to nerve injury which leads to the fragmentation and degeneration of an axon distal to the site of transection [6]. Many years of research using pre-clinical disease models together with a growing body of evidence pointing towards a role in human disease show that PAD is relevant in a wide range of axonal disorders, including many where no physical injury is present [6–12].

These include neurodegeneration secondary to impaired axonal transport, environmental insults, such as toxins, and genetic mutations [5]. Moreover, PAD is druggable, and can be completely prevented in animal models [13]. Understanding and being able to target axon loss has a huge therapeutic potential, especially considering the difficulty of axons to regenerate [14].

While mechanistic studies revolving around the pro-survival nicotinamide mononucleotide adenylyltransferase 2 (NMNAT2) and the pro-degenerative sterile-α and Toll/interleukin 1 receptor (TIR) motif containing protein 1 (SARM1) had been the focus of recent years, the human genetics of PAD had been studied to a much lesser extent at the start of this PhD [5]. Consequently, the aim of this work was to address this knowledge gap and better understand the importance of PAD in the clinic. The work presented and discussed here builds on the mechanistic understanding gained from studies in model organisms, murine and *Drosophila*, and investigates how human gene variants in *NMNAT2* and *SARM1* influence axon vulnerability in disease. The work illustrates why complementary human studies are vital in addition to what we already know from animal models about the role of PAD in disease. Of note, chapter 3 of this thesis revolves around naturally-occurring SARM1 variants in the human population and parts of it have led to a first-author publication [12].

Most importantly, studies conducted in parallel to this PhD by both members of the Coleman group and others, complement my results and their relevance is discussed where appropriate. These findings include the discovery of potentially pathogenic mutations in NMNAT2 in two rare neurological conditions [7, 8], as well as the association of rare SARM1 variants associated with motor neuron disease [9, 10]. The following introductory chapter provides the necessary framework for a proper understanding of PAD, with a particular focus on the two PAD proteins SARM1 and NMNAT2 around which experimental data presented in chapters 3, 4 and 5 revolve.

1.1.2 The burden of neurological diseases

Neurological disorders are the leading cause of disability and premature death worldwide, with stroke and Alzheimer's disease contributing the most to DALY (disability adjusted life years), a standardized metric for disease burden [15]. According to the Neurological Alliance and MHP Health Mandate report in 2014, an estimated 12.5 million people in the UK are affected by nervous system disorders. Many patients with long-term neurological conditions suffer from unmet needs and compromised care provision. With an ageing population, the prevalence of major disabling neurological diseases is expected to rise. This increasing level of demand will impose an ever-growing individual and socioeconomic

burden on society [15]. To this date, many disease mechanisms driving neurodegeneration are poorly understood. Many parallels can be drawn between different neurodegenerative disorders, including overlap of symptoms or functional and structural neuronal deficits driving the quest for potential pan-disease therapeutic targets [16]. Axons, for instance, die early in many neurological disorders disrupting central- (CNS) and peripheral nervous system (PNS) function [6]. Protection of neuronal cell bodies fails to prevent disease in some cases [17, 18]. Moreover, regeneration in the adult CNS is a difficult task. It would require regrowth of an axon over a long distance along the right route and connection with the right target. In addition, these stages would require a well-coordinated and timely regulation of molecular, cellular and systemic events [19]. Thus, understanding how axons degenerate in order to stop destruction and preserve axon integrity and function is an important goal. One of the simplest models used to study axon degeneration remains Wallerian degeneration secondary to physical injury [3]. While one could argue that this represents an outdated system to model axonal loss in disease it is remarkable that non-traumatic neurological disorders with a "dying back" pathology are reminiscent of Waller's description [1] where the axon dies gradually in a retrograde fashion [20]. Crucially, a better understanding of axon degeneration may reveal novel therapeutic targets independent of aetiology or anatomical region affected and therefore provide interventions applicable to a wider group of neurological disorders [5, 21].

1.1.3 The importance of axonal homeostasis

Good health is characterised by a dynamically stable state, where everything is harmoniously integrated or homeostatic. The purpose of homeostasis is to keep variables within a specific range which is essential to the maintenance of physiological functions [22]. The flexibility of tolerating temporary changes characterizes resilient systems [23]. Mammalian nervous systems face several challenges. This is partly related to their complex anatomy and physiology. Nervous systems control essential functions ranging from unconscious bodily processes (like breathing or heart rate), sensing and reacting to our surroundings, to more complex traits of human behaviour, such as emotions or personality. All of this is achieved through a highly complex neuronal network characterised by converging and diverging, excitatory and inhibitory pathways. At the centre of these are neurons. They are post-mitotic, highly polarised cells which grow long processes from the neuronal cell body (soma). These slender cable-like extensions are axons, neuronal compartments dedicated to high speed transmission of information from the soma to the nerve terminal [24].

Relatively speaking, axons are huge structures exceeding the soma's diameter by up to 10,000 x [25] and in some cases reach lengths of over 1 m (sciatic nerve originating in the lumbosacral plexus). To put this in perspective, if the cell body was scaled up to the size of a basket ball, the axon would span 2.4 km. Given this impressive distance, this makes axons the "Achilles heel" of the neuron [3]. In addition, both CNS and PNS axons have poor regeneration capabilities. Axonal transport supplies the majority of components required for homeostasis, including glycolytic enzymes, mitochondria for the supply of ATP, local protein translation as well as other products [26]. Given the constant energy demands and long distances over which these components must be transported, it is not surprising to find that disruption in the axonal transport machinery can cause neurological diseases [27]. Consequently, axon damage impairs this complex logistical activity, resulting in the degeneration of the affected site [28].

1.1.4 Axonopathy, the impairment of axons

Axonopathy, the functional and/or structural impairment of the axon, is a major contributor to the development and progression of disorders affecting the nervous system [29]. Axonal dysfunction, and impaired axonal transport in particular, are often observed at early stages of disease before symptoms or neurodegeneration have occurred. This holds true for a range of pathologies, including neurodegenerative disorders, such as Parkinson's or Alzheimer's disease, glaucoma, degeneration secondary to neurotoxicity and others. In consequence, loss of connectivity between neurons and their communicating targets is likely to play a causative role to neurodegeneration. Despite the widespread loss of axons in the injured and diseased nervous system, the cellular and molecular mechanisms driving axon death remain incompletely understood [5]. The degenerative process, however, is not a passive one resulting from the lack of 'nutrients' as Waller's original wording implied [1]. The delivery of substances to precise subcellular locations is vital to maintaining neuronal function and viability. While axons receive their glucose, oxygen and other necessary nutrients locally or via glia, essential macromolecules are transported from the soma. Therefore, it is not surprising that deficiencies in axonal transport are linked to various neurological diseases [27]. The constant supply of NMNAT2 from the cell body into axons is required for axon survival and its rapid depletion after a block of axonal transport leads to degeneration [30].

1.2 How the discovery of WLD^S mice changed the perception of how axons die

1.2.1 From Augustus Waller to now

The British physiologist Augustus Waller was the first to describe axon degeneration distal to the site of an injury in transected glossopharyngeal and hypoglossal frog nerves (Figure 1.1). Waller rightly predicted: *"It is impossible not to anticipate important results from application of this inquiry to the different nerves of the animal system. But it is particularly with reference to nervous diseases that it will be most desirable to extend these researches."* [1]. It was Lubinska who later proposed the existence of a migrating neuronal trophic substance necessary for the integrity of the axon. Upon injury, this unknown trophic factor would be depleted and once concentrations reached a critically low level, axon destruction would be initiated [31]. Today, the best known match for Lubinska's criteria is NMNAT2 which would be identified as an essential axon survival molecule years later [30].

Degenerating axons undergo histologically distinct phases: (1) Acute axonal degeneration occurs minutes after transection in both the proximal and distal axonal stump which is followed by the formation of bulbar structures. (2) Next comes a defined latent phase where the distal portion of the axon is viable, remains excitable *in vivo* and continues bi-directional axonal transport. (3) This is followed by a rapid axon disintegration of distal axons a point of no return where axons are committed to die. Histologically this is characterised by the breakdown of the cytoskeleton, cell organelles, extracellular influx of Ca^{2+} ions activating Calpain and other proteases, myelin degradation in the form of "ovoids" and subsequent granular disintegration with clearance of cell debris by surrounding glial cells [32–36]. In reaction to this, Schwann cells downregulate myelin genes, myelin protein zero (PO) and myelin basic protein (MBP), and start proliferation [37, 38].

1

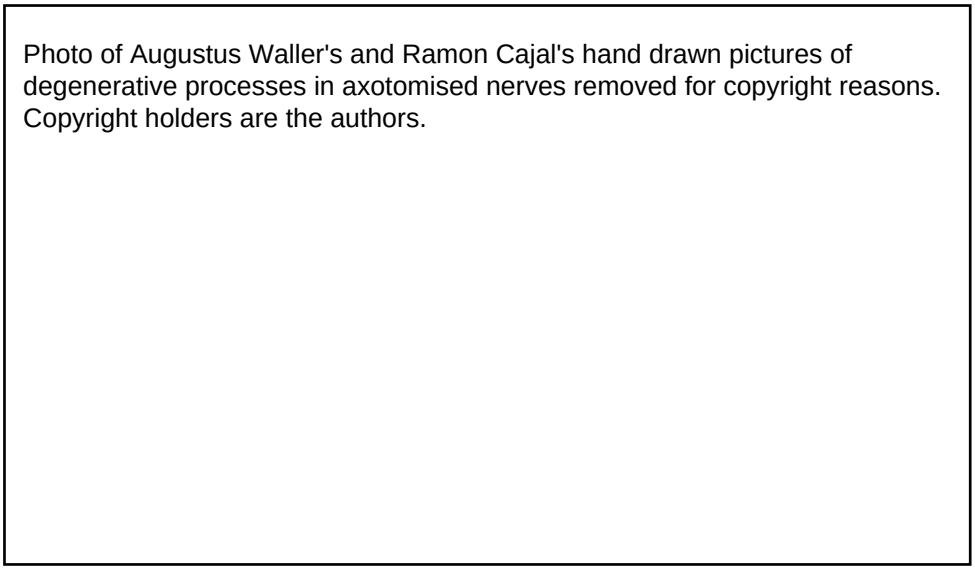


Figure 1.1: **Augustus Waller's and Ramon Cajal's hand drawn observations of Wallerian degeneration. (A)** On the left, Waller's drawing of a frog papillary nerve, three weeks after nerve sectioning. *"the presence of the nervous system element merely indicated by numerous black granules, generally arranged in a row like the beads of a necklace"* (Figure adapted from and text cited from Waller, 1851) [39]. **(B)** On the right, Cajal's drawing of the peripheral stump of the sciatic nerve of a cat 2 days after section showing the agonal reactions and the general breaking up of the nerve fibres; the brushes of neurofibrils, the persistent axial neurofibrils and the terminal intumescences of hypertrophied neurofibrils destined to disappear (Figure and text adapted from Cajal, 1928) [4].

1.2.2 Detailed studies of the WLD^S mouse give mechanistic insights

The discovery of the WLD^S mice, a C57BL substrain carrying a spontaneous mutation resulting in neuroprotection, completely revolutionised the field of PAD research in the 1990s. Originally called C57BL/6/Ola, these mice exhibited a dominant neuroprotective phenotype with prolonged axon survival in the PNS and CNS, including the protection of neuromuscular junctions post axotomy [40, 41]. Transected nerves of these mice remain excitable and survive for 2-3 weeks which is approximately 10x longer than those of wild-type (WT) animals [40, 42, 43]. The causative WLD^S gene is a chimeric gene generated by a tandem triplication of genomic DNA resulting in the overexpression of a fusion protein [44] consisting of the N-terminal Ube4b fragment (ubiquitination factor E4B) fused to the full coding sequence of Nmnat1, both of which are essential to the "newly-acquired" neuroprotective function (Figure 1.2). The resulting WLD^S protein possesses NMNAT enzyme activity which exerts an axoprotective effect [45]. The N-terminal extension does not have any catalytic activity, but instead partially relocates NMNAT1 from the nucleus

to the cytoplasm [46, 47]. This relocation is essential as overexpression of endogenous Nmnat1 (located in the nucleus) does not protect as strongly as the presence of WLD^S conferring a gain-of-function (GoF) [47–49] that overcomes the loss of the axonal pro-survival NMNAT isoform [30]. Nmnat1 overexpression in mice does not protect against injury or toxin-associated axon degeneration on its own [50, 51]. Moreover, depleting WLD^S from axons abolishes its protective function [52, 53]. Non-nuclear WLD^S significantly increases structural and functional preservation of transected neurites. In this case, distal axon stumps are reported to stay intact for up to 7 weeks after injury [46]. Remarkably, the observed phenotype was age-dependent and improvement of neuromuscular function decreased in mice >1 month [54]. Apart from slowed axon degeneration (and regeneration), WLD^S mice appear otherwise healthy.

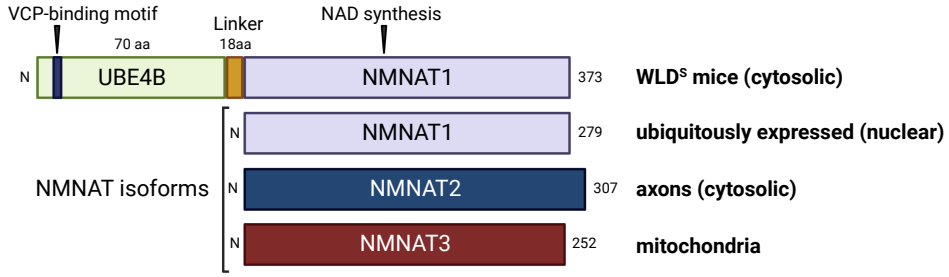


Figure 1.2: **NMNATs and components of the WLD^S chimeric protein.** The slow Wallerian degeneration gene (WLD^S) results from the fusion of the full-length nicotinamide mononucleotide adenylyltransferase 1 (NMNAT1) to the N-terminal 70aa from the ubiquitin ligase UBE4B. UBE4B does not have any catalytic function in this constellation but its valosin-containing protein (VCP) sequence is important for the localization of WLD^S in the cyto- and axoplasm [51, 55]. Mammals have three naturally-occurring NMNATs [56] of which NMNAT2 is the most labile and short-lived protein and specifically expressed in the axon [30, 57]. Created with BioRender.com.

1.2.3 An axon-specific self-destruction mechanism

PAD is an independent cell death mechanism which is well-orchestrated and evolutionary conserved across several organisms [58–61]. Remarkably, degenerative mechanisms in the soma differ from the axon and proceed independently from any influence exerted by degenerating axons [62, 63]. Although axon remodelling during pruning in development resembles injury-induced PAD morphologically, it is mechanistically different [64, 65].

Commonalities between apoptotic cells and degenerating axons exist, including Annexin V positivity of distal cut axons and the loss of mitochondrial membrane potential [66]. These are likely to be secondary to other causes in many cases. Removal of the pro-apoptotic proteins Bcl-2-associated X protein (BAX) and BCL-2 homologous antagonist killer (BAK)

1

[67], overexpression of Bcl-2 [17, 68] or the inhibition of caspase-activity [64] do not prevent axon degeneration. In support of a mechanism that is different to apoptosis, WLD^S does not protect against apoptosis of the soma, secondary to NGF deprivation in culture [62]. WLD^S further fails to prevent motor neuron death [63], as well as the death of retinal ganglion cell (RGC) bodies in a glaucoma model [48]. Similarly, removal of the pro-degenerative *Sarm1* does not prevent RGC death in response to optic nerve injury [69].

Recently, the involvement of PAD was suggested in a TNFα model of glaucoma. It was shown that MLKL, the final executioner of necroptosis, does not activate axon loss directly [70], but instead promotes the loss of NMNAT2 alongside another axon survival protein which is co-regulated with NMNAT2 [30, 71]. Consistent with this, expression of the more stable isoform NMNAT1 potently inhibited axonal necroptosis [70]. Of note, Yang et al had previously reported that inhibiting necroptosis does not block the course of PAD [72], although another study contradicts those findings [73]. Thus, it remains to be clarified whether there is indeed any crosstalk between necroptosis and PAD.

There is evidence showing that SARM1 can induce death of the soma and non-neuronal cells in some instances where artificially active SARM1 constructs are overexpressed [9, 12, 74–76]. For instance, cell bodies of *Sarm1*-deficient SCG cultures are highly resistant to CCCP- and rotenone-induced cell death [77]. Furthermore, WLD^S prevents diabetic neuropathy independently from its axonal actions by blocking beta cell destruction and preserving islet function in Streptozotocin (STZ)-induced diabetes in mice [78]. While SARM1 can induce cell death in non-neuronal cells, its regulation by the pro-survival NMNAT2 is what makes it axon-specific and distinct from other cell death pathways [5].

1.2.4 The evolutionary importance of a distinct axon death pathway

As our understanding of PAD improves, the question as to why an axon-specific destruction mechanism exists in the first place remains. From an evolutionary perspective, a selective clearance mechanism constitutes a useful defence strategy. By confining the cell death to one neuronal compartment, the organism can (1) minimise the damage without getting rid of the soma itself or affecting neighbouring axons, (2) save energy by (3) conserving resources in response to insults and (4) protect against toxic stimuli, including the inhibition of viral shedding [79].

While SARM1 deletion is axoprotective in most disease models [5], recently published data from a mouse model of colitis ulcerosa suggest the existence of a neuroimmune circuit where Sarm1 expression is important to limit local inflammation. Sarm1-driven

enteric degeneration depletes the neurotransmitter norepinephrine, which would otherwise promote the expression of proinflammatory Interleukin-17 cytokines in the mouse model. Consequently, *Sarm1*-deletion exacerbates inflammation despite preserving enteric axons which is suggestive of a protective feedback mechanism to limit colitis inflammation [80]. Similarly, TNFα can activate SARM1 in both retinal ganglion and sensory neurons [70]. Of note, neurodegeneration within the enteric nervous system has not been studied. It will therefore be informative to examine whether SARM1 exerts the same protective effect in other models of gastrointestinal diseases in the future. Given the clinical interest in targeting SARM1 activity, a critical question that remains is whether therapeutically targeting SARM1 can have unwanted side effects.

1.3 Molecular players of programmed axon death

WLD^S provided the initial evidence that NMNATs and NAD signaling play an important role in axon health [6]. Over the last two decades, our knowledge on PAD has been expanded. PAD causes major changes to the NAD metabolome [21, 81] and is mainly regulated by two key proteins with opposing roles: the endogenous labile axoprotective factor NMNAT2 without which axons die [30] and the pro-degenerative SARM1 which is essential for inducing axon death [82, 83]. However, the axon degenerative machinery is more complex and involves various other modulators acting up or downstream of NMNAT2 and/or SARM1, several of which are addressed in the following sections. These PAD players include:

- MYC Binding Protein 2 (MYCBP2) as part of the ubiquitin proteasome system that regulates the turnover of axon survival factors,
- the mitogen-activated protein kinase (MAPK) pathway,
- altered calcium homeostasis and calpain activation,
- Axundead (Axed), a protein downstream of dSarm in *Drosophila*.

1.3.1 NMNAT2, a pro-survival factor

NMNATs are enzymes that catalyse the biosynthesis of nicotinamide adenine dinucleotide (NAD) using ATP and its precursor nicotinamide mononucleotide (NMN) [84]. Mammals have three NMNAT isoforms, NMNAT1-3, all of which show distinct localization patterns and tissue distributions (Figure 1.2) [56]. While re-localization, as well as overexpression of all three isoforms delays degeneration of primary culture neurites similar to WLD^S

expression, NMNAT2 is the only NMNAT whose loss causes axon degeneration [30]. Its constant anterograde supply from the cell body into neurites is required to keep SARM1 activity at bay.

After injury, endogenous NMNAT2 is depleted rapidly in the distal stump of transected neurites and the axonal NMNAT2 pools rapidly decline and – once below a threshold – trigger degeneration. Equally, depleting *Nmnat2* via siRNA is sufficient to kill an axon even in the absence of physical injury [30]. Strong overexpression of exogenous NMNAT2, on the other hand, protects cut SCG neurites for a prolonged period, and this protective effect is dependent on its enzymatic activity [30, 85]. NMNAT2 overexpression significantly delays axon degeneration after sciatic nerve injury in mice [86] and in Mauthner cells in zebrafish [87] and alleviates neurodegeneration in a mouse model of tauopathy [88]. Furthermore, spontaneous synapse and axon loss in *Drosophila* lacking *dNmnat* can be partially rescued through the expression of murine Nmnat2 [89]. In addition, mutant Nmnat2 with a prolonged half-life is neuroprotective in RGC somata and their axons secondary to optic nerve crush model and in a glaucoma model [90].

As a gatekeeper of axon survival, NMNAT2 is an important regulatory point in axonal health. Its rapid turnover is the reason why overexpression only results in a modest protection [91]. Axons have two pools of NMNAT2, golgi-associated palmitoylated and soluble unpalmitoylated NMNAT2. NMNAT2 bound to vesicles undergoes fast axonal transport in primary neuronal cultures [30, 92]. This membrane association is dependent on an intact dual-cysteine palmitoylation site (C164/165) within the isoform-specific targeting and interaction domain (ISTID). ISTID domains are found in all three mammalian Nmnat isoforms and vary highly between isoforms and are believed to account for different localization patterns of the different NMNATs [92, 93].

NMNAT2 half-life can be artificially extended if mutations disrupt vesicle targeting [91]. NMNAT2 stability is modulated by its subcellular localization where vesicle binding results in faster degradation due to ubiquitin-dependent processes [91, 94]. Palmitoylated NMNAT2 is degraded by the MAPK pathway, where dual leucine zipper kinase (DLK) and leucine zipper kinase (LZK) promote its degradation. Conversely, nonpalmitoylated NMNAT2 undergoes degradation through E3 ubiquitin ligases [95]. Highwire E3 ubiquitin ligase promotes dNMNAT2 loss in *Drosophila* [94] and Nmnat2 loss in mice [96]. Likewise, manipulation of the E3 ubiquitin ligases can delay degeneration [97]. Inhibition of the ubiquitin–proteasome system (UPS) delays axon degeneration *in vitro* and *in vivo*, likely by stabilising NMNAT2 levels [98].

Axons of mice lacking any detectable Nmnat2 are truncated both in the peripheral and central nervous system. This suggests NMNAT2 is required during development and axons fail to grow normally in its absence, resulting in an impaired innervation of major target organs (e.g. diaphragm or muscle tissue) and therefore perinatal lethality [99, 100]. The underlying cause for this phenotype is a Wallerian-like mechanism as it can be rescued by unrelated genetic manipulations, including expression of WLD^S, *Sarm1* deletion and expression of the *NMN deamidase transgene* [100–102]. Given the short half-life of NMNAT2 and its critical axoprotective role [30], not just total depletion of NMNAT2 but any reduction of it could make axons more vulnerable to degeneration. Interestingly, compound heterozygote mice carrying two independent *Nmnat2* knockdown alleles expressing approximately 30% of WT levels of Nmnat2 show increased axon loss as they age, including decreased temperature sensitivity. Furthermore, primary neuronal cultures from these mice are more vulnerable to axonal stresses resulting in a lower threshold for degeneration and accelerated degeneration rates [103].

From a disease perspective two factors play an important role. Ageing leads to reduced axonal transport. Together with disease-related impaired axonal transport and other triggers activating the PAD pathway this could synergise leading to neurodegeneration. Improving NMNAT2 stability, increasing its expression levels or enzymatic activity could be promising avenues to pursue for neuroprotective treatments. However, targeting increased NMNAT activity specifically to axons can bring its own challenges.

1.3.2 SARM1, a pro-degenerative factor

SARM1 belongs to the family of five adaptor proteins involved in Toll-like receptor (TLR) signalling [104]. Originally discovered in 2001, it is a highly conserved protein with orthologues in mouse, *Drosophila* (Ect4), and *C. elegans* (TIR-1) [105]. Unlike other mammalian TIR domain-containing molecules, SARM1 is a negative regulator of TLR signalling. It has been shown to inhibit TRIF-dependent NF-kB activation [106, 107] and cause T cell death [108]. During development SARM1 regulates neuronal morphogenesis [109]. Besides its role as a TLR adapter protein in innate immunity, SARM1 was discovered to have a pro-degenerative role in neurons [82, 83].

A genetic forward screen in *Drosophila* discovered that dSarm is essential for inducing degeneration in fly olfactory bulb after axotomy [83]. Similar results were reproduced in mice and re-expression of the WT protein restores degeneration in both cases [82, 83]. Crucially, deletion of *Sarm1* is the only other known component of the PAD pathway that delays degeneration in mice as robustly as the expression of WLD^S or NMNATs.

The structure of SARM1 or isolated SARM1 domains have been determined and refined though cryogenic electron microscopy (cryo-EM) and x-ray crystallography [110–116]. SARM1 is a 724 amino acid-long structurally complex, multi-domain protein which consists of the following domains (Figure 1.3A): an N-terminal allosteric regulatory armadillo repeat (ARM) domain, followed by two tandem sterile alpha motif (SAM) domains, and a TIR domain [82, 110, 117]. The hydrophobic stretch of polypeptides at the N-terminus frequently referred to as 'mitochondrial targeting sequence/signal' or MTS is dispensable for its pro-degenerative function. The N-terminal ARM domain is responsible for autoinhibition, the two central tandem SAM domains help SARM1 oligomers form, and the C-terminal TIR domain is the catalytic site where NAD hydrolysis, ADPR cyclisation and base exchange activities happen [82, 105, 110, 117, 118].

While SARM1 was initially proposed to form dimers [119, 120], studies later showed that both the SAM domains in isolation and full-length SARM1 itself form higher ordered octamers [110, 112–114] where the ARM domains are wrapped around the ring and the TIR domains wedged between the ARM domains on the outside of the ring (Figure 1.3B and C) [116]. While both the inactive and activated human SARM1 remain in an octameric shape [113, 115, 116], a key lock between the autoinhibitory ARM and catalytic TIR domain traps SARM1 in its inactive state [112]. This autoinhibitory state is regulated by an allosteric binding site within the ARM domain which is both NAD- and NMN sensitive [110, 113].

For several years the field of PAD was dominated by two hypotheses of how PAD is activated, the NAD depletion hypothesis and the NMN accumulation hypothesis, both of which were seen as exclusive. The current consensus incorporates elements of both the NAD depletion and NMN accumulation hypotheses where SARM1 activation is triggered by a fall of the NAD:NMN ratio (Figure 1.4) [113, 115].

In healthy axons, NAD binds to the allosteric site in the ARM domain facilitating a "lock-in" state [113]. This arrangement reinforces the autoinhibition of the protein by making sure TIR domains of individual SARM1-molecules stay spatially separated and the protein thus enzymatically inactive (Figure 1.3B). Consequently, artificial mutation of key residues disrupting any of the required ARM-interfaces (ARM-SAM, ARM-TIR and two different ARM domains) results in a conformational change [116]. This brings TIR domains closer and SARM1 becomes catalytically active. When an axon is injured, its homeostatic state is disturbed, axonal NMNAT2 levels together with NAD decrease and therefore NMN rises, SARM1 senses this metabolic change and is activated (Figure 1.3C) [121]. NMN-binding changes the conformation of the protein promoting an activated SARM1, eventually leading to axon death.

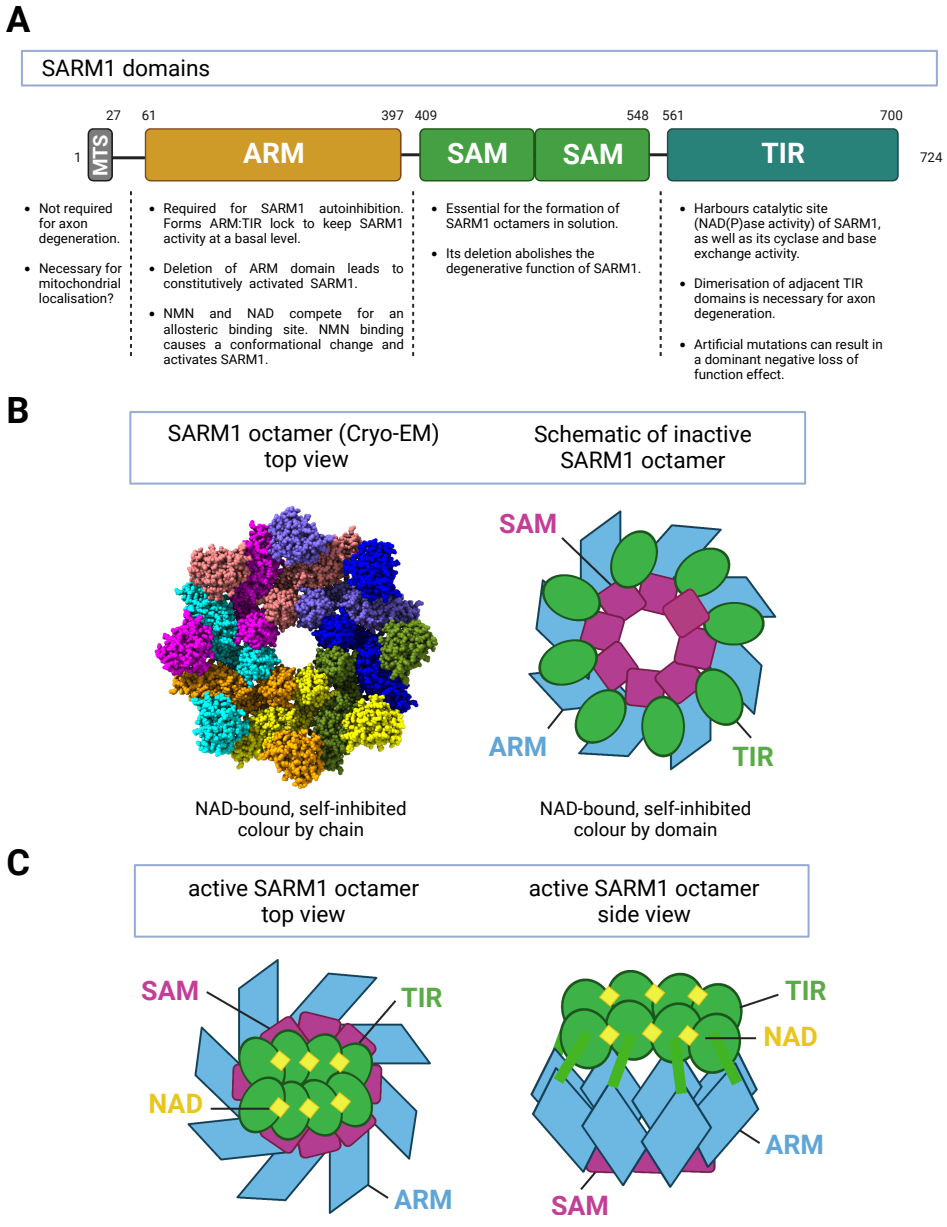


Figure 1.3: **SARM1 domains, its crystal structure and activation mechanism. (A)** Human SARM1 domain structure showing an N-terminal ARM, two tandem SAM domains, and a C-terminal TIR domain and their respective roles in PAD [121]. Numbers highlight amino acid positions. **(B)** Inactive SARM1. On the left, ligand-free hSARM1 cryo-EM structure (PDB: 7CM6) colour-coded by each SARM1 chain. On the right, a schematic of the fully assembled inner and outer octameric SARM1 ring highlighting the arrangement of the individual SARM1 domains right next to it, colour-coded by SARM1 domains [113–115] **(C)** Active SARM1. Upon NMN binding, conformational changes in the ARM domain result in their rotation relative to the SAM-ring and the TIR domains form catalytically-competent active sites. Figure section compiled using information from previous publications [113–116]. Created with BioRender.com.

1

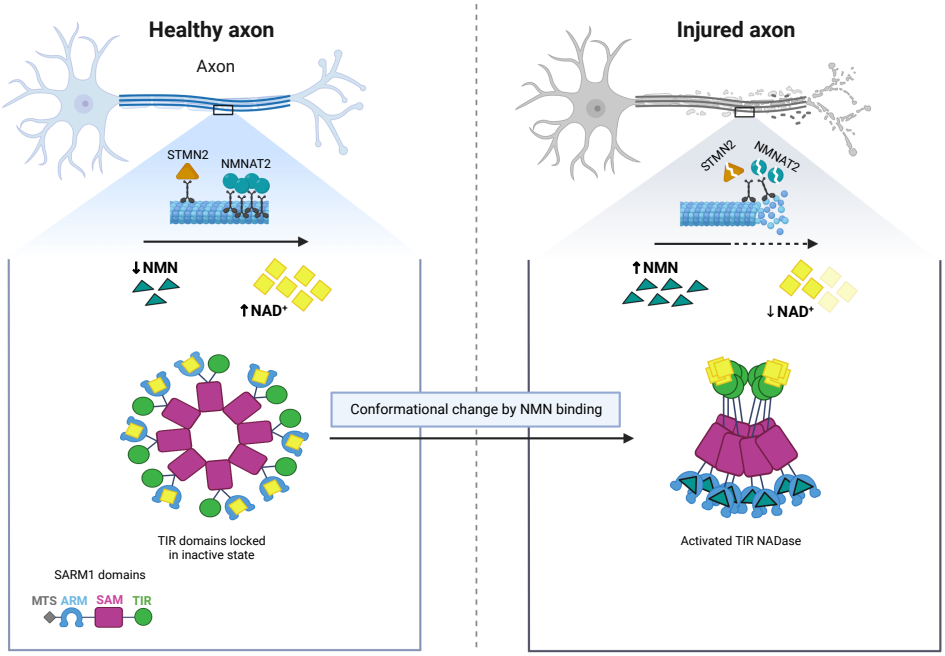


Figure 1.4: **SARM1 and NMNAT2 are regulators of axon health.** Left side: In the inactive state SARM1's ARM domains are bound to NAD (allosteric pocket) and flank adjacent TIR domains, mediating autoinhibition of SARM1 NADase activity. Right side: When an axon is injured, NAD synthesis stops resulting in an NMN buildup. In consequence to the rising NMN/NAD ratio, NMN binds to the ARM domain allosteric pocket, resulting in a conformational change in the ARM domain and multimerisation of the TIR domains. Created with BioRender.com.

More generally, it is believed any insult resulting in reduced NMNAT2 levels eventually activates SARM1-mediated PAD (Figure 1.4). This could be achieved through mitochondrial dysfunction, protein synthesis block, impaired axonal transport, or NMNAT2 mutation directly. All of these examples are well known drivers for pathogenesis and thus provide a rational for how an axon death pathway initially discovered in cut axons could translate to neurodegenerative disease.

SARM1 is a multifunctional glycohydrolase with NAD(P)ase, ADPR cyclisation and base-exchange activities. While SARM1-mediated NAD loss is widely thought to cause PAD, further research into other SARM1 activities and their potential involvement in axon death is required. For instance, both ADPR and its cyclic form cADPR are Ca^{2+} mobilisiers, as is NaADP (Nicotinic acid adenine dinucleotide phosphate) resulting from base-exchange [121]. NAD levels are influenced by other metabolic pathways/enzymes and therefore not a good biomarker for PAD. The rise of cADPR can indicate early axonal damage and, in contrast to Nfl, is SARM1-specific [75].

Studies concerning the exact cellular localization of SARM1 are certainly not in agreement with both mitochondrial and non-mitochondrial SARM1 pools reported [121]. While overexpressed GFP-tagged SARM1 localises to mitochondria [82], endogenous SARM1 is mostly reported to have a partially punctate, non-mitochondrial intracellular location [83]. In support of an axon localization are unpublished data by Coleman lab colleagues Ella Hopkins and Dr. Jonathan Gilley.

The dual role of SARM1 in innate immunity and axon degeneration has prompted questions about whether SARM1 is involved in neuronal damage secondary to viral infections. Examples include rabies infection and cell death secondary to bunyavirus [122, 123]. Furthermore, *SARM1* mRNA and protein levels are upregulated secondary to HPV (Human papillomavirus) transduction in primary human keratinocytes [123]. vesicular stomatitis virus (VSV)-infected *SARM*1$^{-/-}$ mice are protected from neurodegeneration and show reduced cytokine and chemokine levels in the mouse brain. The increase in survival of Sarm1-deficient mice appears to be in line with a blunted inflammatory response. SARM1 further contributes to neuronal cell death observed in encephalitis associated to La Crosse virus (LAVC) as well as under hypoxic conditions [118]. In contrast, Szretter et al suggest SARM1-deletion makes mice more susceptible to West Nile virus infection. A partial explanation could be a context-dependent SARM1 action where the nature of the immune response varies between different pathogens. This may offer a link between SARM1 axon degeneration and innate immunity. However, it is equally likely that these two functions are executed independently but overlap under certain conditions.

1

1.3.3 Stathmin-2

Stathmin-2 (STMN2), also referred to as superior cervical ganglion 10 (SCG10), is a microtubule regulating protein and axonal c-Jun N-terminal kinase (JNK) substrate. Remarkably, both STMN2 and NMNAT2 are palmitoylated proteins regulated by a similar group of zinc Finger DHHC palmitoyltransferases [124]. Like NMNAT2, it is a labile axon survival factor replenished by fast axonal transport [30, 71]. In healthy axons, high levels of STMN2 are maintained through replenishing STMN2 from the cell body. Consequently, transection of an axon leads to STMN2 depletion and promotes axon destruction. JNK inhibition or maintaining high STMN2 levels can delay degeneration. However, these effects are less striking than in the case of NMNAT2 [71]. The loss of STMN2, for instance, is not sufficient to induce degeneration of primary neuronal cultures in the absence of injury, but it renders the axon more vulnerable accelerating the degenerative process [71].

The Drosophila ortholog Stathmin is necessary to maintain the stability of neuromuscular junctions [125]. *STMN2* knockdown in the mouse substantia nigra results in the loss of dopaminergic neurons [126]. Loss of STMN2 has been implicated in neurodegenerative disorders [127]. *STMN2* levels are significantly decreased in Alzheimer's, Parkinson's disease and ALS [126, 128–130]. STMN2 depletion is hypothesised to contribute to the pathogenesis of TDP-43 associated ALS [129, 130]. Loss of mouse *Stmn2* is sufficient to induce ALS-like pathology, including progressive motor neuropathy. However, this is independent of SARM1 [131].

1.3.4 A mitogen-activated protein kinase cascade

The mitogen-activated protein kinase (MAPK) cascade comprises a family of proteins that regulate a wide variety of cellular processes, including proliferation, differentiation, apoptosis and stress responses. These cascades are characterised by a sequential activation of protein kinases named accordingly, MAP4K to MAPK [132]. Interestingly, MAPK signalling is suggested to affect SARM1 both upstream and downstream of it [72, 133]. Dual leucine zipper-bearing kinase (DLK), known as Wallenda in *Drosophila*, is a component of the MAP3K subfamily and known to regulate synaptic architecture [134, 135], as well as axon degeneration and regeneration [136, 137]. Degeneration of DRG primary neuronal cultures derived from *DLK*-deficient embryos is delayed after axotomy and vincristine treatment. Similarly, mice lacking *DLK* show a moderate delay of 52 h in axon degeneration post sciatic nerve injury. Moreover, removal of the *Drosophila* DLK orthologue Wallenda (Wnd) leads to a comparable weak protection [136]. Two other mammalian MAP3Ks, MEKK4 and MLK2, also moderately delay the rate of axon degeneration and there seems

to be functional redundancy between the three MAP3Ks as a combinatorial knockdown results in more long-lasting protection [72]. MAPK signalling via DLK and its paralog LZK promotes the degradation of palmitoylated NMNAT2 and if genetically or pharmacologically inhibited results in increased NMNAT2 levels [95, 133].

1.3.5 Axundead acts downstream of dSarm

Another pro-degenerative protein is Axundead (Axed), discovered through a forward genetic mutagenesis screen in axotomized *Drosophila* wing sensory neurons, where fly *Axed*-null mutants block degeneration triggered by different stimuli, including dSarm GoF and dNMNAT depletion proposing a dNMNAT depletion/dSarm/Axed-pathway with Axed sitting at a convergence point in flies. In mammals, four putative paralogs exist, namely BTBD1, BTBD2, BTBD3 and BTBD6. Whether the axoprotective effect of Axed deletion is preserved in mammals remains to be clarified [138]. All BTBDx proteins have a BTB/POZ domain in common which his a protein-protein binding domain associated to several cellular functions. All 4 mammalian paralogs are largely uncharacterised. However, bTBD3 and 6 are associated to neuronal development.

1.3.6 Mitochondria have a dual role in programmed axon death

The swelling of mitochondria has been reported alongside the destruction of neurofilament [139]. Mitochondria have been proposed to have a dual role in the process of PAD [13]. Mitochondria were initially suggested to play a role in the execution of axon degeneration, the evidence for which is only moderate. However, data support the idea that mitochondrial dysfunction on its own can result in SARM1-dependent axon death. Prominent examples are the protonophore CCCP and Rotenone both of which cause mitochondrial dysfunction [77, 140]. The mitochondrial complex I inhibitor Rotenone is implicated in the loss of dopaminergic neurons seen in PD [141–143]. Rotenone treatment in rats mimics many of the PD like clinical and histopathological features. Given that several diseases have previously been associated to dysregulated mitochondria, including Parkinson's disease, peripheral neuropathies and multiple sclerosis, this makes PAD an attractive target.

1.3.7 The roles of Calcium, Calpain and Calpastatin

Intracellular Ca^{2+} increase is commonly observed during the process of axon destruction, including two distinct phases of intra-axonal calcium level increase, one during the acute axon degeneration phase which also occurs in Wlds animals, as well as those expressing NMN deamidase, and therefore unlikely to be triggering PAD. The late intra-axonal Ca^{2+}

influx occurs downstream of SARM1 and is NMN-dependent. It is this second SARM1-NMN-dependent Ca^{2+} wave which is crucial to the execution of PAD and is therefore crucial to the PAD pathway [144].

Intracellular Ca^{2+} levels are regulated by plasma membrane calcium channels and cell organelles, such as mitochondria and the endoplasmic reticulum. As such, mitochondrial and ER dysfunction have been linked to neurodegenerative disorders. Manipulation of calcium levels with the help of chelators or inhibition of plasma membrane channels, such as L-type calcium channels by dihydropyridines and voltage- and receptor-gated slow calcium channels by bepridil 11 and verapamil 260 all modestly delay axon degeneration *in vitro*. Inhibition of RyR activity protects from degeneration and several points towards Ca^{2+} acting downstream of SARM1.

Calpains, a family of Ca^{2+}-activated cysteine proteases, are implicated in various biological processes, such as remodeling of cytoskeletal/membrane attachments, signal transduction pathways, and apoptosis [145]. Activation of calpains has long been implicated in axotomy-induced axon degeneration [34]. In fact, dysregulated Calpain activity has been linked to neurodegenerative disease [146, 147]. Calpain activity is not just modulated by intracellular Ca^{2+} but also by its endogenous inhibitor calpastatin. Calpastatin, a calpain inhibitor, can delay degeneration for up to 16 h after *in vitro* axotomy and 24 h after *in vivo* optic nerve crush and is naturally depleted post physical injury *in vitro* and *in vivo* [35, 36]. Overexpression of human calpastatin slows down degeneration by initially protecting axonal cytoskeleton and preserving NMJ innervation in transected mouse sciatic nerves with similar protective features observed after optic nerve injury [35, 36].

1.4 Slowing down programmed axon death in pre-clinical disease models

Axotomy is the traditional way of activating PAD and comes with an obvious advantage: Transection affects all axons at a defined site and time which makes it a powerful way to overcome the heterogeneity of axon pathology observed in diseases [6]. While it could be argued that PAD has no significance in neurodegenerative disorders, as axonal transection per se is rare in a clinical context [3], a body of evidence points towards a common degenerative pathway. The most robust protection against degeneration *in vitro* and *in vivo* is achieved by manipulating either of the following: (1) Overexpression of NMNAT function via WLD^S or (2) the removal of *SARM1* [5, 121]. This provides a genetic definition for what is called Wallerian-like degeneration, axon destruction occurring in the absence of a cut or injury [6, 148].

1.4.1 WLD^S delays axon degeneration rates in disease models

The axoprotective effects of WLD^S were first demonstrated in models of physical injury [40, 149, 150]. Protection, however, goes beyond transection or crush, including a wide range of PNS and CNS disorders where expression of mutant WLD^S protein successfully alleviates symptoms.

In the PNS this includes resistance to axon degeneration secondary to treatment with the chemotherapeutics vincristine and paclitaxel [151–153], a model of Charcot-Marie-Tooth (CMT) types 1A and 1B [154, 155], but not CMT type 2D [156]. Furthermore, WLD^S alleviates pain in normal mice [157], as well as in chronic constriction injury [158, 159].

In the CNS, WLD^S has been shown to protect in a mouse model of progressive motor neuronopathy (pmn) [160, 161], gracile axonal dystrophy [162], global cerebral ischemia [163], traumatic brain injury [164] and in neurotoxin-based models of Parkinson's disease [165–168]. WLD^S also attenuates the disease course in experimental autoimmune encephalomyelitis (EAE), a model of multiple sclerosis [169–171]. Interestingly, conditional knockout of astrocytic *SARM1* has been reported to decrease neuronal death, neuroinflammation, inhibited demyelination and improves motor function in EAE mice [172]. WLD^S further delays axonal degeneration in several mouse models of ocular diseases, including glaucoma caused by raised intraocular pressure [48, 173] and protection of RGC axons secondary to injury, toxins and ischemic injury [174–176].

1

1.4.2 *SARM1*-deficiency also efficiently delays axon degeneration in disease models

Like WLD^S, *Sarm1* deletion also protects axons and alleviates pain in mouse models of chemotherapy-induced peripheral neuropathy (CIPN), including the agents Vincristine, Paclitaxel and Bortezomib [177–179], as well as in a model of high-fat diet associated peripheral neuropathy [177]. In addition, *Sarm1* deletion mitigates hepatic sympathetic neuropathy and improves metabolic parameters in high-fat diet (HFD)-challenged mice [180]. Deletion of *Sarm1* rescues axonal, synaptic, and muscle phenotypes in a rat model of CMT type 2A [181]. *Sarm1* deletion further improves axon degeneration and DPN symptoms in a streptozotocin-induced model of diabetes, including rescued outgrowth of DRG primary neuronal cultures, reduced hypoalgesia and alleviation of intraepidermal nerve fiber loss in animals [182].

In the CNS, *Sarm1*-deficiency leads to improved pathology-associated parameters in several models of traumatic brain injury, including fewer protein aggregates, reduced levels of the phosphorylated neurofilament protein, reduced axonal injury, reduced demyelination and reduced corpus callosum atrophy [183–186]. Furthermore, *Sarm1* ablation suppresses neuronal death in brain slices deprived of oxygen and glucose [187]. In addition, deletion of *Drosophila dSARM* reduces dopaminergic neuronal loss [188].

Excitotoxicity upregulates SARM1 expression and promotes degeneration of retinal ganglion cells and their axons [189]. In consequence, absence of *Sarm1* can protect in models of ocular diseases, including axon degeneration in RGCs [69], photoreceptor death in a model of retinal degeneration [74] and retinitis pigmentosa [190]. Depletion of *Sarm1* also rescues retinal degeneration in the NMNAT1-deficient model Leber congenital amaurosis [75]. *Sarm1* deletion completely rescues axon degeneration induced by vacor toxicity, a disused rodenticide and lethal neurotoxin in humans, whose downstream metabolite vacor mononucleotide (VMN) directly activates SARM1 [76]. Of note, *Sarm1* deletion did not improve disease progress in a model of retinal degeneration, although photoreceptor death was significantly reduced, suggesting SARM1 does not occur in retinal epithelium cells/ the choroidal layer and is not required for disease progression [190].

There are some instances where neither the presence of WLD^S, nor *Sarm1* deletion attenuate disease phenotype and progression. One such example is the superoxide dismutase 1 G93A (SOD1G39A) mouse model of ALS [191–193]. In contrast, deleting Sarm1 does protect in a mouse model of ALS-FTD, a TDP-43Q331K mutant, where motor axon degeneration and neuromuscular junction denervation are less severe [194]. Interestingly, *Sarm1* deletion hinders axon degeneration of enteric neurons but exacerbates colon inflammation in a

mouse model of acute dextran sulfate sodium–induced colitis ulcerosa [80].

In addition, examples of other manipulations that protect against PAD *in vivo* exist. Expression of the bacterial NMN deamidase, for instance, delays Wallerian degeneration in mice and zebrafish larvae and rescues axonal defects and lethality of *NMNAT2*-deficient mice. The latter rescue is reminiscent of crosses with WLD^S and *Sarm1* deficient mice [100, 101]. When NMNAT2 is knocked down in mature axons, neurites degenerate even in the absence of an injury [30]. Moreover, genetic *Nmnat2* deficiency in the form of a complete knockdown results in a lethal phenotype in mice. *Nmnat2*-deficient mice die at birth exhibiting absent or truncated axons both in the PNS and CNS with impaired outgrowth [100]. While both *Sarm1* deletion, as well as WLD^S rescue perinatal lethality resulting from Wallerian-like axonopathy in *Nmnat2*-deficient mice, only *Sarm1* deletion confers a life-long rescue beyond the age of three months [101, 195]. A possible explanation for this is the fact that WLD^S substitutes for the lack of NMNAT2, while *Sarm1* deletion blocks the degenerative effects further downstream of PAD [195]. This together with the fact that WLD^S does not occur in humans suggest SARM1 depletion/inhibition has therapeutic advantages over WLD^S.

1.4.3 Manipulation of PAD rates in primary neuronal cultures

The rate of degeneration in culture is faster. Transected primary neurons derived from dorsal root ganglia (DRG) degenerate at a faster rate than superior cervical ganglion (SCG) neurons. It is possible to influence the rate of degeneration through manipulation of the system. WLD^S and *Sarm1*-deficient primary neuronal cultures show delayed axon degeneration after a range of *in vitro* triggers of degeneration: Examples include modest degeneration rate reduction of up to 4-6 h upon NGF-deprivation [196], 24 to 96 h secondary to Vincristine treatment [151, 197], as well as up to 72 h upon exposure to the mitochondrial toxins rotenone and CCCP [77, 140, 198]. Both WLD^S and *Sarm1* deficiency protect against deficits caused by *NMNAT2*-depletion in cultures, including neurite loss and outgrowth [30, 100, 101]. Several other, but less efficient ways exist to delay degeneration in cultures. Exogenous or transgenic expression of NMN deamidase in primary SCG cultures confers a protection reminiscent of the WLD^S phenotype, both secondary to a cut and toxins [102, 199]. Similarly, preventing NMN accumulation with FK866, an NAMPT inhibitor, delays degeneration for 24h after axotomy while NAD levels continue to decline [102, 200].

1

1.5 Bridging the gap between animal studies and human disease

While direct evidence for the role of PAD in humans is lacking, there is accumulating evidence strengthening links between SARM1 and NMNAT2 coding variation and human axonopathies. Recently four cases of rare forms of polyneuropathy were directly associated with human NMNAT2 missense variants published in 2019, where the severity of the disease is representative of the degree of NMNAT2 LoF, as well as phenotypically related to matching mouse genotypes [7, 8, 100, 103]. These include two rare cases of childhood-onset polyneuropathy accompanied by erythromelalgia, episodes of acral burning pain and redness, causatively linked to a homozygous NMNAT2 mutation resulting in a partial loss-of-function causing thermal instability of the enzyme [7]. Lethal missense mutations were observed in the case of two stillborn siblings with fetal akinesia deformation sequence (FADS), which presented with severely reduced skeletal muscle mass and hydrops fetalis. Both protein variants were incapable of supporting axon survival *in vitro* and showed altered protein stability including defects in NAD synthesis, a phenotype reminiscent of NMNAT2-null mice which show both developmental defects in muscle and the nervous system and also die peri-natally [8, 99, 100].

In mice at least, intervention by complete removal of *Sarm1* (which acts downstream of NMNAT2) rescues the extreme phenotype in *Nmnat2:Sarm1* double homozygous mice which remain healthy during their entire lifespan [101, 195]. In addition to the four published NMNAT2 biallelic LoF carriers, two more siblings with a similar early-onset polyneuropathy exist (discussed in chapter 4). These variants were tested for LoF and phenotype causality by myself and the results are discussed in detail in chapter 4 of this thesis. Of note, the patient cases and similar results were published by Dingwall et al. as this work was underway [11].

In all three cases, the severity of the axonopathy correlated with the degree of NMNAT2 LoF and resembles observations in mice with abnormal NMNAT2 levels [99–101]. Biallelic NMNAT2 is rare but the identification of further cases seems likely and could have great potential for transformational PAD-targeting therapies in these patients. With the confirmation that NMNAT2 influences human pathology, milder alleles or heterozygosity appear to be interesting candidates for putative disease modifiers potentially even underlying individual variability of axon loss susceptibility. Interestingly, another rare NMNAT2 mutation c.482T>C (p.Val161Ala) was reported in a 73-year-old patient with a stroke-like onset of brain stem degeneration, also known as Alexander's disease. However, 11 other potentially disease-causing heterozygous variants were identified in the same patient [201].

NMNAT2 transcript levels in human post mortem Alzheimer's brain have been shown to be significantly lower relative to the control group. The results of the study also suggest that lower NMNAT2 mRNA levels negatively correlate with cognitive abilities. More importantly, the study shows 50-fold or more variable levels of human NMNAT2 mRNA expression exists, presumably resulting from natural variation in gene regulation, and it is important to explore what functional consequences this may have on axon health [202]. Indeed, axonal transport of both NMNAT2 and mitochondria, two independently transported cargos, decline with age [203] and mice with low Nmnat2 expression present with early and age-dependent nerve axon defects together with temperature insensitivity and a late-onset decline in motor performance. This is suggestive of reduced NMNAT2 levels below a particular threshold compromising the development of peripheral axons and increasing their vulnerability [103].

While these changes are only evident in mice expressing very low steady-state Nmnat2 levels (roughly 30% of WT level), a more modest NMNAT2 reduction in humans could lead to a similar outcome considering the length, lifespan, as well as the natural exposure to potentially harmful environmental cues. Particularly relevant to chapter 4 of this thesis are the fact that the frequency of predicted NMNAT2 LoF mutations, including splicing and frameshift, is very low in gnomAD (https://gnomad.broadinstitute.org/), a population database which excludes paediatric cases, which is suggestive that heterozygous carriers may have significantly worse outcomes than in mice. It is likely that individuals with reduced NMNAT2 levels will have increased axon vulnerability of selective axon populations secondary to age-related, toxin-induced or disease-dependent stresses.

There are a number of studies that support the hypothesis that SARM1 actively contributes to neurodegeneration, with the strongest links pointing towards ALS in particular. ALS has received particular attention because peripheral axon degeneration often precedes motorneuron death during disease progression [192]. A non-coding risk variant in the SARM1 locus has been repeatedly identified in a meta-analysis of genome-wide association studies of ALS cohorts with estimated odds ratios of 0.845 and 0.9 each [204, 205]. TDP-43 aggregation characteristic of ALS results in reduced STMN2 expression, a survival factor with similar features to NMNAT2 [129, 130]. Finally, a number of SARM1 variants seen in ALS cohorts and other motor neuron disease patients have been shown to have constitutive activity due to loss of autoinhibition with enzymatic activities exceeding that of WT SARM1 by 10-fold [9, 10]. How this relates to SARM1 function is further discussed in chapter 3 of this thesis. Importantly, these single point-mutations are sufficient to induce degeneration.

Previously, data suggesting the relevance of SARM1 and NMNAT2 in human disease were discussed. Along with the similarity to animal models where Sarm1 deletion and the presence of WLD^S are protective this emphasizes important intervention points to modulate the course of degeneration. Over the past 10 years important findings have led to better understanding how the different molecules within the PAD pathway are linked, interact with each and where they are positioned. Moreover, structural biologist have advanced our understanding of SARM1 structure and its mechanism of action. This cumulative knowledge provides a plethora of options for therapeutic intervention to target PAD in disease. Naturally, every target will bring different levels of protection, as well as challenges faced in order to be implemented in the clinic. As of today, the removal of SARM1 appears to have the strongest axon-protective effect. This may change if further crucial players of the pathway, perhaps a homologue to the *Drosophila* axed, are identified.

1.6 Aims of this thesis

Currently, there is a lot of interest in the role of PAD in neurodegenerative axonopathies and other disorders, and several companies are already targeting SARM1 therapeutically [5, 116, 206–208]. Previously discussed sections suggest that PAD-blocking therapies are most promising in the case of (1) rare disorders with biallelic NMNAT2 mutations, (2) conditions where axonal stress is temporary (e.g. CIPN) and (3) axonal disorders where e.g. SARM1 GoF is associated with disease. Further studies of genetic association with disease would be facilitated by identifying more function-altering alleles of NMNAT2 and SARM1. Both loss of function (LoF) and gain of function (GoF) would increase statistical power of disease-association studies so this is the basis for the data chapters presented here.

There are three data chapters in this thesis which will each address a question relating to the role of human variation in the two central regulators of PAD, SARM1 and NMNAT2. These questions include:

1. Are naturally-occurring human SARM1 variants present in the general population? If so, what is their functional effect on NADase activity and axon survival?

    (a) This question will be addressed by screening the population databases gnomAD and dbSNP for SARM1 missense variants likely to result in LoF. The contribution of these variants to injury-induced axon degeneration *in vitro* will be assessed using biochemical assays and a rescue strategy in *Sarm1*-deficient primary neuronal cultures, microinjected with constructs containing the desired mutant alongside WT and the enzyme-dead control E642A SARM1.

   (b) If SARM1 LoF variants are indeed present, they will be tested for their ability to cause dominant negative LoF.

2. The Coleman group knows of two more siblings with rare biallelic *NMNAT2* mutations where both patients are affected by an early-onset polyneurpathy which - to some extent - resembles the phenotype reported by Huppke et al [7]. Are these new disease-associated NMNAT2 LoF variants?

   (a) I will test the patient alleles for LoF and causality to firmly establish biallelic NMNAT2 LoF as pathogenic.

   (b) In addition to the patient variants, a small set of artificial and natural NMNAT2 missense variants in proximity to a functionally-important region of the protein will be tested. The capability of all variants to support axon survival in mouse primary neuronal cultures is functionally assayed alongside WT and the enzyme-dead control H24D NMNAT2. In vitro enzymatic assays are used to test for potential defects in NAD synthesis.

3. Are SARM1 missense variants present in disease cohorts? If so, can the discovery of these help hypothesis generation for future experimental work?

   (a) For this purpose, the UK Biobank and 100,000 Genomes, two UK-based genomic databases, will be screened for SARM1 coding variation.

   (b) Furthermore, allele frequencies of predicted and confirmed SARM1 LoF alleles will be compared between disease and control groups.

2

Materials and Methods

2.1 Generation of constructs

2.1.1 SARM1 and NMNAT2 variant selection strategy

SARM1 coding variants within the protein's ARM, SAM and TIR domains and *NMNAT2* coding variants residing within amino acids 90-105 were selected from the dbSNP (build 137: https://www.ncbi.nlm.nih.gov/snp/; last accessed 05-10-2022) [209] and the Genome Aggregation Database, public release v3.1 (gnomAD; https://gnomad.broadinstitute.org/; last accessed 05-10-2022) both of which served as complementary resources. Variants were filtered as follows: (1) exclusion of non-coding, predicted loss-of-function (pLoF) and synonymous variants, (2) extraction of the respective orthologues and NMNAT isoform sequences from Ensembl [210] followed by multiple sequence alignment to assess evolutionary conservation of residues using Clustal Omega [211], (3) use of SIFT and PolyPhen-2 as *in silico* missense prediction tools [212, 213].

2.1.2 Design and preparation of primers

All oligonucleotides were synthesised by Merck and resuspended in nuclease-free water to a concentration of 100 pmol\µl. Sense and antisense primer pairs were designed as follows: a primer length of 25-45 nucleotides flanking the desired single point mutation in the middle of the sequence and a GC content $\geq$ 40%. In most cases, nucleotides that encoded the amino acid to be changed were substituted such that the change would result in a

single point natural variation. Artificial mutants spanning amino acids 95-102 NMNAT2 (T95A, L99A, H101A, H102A) were created so that the base substitution would result in a codon encoding the amino acid alanine (A) instead. Table 2.1 and Table 2.2 below outline the designed sequences.

2.1.3 Generation of constructs and site directed mutagenesis

Expression vectors encoding the desired constructs were generated by introducing the respective single-point mutation (see Table 2.1 and Table 2.2) following an adapted Quik-Change® II XL site-directed mutagenesis protocol (Stratagene) into the complete open reading frame (ORF) of the canonical 724 amino acid long human SARM1 (NCBI Protein Reference Sequence: NP\055892.2) or the canonical 307 amino acid human NMNAT2 variant (NCBI Protein Reference Sequence: NP\055854). Full-length products were cloned into the expression vector pCMV Tag-4A (Agilent Technologies) and into pLVX-IRES-zsGreen1 (Takara Bio), respectively. NMNAT2 pCMV Tag-4A constructs have a 17 amino acids long linker between the N-terminal Flag tag and the respective protein's ORF. C-terminal Flag-tagged SARM1 variants were expressed from a pLVX-IRES-ZsGreen1 vector backbone (Takara Bio) (alongside ZsGreen expressed from its bicistronic cassette) in all experiments except where otherwise indicated in the text or figure legend. Successful mutagenesis of all constructs and PCR fidelity at relevant steps were checked by subsequent DNA sequencing (Department of Biochemistry, University of Cambridge) (Cogenics). Sequencing reactions consisted of 1000 ng DNA plasmid each diluted in nuclease-free water. The sequencing files were analysed with the help of FinchTV 1.4.0 (Geospiza, Inc., USA). Other plasmids used were pEGFP-C1 expressing enhanced green fluorescent protein (eGFP) used as a transfection control for the SARM1 and NMNAT2 pCMV-Tag4-based expression constructs (BD Biosciences Clontech) and pDsRed2-N1 (BD Biosciences Clontech) expressing variant Discosoma red fluorescent protein (DsRed2) used to label microinjected primary neurons. Mutagenesis reactions were carried out in a 50 µl H_2O reaction mixture, containing 2.5 µl 10 µM forward and reverse primers, 5 µl Pfu 10x reaction buffer, 0.5 µl dNTPs (all Agilent) and 1 µl PfuUltra HF DNA polymerase (2.5 U/ µl, Sigma) which was added last to each reaction mix. The thermal cycling conditions are given in Table 2.3.

Mutation	Sense primer (5'-3')	Antisense primer (5'-3')
P332Q	CTGCAGCGCCTCGTGCAGTTGCTCGACTCTAAC	GTTAGAGTCGAGCAACTGCACGAGGCGCTGCAG
E399K	GCGCCTGCTGGGCAAGGAGGTGCCACGGC	GCCGTGGCACCTCCTTGCCCAGCAGGCGC
E416K	GCTGGAAGGAGGCCAAGGTTCAGACGTGGC	GCCACGTCTGAACCTTGGCCTCCTTCCAGC
G456V	CCAGACCGACCTGGTCATGAAATCGGGCATC	GATGCCCGATTTCATGACCAGGTCGGTCTGG
P549L	GAAATGCTACATCCCTGCTGCCCTGTACTGG	CCAGTACAGGGCAGCAGGGATGTAGCATTTC
R569C	GTCTTCATCAGCTACTGCCGGAACTCAGG	CCTGAGTTCCGGCAGTAGCTGATGAAGAC
R570Q	CATCAGCTACCGCCAGAACTCAGGTTCCCAG	CTGGGAACCTGAGTTCTGGCGGTAGCTGATG
N571K	CAGCTACCGCCGGAAGTCAGGTTCCCAGCTGG	CCAGCTGGGAACCTGACTTCCGGCGGTAGCTG
S572P	CAGCTACCGCCGGAACCCAGGTTCCCAGCTGGCC	GGCCAGCTGGGAACCTGGGTTCCGGCGGTAGCTG
I593T	GCTTCAGTGTCTTCACTGATGTGGAGAAGCTG	CAGCTTCTCCACATCAGTGAAGACACTGAAGC
D594E	CAGTGTCTTCATTGAAGTGGAGAAGCTGGAAG	CTTCCAGCTTCTCCACTTCAATGAAGACACTG
K602N	GCTGGAAGCAGGCAACTTCGAGGACAAACTC	GAGTTTGTCCTCGAAGTTGCCTGCTTCCAGC
I608L	TTCGAGGACAAACTCCTCCAGAGTGTCATGGG	CCCATGACACTCTGGAGGAGTTTGTCCTCGAA
G624ter	GTTGGTGCTATCACCTTGAGCACTGGACAAGTGC	GCACTTGTCCAGTGCTCAAGGTGATAGCACCAAC
K641N	GGATTGGGTGCATAATGAGATTGTGACTGCTT	AAGCAGTCACAATCTCATTATGCACCCAATCC
I643T	GGGTGCATAAGGAGACTGTGACTGCTTTAAGC	GCTTAAAGCAGTCACAGTCTCCTTATGCACCC
I653T	GCTGCGGCAAGAACACTGTGCCCATCATTGATGG	CCATCAATGATGGGCACAGTGTTCTTGCCGCAGC
P655S	GCGGCAAGAACATTGTGTCCATCATTGATGGCTTCG	CGAAGCCATCAATGATGGACACAATGTTCTTGCCGC
S684F	ACGGTATCAAGTGGTTCCACAAATACCAGGAG	CTCCTGGTATTTGTGGAACCACTTGATACCGT
E686K	ATCAAGTGGTCCCACAAATACCAGGAGGCCAC	GTGGCCTCCTGGTATTTGTGGGACCACTTGAT

Table 2.1: **SARM1-specific oligonucleotide primers used for site-directed mutagenesis.**

Mutation	Sense primer (5'-3')	Antisense primer (5'-3')
D90E	GGGAGTGCTACCAGGAAACCTGGCAGACGACC	GGTCGTCTGCCAGGTTTCCTGGTAGCACTCCC
T95A	GACACCTGGCAGACGGCCTGCAGCGTGTTG	CAACACGCTGCAGGCCGTCTGCCAGGTGTC
C96F	CCTGGCAGACGACCTTCAGCGTGTTGGAACACC	GGTGTTCCAACACGCTGAAGGTCGTCTGCCAGG
V98M	GCAGACGACCTGCAGCATGTTGGAACACCACCG	CGGTGGTGTTCCAACATGCTGCAGGTCGTCTGC
L99A	CGACCTGCAGCGTGGCGGAACACCACCGGGAC	GTCCCGGTGGTGTTCCGCCACGCTGCAGGTCG
H101A	GCAGCGTGTTGGAAGCCCACCGGGACCTCATG	CATGAGGTCCCGGTGGGCTTCCAACACGCTGC
H102A	CAGCGTGTTGGAACACGCCCGGGACCTCATGAAG	CTTCATGAGGTCCCGGGCGTGTTCCAACACGCTG
L105F	GGAACACCACCGGGACTTCATGAAGAGGGTGAC	GTCACCCTCTTCATGAAGTCCCGGTGGTGTTCC

Table 2.2: **NMNAT2-specific oligonucleotide primers used for site-directed mutagenesis.**

2.1.4 DpnI digest and transformation

Parental methylated DNA was removed from PCR products by DpnI digest (New England Biolabs, R0176S) at 37°C for 1 h before transforming them into Max Efficiency™ DH5α Competent Cells (Thermo Fisher Scientific, 18258012). 1 µl of each DpnI-digested PCR product was added into pre-chilled Falcon 2059 round-bottom tubes (Corning, 353002) before adding 100 µl competent cells and incubation for 30 min on ice. Cell were then heat-shocked for 45 s at 42°C and subsequently allowed to recover for 2 min on ice before 900 µl S.O.C. medium (Thermo Fisher Scientific, 15544034) was added. Cultures were then left to grow in the 37°C shaker for 1 hour. Cells were spun at 6,000 $x\ g$ on a tabletop centrifuge for 3 min before removing approximately 950 µl of supernatant. Bacterial pellets were carefully resuspended in the remaining volume and plated on lyosgeny broth (LB)-kanamycin (pCMV Ta-4A vector, Thermo Fisher Scientific, 11-815-024) or LB-ampicillin (pLVX-IRES-zsGreen1 vector, Sigma, A0166) agar plates and incubated o/n at 37°C.

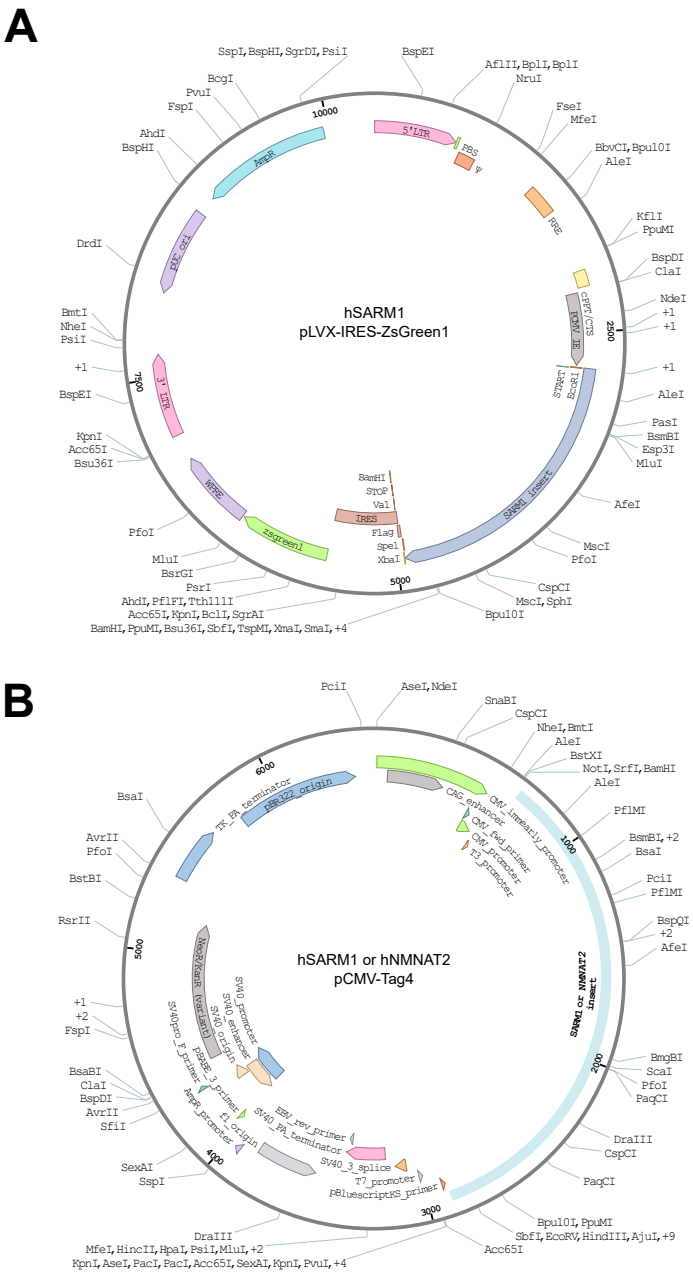


Figure 2.1: **Structure of pLVX-ZsGreen1 and pCMV-Tag 4A plasmid constructs used in chapter 3 and chapter 4. (A)** The pLVX-IRES-ZsGreen1 vector is a bi-cistronic vector, expressing ZsGreen (green arrow in plasmid) and human SARM1 (in blue) and was used for all metabolite assays presented and discussed in chapter 3. **(B)** pCMV-Tag 4A plasmid vectors were used for axotomy assays in chapter 3, as well as chapter 4. The respective insert is highlighted in blue. Generated using https://benchling.com.

Segment	Cycles	Temperature	Time
1	1	95°C Hot-start	30s
2	16	95°C Denaturation	30s
		55°C Annealing	1 min
		68°C Elongation	1 min/kb plasmid*
*5:30 min for NMNAT2 in N-terminal FLAG-tagged pCMV-Tag2 7 min for SARM1 in N-terminal FLAG-tagged pCMV-Tag2 11 min for SARM1 in pLVX-IRES-ZsGreen1			

Table 2.3: **Mutagenesis protocol for generating *SARM1/NMNAT2* expression constructs.**

30 µl total reaction
2 µg Maxi/Miniprep sample
3 µl Buffer
1 µl restriction enzyme No.1
1 µl restriction enzyme No.2
Rest add nuclease-free water

Table 2.4: **Example reaction of a restriction digest.**

2.1.5 Restriction digest and gel electrophoresis

Three µL of the PCR products and restriction enzyme digests (volumes in Table 2.4) were separated by 1% Agarose gel electrophoresis in 1x TRIS-Borate-EDTA-Buffer (TBE) and GelRed™ nucleic acid gel stain (20x). Samples and 1kB DNA ladder were mixed with loading buffer to a ratio of 1:6 and loaded into wells. Gels were run at 200V for approximately 45 min and DNA was visualised under a UV transilluminator.

2.1.6 Mini-, Midi-, Maxipreps

For minipreps, single colonies were inoculated in 2-3 ml of LB broth containing 0.1 mg/mL Kanamycin or Ampicillin and grown overnight in the 37°C bacterial shaker. After incubating for 12-16 hours, bacterial cells were harvested for plasmid preparation using a Qiagen plasmid miniprep kit according to the manufacturer's manual. Alternatively, for the generation of maxipreps the miniprep inoculation was diluted into 250 ml of LB broth containing Kanamycin or Ampicillin, grown overnight at 37°C shaking. DNA mini- or maxi preparations from overnight bacterial cultures were performed using the Qiagen plasmid mini prep kit or the Qiagen Endofree Plasmid Maxi Kit respectively as per manufacturer's instructions followed by quantification using a NanoDrop ND-1000 spectrophotometer (NanoDrop Technologies, Wilmington, North Carolina).

2.2 Cell culture related work

2.2.1 Animals

2

All animal work related to primary cell isolation was regulated under the Animals (Scientific Procedures) Act (ASPA),1986 Amendment Regulations 2012 and Home Office regulations following ethical review by the University of Cambridge Animal Welfare and Ethical Review Body (AWERB) under project licence PPL P98A03BF9. Animals were fed ad libitum and held under standard specific pathogen free (SPF) conditions in the mouse facility. Primary neuronal cultures were isolated from C57BL/6Babr and Sarm1$^{-/-}$ mice (MyD88-5) mice generated by Kim et al, 2007 [118].

2.2.2 HEK 293T cell culture and transfection

Human embryonic kidney (HEK) 293T cells (clone 17, [HEK 293T/17]) obtained from the American Type Culture Collection (ATCC) were authenticated by STR profiling and mycoplasma contamination was excluded. Cells were cultured under standard aseptic conditions in Dulbecco's Modified Eagle Medium (DMEM, from Gibco) with 4.500 mg/L glucose, 110 mg/L sodium pyruvate and 2 mM glutamate (Sigma), supplemented with 1% penicillin/ streptomycin (Invitrogen) and 10% heat-inactivated fetal bovine serum (FBS, from PAA) at 37°C with 5% CO2 in a humidified air incubator. Cell growth and confluency were assessed on a regular basis and cells were passaged when 80-100% confluent. For cell passaging medium was aspirated, and the cell monolayer washed with sterile 1x phosphate buffered saline (PBS, from Gibco). Cell detachment was achieved by incubation with TrypLE Express (milder alternative to Trypsin, from Gibco) for 1 min at 37°C. Upon successful dispersion, 9 mL of fresh complete medium was added to inactivate the TrypLE. For maintenance, cells from the 10 mL cell suspension were seeded into T75 flasks at 1:20. Cells were plated in 24-well plates the night before transfection to reach a confluence of at least 50% the day of transfection. Transfections were performed using Lipofectamine 2000 (Invitrogen) and Opti-MEM™ (Thermo Fisher Scientific) according to the manufacturer's protocol (see Table 2.5 for more detail). In general, 1000 ng SARM1 or NMNAT2 expression construct (wild-type or mutant) or empty vector were transfected per well. In the case of untagged SARM1 or NMNAT2, 750 ng expression vector (wild-type or mutant) or 750 ng empty pCMV-Tag 4A vector as a control were transfected together with 250 ng pEGFP-C1 (used as a control for transfection efficiency) per well. The amount of DNA transfected in each experiment is indicated in the relevant figure legend or chapter sections.

Culture vessel	Area/well	PM (vol.)	DM (vol.)	DNA	LF2000
24-well	2 cm^2	500 µl	2 x 50 µl	1 µg	2 µl
6-well	10 cm^2	2 ml	2 x 250 µl	4 µg	10 µl
60 mm	20 cm	5 ml	2 x 0.5 ml	8 µg	20 µl
10 cm	60 cm	12 ml	2 x 1.5 ml	24 µg	60 µl
PM (vol.) - volume of plating medium DM (vol.) - volume of dilution medium					

Table 2.5: **Protocol for up- or downscaling transfection of HEK 293T cells.**

2.2.3 Primary neuronal cultures from dissociated SCGs

Superior cervical ganglia (SCG) were dissected from postnatal day 0-3 (P0-P3) wt or Sarm1$^{-/-}$ mouse pups according to a standardised protocol [214]. Pups were decapitated and stored on ice until use within 2 hours. SCGs are found next to the carotid bifurcation and were dissected under a stereoscopic dissection microscope. Once cleaned from excessive tissue, ganglia were collected in L15 Leibovitz medium. For the dissociation step, ganglia were first incubated in 0.025% Trypsin (Sigma) in PBS (Ca^{2+}-, Mg^{2+}-free, from Gibco) in a 37°C water bath for 15 min followed by 0.1% collagenase type II in PBS (Gibco) at 37°C for 15 min. Subsequent gentle trituration of ganglia was achieved by pipetting up and down with a p1000 (up to 10x). In most, but not all cases, a preplating step was performed to remove non-neuronal cells. For this purpose, the dissociated neuron suspension was transferred to an uncoated 35 mm petri dish for 2 hours to allow adherence of unwanted glial cells. Eventually, cell suspension was collected with a pipette tip and neurons spun down at 400 *x g* (MSE Mistral 1000 centrifuge) for 5 min. Dissociated cells were then resuspended in a small volume (40 µl per dish) and plated on poly-l-lysine- (20 µg/ml at room temperature, RT, for 1–2 h) and laminin- (20 µg/ml at RT for 1–2 h) pre-coated µ-ibidi dishes (Thisle Scientific). After 2 hours, medium was topped up once neurons adhered to the glass surface of the dish. SCG culture medium was supplemented with nerve growth factor (NGF, 1:3000) and the antimitotic Aphidicolin (1:1000 on day 0, 1:2000 on day 2 and day 5) for further reduction of non-neuronal cells. Medium was replaced on day 1 and every 2-3 days *in vitro* (DIV) after. Detailed information on cell culture media used can be found in Table 2.6.

SCG Medium	Volume	Stock
DMEM (Sigma) - Glucose 4500 mg/l - Sodium pyruvate 110 mg/l	44 ml	n.a.
[dashed] FBS (filtered)	5ml	n.a.
Glutamine	500 µl	200mM (100x)
Penicillin/Streptomycin	500µl	10.000 U/ml
Aphidicolin	1:2000	4 mg/ml
NGF	1:3000	100 ng/ml
Overnight Medium	**Volume**	**Stock**
Hibernate-E Medium	48ml	n.a.
B27	1 ml	20ml/l (2%)
Penicillin/Streptomycin	500µl	10.000 U/ml
Glutamine	500µl	200mM (100x)
NGF	1:3000	100 ng/ml
Imaging Medium	**Volume**	**Stock**
FluoroBrite DMEM	As required	n.a.
FBS (filtered)	5ml	n.a.
Penicillin/Streptomycin	500µl	10.000 U/ml

Table 2.6: **Media preparations used for primary neuronal cultures.**

2.3 Metabolite measurements and NADase activity

2.3.1 In-cell NAD(P) quantification

Cellular NAD(P) levels from transfected HEK 293T cells were analysed at 24 h after transfection using the NAD/NADH-Glo™ and NADP/NAPDH-Glo™ Assay (Promega Biosciences) following an adapted version of the manufacturer's protocol. Essentially, 24-well plates containing transfected HEK 293T cells were placed on ice and cells from individual wells collected by pipetting up and down, centrifuged at 24,000 *x g*, the supernatant removed and then washed once with 500 µl ice-cold PBS containing cOmplete™ Mini EDTA-free protease inhibitor cocktail (Roche). Whole-cell lysates were prepared in ice-cold KHM buffer, containing 110 mM potassium acetate, 20 mM Hepes (pH 7.4), 2 mM MgCl2 supplemented with 0.1 mM digitonin (all Sigma) and cOmplete™ Mini EDTA-free protease inhibitor cocktail (Roche). Cell lysates were clarified by gentle centrifugation (5 min, 1,500 *x g* at 4 °C and all samples diluted to equal concentrations of 0.5 µg/µl using the Pierce™ BCA Protein Assay Kit (Thermo Fisher Scientific).25µl of each lysed sample was mixed with 12.5 µl 0.4M HCl and heated to 60 °C for 15 min before being cooled down to RT. Subsequently, samples were neutralised by adding 12.5 µl 0.5 M Tris base, 10 µl of which was then mixed with 10 µl of the respective Glo detection reagent on ice in wells of a

384-well white polystyrene microplate (Corning). Plates were incubated for 40-50 min at 25°C and luminescence values obtained using the GloMax® Explorer microplate reader (Promega Biosciences). Cell extracts were kept on ice at all points until completion of the experiment. NAD(P) values were calculated in relation to standard curves generated from a serial dilution of the respective nucleotide and data expressed as relative values to the empty vector control. The remaining whole-cell extract samples were stored at -80 °C for subsequent ATP measurements and immunoblotting.

2.3.2 In-cell ATP quantification

The same whole-cell extracts served for analysis of ATP levels using the CellTiter-Glo Assay (Promega Biosciences). Here, 10µl of the cell extract were directly mixed with 10 µl of the detection reagent in wells of a 384-well white polystyrene microplate (Corning) on ice. Luminescence values were read after an incubation period of 15 min in the GloMax® microplate reader (Promega Biosciences). All metabolite values were calculated in relation to standard curves generated from a serial dilution of the respective nucleotides. Data are expressed as relative values measured in wells transfected with the empty vector control.

2.3.3 Purification of FLAG-tagged SARM1 and NMNAT2

Recombinant, Flag-tagged SARM1 and NMNAT2 (WT or variants) were purified from transfected HEK 293T cells. Transfection protocol was adjusted and a larger amount of cells was transfected for SARM1 variants expressed at low levels (+ addition of NR to boost cell viability) and all NMNAT2 constructs (WT and mutants) accounting for the natural lower protein expression of NMNAT2 compared to SARM1. Wells of a 6 well-plate, or 10 cm dishes (all NMNAT2 constructs, as well as SARM1 variants expressed at low levels, including E399K, S572P, G624*, I643T and I653T) were transfected with 4 µg or 24 µg of expression construct, respectively. In the case of SARM1 constructs only, cells were pre-treated with 2 mM Nicotinamide Riboside (NR), an NAD precursor which increases *in cellulo* NAD levels prior to transfection. This delays depletion of NAD and an associated block to de novo protein synthesis to extend the time that proteins are expressed from transfected constructs. This was done to achieve a sufficient yield during the protein purification process of NADase-competent SARM1 variants. Cells were collected 24 h post transfection, washed in 500 µl of ice-cold PBS containing cOmplete™ Mini EDTA-free protease inhibitor cocktail (Roche) and lysed using ice-cold KHM buffer as described above but with lysates being diluted to a final concentration of 1 µg/µl. Lysates were then incubated with 50 µl/ml of washed Pierce™ Protein A/G Magnetic Beads (Thermo

Fisher Scientific) together with 20 µg/ml anti-Flag M2 antibody (Merck F3165) on a rotator overnight at 4 °C. The next day, beads were washed three times in KHM buffer, followed by one wash in PBS (with abovementioned protease inhibitors). Bead-bound protein was then resuspended in PBS containing 1 µg/µl BSA to reduce loss of enzymatic activity when frozen for storage. Immunoblotting was used to determine the concentration of purified bead-bound SARM1 or NMNAT2 protein. Of particular note, G456V SARM1 was not efficiently recognised by the SAM domain antibody used for the initial quantification (kindly provided by AstraZeneca), presumably due to disruption of the epitope. Instead, G456V SARM1 was quantified separately based on Flag immunoblotting relative to WT SARM1.

2.3.4 NADase assays using recombinant SARM1 protein

NADase reactions were optimised to determine the ideal amount of immunoprecipitated SARM1 protein and time points to use [9]. NADase reactions were performed with the recombinant SARM1 attached to beads as the elution of the protein from beads is very inefficient meaning that it was difficult (and expensive) to get sufficient protein for NADase reactions. NADase reactions were set up with bead-bound recombinant SARM1 in 25 µl reactions (in 1x PBS, Gibco) containing 1-5 ng/µl (0.0124-0.0618 pmol/µl) SARM1 together with 25 mM NAD alone or 25 mM NAD with 50 mM NMN. During the setup period, reactions were kept on ice to minimise NAD consumption before the start of the NADase assay at 25°C. Reactions containing bead-bound SARM1 were thoroughly mixed prior to the incubation period, as well as 1-2x during the incubation. NAD consumption was calculated as the difference comparing NAD levels at two timepoints: 0 h vs. an ideal endpoint which was optimised depending on the activity of each variant to obtain rates as close as possible to the most accurate, maximal rate under these conditions. These ranged from 1h-2h for NADase competent (WT-like) SARM1 variants to 24 h for inactive SARM1 LoF variants. 5 µl aliquots of each reaction mix were taken at the start (while still on ice) and at individual endpoints. These aliquots were then mixed with 2.5 µl 0.4M HCl to stop the reaction, followed by neutralisation with 2.5 µl 0.5M Tris base. Samples were then diluted 1:50 in buffer containing 50% PBS, 25% 0.4 M HCl and 25% 0.5 M Tris base to reach the linear range of the NAD/NADH-Glo™ Assay (Promega Biosciences) used to determine NAD levels. 10 µl of the diluted samples were then mixed with 10 µl of NAD/NADH-Glo™ detection reagent on ice in wells of a 384-well white polystyrene microplate (Corning). Plates were incubated for a period of 30-45 min at 25 °C and luminescence values determined using a GloMax® Explorer microplate reader. NAD sample values were calculated in relation to a standard curves generated from a serial NAD dilution.

Control immunoprecipitations using extracts from HEK 293T cells transfected with empty vector revealed that a low level of non-specific NADase consumption was co-purified with the bead/antibody complexes. Although this non-specific activity was small, it significantly changed activity rates calculated for low yield inactive variants, especially G624* SARM1, which were purified using a higher volume of magnetic beads. The non-specific NAD-consuming activity per starting volume of beads (average of n = 4 control immunoprecipitations) was calculated and subtracted this, based on the amount of beads present in each reaction, to obtain a corrected rate for each variant. Noteworthy, in most cases this had almost no effect on the original values obtained. NAD consumption rates were normalised to SARM1 protein concentration and are presented as mol NAD consumed per min per mol recombinant SARM1 (mol/min/mol SARM1).

2.3.5 NAD synthesis assays using recombinant NMNAT2 protein

NMNAT2 protein yield was lower than SARM1 and concentrations therefore appropriately adapted. NAD synthesis reactions were set up with bead-bound recombinant NMNAT2 in 25 µl reactions (in 1x PBS, Gibco) containing 1 ng/µl (0.0124-0.0618 pmol/µl) NMNAT2 together with 1 mM ATP and NMN each, as well as 25 mM MgCl2. Due to the known instability of NMNAT2 preparations after thawing, enzyme was always added as the last component. During the setup period, reactions were kept on ice to minimise NAD synthesis before the start of the assay at 37°C which is the ideal temperature for NMNAT2 activity [8]. Reactions containing bead-bound NMNAT2 were thoroughly mixed prior to the incubation period. NAD synthesis was calculated as the difference comparing NAD levels at two timepoints: 0 h vs. 10 min which was optimised to obtain rates as close as possible to the most accurate, maximal rate under these conditions. 5 µl aliquots of each reaction mix were taken at the start (while still on ice) and at the endpoints. These aliquots were then processed as in the case of NADase assays: mixed with 2.5 µl 0.4M HCl to stop the reaction, followed by neutralisation with 2.5 µl 0.5M Tris base. Samples were then diluted 1:50 in buffer containing 50% PBS, 25% 0.4 M HCl and 25% 0.5 M Tris base to reach the linear range of the NAD/NADH-Glo™ Assay (Promega Biosciences) used to determine NAD levels. 10 µl of the diluted samples were then mixed with 10 µl of NAD/NADH-Glo™ detection reagent on ice in wells of a 384-well white polystyrene microplate (Corning). Plates were incubated for a period of 30-45 min at 25 °C and luminescence values determined using a GloMax® Explorer microplate reader. NAD sample values were calculated in relation to a standard curves generated from a serial NAD dilution. NAD synthesis rates were normalised to NMNAT2 protein concentration and are presented as mol NAD produced per min per mol recombinant NMNAT2 (mol/min/mol NMNAT2).

2.4 Immunoblotting

Western blotting was performed to assess construct expression levels in HEK 293T cells 24 h post transfection. Lysates from transfected HEK 293T cells (0.5 µg protein/µl, see above) were diluted 1:1 (in the case of NMNAT2 constructs) or 1:2 (for SARM1 constructs) in 2x SDS-PAGE loading buffer. SARM1 samples were incubated at 100°C for 3 min. In contrast, NMNAT2 samples were instead incubated at 60°C for 3 min due to higher protein instability. 10 µl of each sample was loaded per lane of a 15 well 4-20% Mini-PROTEAN TGX Precast Protein Gels (Bio-Rad laboratories) and run for 40-50 min at 150-200 V in 1x Tris/Glycine/SDS Electrophoresis Buffer (Bio-Rad laboratories) before being transferred to methanol-activated Immobilon-P PDVF membrane (Millipore) for 60 min in transfer buffer (Tris/Glycine/20% methanol) at 100V. Membranes were then briefly rinsed in water and blocked in 5% milk in TBS (50 mM Trizma base and 150 mM NaCl, PH 8.3, both Sigma) for 1h at RT. Membranes were probed with primary antibodies diluted in 1x TBS with 0.05% Tween-20 (Sigma) (TBS-T) containing 5% milk at 4°C overnight. This was followed by three washes in TBS-T (5-10 min each) and incubation with an appropriate IgG (H+L)-HRP-conjugated secondary antibody (1:3000 in 1xTBS-T containing 5% milk) for 1-2 h at RT. Blots (either whole or cut according to protein size) were probed either sequentially or simultaneously with different antibodies. Primary antibodies used were as follows: mouse monoclonal anti-SARM1 (1:5000, XX), mouse monoclonal anti-FLAG M2 (1:2000, Sigma F3165), mouse monoclonal anti-GFP (1:2000, Sigma, 11814460001), mouse monoclonal anti-ZsGreen (1:1000, OriGene Technologies, TA180002), rabbit monoclonal anti-β Actin (1:5000, Cell signalling technology, 4970) and mouse monoclonal anti-GAPDH (1:2000, Abcam, ab8245). After incubation with antibodies, blots were washed 3x in TBS-T with 5% milk and a final wash in TBS only. Pierce ECL Western Blotting Substrate (Thermo Fisher Scientific) was added for 1 min or the SuperSignal West Dura for 5 min (in case of a weak protein signal) to the membrane prior to chemiluminescence exposure using an Alliance chemiluminescence imaging system (UVITEC Cambridge). Western blot signal intensities were quantified using Fiji (ImageJ).

Primary/ Secondary	Antibody	Raised in	Mono- or Polycloncal	Dilution	Supplier	Cat.No.
Primary	SARM1	Mouse	Monoclonal	1:2000	Hsue lab [109]	-
Primary	FLAG M2	Mouse	Monoclonal	1:2000	Sigma	F3165
Primary	GFP	Mouse	Monoclonal	1:2000	Sigma	11814460001
Primary	ZsGreen	Mouse	Monoclonal	1:1000	OriGene	TA180002
Primary	β Actin	Mouse	Monoclonal	1:5000	Cell signalling technology	4970
Primary	GAPDH	Mouse	Monoclonal	1:2000	Abcam	ab8245
Secondary	Mouse IgG(H+L)-HRP Conjugate	Goat	Polyclonal	1:3000	Bio-Rad	1721011
Secondary	Rabbit IgG(H+L)-HRP Conjugate	Goat	Polyclonal	1:3000	Bio-Rad	1721019

Table 2.7: **Details of antibodies used in the projects discussed in this thesis.**

2.5 Flow cytometric analysis

HEK 293T cells were harvested 24 h post transfection using TrypLE (Thermo Fisher Scientific), neutralised in complete cell medium before being washed once in FACS buffer (1xPBS with 1% BSA) and resuspended in a 200µl volume. To determine cell viability, cells were stained with PI (1:1000, Thermo Fisher Scientific) for 15 min at RT before samples were transferred into ice-cold tubes for immediate analysis. Gating was kept constant throughout all experiments. The percentage of ZsGreen-positive cells among total living cells was determined using a LSR Fortessa (BD Biosciences, San Jose, U.S.) and analysed with FACS Diva 8.0.1 software (BD Biosciences). A minimum of 10,000-20,000 cells were measured per condition.

2.6 Immunostaining

Expression of exogenous SARM1 and NMNAT2 variants in microinjected SCG neurons was confirmed by immunostaining. Medium was carefully aspirated from dishes containing injected neurons, cells were washed with 1x PBS, fixed with 4% paraformaldehyde for 20 min at RT, followed by another wash with 1x PBS. Cell were then permeabilised in 1% Triton X-100 in PBS for 5 min at RT, followed by a wash with 1x PBS. Blocking was performed in 50% goat serum in PBS containing 1% BSA for 30 min at RT. Cells were then incubated with the primary antibody (SARM1 monoclonal antibody 1:500 or Flag M2 monoclonal antibody 1:500) in PBS, 1% BSA for 1 h at RT. After three washes with PBS, cells were incubated with Alexa Fluor-488-conjugated anti-mouse secondary antibody (1:250) in PBS, 1% BSA for 1 h at RT. Cells were washed three times in PBS, then mounted in Vectashield containing DAPI (Vector Laboratories), for nuclear counterstaining, and coverslips sealed with nail varnish. To prevent cell deatchment during the stainin process,

a minimal volume of 300 µl of each solution was used per µ-ibidi dish which is enough to cover the inner surface and solutions were added drop-wise on top of cells. Images were captured with a Leica DFC365FX fluorescence monochrome 188 camera attached to a Leica DMi8 inverted fluorescence microscope (20x objective). Laser filter settings were 405 nm and 425/50 for DAPI, 488 nm and 515/30 for AlexaFluor-488 (Sarm1), and 543 nm and 560 LP for DsRed.

2.7 Axon degeneration experiments

2.7.1 Microinjections

Microinjections were performed using a Zeiss Axiovert 200 microscope with Eppendorf Femtotips (sterile injectioncapillary 0.5µm), a Femtojet transjector and a 5246 micromanipulator system (all Eppendorf). Generated plasmids expressing SARM1 or NMNAT2 together with a DsRed expression construct were diluted in 0.5x PBS(-) and passed through a Spin-X filter (Corning) to avoid needle plugging. The mix was injected into the nuclei of SCG neurons prepared as dissociated cultures and 20-40 SCG neurons/dish individually injected in a row or as clusters to facilitate knowledge of neurite orientation and cell of origin (see Figure 2.2A). More detailed description of types and concentrations of expression constructs used are given in the respective figure legends and thesis sections. In general, construct concentrations were kept low in axon lesion experiments to limit the effects of overexpression. Construct concentrations were increased in the case of immunostaining to allow for sufficient detection of the exogenously expressed protein. In general, for axotomy experiments either WT or Sarm1$^{-/-}$ SCG neurons were injected at 5-7 days *in vitro* and axotomy was performed two days after injection. In contrast, for axotomy experiments using dominant negative SARM1 variants wild-type SCG cultures were injected after 4 days *in vitro*. Axotomy was performed 7 days after injection to allow for formation of dominant negative SARM1 multimers. The DMEM in the SCG medium had to be replaced with phenol red-free FluoroBRITE medium (Thermo Fisher Scientific) for better visualisation/imaging of neurites expressing relatively low levels of ZsGreen due to the longer time window after injection.

2.7.2 Axotomy assays

Neurites were cut manually with a sterile scalpel (No.22 blade) on the second day after injection (Figure 2.2B). The cut was placed just beside the row of injected neuronal bodies to ensure a complete separation of all injected somata from the distal ends of the cut axons.

Numbers of continuous healthy DsRed-labelled axons within the same field were compared distal to the site of a cut at 0 h and 24 h for the purpose of quantification. Fragmented neurites or those displaying abnormal swelling were categorised as degenerating. Numbers displayed on graphs represent the percentage of healthy neurites remaining at 24 h relative to the total number of labelled axons at 0 h after the cut.

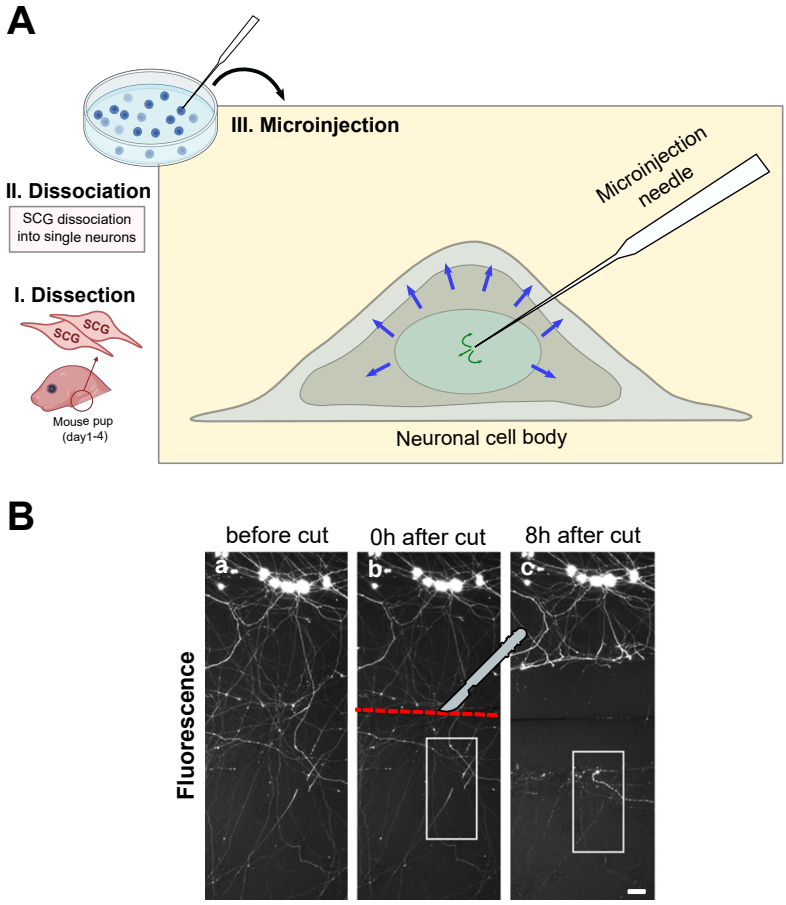


Figure 2.2: **Experimental setup for microinjection assays. (A)** Schematic starting at (I) the dissection of superior cervical ganglia (SCG) from pups aged day 1 to 4, (II) followed by enzymatic dissociation and mechanical trituration and (III) microinjection of dissociated SCG cultures at 4 to 7 days *in vitro* (DIV). Graphical representations of a single neuronal cell body is shown from the side at the point of microinjection. A capillary tip injecting the generated plasmids is briefly dipped into the nucleus but removed before the cell expands to a point of bursting. **(B)** Fluorescence images of a region of a dissociated culture of SCG neurons 48 h after injection showing a small cluster of neurons labelled with DsRed2. The series of images shows the same area before (a), immediately after (b), and 8 h (c) post manual transection with a scalpel blade. A small amount of retraction near the cut site, as visible in (c), is normal. Scale bars correspond to 100 µm. Images were kindly provided by Dr. Jon Gilley from the Coleman lab and adapted, also see Gilley and Loreto, 2020 [214]. Figure created using BioRender.com and Inkscape.

2.8 Model display

Resolved protein crystal structures were retrieved from the PDB database (https://www.rcsb.org/; last accessed 23-07-2022): full-length SARM1 (7LD0) in its autoinhibitory (7CM6) and activated state with the ARM and SAM domains only (7NAL), SARM1 TIR (6O0R). The 3D model of NMNAT2 was obtained from AlphaFold, a sequence homology based programme [215]. Protein structures were visualised and manipulated using ChimeraX [216].

2.9 Database analysis

Aggregate, de-identified data from patients affected by common and rare neurological disorders were analysed using two different disease cohorts as resources: (I) UK Biobank data accessed through the genebass (gene-biobank association summary statistics) browser (https://genebass.org/; last accessed 23-10-2022) and (II) 100,000 Genomes Project. For the purpose of comparison, burden test results from genebass for "pLoF" and "missense" variants were analysed separately. No statistical analysis was performed. Chapter 5 is of an exploratory nature and major limitations are discussed in the respective discussion.

2.10 Statistical analysis

Data were assumed to be normally distributed and variance between groups to be equal. Statistical analysis was performed using GraphPad Prism software version 8 (GraphPad Software Inc., La Jolla, U.S.). Flow cytometry data were analysed with Flow Jo (Ashland, United States). Normally-distributed data were statistically analysed using multiple comparisons (one-way and two-way analysis of variance (ANOVA)) or unpaired and paired *t*-tests followed by Benjamini and Hochberg false discovery rate (FDR) correction or Tukey's multiple comparison test. Correlation in Figure 3.5 was assessed using Pearson's product moment correlation. Details described the respective figure legends. Means ± SEM are plotted for all figures. Statistical analysis with a p value < 0.05 was considered as significant, and values above this cut-off considered not significant (ns). A false discovery rate (FDR) correction was applied to multiple comparisons in some graphs and the adjusted p values shown represent the q values reported in each test.

2.11 Figures and Illustrations

Illustrations were created using BioRender.com and Inkscape.org.

3

SARM1 natural variants cause both intrinsic & dominant LoF influencing axon survival

3.1 Chapter summary

SARM1 is a central executioner of axon death which occurs predominantly in the early stage of neurological diseases preceding loss of neuronal somata. Among other functions understood to a lesser extent, SARM1 has an intrinsic NADase activity executed by its TIR domain without which axon death cannot be induced. Parts of the work presented here have been published in Scientific Reports [12]. This chapter, however, provides a more detailed understanding of the project and includes unpublished findings too. I show that several naturally-occurring human *SARM1* alleles within its SAM and TIR domains result in SARM1 loss-of-function (LoF), including two variants that cause dominant LoF. In addition, one of the alleles studied here has GoF properties, in addition to others recently described by our group [9]. Decreased levels of SARM1 in *Sarm1* hemizygous mice confer a partial protection in a range of disease models [217]. This suggests individuals heterozygous for the identified LoF alleles may have a reduced risk of developing e.g. axonopathy-related pathologies, with even lower risk for individuals carrying dominant LoF alleles. While

overall minor allele frequencies (MAFs) of the identified LoF alleles are low, MAFs vary between different ethnic groups and together these alleles are frequent enough to have a meaningful impact within the healthy human population. I conclude by discussing how the cumulative knowledge of *SARM1* alleles is likely to further support links between SARM1-associated PAD and neurological diseases which would be prime candidates for the use of SARM1-blocking drugs.

3.2 Introduction

Impairment of axons is a common pathological denominator across a wide range of neurological diseases, and maintaining axonal homeostasis is a constant challenge for the human body [5, 6]. Axonal health is highly dependent on the homeostasis of the NAD metabolome and involves a fine interplay between pro-survival and pro-degenerative cues. Axon degeneration has been associated with bioenergetic abnormalities [81, 218], where the antagonistic effects of the NAD-synthesising NMNAT2 and the NAD-consuming SARM1 play a crucial role [30, 82, 83, 101, 115, 117].

3.2.1 A model of how SARM1 is activated secondary to injury

SARM1 is an essential pro-degenerative protein which executes programmed axon death upon injury [82, 83]. In healthy neurons, octameric SARM1 is autoinhibited and, upon injury autoinhibition is relieved within the multimer [115]. NMN, the substrate of NMNAT2, and NAD act respectively as an activator and inhibitor of the enzymatic activity (SARM1 is a multifunctional glycohydrolase, NADase) exerted by the SARM1 TIR domain [113, 115, 117]. More precisely, both nucleotides compete for an allosteric binding site located within the autoinhibitory SARM1 ARM domain [115]. In its inactive state SARM1 has a low level of basal NADase activity [219, 220] and the ARM domains are locked into a conformation that keeps TIR domains at distance [112–115, 221, 222], thereby preventing the formation of catalytic sites (Figure 3.1) [110]. Disruption of this ARM:TIR lock leads to SARM1 activation and neuronal death in vitro [112, 116, 222].

NMNAT2 is a protein absolutely required for axon survival [30]. In healthy axons, it acts as a homeostatic regulator by preventing the accumulation of NMN through NAD synthesis, thereby restraining SARM1 NADase activity [5]. However, as a very labile protein, NMNAT2 is rapidly depleted in axons damaged by injury or other insults leading to rising NMN and declining NAD levels [30, 119, 199] which activate SARM1 [115, 219]. A lack of NMNAT-dependent restraint of SARM1 is also suggested to promote neuronal cell death in some situations [9, 74, 76, 119, 223].

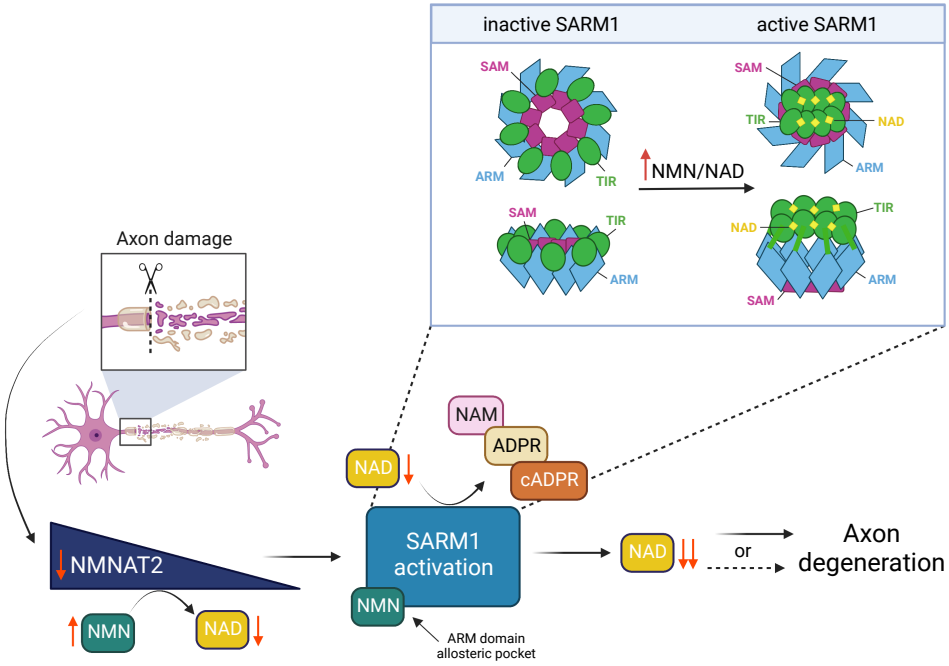


Figure 3.1: **A working model of how SARM1 is activated in injured axons.** Depletion of NMNAT2 results in an increase of NMN and of the NMN:NAD ratio, leading to the activation of the pro-degenerative enzyme SARM1 [82, 83, 101, 115, 117, 144, 199, 219]. SARM1 is a multifunctional glycohydrolase; once activated SARM1 rapidly consumes NAD by metabolising it into NAM, ADPR and cADPR. cADPR accumulation in neurons is specific to the activation of programmed axon death [117]. SARM1 also catalyses base exchange, and with some bases, this resaction is even more efficient than NADase activity [116, 220]. The structural basis of SARM1 activation was recently described in more detail by Shi et al. [116] and is highlighted in the white box: NMN binds to an allosteric ARM domain pocket and thereby induces a conformational change resulting in the activation of SARM1. This is done via the rotation of the ARM domains relative to the octameric SAM-ring. This structural change enables the TIR domains to self-associate and form six catalytically-competent active sites per SARM1 octamer. Figure compiled using information from Merlini et al. and Shi et al. [13, 116]. Created with BioRender.com.

3.2.2 Programmed axon death in human disease

Evidence linking altered protein function of PAD genes to disease susceptibility in humans was limited at the start of this PhD but has been growing since. A body of evidence supports a direct causation for biallelic *NMNAT2* loss-of-function (LoF) mutations in six rare polyneuropathies which broadly resemble equivalent mouse models [7, 8, 11, 100, 103], further discussed in chapter 4, and for *NMNAT1* mutations that cause photoreceptor loss in Leber congenital amaurosis via a SARM1-dependent mechanism [223]. Recently, several *SARM1* alleles encoding pro-degenerative SARM1 gain-of-function (GoF) missense variants or in-frame deletions with constitutively hyperactive NADase were suggested as risk alleles

in ALS and similar motor neuron diseases [9, 10]. Expressing one such SARM1 GoF variant in the mouse CNS causes motor dysfunction and sustained neuroinflammation, all of which are absent in mice treated with the human WT SARM1 [10]. In support of this disease association, two genome-wide association studies (GWAS) independently linked the *SARM1* chromosomal locus single nucleotide polymorphism rs34517613 to sporadic ALS [204, 205]. Although this alone does not confirm that *SARM1* is the causative gene in this locus, a mechanism involving increased SARM1 expression as a result of altered transcriptional regulation would be a very plausible explanation for the linkage.

3.2.3 Aims of this chapter

There is currently a lot of interest in the role of SARM1 in neurodegenerative axonopathies and other disorders, and several companies are targeting SARM1 therapeutically [116, 206–208]. Crucially, genetic ablation of *Sarm1* leads to robust and reliable protection against axonopathies in animal models mimicking diseases of the central and peripheral nervous system without inflicting any apparent impediments on the animals [5, 70, 177–179, 182–184, 194, 221, 224]. Moreover, Sarm1 has effects via a haploinsufficiency mechanism in mice. Loss of one allele results in a significant depletion of its NADase activity and delays PAD secondary to injury [217, 223]. As such, it is anticipated that human SARM1 alleles encoding full LoF variants might confer meaningful axon protection even in heterozygous individuals. There is a number of predicted LoF variants in SARM1 resulting in a premature stop codon, frameshift or change of splicing sites adjacent to exons. It is possible that a very small percentage of individuals within the human population may be nullizygous or even compound heterozygous for SARM1 LoF alleles [217]. Interestingly, a small number of artificial SARM1 mutants have previously been identified to exert a dominant negative effect when expressed in WT neurons significantly reducing the pro-degenerative effect, both *in vitro* and *in vivo*. In the context of the octameric SARM1, this dominant negative effect is predicted to result from co-expression of mutant and WT SARM1 eventually impairing TIR-TIR domain interactions within the octameric ring [82, 120, 197]. In addition to the NMNAT2 LoF and SARM1 GoF alleles that had been linked to human neurodegenerative phenotypes, it thus seemed likely that other function-altering alleles, especially SARM1 LoF alleles, would exist in the human population. This chapter investigates whether naturally-occurring SARM1 alleles encoding LoF coding variants exist in the general population as these are predicted to be protective. A total of 20 missense and nonsense variants are tested for their SARM1 NADase and axon survival functions *in vitro*. The findings have intriguing implications in relation to individual susceptibility to human neurodegenerative axonopathies which is discussed at the end of this chapter.

3.3 Results

3.3.1 Candidate selection of naturally-occurring variants in human SARM1

Previous structure-function studies of SARM1 have shown that disruption of the SAM multimerization domains or catalytic TIR domain is more likely to result in (protective) LoF than disruption of the autoinhibitory ARM domain, which mostly causes pro-degenerative GoF [9, 10, 82, 110, 112, 113, 115, 117, 120, 208, 222]. In fact, artificially-induced single point mutations within the TIR domain can lead to NADase LoF resulting in a protection against degeneration in cultured primary neurons [117, 120]. Loss-of-function genetic variants are frequently associated with disease. Yet, in the case of the pro-degenerative SARM1, they would be expected to be protective [5]. This prompted the idea that rare human LoF SARM1 variants must be present in the healthy human population as they may not be subject to evolutionary pressure. To address this hypothesis a list of naturally-occurring missense and nonsense SARM1 variants primarily, but not exclusively, located within its SAM and TIR domains was curated using dbSNP and Genome Aggregation Database (gnomAD), as complementary sources [225, 226].

A total of 20 coding single-nucleotide polymorphism (SNPs) were selected from these lists, comprising 19 missense and one nonsense mutation that were considered to have good potential for LoF. Selection criteria included were: overlap or close proximity to previously reported artificial, inactivating mutations in the NADase catalytic pocket [110, 120], evolutionary conservation of the consensus residue, physicochemical consequences of the amino acid changes, allele frequency and in silico prediction tools to determine potential deleteriousness of any changes (Figure 3.2 and Table 3.1). All SARM1 variant carriers listed in gnomAD are heterozygous only, however the existence of compound heterozygous individuals is possible and cannot be excluded. Noteworthy, P332Q SARM1 is the most common SARM1 variant (Population frequency of 1.2% overall and the highest in European non-Finnish) found in gnomAD and was characterised in two independent studies while this work was ongoing [9, 10].

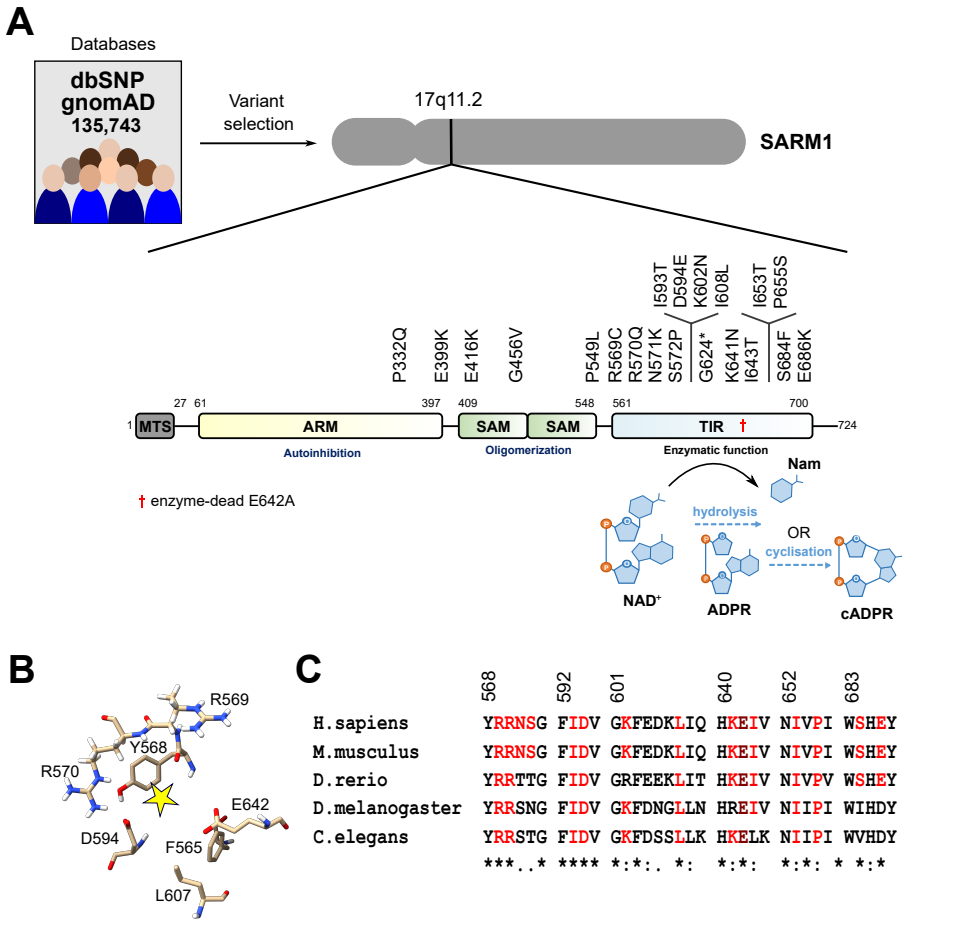


Figure 3.2: **Naturally-occurring SARM1 coding variants assessed in this study. (A)** Protein architecture highlighting important domains of the canonical 724 amino acid human SARM1 protein and showing the approximate locations of the missense and nonsense ARM, SAM and TIR domain variation encoded by SARM1 alleles selected from the databases gnomAD and dbSNP. Noteworthy, all numbering is based on GRCh38/ hg38. The catalytic activity of the TIR domain results in the hydrolysis of NAD producing nicotinamide (NA) and a mixture of ADP-ribose (ADPR) and cyclic ADP-ribose (cADPR). Different papers have different start and end amino acid numbers for the SARM1 domains, these were adapted from [9, 227]. MTS, "mitochondrial" targeting sequence; ARM, HEAT/Armadillo motif domain; SAM, sterile alpha motif domains; TIR, Toll/Interleukin receptor domain. **(B)** Stick representation of SARM1 TIR domain residues in the catalytic pocket interacting with the ligand β-D-ribose (indicated as a star), PDB ID: 6O0Q, visualised in ChimeraX. **(C)** Multiple sequence alignment of selected human SARM1 TIR missense variants along with selected orthologues. Alignment was performed using ClustalOmega. (*, asterix) - fully conserved residue; (., period) - conservation between groups of weakly similar properties. This graph was generated in InkScape.

SARM1 domain	Coding variant[a]	rsID	Genomic location and change[b]	MAF[c]	Polyphen	SIFT score
ARM	P332Q	rs140811640	28381727 C>A	0.006371	0.712	0
ARM	E399K	rs375645219	28384462 G>A	0.000457	0.98	0
SAM	E416K	rs147156050	28384513 G>A	0.00058	0.082	0.02
SAM	G456V	rs140340827	28384903 G>T	0.00066	0.782	0
SAM	P549L	rs1241475032	28388189 C>T	0.000020	0.995	0.28
TIR	R569C	rs571724138	28388248 C>T	0.000046	0.998	0
TIR	R570Q	rs539229444	28388252 G>A	0.000085	0.997	0
TIR	N571K	rs150052156	28388256 C>G	0.000013	0.0025	0
TIR	S572P	rs781797528	28388257 T>C	0.000013	0.14	0.01
TIR	I593T	rs782196205	28388394 T>C	0.000013	0.721	0
TIR	D594E	rs782407924	28388398 T>A	0.000004*	0.998	0
TIR	K602N	rs35201495	28388422 G>T	0.000079	0.961	0.04
TIR	I608L	rs1490414328	28388438 A>C	0.000008**	0.033	1
TIR	G624*	rs141324431	28388486 G>T	0.000033	-	-
TIR	K641N	rs1344370780	28388539 G>T	0.000013	0.998	0
TIR	I643T	rs1224037543	28395909 T>C	0.000008**	0.997	0
TIR	I653T	rs782525385	28395939 T>C	0.0000066	0.997	0
TIR	P655S	rs776939252	28395944 C>T	0.000046	0.999	0
TIR	S684F	rs782256561	28396162 C>T	0.000033	0.994	0.03
TIR	E686K	rs1460394367	28396167 G>A	0.000013	0	0

[a] Numbering according to the canonical 724 amino acid long human SARM1.
[b] Numbering according to the GRCh38 genome build.
[c] Minor allele frequency referring to the gnomAD population except where indicated (*, *gnomADExome*; **, *TOPMED*.

Table 3.1: **Human SARM1 ARM, SAM and TIR domain coding variants in gnomAD and dbSNP.**

3.3.2 NAD levels in transfected HEK 293T cells are altered by naturally-occurring human SARM1 variants

As an initial screen for potential NADase LoF, SARM1 variants encoded by the selected SARM1 alleles were tested for their ability to deplete NAD in transfected HEK 293T cells which do not express any endogenous SARM1 (see Figure 4.4.A). This assay was established as an indirect way to measure the activity of exogenously expressed Flag-tagged SARM1. In-cell NAD levels were measured 24h after transfection with FLAG-tagged SARM1 constructs co-expressing ZsGreen using the bioluminescent NAD/NADH-Glo™ assay (Figure 3.3.A). Of note, earlier time points resulted in greater variability of NAD values which may be due to asynchronous protein expression (data not shown). This assay has the scope to test for both SARM1 LoF and GoF variants [9]. However, here the conditions were adapted (see chapter 2 for detailed information on the used protocol) to optimise the detection of NADase LoF specifically. Under these conditions, full-length wild-type (WT) SARM1 causes a robust depletion of cellular NAD 24 h after standard transfection of HEK 293T cells (due to high overexpression of a low, constitutive NADase activity) (Figure 3.3.B). Naturally, this masks any differences in NAD depletion compared to potential GoF variants that may be present.

While a number of the selected variants (P332Q, E399K, E416K, G456V, P549L, R570Q, N571K, I593T, K602N and I608L SARM1) behaved like WT SARM1, resulting in an NAD depletion of over 90%, several natural TIR domain variants – R569C, S572P, D594E, G624*, I643T, I653T, P655S, S684F, and E686K SARM1 – failed to deplete NAD significantly (Figure 3.3.B). These NAD levels were comparable to results obtained from the empty vector control and the enzyme-dead E642A SARM1 which is deficient for NADase activity [117]. The latter group of constructs was thus predicted to result in substantial NADase LoF. Consistent with these results, variants that failed to deplete NAD (and thus putative NADase LoF) also failed to deplete NADP, an NAD analogue and alternative SARM1 substrate [110, 220, 228, 229] (Figure 3.3.C). As expected, ATP levels matched these observations even though differences were less significant at 24 h post transfection (Figure 3.3.D). This is a likely lagging consequence of NAD loss, also observed elsewhere [9, 120]. Another likely contributing factor to the lower depletion of ATP could be the fact that cell lysates were obtained using a gentle KHM lysis buffer where compartmentalised organelles, such as mitochondria, likely remain intact. Interestingly, K641N SARM1 led to a significant but less drastic reduction of metabolite values which is suggestive of a moderate LoF. Furthermore, a slight reduction in NAD and NADP consumption by R570Q and I593T SARM1 could be suggestive of very modest LoF (Figure 3.3.B and A).

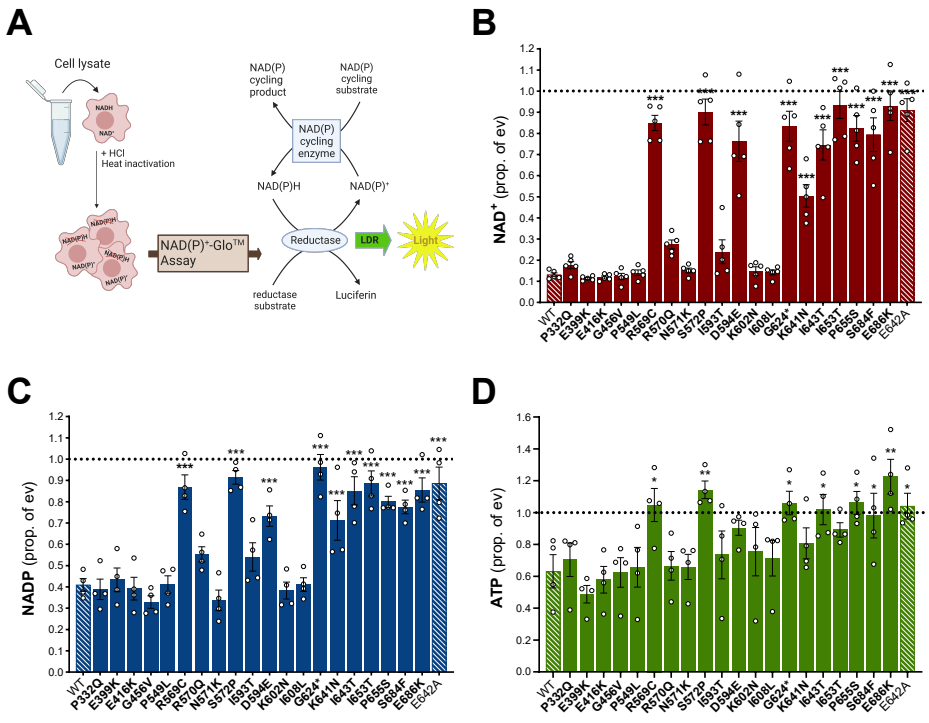


Figure 3.3: **In-cell NAD levels are not depleted by several SARM1 TIR domain variants. (A)** Schematic diagram of the bioluminescent NAD(P)-Glo assays used to assess NAD(P) levels, generated using BioRender.com. **(B, C, D)** Endogenous NAD, NADP and ATP levels acquired from HEK 293T cells 24h after transfection with 1µg WT or mutant SARM1 expression vectors co-expressing fluorescent ZsGreen. Values are shown relative to those from cells transfected with empty vector (ev) control only (values at 1 and indicated by a dashed line). Mean ±SEM with single data points are given (n=4-5); *p <0.05, **p <0.01, ***p <0.001, multiple comparisons using a one-way ANOVA with Benjamini and Hochberg false discovery rate (FDR) correction showing significance as compared to WT SARM1. Bars for the positive and negative controls (respectively WT SARM1 and the enzyme-dead E642A SARM1 artificial mutant) are hatched to distinguish them from the selected variants (text bold, filled bars).

3.3.3 Investigation of human SARM1 variant expression levels in transfected HEK 293T cells

Successful transfection was confirmed by ZsGreen expression in transfected HEK 293T cells (Figure 3.4.A) prior to cell collection for measurement of in-cell endogenous metabolites shown in Figure 3.3. Importantly, western blotting using the same cell lysates suggested that the lack of NAD consumption in the transfected HEK 293T cells could, in most cases, not be explained by insufficient SARM1 expression (Figure 3.4.B). In fact, the majority of the putative LoF variants – R569C, D594E, K641N, P655S, S684F and E686K SARM1 – were

expressed at the same or even higher levels than WT SARM1. Even in the cases where expression was found to be noticeably lower - S572P, I643T and I653T SARM1 – the degree to which expression was reduced would, with the exception of I593T and G624* SARM1, most likely not be sufficient to account for the observed NADase LoF. G624* SARM1 is barely expressed (Figure 3.4.B) which is likely a result of impaired protein stability caused by the truncation rather than insufficient transfection (bright ZsGreen expression as seen in Figure 3.4.A). While its low expression could certainly compromise its SARM1 NADase function if G624* was NADase-competent, the fact that G624* SARM1 lacks key catalytic residues [110, 208] as a result of the C-terminal truncation of the TIR domain - including the essential E642 residue [117] – predicts it to be full NADase LoF anyway.

As observed with other SARM1 GoF variants [9], E399K SARM1 was also barely detectable by immunoblotting figure 3.4.B. In contrast to G624* SARM1, however, overexpression of E399K led to a robust depletion of NAD and NADP of in-cell metabolites values, as was shown earlier in Figure 3.3. This suggests that NAD depletion can be achieved by substantially lower amounts of full-length E399K SARM1 further supporting the idea that it is a potential GoF natural SARM1 variant. Of note, it was difficult to load the right amount of protein on the gels so that both candidate LoF and GoF SARM1 variants were detectable, as adjustment in either way would result in the expression outside of the linear range for the other variants. E399K SARM1 is expressed at roughly a fifth of the WT SARM1 protein (data from Coleman group member Dr. Jon Gilley, not shown).

Levels of co-expressed ZsGreen vary in transfected HEK 293T cells even when overall transfection efficiency appears comparable between different variants (Figure 3.4). A plausible explanation previously suggested is that NAD depletion resulting from overexpressed functional ("WT-like") SARM1 variants suppresses de novo protein synthesis in an NADase-dependent manner [9, 230]. As a result, cells with substantial NAD depletion are expected to have lower ZsGreen expression levels than cells where NAD levels remain high. In support of this hypothesis, fluorescence imaging of wells transfected with the putative natural GoF E399K SARM1 show suppressed ZsGreen expression, almost within a non-detectable range when compared to other SARM1 variants (Figure 3.4.A). Similar observations have been reported in ALS-associated SARM1 GoF variants [30]. Noteworthy, protein stability of variants was not examined in this case. Thus, it cannot be excluded that reduced stability of E399K SARM1 also contributed to low expression levels detected by immunoblotting.

While this model explains observations for the majority of the SARM1 variants that were tested there are exceptions to it. Cells expressing the NADase-competent variants G456V

and K602N SARM1, for instance, express ZsGreen levels which are higher than what would be expected (Figure 3.4.B). This could be the result of a subtle LoF resulting in slower NAD depletion compared to WT SARM1 (but still fast enough to cause maximal NAD depletion by the assay endpoint) allowing for a longer period of ZsGreen expression (and SARM1 expression as well). In addition, the empty vector control is representative of NAD levels but not for ZsGreen expression (Figure 3.4.B). In fact, the consistently low ZsGreen expression from empty vector is likely a transcriptional or translational consequence of an empty first cistron in the bicistronic expression cassette and therefore completely independent of NAD levels. Alternatively, expression of SARM1 may happen up until a threshold activity of the enzyme is reached where it starts suppressing further activity/destruction by impairing translation/transcription of more protein.

To assess the strength of association between in-cell NAD values (indirectly reflecting enzyme activity) and relative ZsGreen expression a Pearson correlation analysis was performed and, indeed, revealed a moderate positive correlation between relative NAD and relative ZsGreen values for each SARM1 variant (Figure 3.5).

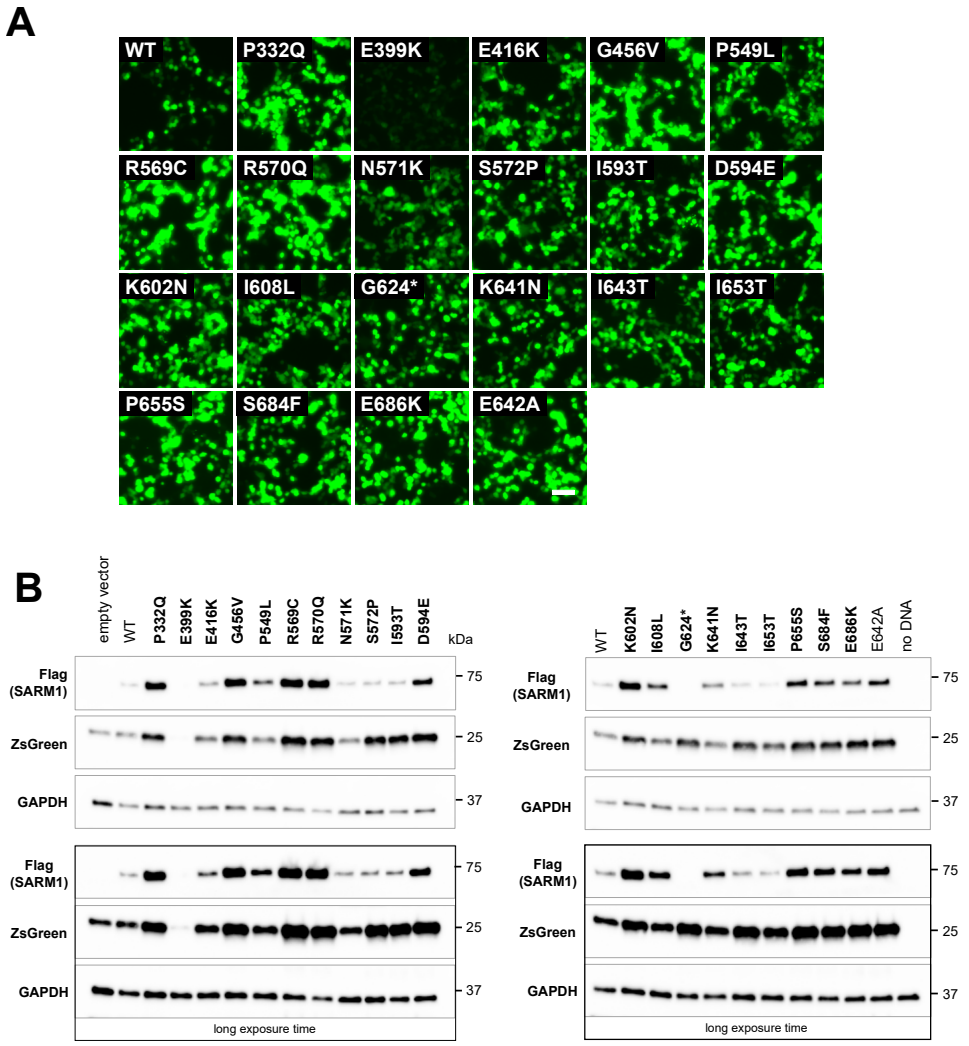


Figure 3.4: **SARM1 variant expression levels in transfected HEK 293T cells. (A)** Representative micrographs of HEK 293T cells transfected with bicistronic constructs stably expressing the selected SARM1 variants as shown together with ZsGreen. ZsGreen intensity differed depending on the activity of the respective SARM1 variant being expressed, however, similar amounts of cells were transfected (total ZsGreen positivity) in each case. This is further elaborated in Section 3.3.4 and the corresponding Figure 3.6. Lower ZsGreen expression is likely a result of NADase-competent (WT-like) SARM1 protein, as observed by Gilley et al. [9]. Scale bar, 50 µm. **(B)** Representative immunoblots showing SARM1 level expression in HEK 293T cell lysates 24 h after transfection. A Flag antibody was used to detect Flag-tagged SARM1 protein (~70 kDa), as well as antibodies against co-expressed ZsGreen (~26 kDa, acting as an indicator for transfection efficiency) and GAPDH (~36 kDa, acting as a loading control). A long exposure of the blots (lower panels highlighted by a thicker frame) was included to show that E399K and G624* SARM1, both not visible under shorter exposures, are expressed but at a very low level. In contrast to G624*, the putative GoF E399K SARM1 also suppressed the expression of ZsGreen.

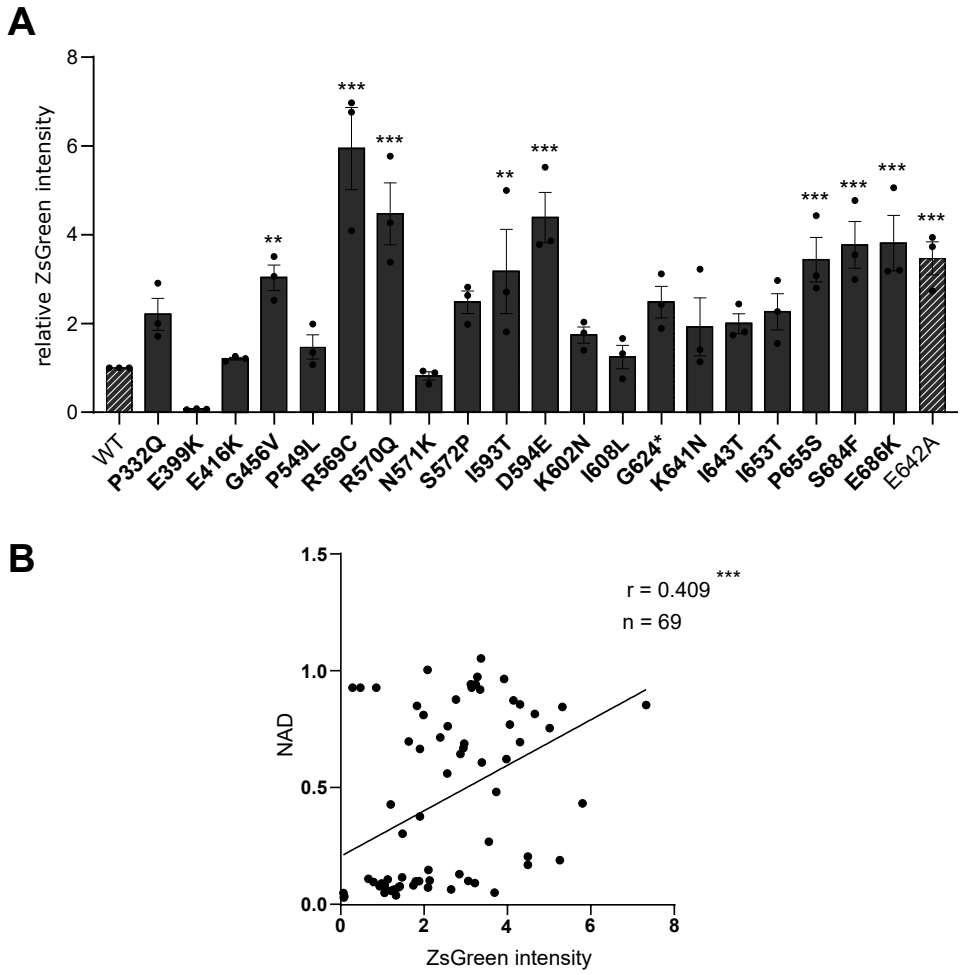


Figure 3.5: **Moderate positive correlation between ZsGreen fluorescence and in-cell NAD values. (A)** Immunoblot quantification of individual ZsGreen levels relative to the loading control GAPDH. ZsGreen expression values are shown as a proportion to those obtained from WT SARM1 (value equals 1). Representative bands are shown in Figure 3.4. Values were obtained from three independent experiments and are shown as ±SEM ***P <0.0001, NS: not significant, multiple comparisons using a one-way ANOVA with FDR correction comparing band intensities to that of the WT protein. Bars for the positive and negative controls (respectively WT SARM1 and the enzyme-dead E642A SARM1 artificial mutant) are hatched as in Figure 3.3. **(B)** Pearson's correlation coefficient revealed a moderate positive correlation between ZsGreen expression levels and the corresponding in-cell NAD levels (as shown in Figure 3.3 in transfected HEK 293T cells, r=0.409 (with r = 1 reflecting a perfect positive correlation), n=69, ***p <0.001.

3.3.4 Transfection efficiency of HEK 293T cells is consistent between different human SARM1 variants

Although ZsGreen expression in transfected HEK 293T cells did not appear to differ between variants when compared under the microscope (Figure 3.4.A), flow cytometry was used as a simple, rapid and robust tool to quantify and therefore rule out variable transfection efficiency between different SARM1 variants. Indeed, transfection efficiency was equal across cells transfected with different human SARM1 variants, including E399K SARM1, and this was independent of their efficiency to deplete NAD. While WT SARM1 and other NADase-competent SARM1 variants (e.g. G456V, P549L among others) depletes NAD levels by > 90% it was surprising to see that the average transfection efficiency was only around 50-60% and thus much lower than expected. While this was not followed up further due to time constraints, a potential explanation for this observation could be the transport of NAD between adjacent cells as a form of a rescue mechanism.

ZsGreen fluorescence was barely detectable in cells overexpressing the natural GoF variant E399K SARM1. To confirm that this was a result of low ZsGreen expression and not due to increased cell death, cells were stained with propidium iodide, a cell impermeable nucleic acid intercalating dye. As expected, cell death rates were very low across all mutants (Figure 3.6), including E399K SARM1 for which there had been doubts initially. This observation is in line with previous reports, suggesting NAD levels must decline by >95% to have a compromising effect on cell viability [231]. While reduced cell viability has previously reported in transfected HEK cells expressing active SARM1 mutants in several studies [82, 111, 114, 232], our lab recently showed that the reported difference is likely a cell density-dependent effect as high rates of cell death are only observed when HEK 293T cells are transfected with the same construct at lower densities [9].

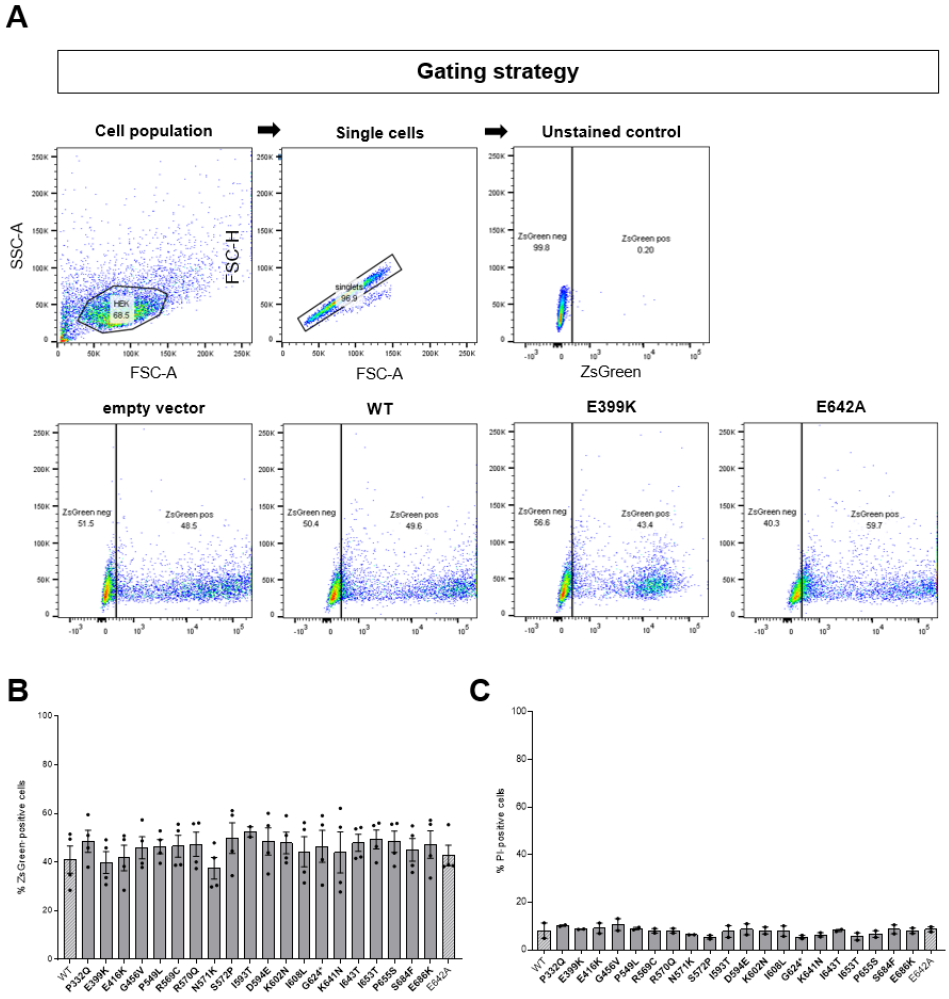


Figure 3.6: **HEK 293T transfection efficiency of different human SARM1 constructs is comparable.** **(A)** Representative flow cytometry dot plots showing the gating strategy used for assessing the percentages of ZsGreen-positive HEK 293T cells. **(B)** Transfection efficiency was quantified by flow cytometry with values given as the percentage of ZsGreen-positive cells with respect to the total number of cells in each condition. Data are presented as mean ±SEM of four independent experiments. Differences in SARM1 (and ZsGreen) expression detected in Figure 3.4.A and B are therefore not the result of substantial differences in transfection efficiency and this was true for all variants, not just those shown. **(C)** Cell death rate given as the percentage of propidium iodite (PI)-positive cells. Transfection efficiency was quantified by flow cytometry with values given as the percentage of ZsGreen-positive cells with respect to the total number of cells in each condition. Data are presented as mean ±SEM of two independent experiments. Multiple comparison using a one-way ANOVA with FDR correction comparing values in part (B) and (C) to the respective WT SARM1 revealed no significance.

3.3.5 Several natural human SARM1 TIR domain variants lack constitutive (basal) NADase activity

Measuring in-cell NAD levels in transfected HEK 293T cells (Figure 3.3A) is only an indirect way of assessing NADase activity of exogenously expressed SARM1 variants. To determine NADase activity directly, full-length Flag-tagged SARM1 constructs were transiently expressed in HEK 293T cells and purified by immunoprecipitation, as previously described [9]. Prior to transfection, cells were supplemented with nicotinamide riboside (NR) to boost NAD levels and thereby cell viability and final protein yield. This was particularly important in wells expressing NADase-competent SARM1 variants and the highly active natural GoF E399K SARM1 where NAD levels would be lower. The NADase activities were tested using the bead-bound SARM1 protein complexes, as illustrated in Figure 3.7, directly.

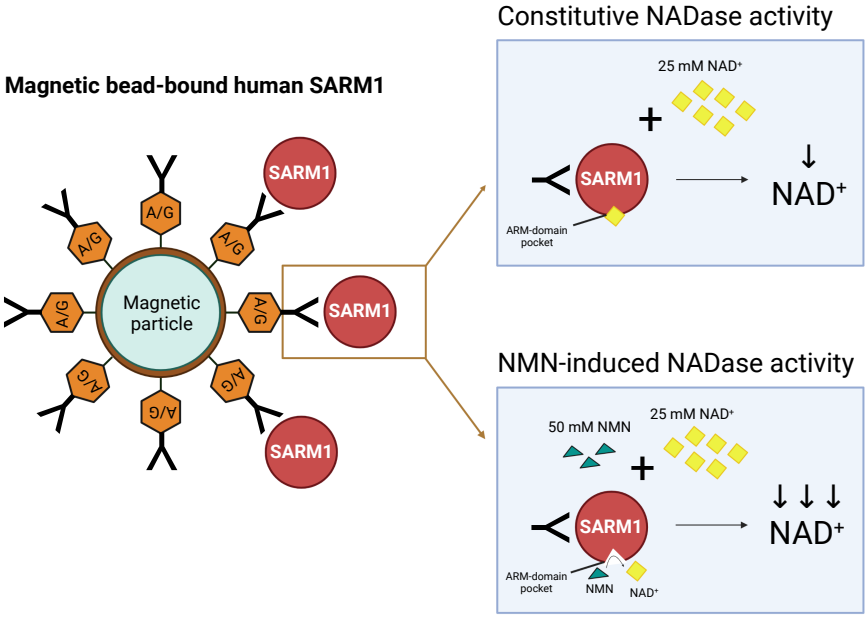


Figure 3.7: **Schematic illustration of the *in vitro* NADase assay using purified bead-bound human SARM1.** Immunoprecipitated SARM1 is bound to magnetic beads pre-coupled with protein A/G captured with an M2 Flag antibody. Protein elution was not performed as it compromises NADase activity of WT SARM1 in the assays used. Constitutive (basal) and NMN-induced NADase activities were assessed in the presence of 25µM NAD only or both 25 µM NAD and 50 µM NMN, a physiological activator of SARM1 which competitively binds to an ARM-domain pocket. The figure was created using BioRender.com.

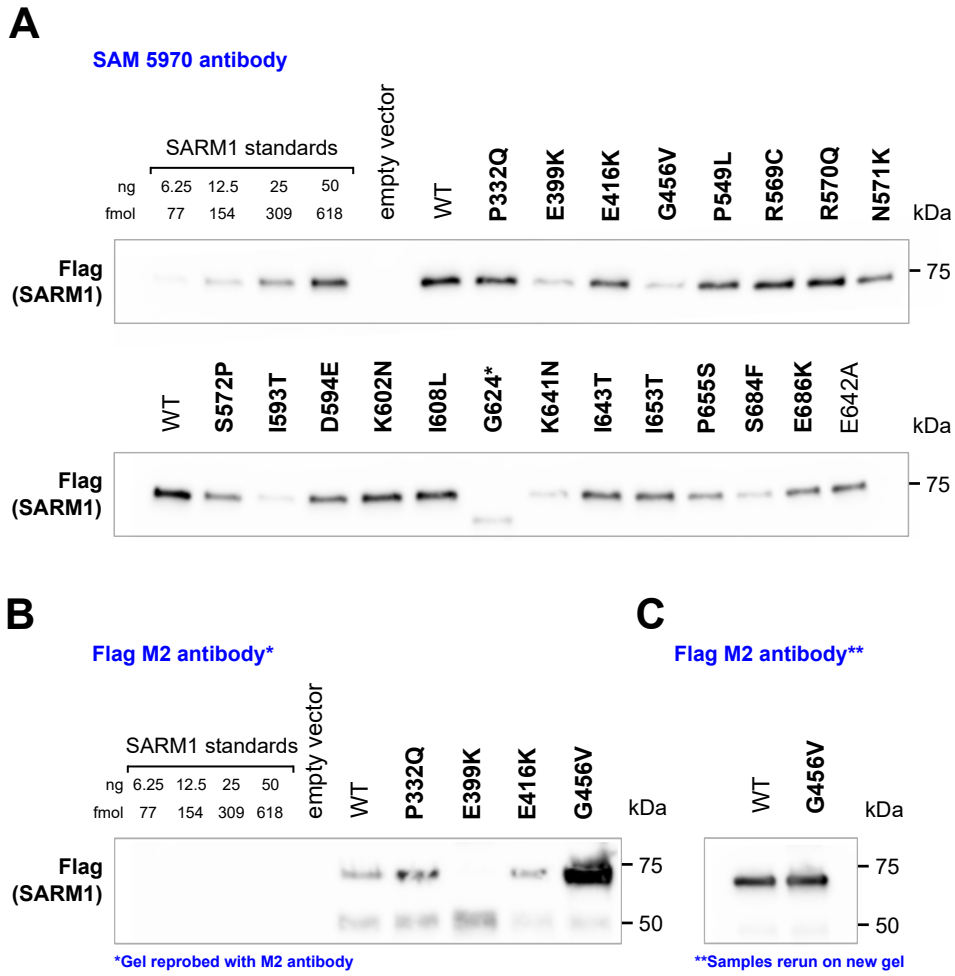


Figure 3.8: **Immunopurification of recombinant SARM1 variants used in NADase assays.** Representative western blots of immunoprecipitated WT and natural variant SARM1. A detailed description can be found in the Materials and Methods section. **(A)** SARM1 protein bound to the equivalent of 0.625 µl of magnetic bead suspension were loaded per lane next to a dilution series of purified SARM1 which served as a standard curve for quantification of the purified SARM1 variants. In contrast to the WT and natural SARM1 variants, the purified SARM1 standards (kindly provided by collaborators at AstraZeneca) were not Flag-tagged. Therefore, blots were probed with a polyclonal antibody raised against the SAM domains of human SARM1 instead. Upon initial performance of the NADase assay, G456V SARM1 appeared to have a higher basal NADase activity (data not shown). **(B)** Indeed, reprobing of the same membrane with a Flag M2 antibody showed an artificially increased G456V SARM1 signal as the protein band had previously been insufficiently recognised by the SAM 5960 antibody, likely due to a disruption of the epitope. The untagged SARM1 standards are not visible. **(C)** Thus, G456V SARM1 was quantified on a separate gel based on Flag immunoblotting relative to WT SARM1. Molecular weight markers (kDa) are shown on the right of all panels. Faint bands at ~50 kDa in (B) and (C) correspond to non-specific binding to the heavy chain of the Flag antibody used for the immunoprecipitation.

Consistent with previous reports, WT SARM1 activity was negatively affected when purified protein was eluted from beads which is why both basal and NMN-induced NADase activity (section 3.3.5 and section 3.3.6) were assessed using bead-bound SARM1 protein. In fact, SARM1 has previously been reported to lose activity during the purification process unless assayed at a high concentration (>20 μM) or on-beads [110, 233]. At first, constitutive (basal) NADase activity using equal amounts of purified WT and variant SARM1 was measured in the presence of 25μM NAD alone, a value which is close to the Michaelis constant (K_m) for the catalytic site of WT SARM1 (see Figure 3.7) [114, 117, 220]. Enzymatic rates were calculated by comparing starting NAD values with individual end points for each SARM1 variant (determined using the bioluminescent NAD/NADH-Glo^{TM} assays) and displayed as mol/min/mol SARM1 enzyme. The NADase consumption rate obtained for WT SARM1 was 1 mol/min/mol enzyme (Figure 3.9) which is within the same range as values previously reported by the Coleman group using the same assay [9].

Indeed, several SARM1 TIR domain variants – R569C, S572P, D594E, G624*, K641N, I643T, I653T, P655S, S686F and E686K SARM1 – which had previously failed to deplete NAD in transfected HEK 293T cells (and were therefore potential SARM1 LoF, see Figure 3.3), also had little to no basal NADase activity in these recombinant protein assays. This lack of activity matched that of NADase-dead E642A SARM1 suggesting a complete LoF for constitutive NADase activity for these SARM1 variants (Figure 3.9.A). Surprisingly, R570Q and I593T SARM1, which had efficiently depleted NAD in transfected HEK 293T cells in previous assays (Figure 3.3.A), appeared to be full LoF for basal NADase activity in these assays (Figure 3.9.A). In contrast, strikingly increased NAD consumption rates were found for the presumed natural GoF variant E399K (Figure 3.9.A), whose rate was approximately 10x higher than that of WT SARM1 and therefore similar to the previously identified ALS-associated GoF T385A SARM1 [9]. Interestingly, P332Q SARM1 had a slightly reduced NADase activity suggestive of a partial LoF. This observation is consistent with previous reports [9, 10]. All other variants – E416V, G456V, P549L, N571K, K602N and I608L, with the exception of N571K SARM1 – had basal NADase activity rates comparable to WT SARM1, consistent with results obtained from transfected HEK 293T cells where these SARM1 variants deplete NAD efficiently (Figure 3.3.A). N571K SARM1 showed a moderately reduced NAD consumption rate (Figure 3.9.A).

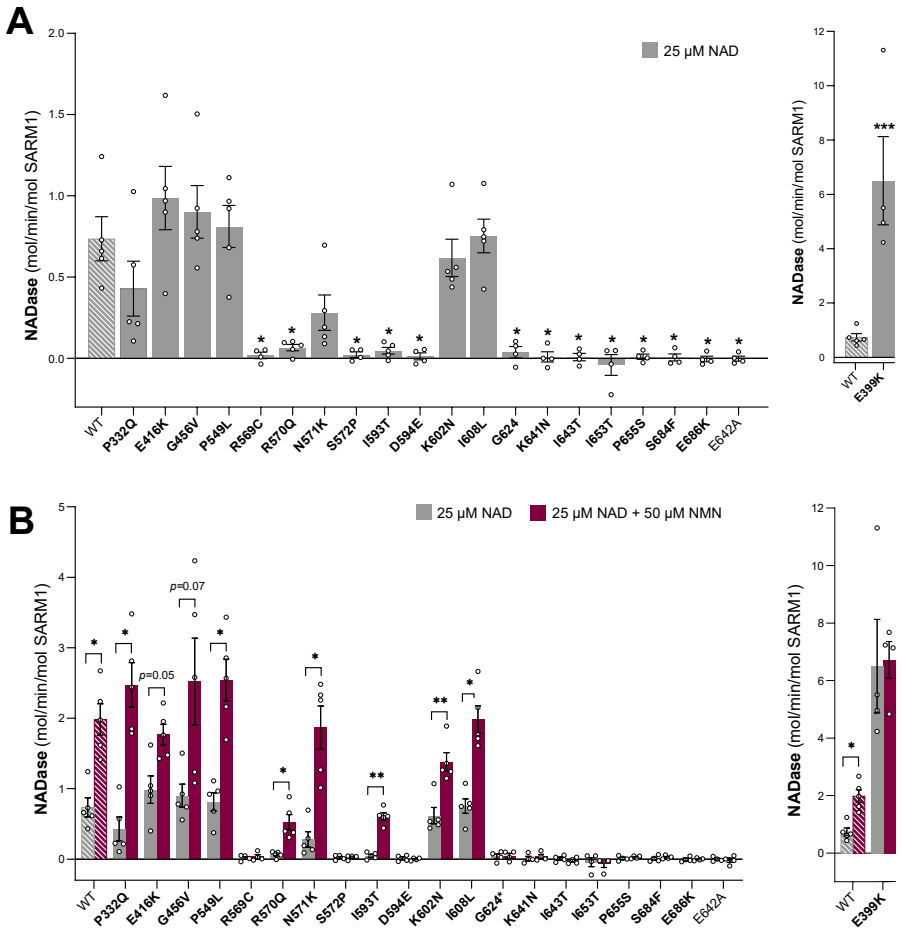


Figure 3.9: **Several SARM1 TIR domain variants are LoF for basal (constitutive) and NMN-induced NADase activity. (A)** Basal NADase activities of recombinant WT SARM1, enzyme-dead E642A (representing a full LoF control), and the selected naturally occurring SARM1 variants in the presence of 25 µm NAD alone. E399K SARM1 is plotted separately as it has a much higher basal activity than the rest of the tested SARM1 variants. All values are presented as means ±SEM with individual data points (n = 4 or 5) plotted. * p <0.05, *** p <0.001, multiple pairwise comparisons to WT SARM1 with FDR correction. **(B)** Side-by-side comparison of basal and NMN-induced NADase activities of all SARM1 variants in the presence of 25 µM NAD with or without the addition of 50 µM NMN. Constitutive activities (no NMN) are the same values as shown in (A) and NADase consumption rates (+NMN) calculated from assays where both conditions were performed in parallel. E399K SARM1 is again plotted separately next to WT SARM1. Data are shown as means ±SEM with individual data points (n = 4 or 5) plotted. * p <0.05, ** p <0.01, multiple paired t-tests with FDR correction of basal (NAD alone) versus induced activity (NAD+NMN) for each SARM1 variant. A detailed description of rate calculations can be found in the Materials and Methods section. Rate measurements were determined as the difference between NAD levels in the original reaction at t = 0h and at individual SARM1 variant's reaction endpoint (15 min, 1h, 2h or 24h). Endpoint NAD levels for LoF variants should, in theory, be identical to the starting level. However, fluctuations on either side of the starting value are unavoidable due to pipetting variation. This explains why small negative rates can be obtained using this method. As in Figure 3.3, bars for controls in parts A and B are hatched to facilitate easy differentiation from the tested variants (bold text, filled bars).

3.3.6 Human SARM1 TIR domain variants which display no basal NADase activity also lack NMN-induced NADase activity

In a next step, NADase inducibility of each SARM1 variant was tested in the presence of NMN, a physiological activator of SARM1 NADase activity [76, 102, 115, 199, 219]. NMN binds an allosteric site on the SARM1 inhibitory ARM domain, and together with NAD competes to bind the same activation site, as illustrated in Figure 3.7 [113–115]. In this set of experiments, equal amounts of WT or variant SARM1 were mixed with 25 μM NAD and 50 μM NMN. This NMN concentration is higher than expected values in neurons and/or axons (before and after injury) and thus reliably induces maximal NAD consumption of recombinant WT SARM1 achieving rates approximately 2.5-3x higher than those at basal levels [9].

In line with previous results, several SARM1 TIR domain variants which had failed to deplete NAD levels in transfected HEK 293T cells (Figure 3.3.A) and had no basal NADase activity (Figure 3.9.A) – R569C, S572P, D594E, G624*, K641N, I643T, I653T, P655S, S684F, and E686K SARM1 – also lacked inducible NADase activity in the presence of the activator NMN (Figure 3.9). This lack of inducibility was comparable to the enzyme-dead artificial E642A SARM1 mutant, suggestive of a complete loss of TIR domain catalytic activity in these mutated SARM1 residues. Surprisingly, despite having no constitutive NADase activity, R570Q and I593T SARM1 were found to have some inducible NADase activity in the presence of NMN suggesting that they were not completely enzyme-dead when NMN was present (Figure 3.9.B). As expected, the putative GoF E399K SARM1 did not show any further increase in its already high NADase activity in the presence of NMN. This NMN-insensitivity mirrors the behaviour of previously characterised GoF SARM1 variants associated to ALS and other motor nerve disorders, as well as the SAM-TIR mutant lacking the autoinhibitory ARM domain with its NAD/NMN-docking site [9]. In contrast, all other variants – E416V, G456V, P549L, N571K, K602N and I608L SARM1 – with WT-like basal NADase activity rates also showed increased levels of activity in the presence of NMN similar to those observed using WT SARM1 (Figure 3.9.B). These results were in line with previous observations made in transfected HEK 293T cells where NAD was efficiently depleted by the same SARM1 variants (Figure 3.3.A). Even N571K SARM1 which had a slightly reduced basal NADase activity in the presence of NAD alone was NMN-inducible to a level comparable to the aforementioned WT-like SARM1 variants. Both basal and NMN-induced NADase activity were displayed as a consumption rate in mol/min/mol SARM1 enzyme (Figure 3.9). While it seemed that fold induction showing NMN-induced activity relative to the basal (constitutive) activity could be informative, values for some SARM1

variants seemed deceiving. For instance, fold induction calculated for R570Q and I593T SARM1 (data not shown) resulted in very high values which could falsely be misinterpreted as higher enzymatic activity. In addition, minor pipetting errors are magnified in these circumstances and contribute to a greater variability.

The complete lack of constitutive NADase activity for R570Q and I593T SARM1, and to a lesser extent the relatively low constitutive activity of N571K SARM1, stands in conflict with the fact that all variants sufficiently deplete NAD in transfected HEK 293T cells (compare Figure 3.3.A with Figure 3.9.A). Both recombinant R570Q and I593T SARM1 show detectable NADase activity in the presence of NMN, however, there is not enough evidence supporting that NMN-induced activity significantly contributes to cellular NAD consumption in transfected HEK 293T cells. HEK 293T cells, though, have some NMN while the basal NADase assay discussed in section 3.3.5 and Figure 3.9.A does not. Therefore, it seems plausible that NMN explains at least some of the apparently differing properties of these variants in the different assays. Furthermore, NMN-induced NADase activities of recombinant R570Q and I593T SARM1 are 3-4x lower than that of WT SARM1 (Figure 3.9.B). A possible explanation instead could be that the developed NADase assay using recombinant SARM1 protein may not reflect the true NADase activities for these variants in the context of a living cell. While the same could be argued for other identified LoF variants within that domain region – namely, R569C, S572P, and D594E SARM1 – all of these SARM1 variants lack both constitutive and NMN-inducible NADase activity (Figure 3.9) and fail to deplete NAD in transfected HEK 293T cells (Figure 3.3.A), all of which is consistent with a LoF SARM1 phenotype.

3.3.7 Most SARM1 TIR domain variants that lack NADase activity also fail to trigger neurite degeneration

In order to assess how the observed lack of NADase activity relates to the pro-degenerative function of the natural SARM1 variants under investigation, a well-established rescue strategy in microinjected primary neuronal cultures was employed: Axons of neuronal cultures lacking SARM1 are strongly resistant to degeneration induced by injury or other types of insult. However, this protective phenotype is overcome when full-length WT SARM1 is exogenously reintroduced via microinjection into Sarm1-deficient mouse cultures and, in consequence, the degenerative phenotype is restored (concept and technique as shown in Figure 2.2) [82, 83]. Thus, the extent to which exogenous expression of WT SARM1 or the selected ARM, SAM and TIR domain SARM1 variants could restore normal injury-induced neurite degeneration in primary neuronal cultures of *Sarm1*$^{-/-}$ neurons was

tested. Microinjection was used to introduce controlled amounts of WT or mutant SARM1, accompanied by fluorescent DsRed protein for the visualization of the microinjected somata of *Sarm1*$^{-/-}$ neuronal cultures and their neurites (Figure 3.10.A). While microinjection is a low-throughput technique it is particularly useful in these types of assays where a small number of neurons within a specific area of the dish are targeted. The binding of NMN is required to trigger injury-induced SARM1 activation and axon destruction [76, 115, 219]. In line with this, most of the natural SARM1 variants that behaved like the WT protein when induced with NMN in the recombinant protein assays (Figure 3.9.B) – P332Q, E416K, G456V, P549L, N571K, K602N and I608L SARM1 – also successfully restored degeneration of transected *Sarm1*$^{-/-}$ SCG neurites (Figure 3.10.B and C). As expected, the putatitve GoF E399K SARM1 variant also efficiently restored degeneration (Figure 3.10.B). Conversely, several of the variants that were LoF for SARM1 NADase activity in previous assays – R569C, S572P, D594E, G624*, I653T, P655S, S684F and E686K SARM1 – also failed to restore degeneration resulting in approximately 90% intact neurites 24 h post axotomy. This was in line with observations made for the enzyme-dead control E642A SARM1 (Figure 3.10.B and C). Intriguingly, some natural SARM1 variants were an exception to this rule. Indeed, the variants I643T and K641N SARM1, both of which had failed to demonstrate NADase function in the recombinant protein assays (Figure 3.9), displayed an intermediate phenotype only resulting in a partial LoF in the neurite degeneration assay (Figure 3.10). This, however, is compatible with the fact that K641N SARM1 also resulted in a partial consumption of NAD and NADP in transfected HEK 293T cells (Figure 3.3). In contrast, K602N and even more so E416K SARM1 were partial LoF in the neurite degeneration assay, while they previously appeared to have a WT-like NADase function (compare Figure 3.9 and Figure 3.10.B). Of the variants that robustly depleted NAD in transfected HEK 293T cells, but only had small inducible NADase activity, R570Q SARM1 fully restored neurite degeneration which is suggestive of a functional SARM1 protein, whereas I593T SARM1 did not restore degeneration and therefore had a LoF phenotype in the degeneration assay. The obtained data for variant R570Q SARM1 fit the idea that it is only active in the presence of NMN (in-cell NAD consumption in HEK 293T cells where NMN is present as shown in Figure 3.3; no basal NADase activity but inducibility in the presence of NMN as shown in Figure 3.9) , however, this explanation does not fit variant I593T SARM1 which appears LoF in the degeneration assay (Figure 3.10.B).

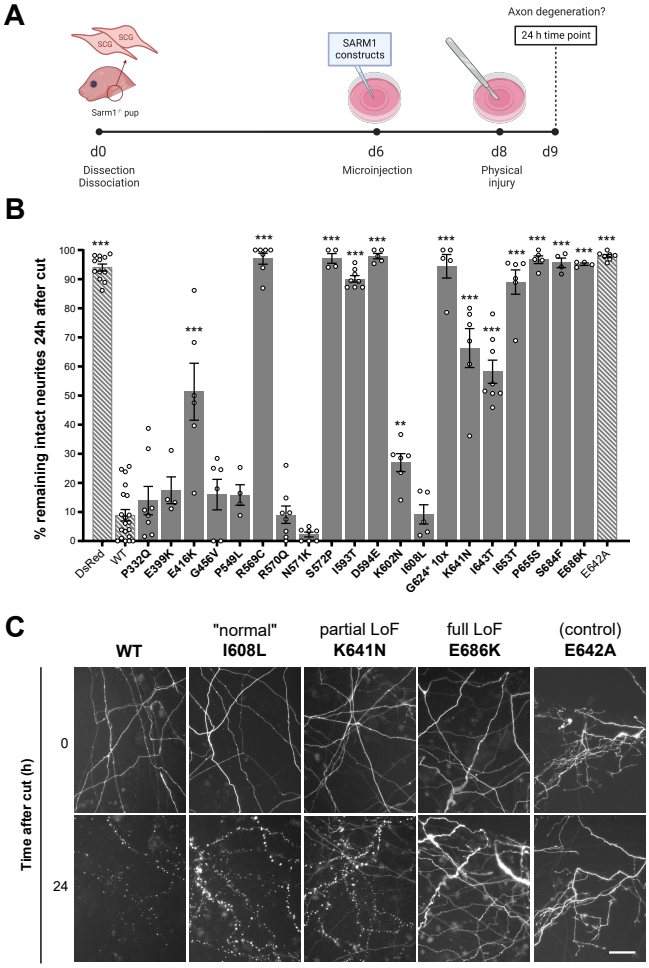


Figure 3.10: **NADase LoF SARM1 TIR domain variants fail to induce degeneration in response to physical injury. (A)** Schematic representation of the experimental design. **(B)** *Sarm1*$^{-/-}$ SCG neurons were microinjected with 2.5-5 ng/µl of selected SARM1 expression constructs (pCMV-Tag4 vector backbone) together with 40 ng/µl pDsRed2 encoding DsRed for the visualisation of injected neurites. Manual transection of DsRed-labelled neurites was performed with a razor blade 48 h after microinjection. Axon degeneration was quantified by determining the percentage of intact DsRed-labelled neurites 24 h after transection relative to those present at the the time of the cut (0 h). Data shown as means ±SEM with individual data points plotted (n = 4-20). Each represents the average neurite survival from independent assays of multiple injected neurons per assay. *** $p < 0.001$, multiple comparisons using a one-way ANOVA with false discovery rate (FDR) correction showing significance as compared to WT. Of note, cut neurites in pDsRed2 only control injections did not undergo degeneration (94.0 ±1.2% neurite survival at 24h) similar to neurites microinjected with the enzyme-dead E642A SARM1. **(C)** Representative fluorescence images, as those used for the quantification in (B), of cut DsRed-labelled neurites of Sarm1-deficient primary neuronal cultures injected with the generated SARM1 constructs expressing either variant or WT protein at 0 and 24 h post transfection. Controls (wild-type and enzyme-dead E642A SARM1) and three exemplary phenotypes are shown: I608L SARM1 resembling wild-type SARM1 ("normal"), K641N SARM1 displaying a partial LoF phenotype, and E686K SARM1 displaying full LoF. Scale bar, 50 µm.

3.3.8 SARM1 LoF variants used for microinjection into SCG neurons are sufficiently expressed

While unrepresentative NADase activities obtained in the recombinant protein assays for a few of these variants (see discussion in section 3.3.5) could explain some of the observed discrepancies, another plausible explanation could be differences in expression levels. For example, low expression of a functional (NADase competent) SARM1 variant may limit its ability to restore degeneration in microinjected *Sarm1*$^{-/-}$ SCG cultures, whereas high expression of variants with a partial LoF may be sufficient to induce degeneration masking the partial phenotype. As previously mentioned, microinjection is a low throughput technique with which only a handful of neuronal cell bodies can be injected. Therefore, expression level analysis based on western blotting is not feasible. Instead immunostaining was used to test for differences in expression levels of human SARM1 variants in microinjected *Sarm1*$^{-/-}$ SCG cultures. Staining revealed that levels of SARM1 variants were broadly similar to WT SARM1 in the cell bodies of the injected neurons. However, this is not a sensitive enough method to rule out a functionally relevant deficiency or excess specifically within the neurites themselves.

Complementary to the staining, western blotting using extracts of transfected HEK 293T cells was performed to prove that the expression constructs used in the axotomy assay result in the expression of SARM1 proteins of the expected size. In anticipation of poor expression of the truncated construct (see Figure 3.4B), G624* SARM1 was injected at a concentration 10x times higher than that of WT and other natural SARM1. However, the expression levels of G624* SARM1 still appeared substantially lower than that of WT and other SARM1 variants in the injected neurons. While this complicates the interpretation of its effects in the degeneration assay (Figure 3.10A), it is expected that - even if expressed at WT levels - G624* SARM1 would be incapable of restoring degeneration in cut *Sarm1*$^{-/-}$ SCG neurites because it lacks NADase activity in the NADase assays using recombinant protein.

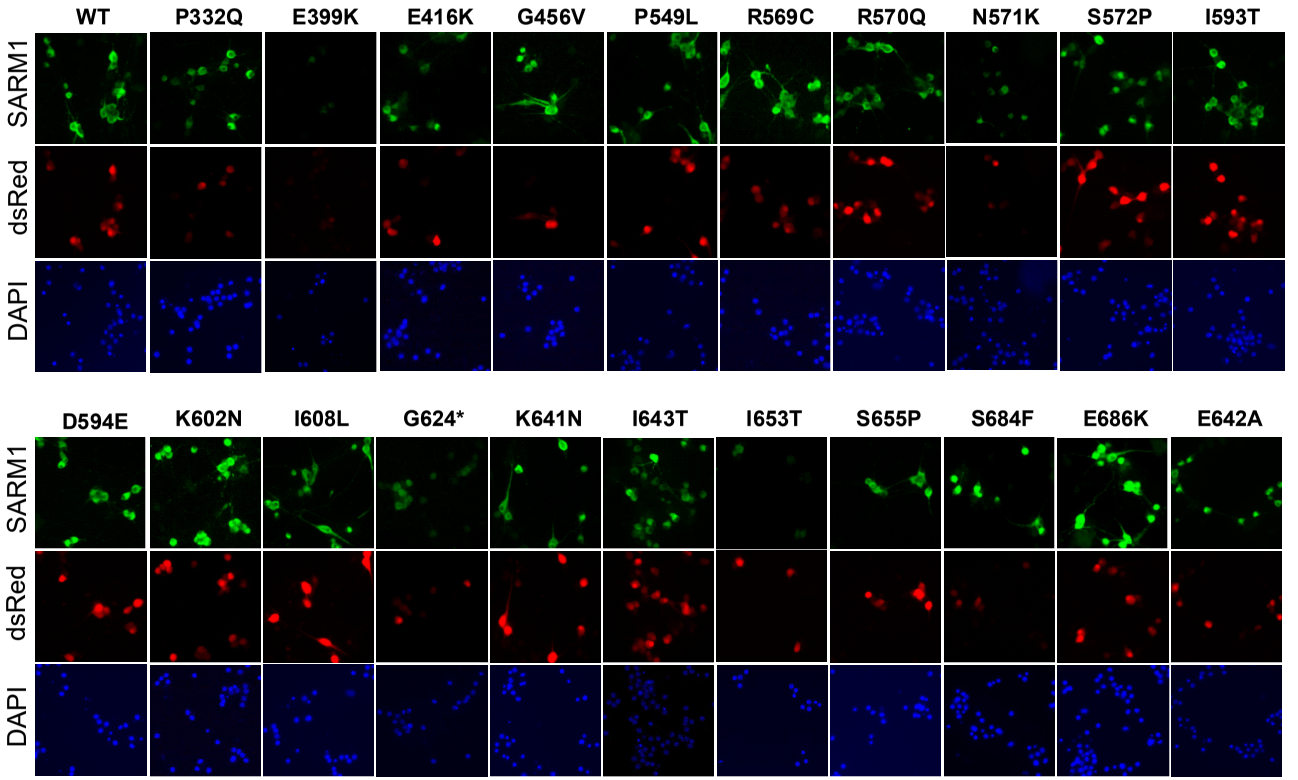


Figure 3.11: **Expression levels of natural SARM1 variants expressed from pCMV-Tag4A backbones in microinjected *Sarm1*$^{-/-}$ SCG neurons. (A)** *Sarm1*$^{-/-}$ SCG neurons were co-injected with 25 ng/µl pCMV-Tag4A expression constructs for untagged WT or variant SARM1 and 25 ng/µl pDsRed2. Neurons were immunostained with a SARM1 antibody 24 h after injection, followed by nuclear counterstaining with DAPI. Representative images of SARM1 immunostaining, DsRed fluorescence (as a marker of microinjected cells), and DAPI staining are shown for each SARM1 variant, as indicated. Scale bar, 50 µm.

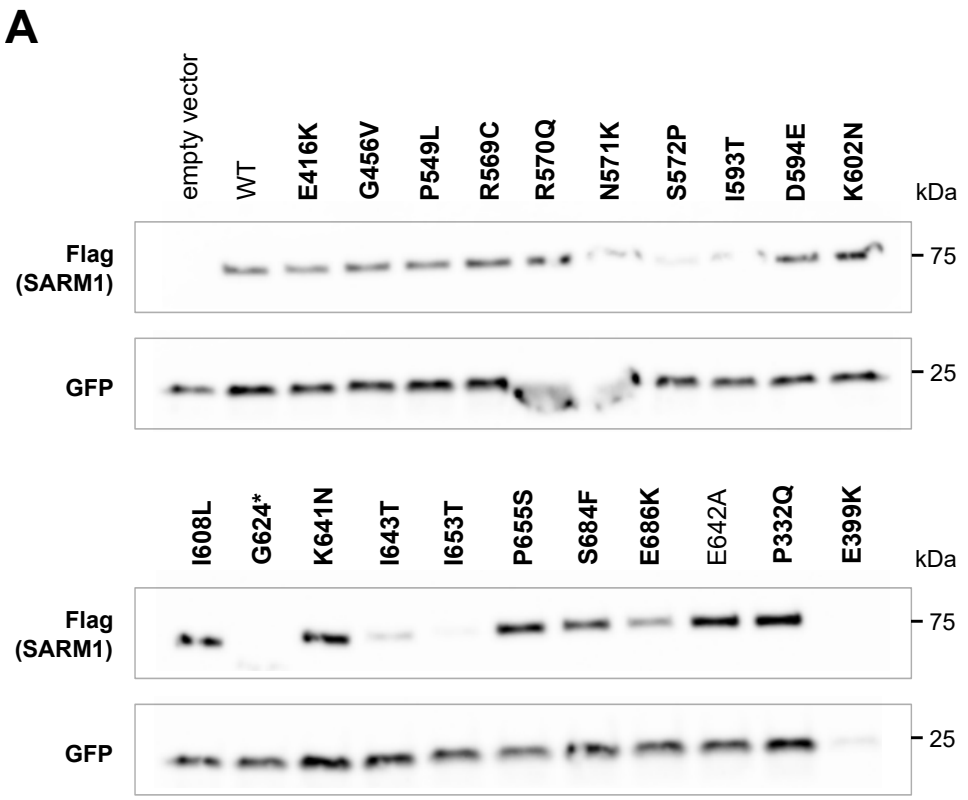


Figure 3.12: **SARM1 variant expression levels from pCMV-Tag4A backbones in transfected HEK 293T cells. (A)** Representative immunoblots (of n=4) showing SARM1 level expression from untagged pCMV-Tag4A constructs in HEK 293T cell lysates 24 h after co-transfection with 0.75 µg WT or mutant SARM1 and 0.25 µg pEGFP-C1 encoding eGFP protein (total of 1 µg DNA transfected). Blots were probed with antibodies for SARM1 (~70kDa) and eGFP (~26 kDa, used as a control for transfection efficiency for the untagged constructs). All SARM1 variants are expressed and of the expected size. As previously observed, E399K and G624* SARM1 are very faintly expressed. transfection.

3.3.9 SARM1 LoF variants do not have cytotoxic effects on neuronal cell bodies

Interestingly, exogenously-expressed SARM1 was observed to have moderately cytotoxic effects on microinjected neuronal cell bodies in the degeneration assays. This largely correlated with NADase-competence of the respective SARM1 mutants. While WT SARM1 and other NADase-competent variants caused some cell death between 24h and 48 h after microinjection (and prior to performing axotomy with a scalpel), no such effect was observed for SARM1 variants with a LoF for NADase activity. Indeed, cytotoxicity largely mirrored variant functionality in the axotomy assays, albeit the effect was weaker and more variable. Notably, microinjection provides a greater degree of control over the concentrations of construct introduced than e.g. viral transduction. Small amounts of SARM1 expression constructs were purposefully injected in these assays to avoid excessive overexpression. The observations may reflect a potential synergistic toxic effect of an acute increase in NADase activity in neurons lacking Sarm1 in the first place together with the stresses associated with an invasive method, such as microinjection.

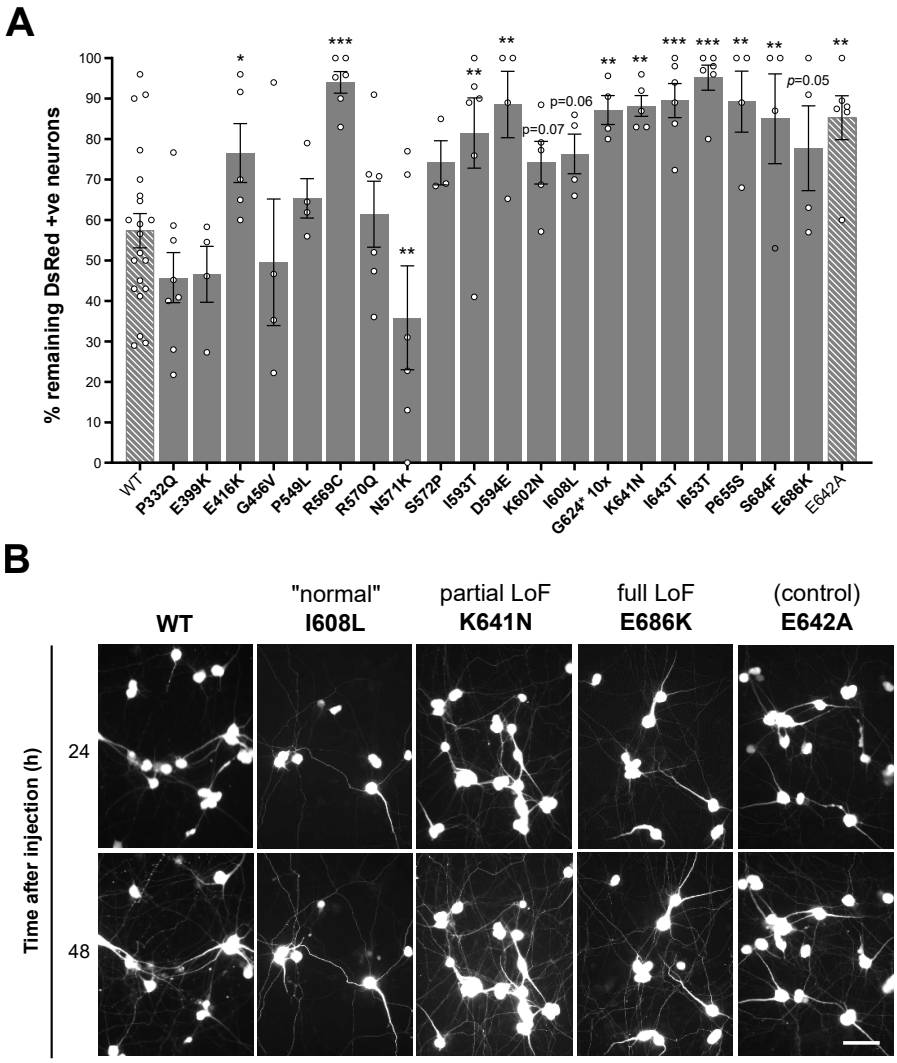


Figure 3.13: **Natural human SARM1 variants with a LoF phenotype do not have cytotoxic effects. (A)** Survival of microinjected *Sarm1*$^{-/-}$ SCG neurons prior to transection for the degeneration assay quantified in Figure 3.10. Death or loss of microinjected neurons was determined by comparing cell body size and shape of DsRed-labelled somata, at 24 h and 48 h after injection. Cell death was quantified as the percentage of the number of morphologically normal cell bodies at 48 h post microinjection compared to the total number of those present at 24 h. Data shown as means ±SEM with individual data points plotted (n = 3-20). * p <0.05, ** p <0.01, *** p <0.001, multiple pairwise comparisons to WT SARM1 with a FDR correction. **(B)** Representative fluorescence images, as those used for the quantification presented in (A) of microinjected *Sarm1*$^{-/-}$ neuronal cell bodies injected with constructs expressing WT or variant SARM1 at 24 and 48 h after microinjection. As in Figure 3.10.C, controls (wild-type and enzyme-dead E642A SARM1) alongside three exemplary phenotypes are shown: I608L SARM1 resembling wild-type SARM1 ("normal"), K641N SARM1 displaying a partial LoF phenotype, and E686K SARM1 displaying full LoF. Scale bar, 50 μm.

3.3.10 GoF E399K SARM1 does not accelerate injury-induced neurite degeneration relative to WT SARM1

Next, the question occurred whether the greatly enhanced constitutive SARM1 activity of the natural GoF E399K SARM1 accelerates axon degeneration post axotomy relative to WT SARM1. Upon injury, cellular NAD levels begin to drop - as a consequence of NMNAT2 depletion and NMN-induced activation of SARM1. While WT SARM1 responds with an NMN-induced increased NAD consumption rate, E399K SARM1 is in a hyperactivated state which cannot be further induced by endogenous cellular NMN (based on results obtained in Figure 3.9B). As illustrated in Figure 3.14, it was, therefore, hypothesised that E399K SARM1 reaches a critical threshold of cellular NAD levels sooner than the WT protein and therefore axons expressing E399K SARM1 degenerate faster.

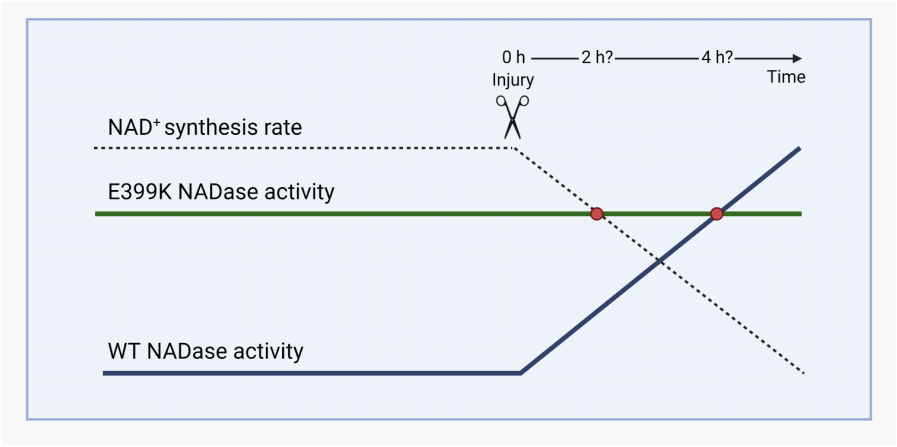


Figure 3.14: **A simplified model based on which it was hypothesised that NADase GoF E399K SARM1 variant would lead to accelerated degeneration relative to the WT protein.** During a homeostatic state the NAD synthesis rate stays stable and SARM1 remains in an autoinhibited state. It is interesting that E399K is tolerated in individuals of an older age, when its activity is more potent than the ARM deleted version of SARM1. This is further addressed in the discussion.

To address this question, a time-course analysis was performed comparing the degenerative capacity of E399K SARM1 alongside the WT protein and appropriate controls in injected *Sarm1*$^{-/-}$ SCG neuronal cultures (Figure 3.15). A DsRed expression construct was again co-injected to facilitate the visualization of the microinjected somata and their neurites. Contrary to what was expected, E399K SARM1 did not lead to an accelerated degeneration when compared to the WT protein. In fact, degeneration in *Sarm1*$^{-/-}$ cultures expressing the NADase natural GoF SARM1 variant appeared to degenerate more slowly than cultures expressing WT SARM1 (Figure 3.15). While this observation is quite puzzling it may suggest

that acute expression of a constitutively hyperactivated SARM1 initiates compensatory responses within the injected cell limiting the degenerative effect of the protein. Since no differences were observed, another possibility could be that expression of E399K SARM1 makes injected neurites more sensitive to otherwise sub-threshold insults (e.g. low dose of Vincristine or change of medium). However, this was not further analysed, due to time constraints and focus on other projects. Interestingly, the intensity of DsRed in E399K SARM1 expressing neurites was greatly reduced compared to other expression constructs used in the experiment (Figure 3.15B). It is likely that strong NADase GoF suppresses DsRed expression through the suppression of de novo protein synthesis - as it does with ZsGreen (see Figure 3.4) – and similar observations have been made with other published disease-associated GoF SARM1 variants [9].

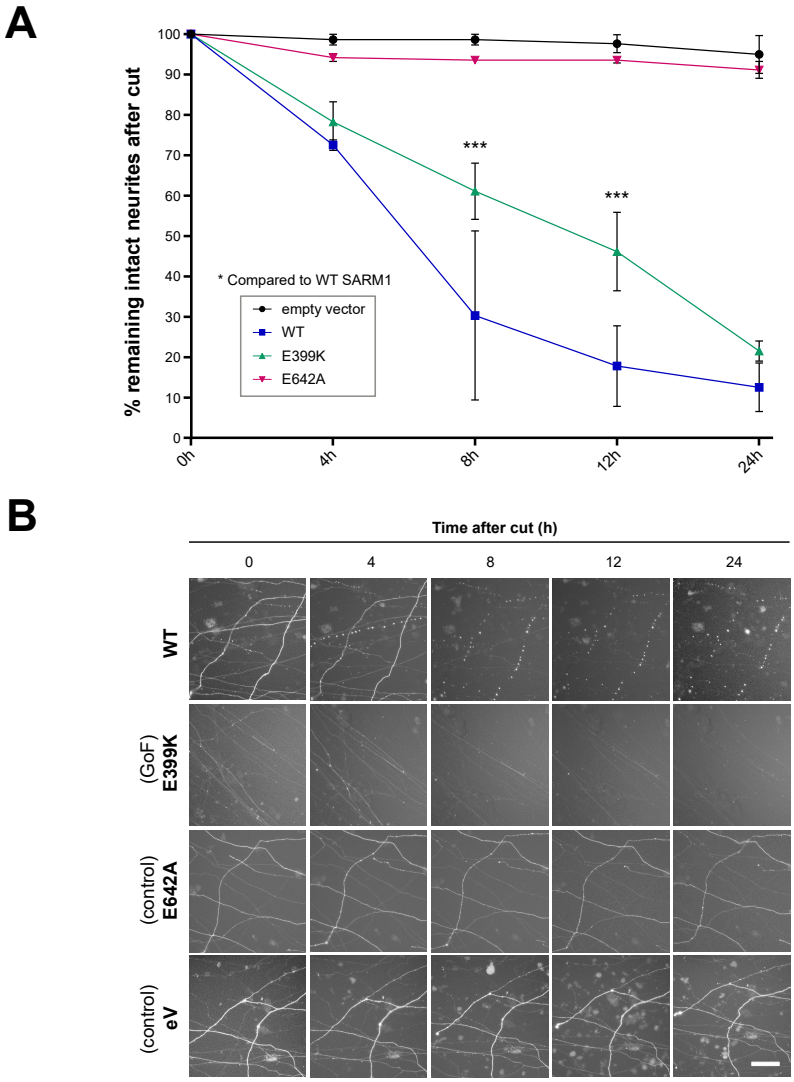


Figure 3.15: **NADase GoF E399K SARM1 variant does not accelerate degeneration in response to physical axotomy. (A)** As in Figure 3.10, *Sarm1*$^{-/-}$ SCG neurons were microinjected with 5 ng/µl of selected SARM1 expression constructs (pCMV-Tag4 vector backbone) together with 40 ng/µl pDsRed2 encoding DsRed for the visualisation of injected neurites. Manual transection of DsRed-labelled neurites was performed with a razor blade 48 h after microinjection. Axon degeneration was quantified by determinin the percentage of intact DsRed-labelled neurites 4 h, 8 h, 12 h and 24 h after transection relative to those present at the the time of the cut (0 h). Data shown as means ±SEM with individual data points plotted (n = 3), ***p < 0.001, repeated measures two-way ANOVA followed by Tukey's multiple comparison test to determine whether E399K SARM1 was degenerating at a significantly different rate compared to WT SARM1 at any of the given time points. **(B)** Representative fluorescence images, as those used for the quantification in (A), of cut DsRed-labelled neurites of Sarm1-deficient primary neuronal cultures injected with SARM1 constructs expressing either E399K, the enzyme-dead E642A or WT SARM1 at the indicated time points. Scale bar, 50 µm.

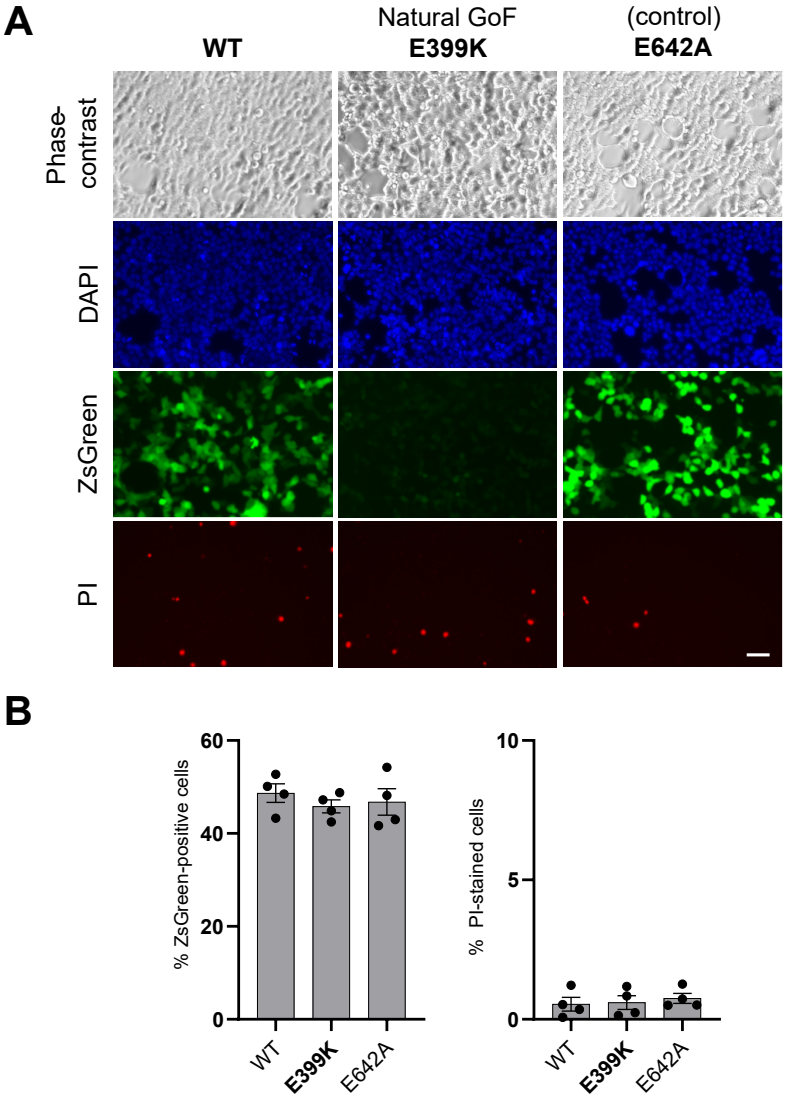


Figure 3.16: **Transfection efficiency and cell death rates of cells transfected with E399K SARM1 GoF variant are similar to WT SARM1.** Transfection efficiency and cell death rates for E399K SARM1 were assessed manually before and independently from the flow cytometry data shown in Figure 3.6. **(A)** Representative micrographs of HEK 293T cells transfected with bicistronic constructs stably expressing E399K, WT or the enzyme-dead control E642A SARM1. Scale bar, 50 µm. **(B)** Similar amounts of cells were transfected (total ZsGreen positivity) in each case. **(C)** The lower ZsGreen signal, as shown in (A), was not due to higher cell death rates, confirming data in Figure 3.6. Multiple comparison using a one-way ANOVA with FDR correction revealed no statistical significance when comparing values of E399K SARM1 to that of the WT protein.

3.3.11 D594E and E686K SARM1 act as dominant negatives on axon degeneration

In solution, SARM1 molecules form an octameric ring [110–113] and this multimerisation is necessary for the pro-degenerative function of the protein [82, 110]. A small number of artificial SARM1 mutants have previously been shown to have a dominant-negative effect when expressed in wild-type cultures. This likely results from co-expression of mutated and endogenous WT SARM1 which presumably form octamers where the dominant negative SARM1 mutants disrupt TIR domain interactions and NADase activity of endogenous (WT) SARM1 monomers within the hetero-oligomers. This block SARM1' pro-degenerative activity and prevents axon degeneration [82, 120, 197]. It, therefore, appeared reasonable to investigate whether any of the naturally-occurring SARM1 TIR domain variants with a confirmed LoF for NADase activity and pro-degenerative capacity also have dominant negative properties. This was of particular interest, as all identified LoF SARM1 TIR domain variant carriers listed in gnomAD are heterozygous. However, compound heterozygosity for these variants cannot be excluded, as gnomAD does not list any information on which variants within it occurred together in the same individual [226].

To address this question, the previously identified SARM1 LoF variants (see Figure 3.9 and Figure 3.10) were microinjected into wild-type SCG primary culture neurons and their effect on degeneration secondary to a cut assessed. Unlike previous axotomy experiments, transection of neurites occurred seven instead of two days after injection to allow sufficient time for the formation of the putative hetero-oligomers between the endogenous WT mouse SARM1 and the exogenously expressed human SARM1 mutant (Figure 3.17A). Given that prolonged and robust expression of DsRed and other fluorescent dyes can be toxic to cells [30], a low concentration of a single bicistronic expression construct encoding SARM1 and ZsGreen (as used for experiments in e.g. Figure 3.3 and Figure 3.9) was injected in these experiments, rather than separate constructs encoding SARM1 and DsRed. This relatively low expression of ZsGreen was sufficient to visualise microinjected neurites for quantification purposes, at the same time avoiding significant cytotoxicity (observed by eye, not quantified).

K193R SARM1 is a confirmed strong dominant negative artificial mutant [197] and it was thus used as a positive control in this set of experiments. It showed a strong protective phenotype against degeneration under these conditions, protecting over 95% of neurites for up to 24 h after axotomy (Figure 3.17B and C), thereby establishing this experimental setup as a valid screening method for dominant negative SARM1 mutants (Figure 3.17). Most of the identified natural LoF SARM1 variants failed to block the normal, rapid de-

generation of injured wildtype neurites. Two variants, however, were an exception to this observation: D594E and E686K SARM1 showed clear dominant LoF properties, with E686K protecting injured neurites as robustly as K193R SARM1, and D594E having only a slightly weaker effect (Figure 3.17B and C). This suggests that individuals heterozygous for the alleles encoding D594E or E686K SARM1 may have a stronger protection against axonal degeneration disorders involving PAD compared to other SARM1 LoF allele carriers. Phenotypically this may even resemble a SARM1 LoF homozygous phenotype, although previous *in vivo* data using dominant-negative SARM1 mutants in mice suggest a slightly weaker effect than in the case of a genetic ablation of Sarm1 [197].

The above result does not exclude the possibility that the observed dominant negative LoF phenotype for D594E or E686K is due to a compensatory mechanism activated in wild-type SCG primary culture neurons. So, to confirm that these two variants had indeed dominant negative LoF properties, it was reasoned that exogenous co-expression of WT SARM1 alongside D594E or E686K SARM1 co-injected into *Sarm1*$^{-/-}$ SCG primary neuronal cultures in a 1:1 ratio would lead to similar protection post axotomy, as observed in Figure 3.17. While Δ TIR had initially been described as a strong dominant negative completely blocking axon degeneration [82], this strong effect was not reproduced in later studies [197], neither was it in this experiment. In fact, on average < 20% of neurites were intact 24 h after transection (Figure 3.18B and C).

Whether expression of SARM1 dominant negative mutants also delays axonal loss of NAD(P) or ATP was not tested using microinjection as this technique does not provide sufficient material for metabolite assays to be carried out. Alternatively, WT and the putative dominant LoF SARM1 variants could have been co-expressed in a 1:1 ratio in HEK 293T cells (which have very low levels of endogenous SARM1) to test for NAD depletion. In addition, WT SARM1 and a dominant LoF SARM1 variant could have been co-immunoprecipitated from co-expressing HEK 293T cells to directly measure NADase activity of the hetero-oligomers, similarly to what has been done with SARM1 GoF variants [9]. While all of this would have been reasonable, other experiments were prioritised at this point.

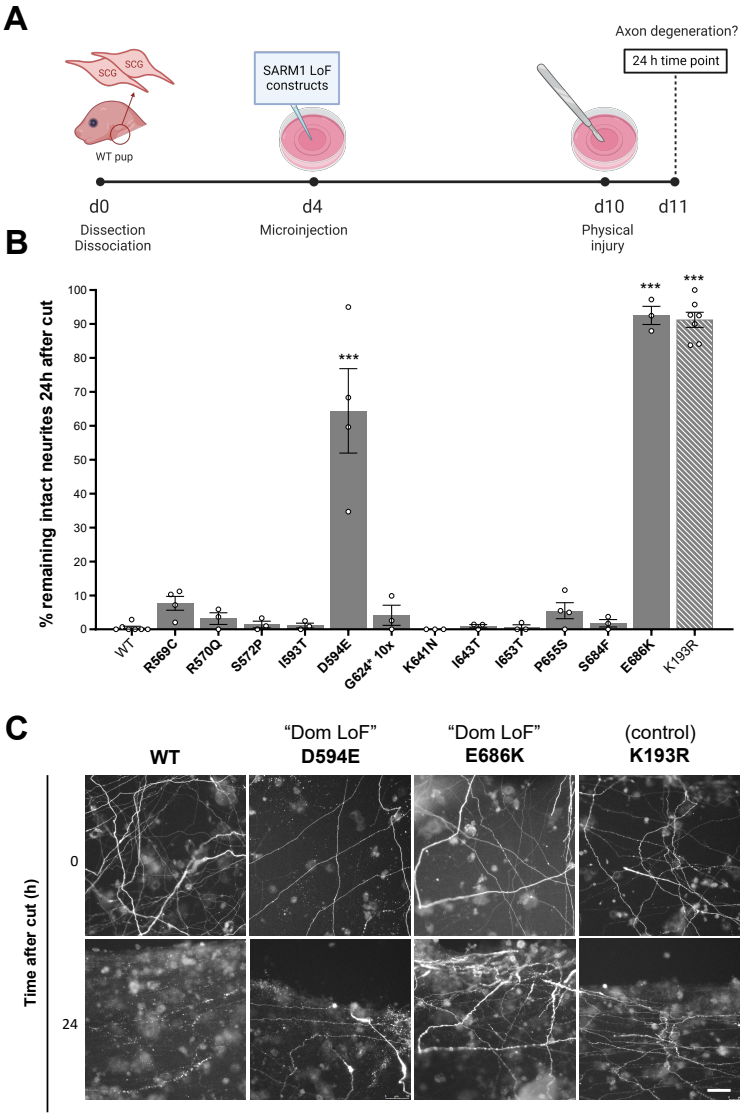


Figure 3.17: **D594E and E686K SARM1 have dominant LoF properties in axotomised wild-type SCG cultures. (A)** Schematic representation of the experimental design. **(B)** Wild-type SCG neurons were injected with 5 ng/µl bicistronic expression constructs (pLVX-IRES-ZsGreen1 vector backbone) encoding WT or variant/mutant human SARM1 with a C-terminal Flag tag and ZsGreen. Co-expressed ZsGreen allowed visualisation of the neurites of the injected neurons, and these were transected 7 days after injection. Degeneration was quantified by determining the percentage of intact ZsGreen-labelled neurites remaining 24 h after transection compared to at the time of cut (0 h). Data are presented as means ±SEM with individual data points (n = 3-6). *** $p < 0.001$, multiple pairwise comparisons to WT SARM1 with FDR correction. **(C)** Representative fluorescence images, as used for the quantification shown in part a, of transected ZsGreen-labelled neurites of neurons injected with constructs expressing the indicated SARM1 variants at 0 and 24 h after the cut. Scale bar, 50 µm.

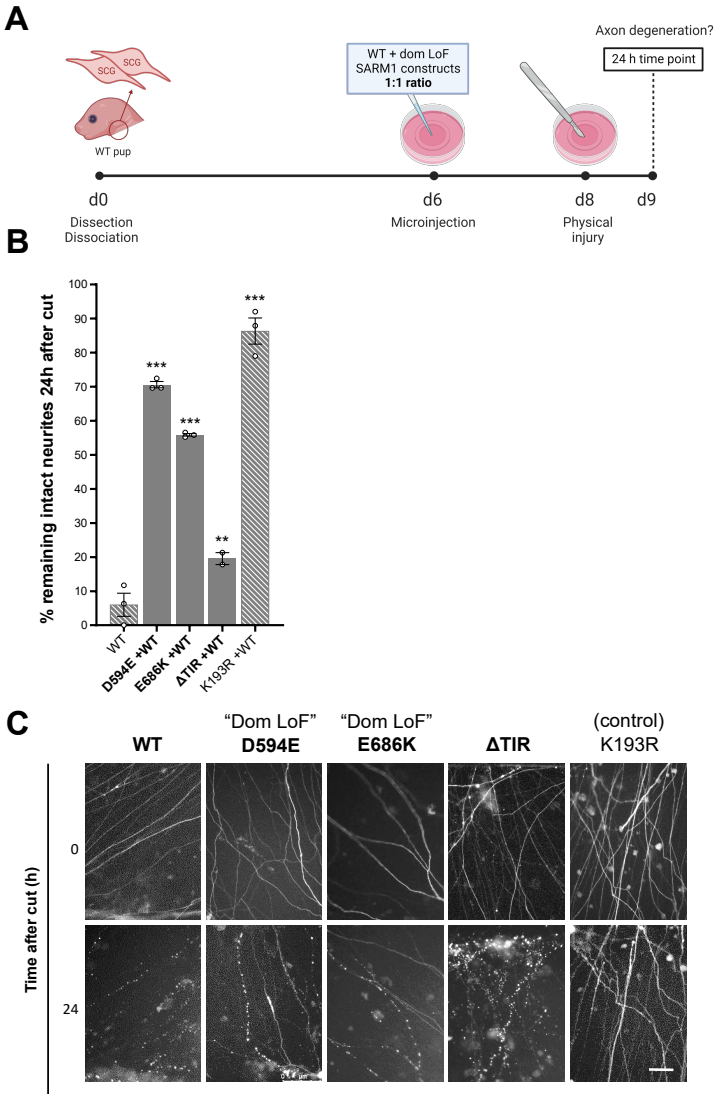


Figure 3.18: **Co-expression of WT SARM1 together with D594E or E686K SARM1 results in a dominant SARM1 LoF. (A)** Schematic representation of the experimental design. **(B)** *Sarm1*$^{-/-}$ SCG neurons were co-injected with 2.5 ng/µl bicistronic expression constructs (pLVX-IRES-ZsGreen1 vector backbone) encoding WT and 2.5 ng/µl variant/mutant human SARM1 with a C-terminal Flag tag and ZsGreen. Co-expressed ZsGreen allowed visualisation of the neurites of the injected neurons, and these were transected 2 days after injection. Degeneration was quantified by determining the percentage of intact ZsGreen-labelled neurites remaining 24 h after transection compared to at the time of cut (0 h). Data are presented as means ±SEM with individual data points (n = 3 except for Δ TIR with n = 2). ** $p < 0.01$, *** $p < 0.001$, multiple pairwise comparisons to WT SARM1 with FDR correction. **(C)** Representative fluorescence images, as used for the quantification shown in part a, of transected ZsGreen-labelled neurites of neurons injected with constructs expressing the indicated combinations of SARM1 variants at 0 and 24 h after the cut. Scale bar, 50 µm.

3.4 Discussion

3.4.1 Summary of findings

Of >100 natural SARM1 variants listed in the dbSNP and gnomAD databases, 20 SARM1 missense and nonsense variants with a high potential to result in LoF mutants were tested for I) their ability to deplete NAD in transfected HEK 293T cells, II) their constitutive (basal) and NMN-induced NADase activity using purified SARM1 protein and III) their ability to promote injury-induced axon degeneration in an *in vitro* assay of transected SCG neuronal cultures by comparing them to WT and the enzyme-dead E642A SARM1. These findings are summarised as variant categories in Table 3.2 and include:

1. **Dominant negative LoF variants D594E and E686K SARM1** which block neurite degeneration even in the presence of endogenous (WT) mouse Sarm1 in SCG neuronal cultures (Figure 3.17 and Figure 3.18).

2. **Variants that result in clear LoF in all performed assays but are not dominant negative** - R569C, S572P, G624*, K641N, I643T, I653T, P655S, and S684F SARM1 all of which reside within the catalytic TIR domain. They fail to deplete NAD in transfected HEK 293T cells (Figure 3.3), they lack NADase activity even in the presence of the physiological SARM1 activator NMN (Section 3.3.5), and they fail to restore degeneration of neurites in *Sarm1*$^{-/-}$ primary neuronal cultures (Figure 3.10). Their locations within the SARM1 TIR domain crystal structure are shown in Figure 3.19.

3. **One variant which results in clear GoF in all performed assays** – E399K SARM1.

4. **Variants that are LoF in some assays but display an NADase activity which is NMN-inducible** – R570Q and I593T SARM1.

5. **Variants that result in modest or weak LoF.** P332Q SARM1 has a consistently lower basal NADase activity than the WT protein. This is also reported elsewhere [9]. E416K and K602N SARM1, both of which only partially restore degeneration in *Sarm1*$^{-/-}$ primary neuronal cultures, behave like WT SARM1 in other assays.

6. **Variants that are WT-like in all performed assays** - G456V, P549L, N571K and I608L SARM1.

SARM1 domain	Coding variant[a]	In-cell NAD consumption[b]	NADase activity[c]		*Sarm1*$^{-/-}$ rescue[d]	Dominant negative[e]	Cytotoxicity[f]	Consequence/ Phenotype
			Basal	inducible				
-	WT	+	+	+	+	-	+	WT protein
ARM	P332Q	+	+/-	+	+	NA	+	Weak LoF
ARM	E399K	+	++++	-	+	NA	+	GoF
SAM	E416K	+	+	+	+/-	NA	-	Weak LoF
SAM	G456V	+	+	+	+	NA	+	WT-like
SAM	P549L	+	+	+	+	NA	+	WT-like
TIR	R569C	-	-	-	-	-	-	LoF
TIR	R570Q	+	-	+	+	-	+	LoF?
TIR	N571K	+	+	+	+	NA	+	WT-like
TIR	S572P	-	-	-	-	-	-	LoF
TIR	I593T	+	-	+	-	-	-	LoF?
TIR	D594E	-	-	-	-	+	-	Dominant negative
TIR	K602N	+	+	+	+/-	NA	-	Weak LoF
TIR	I608L	+	+	+	-	NA	-	WT-like
TIR	G624*	-	-	-	-	-	-	LoF
TIR	K641N	+/-	-	-	-	-	-	LoF
TIR	I643T	-	-	-	-	-	-	LoF
TIR	I653T	-	-	-	-	-	-	LoF
TIR	P655S	-	-	-	-	-	-	LoF
TIR	S684F	-	-	-	-	-	-	LoF
TIR	E686K	-	-	-	-	+	-	Dominant negative
TIR	E642A	-	-	-	-	-	-	Control for LoF

[a] Numbering according to the canonical 724 amino acid long human SARM1.
[b] Compare Figure 3.3; [c] compare Figure 3.9; [d] compare Figure 3.10; [e] compare Figure 3.17 and Figure 3.18; [f] compare Figure 3.13.

Table 3.2: **Summary of findings for natural SARM1 variants presented in this chapter.** The results of the functional studies for all tested SARM1 variants are summarised and compared to the positive and negative controls (respectively WT SARM1 and the enzyme-dead E642A SARM1) highlighted in grey.

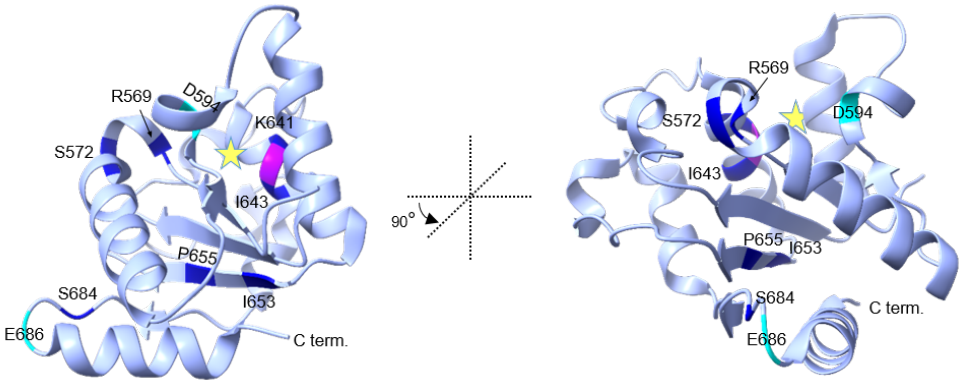


Figure 3.19: **Locations of SARM1 missense variants that confer full LoF in the SARM1 TIR domain crystal structure.** Ribbon diagram of the reported crystal structure of the human SARM1 TIR domain showing the locations of residues that are altered by the natural missense coding variants identified in this study to cause LoF. The structure presented is based on PDB ID:6O0R (bound to ribose) with the position of the predicted NAD substrate-binding pocket indicated by a star. Two views are shown differing by a rotation of 90° anti-clockwise along the vertical axis. The locations of residues that are altered to confer basic LoF are shown in dark blue and those that are altered to confer dominant LoF properties are shown in cyan. The catalytic E642 residue is labelled magenta. ChimeraX (http://www.rbvi.ucsf.edu/chimerax/) was used to generate the structures shown.

3.4.2 SARM1 LoF may be underrepresented in disease groups

Evidence exists that SARM1 alleles encoding variants with altered function can act as potential modifiers of disease risk, likely altering penetrance or expression. While the work of this chapter was ongoing, the Coleman group and others reported that SARM1 alleles encoding variants within its autoinhibitory ARM domain can lead to constitutively hyperactive NADase function and increased pro-degenerative capacity. These variants are highly enriched in individuals with ALS and related motor nerve disorders [9, 10].

In consequence, a relative paucity of carriers of SARM1 alleles encoding LoF variants could be predicted among individuals with these pathologies compared to the general human population [12]. Underrepresentation of LoF variants in ALS patients would, for instance, further support the hypothesis that SARM1 contributes to ALS. In addition to the recently suggested disease association (ALS) with SARM1 GoF variants there are two GWAS where variation in the *SARM1* chromosomal locus has been linked to ALS [9, 10, 204, 205]. If SARM1 LoF variants were to be underrepresented in disease cohorts, this would suggest that lowering SARM1 activity is a useful therapeutic strategy in ALS and related disorders [234]. Confirmation of this has not been possible yet due to the low frequency of the confirmed LoF alleles and the restricted size of currently available patient cohorts.

Nevertheless, this will become possible in the future as more SARM1 LoF variants are identified, and as disease cohorts increase. As such, it is predicted that carriers of SARM1 LoF alleles could have varying degrees of reduced susceptibility to different neurological conditions. It is also likely that any protective effect would only be detectable in a population where disease is expected, for example by modifying age-of-onset in carriers of pathogenic mutations. One such example could be Apolipoprotein E ϵ4 (APOE ϵ4) allele carriers with Alzheimer's disease. This will also facilitate identifying potential links between SARM1 variant alleles and other neurological disorders where SARM1 is predicted to play a modifying role. Any association of natural SARM1 LoF alleles with the absence or delayed onset of disease would support the idea that drugs targeting programmed axon death could be effective in that disorder.

3.4.3 SARM1 LoF frequency in the human population

The identified LoF variants are all rare, with ~0.17% of the general population (based on the sum of the global MAFs) being carriers of an allele encoding a SARM1 variant that shows any degree of LoF in the neurite degeneration assay (Figure 3.10). As discussed above, the varying degrees of NADase LoF determined for recombinant R570Q, N571K and I593T SARM1 might not be representative of their activities due to limitations of the

assay. The failure of E416K, I593T, and K602N SARM1 to fully restore degeneration of SCG neurites, however, could reflect partial LoF phenotypes with functional relevance in carrier individuals which remains to be clarified in future studies. Furthermore, only a small proportion of all the existing natural missense or nonsense variation within the SARM1 SAM and TIR domains have been tested. There is a high probability that other LoF alleles exist among the remainder. In addition, there are naturally occurring splice, nonsense and frameshift variants in gnomAD encoding SARM1 variants lacking the catalytic TIR domain that are also predicted to be full LoF alleles (This is further expanded on in chapter 5). Therefore, the total number of carriers of SARM1 LoF alleles is likely to be at least ~0.2-0.3%, and possibly substantially higher in some ethnic groups, which would be enough to have a meaningful impact on axon health at the population level. This prevalence may vary across different population groups and could potentially be higher due to LoF variants in non-coding regions of unknown significance. In fact, MAFs for several of the identified LoF alleles are much higher among individuals of South Asian and African/African American ancestry. Whole genome sequencing data of ALS patients within these populations could further help support this hypothesis.

Mice lacking SARM1 are overtly normal, even into old age [118, 195]. The fact that the *SARM1* gene has been evolutionarily conserved argues that there must be significant selective pressure to retain SARM1 functionality. This could either reflect that the alternative function of SARM1 in innate immunity is essential [235], which would not be challenged in mice housed in a pathogen-free environment, or that axon protection resulting from *SARM1*-deficiency confers a subclinical phenotype that only impacts survival in the wild or other circumstances, such as infection by some viruses. While targeting SARM1 is therapeutically promising [5, 206–208, 217], the question occurs whether complete elimination of SARM1 could interfere with natural homeostatic processes, such as the clearing of damaged axons following injury or other insults. Importantly, the discovery of the dominant negative mutants D594E and E686K SARM1 is the closest we have come yet to answering this question as the individuals carrying these variants had reached healthy adulthood at the time of recruitment for gnomAD.

3.4.4 SARM1 LoF variants are located within the TIR domain

All LoF variants identified here encode changes in the SARM1 catalytic TIR domain (see Figure 3.19). Several of these either overlap with or are in proximity to residues that are known or predicted to be involved in catalysis and/or substrate binding. These include F565-R570, D594, and E642 [110, 117]. Other variants are close to other functionally-important residues that may modify TIR domain conformation to alter activity [110, 229], such as

H685, mutation of which results in a dominant negative variant [197].

Interestingly, the mutation E686K SARM1 changes a residue that is important for an autoinhibitory interaction between the ARM and TIR domains within the SARM1 octamer that normally restricts TIR-TIR interactions to limit catalytic activity [112, 113, 222]. If E686K change stabilises the ARM-TIR interaction it could represent an alternative LoF mechanism. However, an artificial E686A mutation actually increases NADase activity [222], and switching a negative charge to a positive charge at this residue would arguably cause greater disruption of the ARM-TIR interaction and greater GoF. Instead, E686K likely causes a change within the TIR domain itself resulting in an inherently catalytically inactive SARM1 variant that would negate any potential GoF effect relating to the ARM-TIR interface.

While several of the tested SARM1 variants/mutants have a loss of enzyme activity, only two (D594E and E686K SARM1) have dominant LoF effects. Importantly, loss of enzyme activity itself is not an absolute requirement for dominant LoF effects as the dominant LoF mutant K193R SARM1 (residue K193 interacts with the phosphate moiety of NMN) retains basal enzyme activity at a level comparable to the WT protein [115, 197]. While K193A SARM1 is able to bind NMN the enzyme is not further activated and thus does not lead to degeneration of primary neuronal cultures (Figure 3.17 and Figure 3.18) [115].

Instead, dominant LoF variants may prevent the NMN binding-dependent conformational changes that would otherwise result in the pro-degenerative activation of enzyme activity of any WT SARM1 protomers within the hetero-oligomers. This would presumably occur via a combination of intra- and inter-protomer interactions within the octameric structure. In this respect, the involvement of the E686 residue in one of the ARM-TIR interactions could be important in relation to the dominant LoF effects of E686K SARM1.

The amino acid changes in the strong dominant LoF E686K SARM1 and weaker D594E SARM1 identified here are close to the previously reported strong and weaker dominant-negative changes, H685Y and K597E [120, 197]. However, there seems to be no obvious relationship between these two regions, or the location of K193, within the SARM1 structure. The way in which the dominant LoF variants/mutants in each separate SARM1 region confer their effects may thus be different. It is predicted that heterozygous carriers of either of the two dominant LoF variants will possess axons with a resistance to degeneration similar to that seen in mice completely lacking SARM1 [82, 83], provided that physiological levels of expression confer a robust dominant negative effect.

Individuals that are heterozygous for intrinsic (non-dominant) LoF will likely have a more modest, but still meaningful axon protection phenotype given that Sarm1 haploinsufficiency

provides some degree of protection against programmed axon degeneration triggered by injury and other stresses in mice and primary neurons [75, 217]. In addition, the results obtained in the dominant negative assays provide the first indirect evidence that endogenous (WT) mouse Sarm1 expressed in SCG primary neuronal cultures oligomerises with human SARM1 variant monomers. Otherwise, the dominant negative effect would be difficult to explain. In fact, study of sequence homology reveals 94% identity and 98.1% similarity between human and mouse SARM1 protein sequences.

3.4.5 Do compensatory mechanisms for SARM1 GoF exist?

The reported modest NADase GoF for E399K SARM1 is reflected in an increased basal NADase activity which cannot be further activated with the addition of the physiological activator NMN [76, 115, 199, 219]. This lack of response to NMN-inducibility makes it unlikely that the increased E399K activity is related to changes or interactions with the NMN/NAD binding pocket of SARM1. It is more likely that the mutation of the E399 residue induces a conformational change leading to a more active SARM1. Of note, even though *in vitro* cultures expressing E399K SARM1 do not degenerate faster over time compared to those injected with WT protein (Figure 3.15), biologically-relevant consequences in humans cannot be ruled out.

E399K SARM1 carriers are likely to have been overtly normal at the time of recruitment given the exclusion criteria of the gnomAD database [226]. Nevertheless, it is important to establish the extent of the penetrance of E399K SARM1 in the affected individuals and to see whether carriers have a subclinical phenotype or perhaps even show association with axonopathy at a later time in life. The fact that these individuals survive with such high constitutive SARM1 NADase activity is unexpected [9]. Chronic expression of constitutive hyperactivated SARM1 may induce compensatory changes via an as yet unknown mechanism. Similarly, low levels of NMNAT2 during development trigger compensatory mechanisms in primary neuronal cultures which are independent of expression levels of other enzymes involved in the NAD salvage pathway or SARM1 expression [100]. In particular, it will be important to determine the mechanism(s) responsible for these compensatory changes allowing for apparently normal axonal growth and health.

3.4.6 Limitations of the study

Given the very low levels of endogenous SARM1 in our HEK 293T cell line, the data will largely reflect the properties of each SARM1 variant in isolation. The findings could be expanded in the future by showing a LoF effect *in vivo* and in humans: (I) This could be

done with the help of mouse studies where one of the confirmed SARM1 LoF variants is expressed in a knock-in mouse model and a reduced susceptibility to injury-induced or disease-associated axonal degeneration is shown. The results could be directly compared with previously reported findings in mice heterozygous for *Sarm1* [217]. However, a generated knock-in mouse is likely to mimic the phenotype of mice that only harbour one *Sarm1* allele. Moreover, *in vivo* studies are time-consuming, tightly regulated, but also expensive to perform. (II) The current findings could be extended by collecting clinical information of individuals carrying the confirmed SARM1 LoF mutants (e.g. showing decreased susceptibility to PAD triggers, such as chemotherapy-induced peripheral neuropathy). This will become feasible as appropriate databases expand.

3.4.7 Conclusion

In summary, the results from this chapter show that multiple coding variants encoded by natural human SARM1 alleles impair the ability of SARM1 to drive axon degeneration *in vitro*. Most importantly, this is the first occasion where a dominant negative effect is described for human variants. Together with observations made by Gould et al. showing that Sarm1 haploinsufficiency confers partial protection in a range of disease models [217], this suggests that carriers of SARM1 LoF alleles could be at reduced risk of a number of neurological disorders. The combined frequency of LoF alleles is likely to be high enough to have a meaningful impact on population health and association of SARM1 LoF alleles with low risk or delayed onset of any disorder would support the use of SARM1-blocking drugs in those cases. Of note, parts of this chapter have led to a first-author publication [12] and the findings discussed add to our understanding of the human genetics of SARM1.

4

Functional characterisation of two patient & other rare NMNAT2 missense variants

4.1 Chapter summary

In healthy axons, the pro-survival NMNAT2 inhibits activation of SARM1, the central executioner of PAD [5]. Despite being very rare, NMNAT2 LoF coding variants exist and alter axon vulnerability. These have primarily been described in the context of rare polyneuropathies [7, 8], though, any role NMNAT2 may play in common neurodegenerative disorders remains unexplored and to be addressed in the future [234]. This chapter presents new functional data on a subset of natural NMNAT2 missense variants present in the human population, as well as artificial mutants located within the same part of the protein sequence hypothesised to be candidate LoF for NMNAT2. This set of characterised NMNAT2 variants includes a newly identified rare LoF NMNAT2 missense variant discovered through clinical exome sequencing in two patients with chronic polyneuropathy, both of which are compound heterozygous and carry an additional NMNAT2 variant, R232Q NMNAT2, a known LoF allele [8]. At first, the capability of the selected variants to support transected axon survival in mouse primary neuronal cultures was assayed when overexpressed. Subsequently, *in vitro* enzymatic assays and steady-state protein expression levels were used to help shed light on mechanism of those NMNAT2 variants failing to support neurite

survival and served as additional measures of any LoF not detected by that assay. In summary, a total of three new LoF NMNAT2 variants were identified, two of which confer a partial loss for NAD synthesis activity. These include V98M NMNAT2, the allele of unknown significance reported in the patient case. In summary, the data shown support the idea that biallelic NMNAT2 LoF is causal for some rare disorders. How these variations may influence axon vulnerability and disease susceptibility in some individuals is discussed in one of the last sections. Of note, while this work was still in progress, Dingwall et al reported similar results and independently published a bioRxiv pre-print of the same patient cases presented here. Their findings confirm part of my data obtained here independently [11].

4.2 Introduction

NMNATs are NAD-synthesizing enzymes which play an important role in neuronal maintenance in both *Drosophila* and humans [236–241]. Of these, the isoform NMNAT2 is an endogenous axon maintenance factor without which axons cannot survive [30]. Its constant replenishment is likely achieved through axonal trafficking on the surface of Golgi-derived vesicles [91]. Efficient knockdown of *Nmnat2* in primary neuronal cultures results in spontaneous degeneration in the absence of injury. This cannot be compensated for by endogenous NMNAT1, nor NMNAT3, arguing against redundancy among the NMNAT isoforms [30]. When a nerve is injured, axonal transport is blocked. This results in the depletion of the highly labile protein NMNAT2 (and other cargoes that depend on axonal transport) [30, 85], causing NMN build up alongside NAD loss [144, 199]. This imbalance in the energy metabolism eventually leads to the activation of SARM1 and death of the axon (see Figure 3.1) [5].

Nmnat2-deficient mice die at birth as a result of severe defects in peripheral innervation (including the phrenic nerve) and also exhibit truncated axons in the peripheral and central nervous system [99, 100]. The cause appears to be limited axon extension, rather than a dying-back degeneration of existing axons, suggestive of an essential role for NMNAT2 during axon development [100]. Importantly, the underlying mechanism involves PAD as the following manipulations all improve the phenotype: a) the use of WLD^S mice [100], b) *Sarm1*-deletion [101] and c) expression of the bacterial NMN deamidase transgene [199]. Strikingly, *Nmnat2*-deficient mice rescued by *Sarm1* deletion survive into old age with no overt phenotype [195]. This raises the important question of whether human diseases associated with NMNAT2 LoF would respond in a similar way if the affected individuals were to be treated with anti-SARM1 therapies.

Mice heterozygous for a silenced *Nmnat2* allele are viable and appear overtly normal into old age [100, 101]. They only express reduced levels of synaptic proteins in the hippocampus [202] and NMNAT2$^{+/-}$ primary neuronal cultures are modestly more sensitive to vincristine treatment [242]. However, reducing NMNAT2 levels below a particular threshold (which is estimated to be roughly 30%) compromise axon development and survival [103]. *Nmnat2*$^{gtBay/gtE}$ compound heterozygous mice result from a cross of mice heterozygous for two different *Nmnat2* gene trap alleles which results in an NMNAT2 expression of 30% [195]. While *Nmnat2*$^{gtBay/gtE}$ mice are viable and appear overtly normal for up to 12 months the animals display deficits later on. These include early and age-dependent deficiency in peripheral nerve axons (reduced numbers of myelinated sensory axons), temperature insensitivity and a later-onset decline in motor performance. Similarly, *Nmnat2*$^{gtBay/gtE}$ primary neuronal cultures display a slower neurite outgrowth, and increased sensitivity to axonal stress, such as Vincristine treatment [103].

NMNAT2 has been suggested to have a protective role for maintaining neuronal health. Reduced *NMNAT2* mRNA levels have been reported in Parkinson's, Huntington's, Alzheimer's diseases, as well as in tauopathy [243–248]. In addition, *NMNAT2* expression is also decreased in spinal cord tissue of ALS patients compared to respective control groups [249]. Moreover, *Nmnat2* mRNA and protein levels significantly decline prior to the appearance of cognitive deficits in a mouse model of human tauopathy [88]. Wobbler mice modelling motor neuron disease also express reduced *Nmnat2* levels prior to symptom onset [250]. In line with a neuroprotective role of NMNAT2, its overexpression is neuroprotective in both mouse and *Drosophila* [88, 202]. This is suggestive of constitutively low or declining NMNAT2 expression contributing to clinical and subclinical phenotypes. Crucially, there is evidence of widespread natural variation in human *NMNAT2* mRNA expression the significance of which is yet to be explored in the context of axonal health [202].

At present, our knowledge of the consequences of very rare NMNAT2 coding variants in humans is limited to six polyneuropathy cases all of which are associated with biallelic NMNAT2 LoF of varying degrees [7, 8, 11]. In all cases, the severity of the disease was representative for the degree of protein LoF and phenotypically matching previously reported mouse genotypes. A homozygous missense mutation conferring a partial LoF was causatively linked to a rare case of childhood onset polyneuropathy accompanied by erythromelalgia resulting in thermal instability of the NMNAT2 enzyme and increasing axonal levels of NMN, the physiological activator of SARM1 [7]. Similarly, a companion case report described two biallelic LoF mutations in two stillborn fetuses with fetal akinesia deformation sequence (FADS), presenting with severely reduced skeletal muscle mass and hydrops fetalis at birth. Both protein variants were incapable of supporting axon survival in

vitro and showed altered protein stability including defects in NAD synthesis, a phenotype reminiscent of *NMNAT2*-null mice [8].

4.2.1 Aims of this chapter

This chapter discusses a rare case of biallelic compound heterozygous NMNAT2 mutations found in two brothers affected by a chronic polyneuropathy of unknown origin. While one variant is a previously known LoF [8], biochemical and cell biological analysis were performed to characterize the other patient mutation V98M NMNAT2. Furthermore, extended analysis of the adjacent region 90-105aa was performed as previous findings had implied its functional importance for the catalytic activity of the protein. Of note, similar results related to the patient cases were published by Dingwall et al. as this work was ongoing [11].

4.3 Results

4.3.1 Biallelic compound heterozygous NMNAT2 mutations in two siblings with a severe chronic neuropathy

The Division of Genomic Diagnostics at the Children's Hospital of Philadelphia, US, contacted the Coleman group regarding a case of two siblings with chronic peripheral neuropathy of unknown origin (see Figure 4.1A). The Division had followed up a GeneMatcher submission for *NMNAT2*, an online database that facilitates the collaboration of researchers and clinicians working on rare clinical phenotypes associated to genes of interest [251]. Whole exome and Sanger sequencing performed at the Children's Hospital of Philadelphia confirmed two rare compound heterozygous NMNAT2 variants in the two brothers, c.695G>A (R232Q) and c.292G>A (V98M). Of these, R232Q NMNAT2 is a characterised and confirmed NMNAT2 LoF allele previously identified in two stillborn siblings with fetal akinesia deformation sequence (FADS) [8]. The other variant V98M NMNAT2 was of unknown significance, however predicted to be a likely candidate for complete or partial LoF based on the following criteria: (1) It is a rare variant with a minor allele frequency (MAF) of $7/10^6$ in gnomAD. (2) Primary sequence alignment revealed Valine at position 98 is highly conserved across different organisms and human NMNAT isoforms, (3) V98M is located in a part of the protein sequence where other LoF mutations are clustered. In fact, it is in close proximity to T94M, a mutation that confers partial LoF [7], as well as W92 and T95, two conserved residues involved in pyridine nucleotide binding of the substrate NMN required for NAD synthesis by NMNAT2 [252, 253]. Furthermore, mutation of W92

to Glycine reduces its NAD synthesis activity by 95% [85, 202, 254]. (4) In addition, the in-silico prediction tools SIFT and Polyphen predict V98M to be damaging. Both parents are heterozygous for either of the NMNAT2 variants (Figure 4.1B).

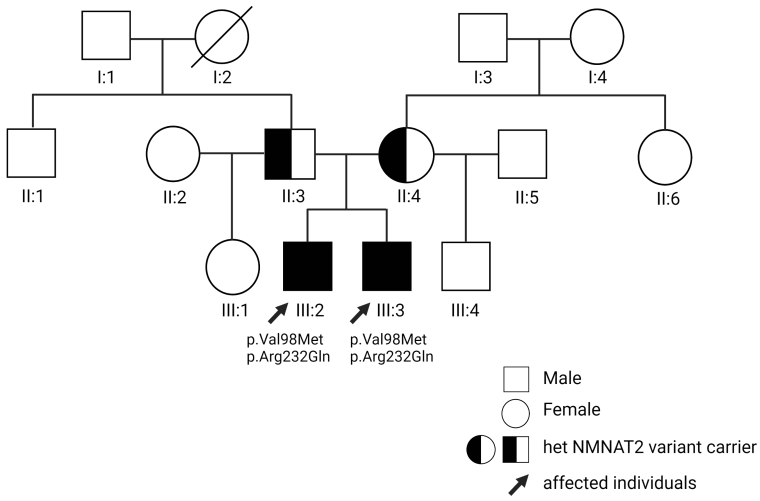


Figure 4.1: **Rare compound heterozygous NMNAT2 variants in two siblings with chronic neuropathy.** Family pedigree of the affected individuals. Patients are indicated by blackened symbols and arrows. The probands' parents are healthy and have no neurological manifestation despite being heterozygous carriers for each NMNAT2 variant.

4.3.2 Clinical features of the patients with NMNAT2 variants

Both brothers suffer from a chronic sensorineural polyneuropathy and have had a similar disease course. Proband I initially presented with an acute onset of flaccid quadriparesis and respiratory failure at the age of 1-2 years resulting in a hospitalization. Further reported symptoms included skeletal muscular atrophy, skeletal deformities (Figure 4.1A), such as kyphoscoliosis and pes equinovarus, joint laxity, flexion contracture and failure to thrive. Electrophysiological examination (nerve conduction study and electromyography) pointed towards both sensory and motor axon defects. Although a multifocal demyelinating neuropathy was diagnosed initially in both cases, repeated examination later showed no such evidence in either of the probands' examined extremities. Clinical features, including missing information later published by Dingwall et al. [11], are summarised in Table 4.1. Both parents are healthy and no further members with a similar neurological condition

are known in the extended family (Figure 4.1B). The reported neurological phenotype of the two patients is intermediate compared to cases reported by Huppke et al and Lukacs et al [7, 8]. Furthermore, both brothers share symptoms (incl. polyneuropathy and erythromelalgia) with one of the aforementioned clinical case reports associated to a biallelic NMNAT2 partial LoF [7]. Furthermore, the fact that one of the identified NMNAT2 alleles is a confirmed full LoF [8] and existing data from primary culture work and mouse studies added additional support for an NMNAT2 LoF hypothesis [30, 99, 100, 103]. Together this strengthened causality between the reported phenotype and the biallelic NMNAT2 mutations. It supports a recessive mode of inheritance of NMNAT2-associated human axonopathy. Therefore, this was followed by function characterisation of the NMNAT2 variant in question.

Symptoms	Clinical features	
	Patient I	Patient II
NMNAT2 mutation	Val98Met, Arg232Gln	Val98Met, Arg232Gln
Sex/age, y	M/20	M/17
Ethnicity	black, African American	black, African American
Age of onset	13 months	15 months
Presenting symptoms	Episodic attacks characterised by neuropathic pain, worsening erythromelalgia and flaccid lower limbs.	Episodic attacks characterised by neuropathic pain, worsening erythromelalgia and flaccid lower limbs.
Initial symptoms	Respiratory failure accompanied by hypotonia and fatigue requiring mechanical ventilation	Respiratory failure accompanied by hypotonia and fatigue requiring mechanical ventilation
Motor development	Delayed	Delayed
Weakness/ atrophy	flaccid quadriparesis, proximal and distal skeletal muscular atrophy	flaccid quadriparesis, proximal and distal skeletal muscular atrophy
Mobility	joint laxity, flexion contracture,	joint laxity, flexion contracture,
Skeletal deformation	Kyphoscoliosis, equinovarus	Kyphoscoliosis, equinovarus
Fundi	bilateral optic atrophy	bilateral optic atrophy
NCS	Chronic sensorineural polyneuropathy	Chronic sensorineural polyneuropathy
Disease progression	progressive	progressive
Others	failure to thrive, impaired movement with wheelchair dependence	failure to thrive, impaired movement with wheelchair dependence
Aid for walking	Wheelchair	Wheelchair

Table 4.1: **Summary of clinical features in affected siblings.**

4.3.3 Strategic candidate selection of other NMNAT2 variants within region 90-105 aa

To understand the importance of the protein region adjacent to the affected patient residue V98, *in vitro* NMNAT2 characterization was extended to other variants, including nearby residues considered to have a high potential for LoF when mutated. Natural variants studied were based on the gnomAD dataset v3.1.2 [226] which lists a total of 84 coding non-synonymous NMNAT2 variants. Selection of natural variants or artificial mutants for candidate NMNAT2 LoF was based on the following criteria: (1) Proximity to previously reported NMNAT2 LoF mutations, as discussed in Section 4.3.1. (2) Evolutionary

NMNAT2 coding variant[a]	Type	rsID	Gen. location and change[b]	MAF[c]	*in-silico* prediction tools	
					Poly-Phen	SIFT Score
D90E	Natural	rs1336389282	1:183290179 C>A	0.00002	1	0.656
W92R	Natural	rs559396436	1:183290175 T>C	0.000007	0	0.994
C96F	Natural	rs1439964553	1:183290162 G>T	0.000007	0.01	0.542
V98M*	Natural	rs759119922	1:183290157 G>A	0.000007	0.02	1
L105F	Natural		1:183290136 G>A	0.000007	-	-
R232Q*	Natural	rs1382955168	1:183261261 C>T	0.000007	0	0.968
T95A	Artificial	-	1:183290166 A>G	-	-	-
L99A	Artificial	-	1:183290154 TT>GC	-	-	-
H101A	Artificial	-	1:183290148 CA>GC	-	-	-
H102A	Artificial	-	1:183290145 CA>GC	-	-	-

[a] Numbering according to the canonical 307 amino acid long human NMNAT2.
[b] Numbering according to the GRCh38 genome build.
[c] Minor allele frequency referring to the gnomAD population.
* Patient variants highlighted by asterisks.

Table 4.2: **Human NMNAT2 natural and artificial coding variants analysed in this study.**

conservation across model organisms, and (3) physicochemical consequences of amino acid changes and allele frequencies (see Figure 4.2 and Table 4.2). Site-directed mutagenesis was employed to generate expression vectors (pCMV-Tag4 vector backbone) carrying the following candidate LoF NMNAT2 residues (Table 4.2) ranging from amino acid 90 to 105: D90E, W92R, T95A, C96F, V98M, L99A, H101A, H102A, L105F NMNAT2 (see Figure 4.2). Mutated protein preparations were subsequently tested in a series of functional assays aimed at detecting differences in NMNAT2 protein function *in vitro*. To support the reading flow in the following, variants are referred to as either natural, when listed in gnomAD [226], or artificial, where residues were intentionally substituted so that they encoded an alanine (A) amino acid instead. Alanine substitution was used to test for the contribution of specific aa side-chains while preserving native NMNAT2 protein structure. The residue H24 is part of the predicted ATP binding site and highly conserved across species and NMNAT isoforms [85]. Its mutation to H24D NMNAT2 results in an enzyme-dead NMNAT2 protein [254]. Structure prediction suggests it contacts with the NAD phosphate bonded to nicotinamide ribose. R232Q NMNAT2, one of the patient variants (Figure 4.1B), is a known NMNAT2 LoF variant [8] and was included in the experiments to serve as a reference point for the new variants being tested. Together with T94M, these three variants were continuously used as positive control for LoF for experiments discussed in the following sections.

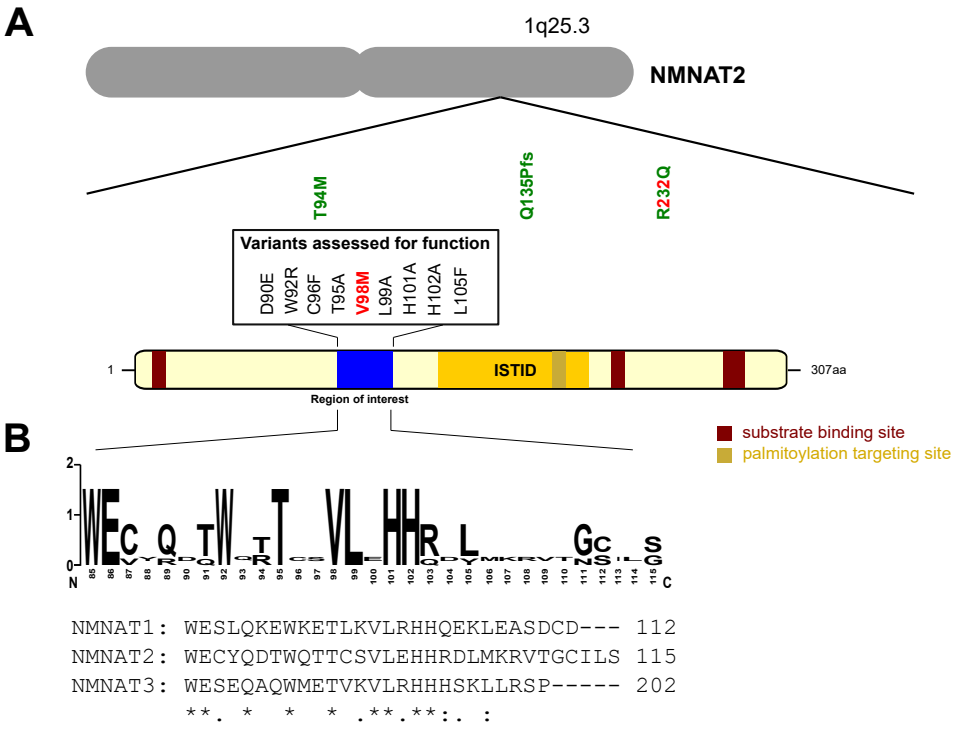


Figure 4.2: **Selection strategy of NMNAT2 variants targeted for mutagenesis in the present study. (A)** Domain architecture of the 307 amino acid (aa) human NMNAT2 protein showing the locations of the missense variation (region of interest highlighted in blue) encoded by selected *NMNAT2* alleles and artificial mutations characterised in this study. Patient variants are highlighted in red. Previously identified disease-associated variants T94M, Q135Pfs and R232Q NMNAT2 are shown in green [7, 8]. Important NMNAT2 structures are highlighted, including palmitoylation sites (C164/165) important for targeting to Golgi and vesicle membranes in Hela cells [92, 93] and primary neuronal cultures [91], substrate binding sites (H24) and the isoform-specific targeting and interaction domain 2 (ISTID2) (residues R108-I190) in orange [85, 93]. **(B)** Several amino acids within the NMNAT2 region 85 – 115aa are highly conserved across different model organisms and isoforms. The top panel shows an amino acid conservation logo plot determined by multiple sequence alignment of NMNAT2 sequence from 5 species (human, mouse, zebrafish, *C. elegans* and *Drosophila*) obtained via WebLogo [255]. The lower panel shows a multiple sequence alignment of the three human NMNAT isoforms generated by ClustalOmega. Asterisks highlight identical amino acids; double and single dots mark strong and weak conserved amino acids, respectively. Gaps are shown as dashes.

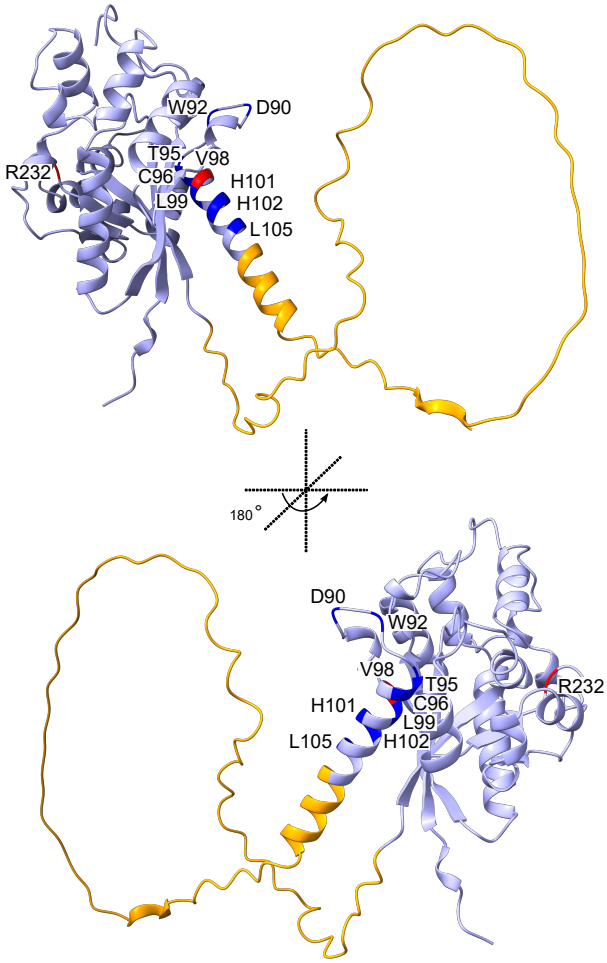


Figure 4.3: **Locations of characterised missense variation in the predicted NMNAT2 protein structure.** Ribbon diagram of the predicted structure of human NMNAT2 showing the locations of the candidate LoF residues (highlighted in dark blue) that were altered in this study, NMNAT2 residues V98 and R232 affected in the two patients are highlighted in red. The ISTID2 is labelled in orange. AlphaFold (`https://alphafold.ebi.ac.uk/`), a homology-based modelling method [256, 257], was used to predict NMNAT2 structure and visualization was performed using ChimeraX [258]. Two views are shown differing by a rotation of 180° anti-clockwise along the vertical axis.

4.3.4 Metabolite analysis of NMNAT2 variants expressed in NRK1-HEK cells is not conclusive

Firstly, it seemed important to establish a simple screening method for the identification of potential NMNAT2 LoF variants before performing more advanced functional analysis. For this purpose, an initial screening assay was established to test the selected NMNAT2 variants (Table 4.2) for their ability to produce NAD in transfected HEK 293T cells. HEK 293T cells seemed to be a suitable testing system as NMNAT2 is not endogenously expressed (Figure 4.4A). The rationale behind this assay was the possibility that NMNAT activity may be rate-limiting for NAD synthesis in HEK 293T cells, at least under the supplementation with NAD precursor molecules, so that differences in the amount of exogenously-expressed NMNAT2 activity added could be measured from the NAD increase relative to the empty vector (or GFP only) control. In-cell NAD levels were measured 24h after co-transfection with FLAG-tagged NMNAT2 constructs together with peGFP encoding GFP (transfection efficiency control) using the bioluminescent NAD/ NADH-Glo^{TM} assay. While the assay was believed to have the scope to test for NMNAT2 LoF variants, this approach proved to be unsuccessful and no differences in NAD levels where detected when comparing in-cell NAD values from well transfected with WT NMNAT2 and the empty vector control (data not shown).

Following this initial pilot experiment, it was concluded that HEK 293T cells expressed sufficient amounts of NMNAT1 (Figure 4.4A) so that differences in NAD synthesis activity between overexpressed NMNAT2 constructs and the empty vector control would not be detectable. How much NAD is produced is not just dependent on spare NMNAT activity within the cell but also the production of the NAD precursor molecule NMN (Figure 4.4B). To overcome the aforementioned obstacle, it seemed reasonable to boost NMN levels to test whether NMNAT1 could become rate-limiting, allowing the additional NAD produced by the exogenously-expressed NMNAT2 to be quantified. Boosting NMN was attempted using different strategies, as highlighted in Figure 4.4B: (1) The use of NRK1-HEK cells, a cell line stably expressing the enzyme nicotinamide riboside kinase (NRK1) needed for the conversion of nicotinamide riboside (NR) to NMN [259]. (2) The addition of NR only or (3) the addition of NR together with Nam. Under normal conditions, NAMPT, the enzyme for conversion of Nam to NMN, is rate limiting. However, this is experimentally bypassed through the addition of the NMN precursor NR (Figure 4.4B).

As expected, absolute NAD values significantly increased with each treatment with NAD values being lowest in untreated cells, followed by an increase in the presence of NR and even higher levels reached when NR was supplemented together with Nam (Figure 4.4C).

Conditions	NMN	NAD	NMNAT1/3	NMNAT2
HEK 293T cells, untreated	Normal	Normal	Unsaturated	Overexpressed
[dashed] NRK1-HEK cells, untreated	↑↑	↑↑	Unsaturated	Overexpressed
[dashed] NRK1-HEK cells, + NR (24h)	↑↑↑↑	↑↑↑↑	Unsaturated	Overexpressed
[dashed] NRK1-HEK cells, + NR, +Nam (24h)	↑↑↑↑↑↑↑↑	↑↑↑↑↑↑↑↑	Unsaturated	Overexpressed

Table 4.3: **Overview of changes caused by experimental manipulations employed in Figure 4.4 C and D.** Table summarizing what effect experimental manipulations of cultures had on NMN levels, NAD levels, as well as NMNAT activities.

However, NAD values between individual empty vector controls and the WT NMNAT2 obtained for each treatment were not statistically significant (Figure 4.4C and D). This observation was even more obvious when in-cell NAD values of WT NMNAT2 were expressed relative to the empty vector control (Figure 4.4D). Noteworthy, the small amount of variation between ev and WT NMNAT2 NAD levels observed is likely a result of technical variability. Overall, the obtained data suggest that despite boosting NAD levels through the addition of NMN precursors NR and Nam, endogenous NMNAT activity in NRK1-HEK cells is not saturated to a degree where differences in activity of overexpressed NMNAT2 could be seen. It is acknowledged other explanations may exist. To prove that NMNAT1 was indeed hindering this NRK1-HEK cell based screening approach, other manipulations, such as the knockdown of NMNAT1 or overexpression of the enzyme NAMPT, could have been employed. This, however, would defeat the point of setting up an easy screening assay in the first place. Secondly, it would require further external manipulation of the cell system that may result in a micro-environment not representative of physiological conditions. Therefore, other assays were prioritised at this point.

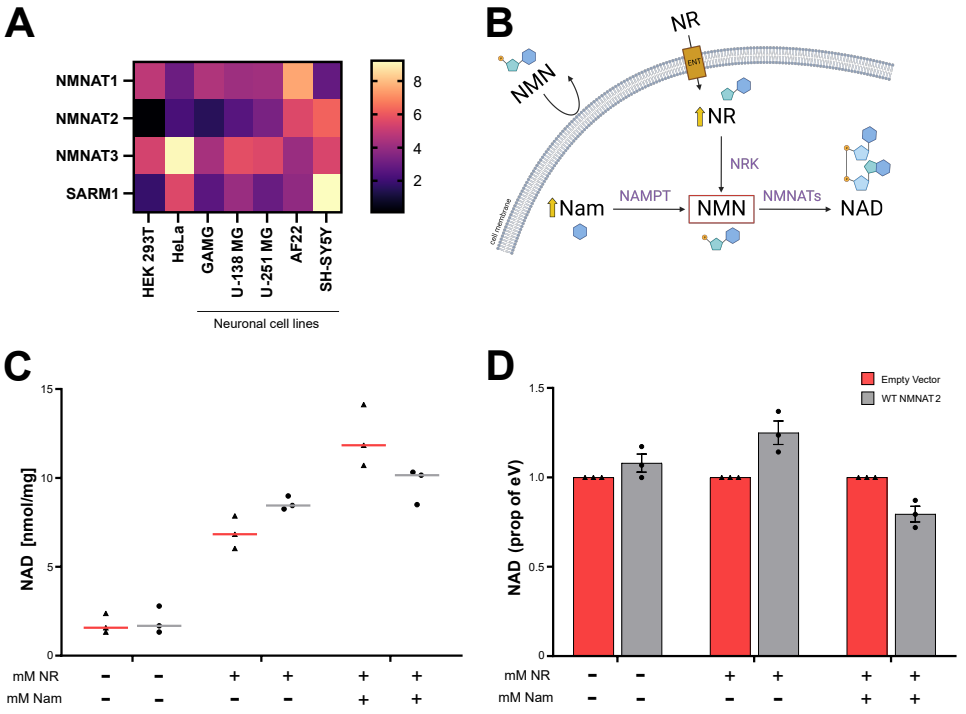


Figure 4.4: **NRK1-HEK cells are not a good model to indirectly screen for differences in NMNAT2 variant enzyme activity. (A)** NMNAT isoform and SARM1 mRNA expression levels in commonly used cell lines obtained from the HPA (www.proteinatlas.org). The heat map depicts transcript expression levels as normalised values (Number of transcript per kilobase million, nTPM). NAMPT levels are not shown as they are significantly higher and would therefore not allow for visual-based distinction between NMNAT and SARM1 expression levels on the heat map. **(B)** Schematic diagram showing NAD biosynthesis through the salvage pathway and how experimental manipulations, such as the addition of NR and/ or NAM, impact NMN synthesis and subsequently boost NAD production. NAD, nicotinamide adenine dinucleotide; NAM, nicotinamide; NAMPT, nicotinamide phophoribosyltransferase; NMN, nicotinamide mononucleotide; NR, nicotinamide riboside; NRK, nicotinamide riboside kinase. **(C)** Absolute and **(D)** relative in-cell NAD levels 24 h after transfection with either empty vector or wild-type NMNAT2. Cells were either (I) left untreated or supplemented with (II) 2 mM NR or (III) 2 mM NR together with 1 mM Nam to boost NAD production. Unpaired t-tests comparing NAD levels of WT NMNAT2 and the empty vector control were performed for each condition and showed no statistical significance.

4.3.5 Several NMNAT2 variants within region 90-105 aa show reduced capacity to promote neurite survival

To test whether V98M NMNAT2 could be an underlying cause of the patients' symptoms and whether the selected NMNAT2 region 90-105 aa was of any functional importance, the chosen natural and artificial missense variants (Table 4.2) were tested for their relative capacity to promote axon survival in WT SCG cultures after transection. To answer this question, a well-established microinjection method was employed in a similar approach to chapter 3 (also see Figure 2.2) [214]. This could help distinguish the level of axo-protection between different NMNAT2 proteins [30, 91].

The ability of the NMNAT2 mutants to preserve the integrity of axotomised neurites was assessed relative to WT NMNAT2 and positive controls for NMNAT2 LoF, including the enzyme-dead H24D and the known natural LoF variant R232Q NMNAT2. Each Flag-tagged NMNAT2 expression construct was injected at a concentration where exogenously expressed WT NMNAT2 would preserve around 70-80% of cut axons 24h post transection (Figure 4.5). Noteworthy, NMNAT2 overexpression only has a modest effect unless expression levels are very high due to its high turnover rate [30]. In contrast, the enzyme-dead mutant H24D NMNAT2 conferred no protection at all (Figure 4.5), consistent with previous findings [7, 91]. Out of 10 NMNAT2 mutants tested, seven – W92R, C96F, V98M (patient variant), T95A, L99A, H101A and H102A NMNAT2 - were found to have a significantly reduced capacity to confer protection at 24h post transection (Figure 4.5). Similarly, expression of R232Q NMNAT2, the other patient variant, led to little preservation of cut neurites in line with published results [8]. Lack of protection in the case of W92R, T95A and R232Q NMNAT2 was comparable to the lack of protection seen after injection with empty vector and H24D NMNAT2. In contrast, D90E and L105F NMNAT2 were the only injected mutants able to protect cut neurites 24 h after axotomy to a degree comparable to the WT NMNAT2 (60-70%) (Figure 4.5).

To exclude cytotoxicity, soma integrity was assessed at 24 and 48 hours after injection (prior to performing neurite transections). As expected, no NMNAT2-associated cell death was observed related to either wild-type or mutant NMNAT2 (Figure 4.6). At this point, it was concluded that the reduced capacity to maintain neuronal health of V98M NMNAT2 (Figure 4.5) together with the known full LoF R232Q NMNAT2 is likely to make a significant contribution to the symptoms of the two patients. Complete NMNAT2 LoF appears irreconcilable with life. This is supported by both mouse and human data [8, 99, 100]. In fact, R232Q NMNAT2 is described together with another complete LoF variant, both of which result in a biallelic LoF where each NMNAT2 variant is unable to prevent axon degeneration

when overexpressed in culture [8]. The fact that the affected brothers' phenotype is severe but not lethal and the symptoms intermediate to the two published clinical case reports strongly supported the idea that V98M is unlikely as strong of a LoF as R232Q NMNAT2 is [7, 8].

After identifying several potential NMNAT2 LoF variants through the axotomy assay it was concluded that the observed failure to protect transected neurites could be either due to impaired enzymatic NAD synthesis function or perhaps insufficient protein expression or impaired protein stability. In order to test this hypothesis, protein expression and enzymatic activities of the mutant NMNAT2 constructs were subsequently tested.

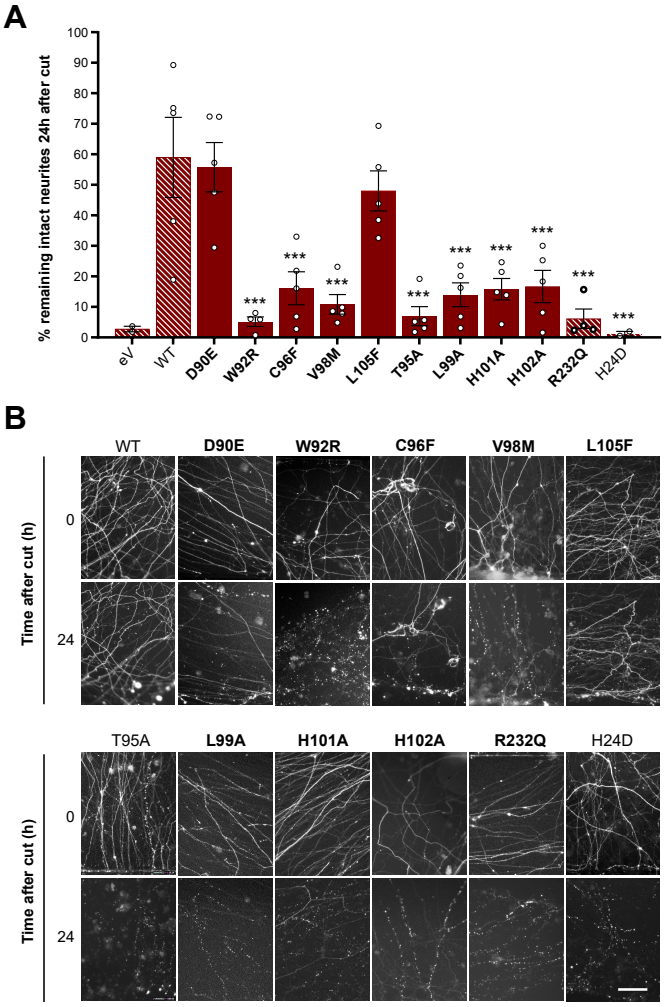


Figure 4.5: **Selected NMNAT2 variants are unable to promote injury-induced neurite degeneration as efficiently as the wild-type protein. (A)** Cultured SCG neurons from wild-type animals were microinjected with 10 ng/µl of selected human NMNAT2 constructs (pCMV-Tag4 vector backbone) together with 40 ng/µl pDsRed2 encoding DsRed necessary for the visualisation of injected neurites. Two days post microinjection *in vitro*, DsRed-labelled neurites of the cultures were severed using a scalpel and thereby completely separated from their cell bodies to prevent further supply of the protein from the soma. As previously described (Section 2.7.2 and Figure 3.10), degeneration was quantified by calculating the percentage of intact DsRed-labelled neurites remaining 24 h after transection relative to those present at the time of the cut (0 h). Bars for the controls (respectively WT NMNAT2, R232Q and the enzyme-dead H24D NMNAT2) are hatched to differentiate them from the selected variants (bold text, filled bars). Data are presented as means ±SEM with individual data points shown (n = 4-5, except for the empty vector and H24D control). Multiple comparisons using a one-way ANOVA with Benjamini and Hochberg false discovery rate (FDR) correction showing significance as compared to WT; *** $p < 0.001$. **(B)** Representative fluorescence images, as used for the quantification shown in part A, of transected, DsRed-labelled neurites of wild-type neurons microinjected with the generated constructs expressing WT or variant/mutant NMNAT2 (as labelled) at 0 and 24 h after the cut. Scale bar corresponds to 50 µm.

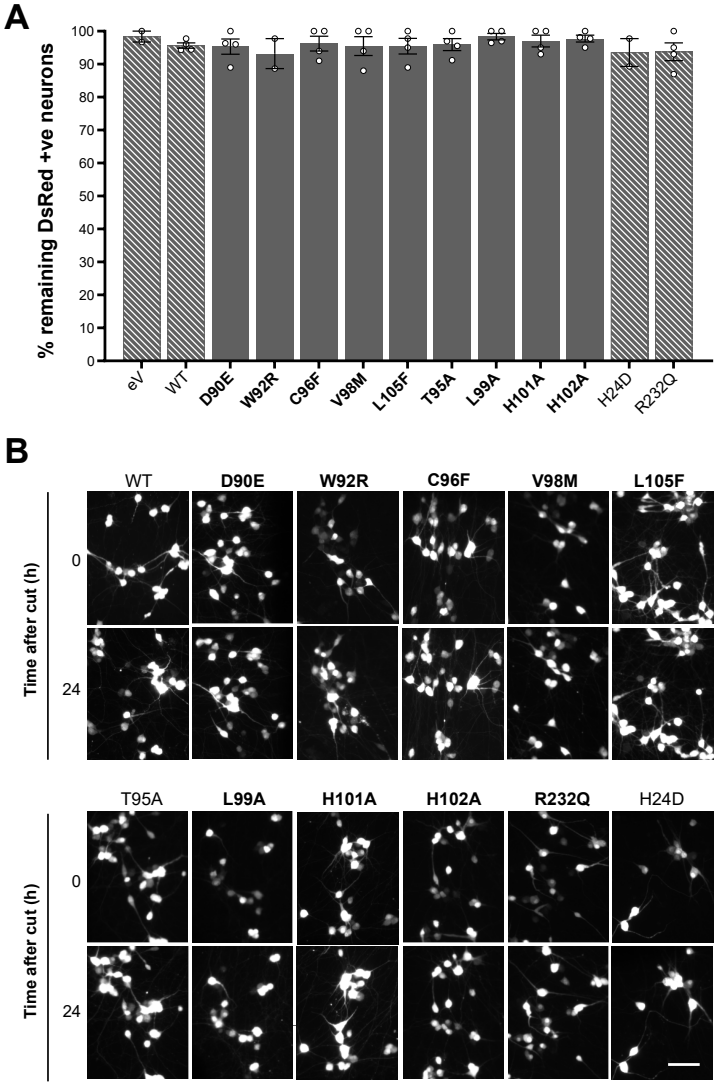


Figure 4.6: **Generated NMNAT2 variants do not have cytotoxic effects on primary neuronal cultures. (A)** Viability of dsRed-labelled WT SCG cell bodies prior to transection was assessed by comparing cell body morphology at 24 h and 48 h post microinjection, similar to Figure 3.13. The number of morphologically healthy cell bodies remaining at 48 h is shown as a percentage of the total number of those present at 24 h post microinjection, a method previously shown to reflect accurate survival rates [30] Means ±SEM, including individual data points (n=2-4) are shown, multiple pairwise comparisons to WT SARM1 with a FDR correction did not show any statistical significance. **(A)** Representative fluorescent images as used for the quantification in (A) of microinjected WT neuronal cell bodies injected with constructs expressing WT or variant NMNAT2 (as indicated) at 24 and 48 h after microinjection. Scale bar corresponding to 50 µm.

4.3.6 NMNAT2 LoF variants used for microinjection into SCG neurons are sufficiently expressed

To understand whether the observed failure of the NMNAT2 variants to protect transected SCG cultures, as shown in Figure 4.5, was a result of insufficient protein expression, steady-state NMNAT2 construct expression levels were checked. This is important as low expression of a functional (NAD synthesizing) NMNAT2 variant may lead to degeneration in microinjected WT SCG cultures despite being enzymatically active, whereas high expression of an NMNAT2 variant with a partial LoF for NAD synthesis may be sufficient to protect injected cultures masking the partial phenotype.

Total lysates of transfected HEK 293T cells were analysed by western blotting using an anti-FLAG antibody to detect overexpressed WT or variant/mutant NMNAT2 (Figure 4.7). As expected, NMNAT2 bands migrating at the corresponding molecular weight (~34kDa) were observed in cells transfected with NMNAT2-expressing constructs but not in the empty vector control sample (Figure 4.7A). A slightly slower migrating band was observed for R232Q NMNAT2 which was consistent with a previous report [8]. Surprisingly, observed steady-state expression intensities were variable between NMNAT2 mutants. In fact, of the tested NMNAT2 variants D90E NMNAT2 was the only mutant with expression levels comparable to that of the WT protein (Figure 4.7A and B). R232Q NMNAT2 was even higher expressed than WT NMNAT2 [8]. In contrast, C96F, V98M, L99A, as well as H102A NMNAT2 were not well expressed (Figure 4.7A and B). Perhaps the lower expression levels suggest the region may be important for protein stability. This low protein expression could be replicated in the neurons of human carriers of these variants, and thus be clinically relevant. However, this requires confirming directly in such tissue to be sure. Two alternative explanations for low NMNAT2 expression are reduced protein synthesis and a shorter protein half-life, or a combination of both. Due to time constraints this was not further analysed.

In addition to western blotting, expression of exogenously-introduced NMNAT2 in microinjected SCG cultures was shown using immunohistochemistry, as the amount of injected cells would not yield material sufficient for detecting via immunoblotting (see Section 3.3.8) for similar rationale). Similar to previous observations, NMNAT2 variants resulted in a perinuclear staining typical of Golgi-associated proteins [56, 85] (Figure 4.8). Noteworthy, staining intensity was not quantified as this only served to prove that introduced NMNAT2 constructs were indeed expressed in primary neuronal cultures. Information on NMNAT2 construct expression levels together with NAD synthesis activity would provide more conclusive results for the functional interpretation of the NMNAT2 constructs.

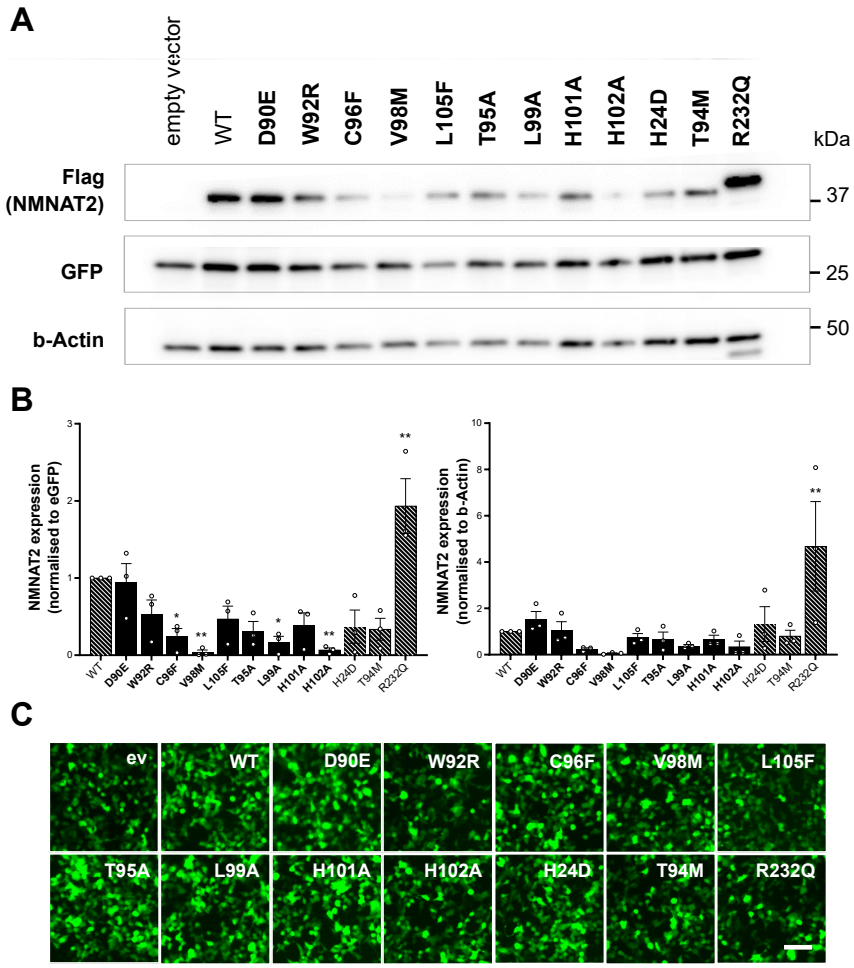


Figure 4.7: **Steady-state expression of NMNAT2 variants from pCMV-Tag4-based constructs used for microinjection into SCG neurons. (A)** Representative immunoblot (n = 3) from HEK 293T extracts 24 h after co-transfection with pCMV expression constructs for Flag-tagged WT or variant NMNAT2 and an expression construct for eGFP. Cells transfected with empty Vector are also shown (no FLAG band). Blots were probed with antibodies for Flag to detect NMNAT2 (~35 kDa). Co-transfected eGFP (~25 kDa) served as a transfection efficiency control and b-Actin (~40 kDa) is an endogenously expressed housekeeping protein. All generated NMNAT2 constructs were expressed and of the expected size. R232Q NMNAT2 migrates slightly slower than WT NMNAT2, as previously reported [8].**(B)** Quantification of normalised Flag-NMNAT2 levels to eGFP (left graph) and to b-actin (right graph) are shown, with data presented relative to WT NMNAT2. Individual values (n=3) and means ±SEM are shown; * $p < 0.05$ and ** $p < 0.01$; multiple comparisons using a one-way ANOVA with FDR correction comparing band intensities to that of the WT protein. **(C)** Representative eGFP fluorescence imaging of HEK 293T cells 24 h after transfection with respective NMNAT2 variants or the WT protein. Scale bars corresponding to 50 µm.

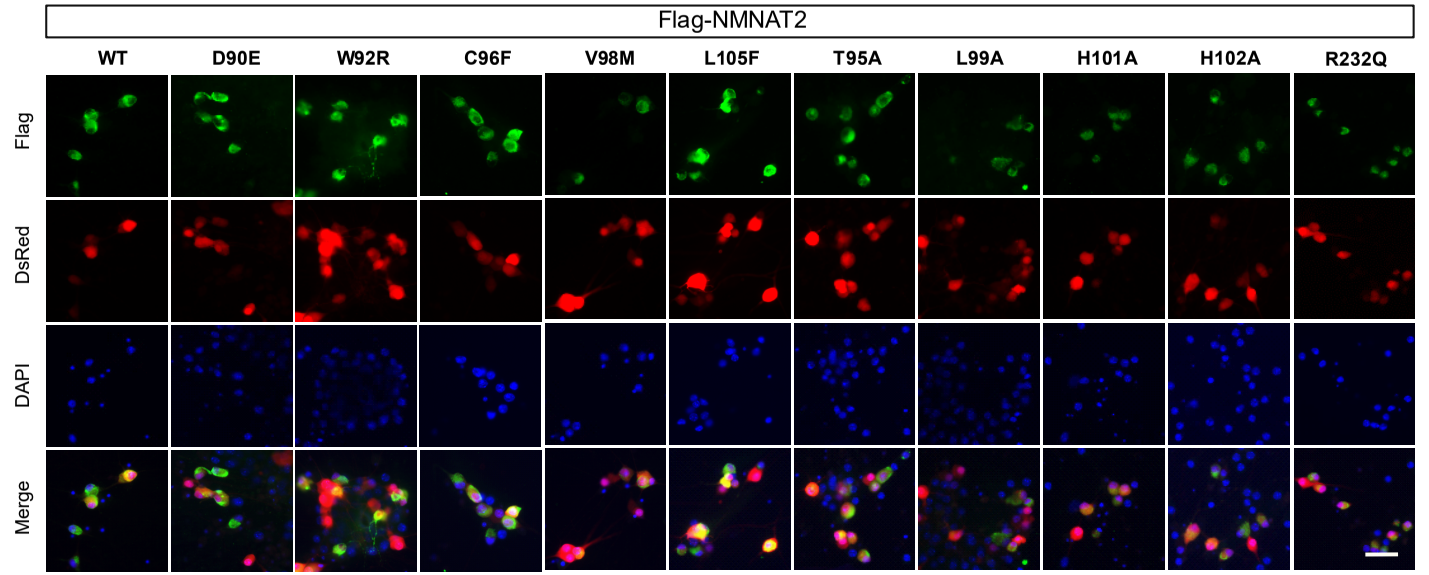


Figure 4.8: **Expression levels of NMNAT2 variants expressed from pCMV-Tag4A backbones in microinjected WT SCG neurons. (A)** Representative fluorescent images of dissociated wild-type SCG neuronal cultures after microinjection with expression constructs for WT or variant NMNAT2 (25 ng/l) and DsRed (25 ng/µl). Neurons were immunostained 24h post injection, followed by nuclear counterstaining using Vectashield with DAPI. DsRed labels injected neurons while Flag immunostaining indicates expression of the injected NMNAT2 protein. Scale bars corresponding to 50 µm.

4.3.7 Enzymatic activities in comparison: W92R, V98M and T95A NMNAT2 have reduced NAD synthesis capacities

Previously, measuring NAD levels in transfected NRK1-HEK cells (see Figure 4.4) did not prove suitable to detect differences in enzymatic function of NMNAT2 variants and would have, anyhow, only provided an indirect measure of NAD synthesis activity. Thus, enzymatic activity of the respective NMNAT2 variants was tested directly using recombinant protein (Figure 4.9). It is acknowledged that a full biochemical characterisation of the enzymatic activity, including measurements at physiological and pathological levels, requires assessment of activity across a range of substrate concentrations, to calculate the K_M for each substrate [7, 8]. This requires expertise and equipment available in our collaborator's group but this was beyond their capacity at the current time. So, as an initial investigation, the V_{max} was tested in our laboratory to perform an initial screen for NMNAT2 NAD synthesis LoF. After protein purification from HEK 293T cells a standard curve of FLAG-tagged SARM1 was used to determine relative concentrations of the purified FLAG-tagged NMNAT2 mutants of unknown concentration (Figure 4.9). Differences in enzyme molecular weight (factor 0.47) between NMNAT2 and SARM1 were taken into account when converting the protein concentration.

NAD synthesis activity of equal amounts of each purified NMNAT2 protein was measured in the presence of 1mM ATP and NMN each, as well as 5mM $MgCl^2$. Assay conditions were chosen so that the substrates were abundant with individual concentrations exceeding the respective concentrations for the K_M by 10-50x. This would guarantee catalysis reactions with a velocity close to the NMNAT2 V_{max}. In contrast, lower concentrations closer to the K_M may lead to greater variability of results. In addition, NMNAT activity requires divalent cations for optimal activity, which is highest at the presence of Mg^{2+}.

Initially, enzymatic activities of WT NMNAT2 and R232Q NMNAT2 (as a positive control for LoF) were measured at 25°C (RT) and 37°C. As previously reported, the activity of WT NMNAT2 was almost twice as high at 37°C when compared to 25°C (not shown). The obtained values were within the expected range [7, 8]. In addition, a time course of NAD synthesis at 0, 15 and 30 min was performed under "conventional" assay conditions to identify an ideal end point within linear NAD production (Figure 4.10). While an earlier end point, such as 5 min, seemed more appropriate, end values at 10 min after incubation were collected to avoid pipetting variability at the expense of obtaining NAD values within a sub-optimal linear range, though still far from being saturated. An empty Vector control ruled out any potential background activity associated to the beads rather than the purified NMNAT2 protein itself. In line with the results from the axotomy assay shown in

Figure 4.5.A, the NMNAT2 variants that previously behaved like the WT protein and successfully restored degeneration of transected WT SCG neurites, also displayed enzymatic activity levels similar to WT NMNAT2. Conversely, several of the variants that appeared to be LoF in the previous axotomy assays - W92R, V98M, T95A, L99A and H101A NMNAT2 - showed reduced, though not completely absent, NAD synthesis activities. While C96F NMNAT2 had a slightly lower enzymatic activity than WT NMNAT2 this difference was minimal and therefore not statistically significant. Perhaps the discrepancy in the axotomy and enzymatic activity results can be explained by insufficient expression of C96F NMNAT2 in microinjected cultures.

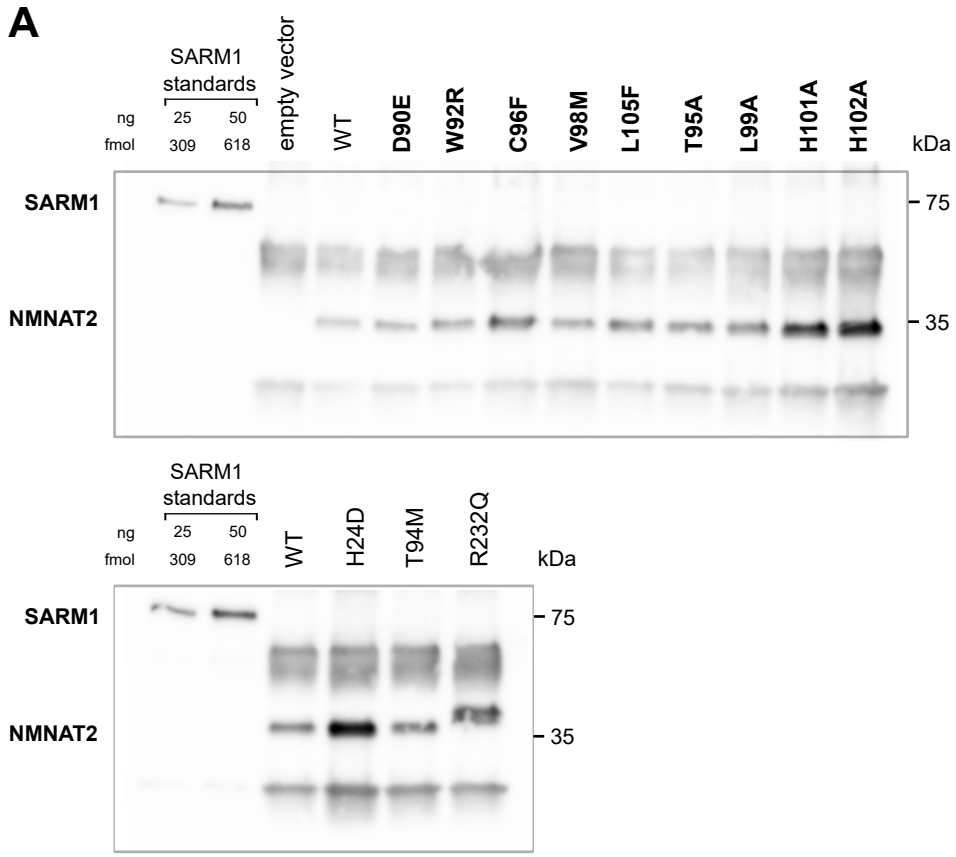


Figure 4.9: **Immunopurification of recombinant NMNAT2 variants used in NAD synthesis assays.** Representative western blots (n=4) of immunoprecipitated WT and natural variant NMNAT2 next to two SARM1 standards (on the left of each blot) used for relative NMNAT2 protein quantification. A detailed description can be found in the Materials and Methods section. **(A)** NMNAT2 protein bound to the equivalent of 1.777 µl of magnetic bead suspension were loaded per lane next to a dilution series of purified SARM1 which served as a standard curve for quantification of the purified NMNAT2 variants as no NMNAT2 standards were available. In contrast to the WT and natural NMNAT2 variants, the purified SARM1 standards (kindly provided by collaborators at AstraZeneca) were not Flag-tagged. Therefore, blots were in addition probed with a polyclonal antibody raised against the SAM domains of human SARM1. The amount of NMNAT2 protein was quantified based on Flag immunoblotting relative to the standard curve obtained from the SARM1 standard loaded. Te difference in the MW of both proteins being a factor of x0.47 was taken into account for this. Molecular weight markers (kDa) are shown on the right of each panel. Noteworthy, bands at ~50 kDa and ~20 kDa correspond to non-specific binding to the heavy and light chain of the Flag antibody used for the immunoprecipitation.

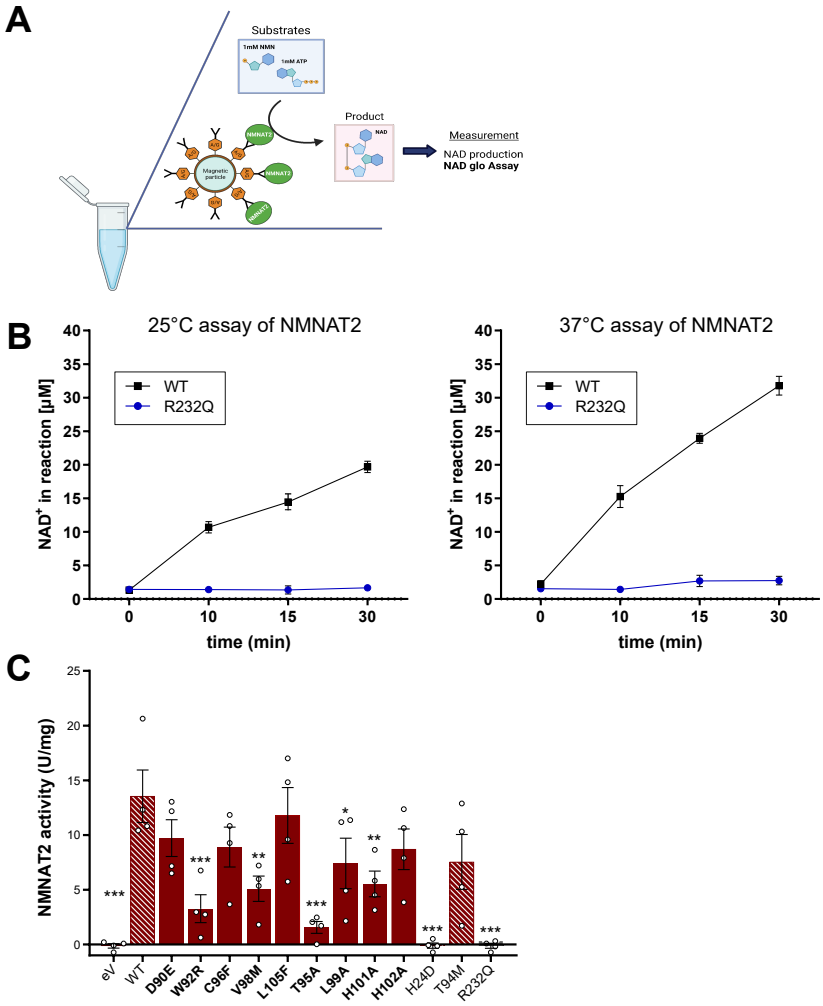


Figure 4.10: **Comparison of NAD synthesis activity of recombinant NMNAT2 protein. (A)** Schematic illustration of the NAD synthesis assay using purified bead-bound human NMNAT2. Enzymatic activities of WT or mutant/variant NMNAT2 was measured in the presence of the substrates NMN and ATP together with $MgCl^2$. **(B)** Time-course analysis of WT and R232Q NMNAT2 activity at 25°C and 37°C performed to establish ideal temperature conditions [8]. **(C)** NMNAT2 specific activity of Flag-tag purified preparations measured at 37 °C with saturating concentrations of substrates NMN and ATP. Activity was measured as a rate. Values are presented as the mean ±SEM from n = 4 independent measures, multiple comparisons using a one-way ANOVA with FDR correction showing significance as compared to WT; $p < 0.05$, ** $p < 0.01$ and *** $p < 0.001$. Detailed description of rate calculations can be found in the Materials and Methods. Rate measurements were determined as the difference between NAD levels in the original reaction at t = 0h and at reaction endpoint (10 min). Specific enzyme activity is given as the number of NMNAT2 enzyme units per mg protein (U/mg) which is corresponding to µmol/min/mg. Details of the assay procedure are provided in the Materials and Methods section.

4.4 Discussion

4.4.1 Summary of findings

The results of this chapter provide useful insight into the functional importance of residues within the NMNAT2 region 90-105 aa (Table 4.4). Firstly, a third human axonopathy family, again with two affected offspring, with biallelic NMNAT2 LoF in two brothers and chronic polyneuropathy, is described. This further supports the model, now based on both human cases and mouse models, that NMNAT2 LoF variants result in wide-ranging axonal phenotypes whose severity appears to correlate with the degree of LoF. Furthermore, a group of 10 natural and artificial human NMNAT2 variants of which two encode naturally occurring partial LoF NMNAT2 missense variants lacking NAD synthesis capacity and consequently fail to protect when overexpressed in primary SCG neuronal cultures is characterised. Furthermore, the artificial mutation of residue T95 into an Alanine results in a full NMNAT2 LoF variant. Interestingly, expression of several NMNAT2 variants seems compromised which could be suggestive of residues being important for protein stability, potentially explaining their inability to support neurite survival. However, this requires further experimental exploration to be addressed in the future. Together with previous results, the data discussed here will be of substantial benefit and will gain more clinical relevance as the field uncovers further disease-relevant variants of NMNAT2 and other programmed axon death genes similar to the limited exploration performed in chapter 5.

4.4.2 Technical limitations

Some technicalities that could have impacted the study are discussed in the following.

1. Screening for candidate NMNAT2 LoF coding variants was based on overexpressed variants that would fail to protect WT primary cultures post axotomy. Axotomy is a general, and easily quantifiable model for other causes of axonal stress, in particular axonal transport impairment [30]. While this assay is an established method, it is worth acknowledging that less severe insults, such as the treatment with a cytotoxic agent (e.g. Vincristine, Taxol or similar), would be clinically more relevant.

2. Enzymatic studies were performed using bead-bound recombinant protein together with the respective substrates necessary to initiate NAD production and values measured using the bioluminescent NAD/NADH-Glo^{TM} assay. While this is an efficient way to perform rough screening for potential NMNAT2 LoF mutants, it is not as accurate as other methods, including high-performance liquid chromatography (HPLC), to detect more subtle differences in enzyme activity or kinetic parameters.

NMNAT2 coding variant [a]	Mutant type	Neurite survival [b]	NAD synthesis activity (V_{max}) [c]	Steady-state expression [d]	Proposed functional consequence
D90E	natural	+	+	WT-like	similar to WT
W92R	natural	-	-	WT-like	LoF due to reduced enzyme activity
C96F	natural	+/-	+	reduced	LoF due to lower expression level
V98M*	natural	-	+/-	very reduced	partial LoF due to reduced enzyme activity and lower expression level
L105F	natural	+	+	WT-comparable	similar to WT
R232Q*	natural	-	-	>WT	known full LoF
T95A	artificial	-	-	normal	LoF due to reduced enzyme activity
L99A	artificial	+/-	+/-	reduced	partial LoF due to slightly impaired enzyme activity and low expression
H101A	artificial	+/-	+/-	normal	partial LoF due to slightly impaired enzyme activity
H102A	artificial	+/-	-	reduced	LoF due to lower expression level

[a] Numbering according to the canonical 307 amino acid long human NMNAT2.
[b] Compare Figure 4.5; [c] compare Figure 4.10; [d] compare Figure 4.7

Table 4.4: **Summary of findings from functional analyses of natural and artificial NMNAT2 variants presented in this chapter.**

This could include kinetic analysis of different variants measuring initial rate plots as a function of NMN substrate concentration measured at varied fixed concentration of ATP substrate and vice versa. Encouragingly, no value differences in the enzymatic activity of WT NMNAT2 were observed when comparing our results to published studies, where protein had been purified from bacteria, protein amount quantified using the Bradford Assay and NAD values of eluted protein measured using HPLC [7, 8, 11].

3. While LoF could not be confirmed for several NMNAT2 variants, the findings in this study may have other implications. The results raise the question whether the apparent normal enzymatic activity of some variants, including C96F, L99A, H101A or H102A NMNAT2 is – similar to T94M NMNAT2 [7] - temperature dependent and decreases at higher body temperatures, such as during the course of a systemic infection. Other factors, including the effect of much longer axons in humans and ageing could play a role too. Lack of time did not allow for follow up studies, including testing the stability of each protein. A more detailed analysis of these constructs may be provided in future work. The most common NMNAT2 missense variants are I113V NMNAT2 (MAF 0.01598) and R162Q NMNAT2 (MAF 0.0002352), the latter of which does not result in LoF as shown by unpublished data by Coleman lab member Dr. Jon Gilley. While this suggests there is no evolutionary selection against this

particular variant and perhaps I113V NMNAT2 too there may indeed be pressure against those with much lower MAFs.

4. Interestingly, gnomAD constraint score pLI (predicted LoF) for NMNAT2 is 0.99 which indicates that the gene or transcript cannot tolerate protein truncating variation. SARM1, which is about double the size of NMNAT2, has 50 missense alleles with a higher MAF than this suggesting there is evolutionary selecting against many NMNAT2 variants. Whether this may be explained by early onset disease in very rare biallelic cases remains to be addressed. Overall, these data are in models and are a guide to what could occur in patients or carriers but may not fully represent them. Thus, differences may be found in humans. To strengthen findings, there is a need to generate knock-in transgenic mice similar to the mouse model described by Dingwall et al [11]. To prove relevance in human cells, NMNAT2 null human induced pluripotent stem cells (iPSC) lines could be generated and used for further neuronal differentiation or organoid growth. Axon outgrowth deficiency could be one of the parameters investigated and whether this is rescued by targeting SARM1.

5. As NMNAT2 is crucial for axon survival in the central and peripheral nervous system, better understanding of its structure and the role of distinct amino acid residues may reveal features that provide the basis for a rational design of drugs targeting dangerously low NMNAT2 levels, either by increasing stability or enhancing enzymatic activity, in patients with several neurological phenotype and hence preserve neurons and axons in these cases. Most promising patient targets are those with rare axonopathies, as described by others [7, 8, 11].

4.4.3 Adults carrying heterozygous NMNAT2 LoF mutations appear clinically healthy

As in the two other clinical reports previously published by members of the Coleman group, both parents of the affected brothers described in Section 4.3.2 are reported to be clinically healthy. If carriers for missense heterozygous NMNAT2 mutations can be healthy, this raises the question why they are so rare. Not only are nonsense/frameshift NMNAT2 alleles nearly absent in gnomAD, but so are missense NMNAT2 alleles in general scarce. It is interesting to point out that heterozygous mice carrying a single gene trapped NMNAT2 allele are healthy at birth and at least up until the age of 24 months and show no signs of abnormality [99, 100, 103]. However, it has been previously described that the neurites are more sensitive to chemotherapeutic treatment in culture. Thus, reducing NMNAT2 expression by 50% does not have any overt effects in mice. While the age of the parents

is unknown they are at or close to a childbearing age and appear healthy. It remains unknown, however, whether they have any sub-clinical symptoms, or, limited ability to cope with other neurodegenerative stresses (2nd hit), including ageing, and show greater susceptibility to axon damage. This could include skewed age of onset or displaying or more severe phenotype (e.g. CIPN, DPN). This second-hit hypothesis could be tested - in part - by generating knock-in transgenic mouse models heterozygous for one LoF NMNAT2 allele and exposing the animals to stress or minor insults. It would be useful to know whether parents in either of the reported NMNAT2 cases should be subjected to additional more thorough investigations targeted at picking up subclinical neurological deficits. Low NMNAT2 expression could be a risk factor for axonal loss, especially in the context of 'two hit' cases, as supported by published results in our lab [103]. Although the study of non-coding, potential regulatory sequences exceeded the scope of this thesis project, the data presented provides evidence of some coding alleles with reduced expression, that could be explained by lower levels of transcription/translation and/or by a shorter half life.

4.4.4 Biallelic NMNAT2 LoF associated to human axonopathies

Proving causality between NMNAT2 variants and rare disease phenotypes has proven challenging due to the following reasons. Firstly, NMNAT2 variants are generally very rare within the human population suggesting they are selected against. Another drawback is limited sample size. Including the patient case discussed in this chapter, rare human axonopathies have been associated to NMNAT2 variants in three unrelated families where affected individuals are biallelic NMNAT2 LoF. This is further supported by existing mouse data (both in full knockout models and compound heterozygous animals [30, 99–101, 103, 195]. In order to further strengthen this hypothesis, there is in need of identifying additional affected individuals with similarly rare NMNAT2 variants.

4.4.5 Importance of genomic databases & future directions

This problem could be addressed in the future by establishing databases collecting genomic (exome or targeted sequencing to limit costs) and clinical information of patients focusing on the following phenotypes: unsolved cases of rare chronic neuropathy, cases of unexplained erythromelalgia where SCN9A mutations have been excluded, cases of foetal loss, stillbirth, perinatal lethality associated to respiratory failure, early-onset muscular weakness and the failure to thrive. These are most likely to help identify further cases of biallelic LoF NMNAT2 mutations, as well as heterozygous carriers in humans. Overall, this could help gain further insight into the nature of the disorders and, for instance help advise regarding

future pregnancies in affected families. NMNAT2-associated disease phenotypes have become an area of considerable current research. While this study focused on a rare genetic cause of neuropathy, the increasing availability of genomic and structural data will help shed light on the importance of NMNAT2 in human disease. Affected individuals could be identified by targeted genetic testing and could later undergo specific Wallerian-pathway targeted treatment. Interestingly, NMNAT2 impairment is most obvious in the peripheral nervous system, which is likely due to the length of peripheral nerves and the short half-life of the protein itself.

5

Screening genomic databases for disease-associated coding variants in PAD genes

5.1 Chapter summary

Results from previous sections, chapter 3 and chapter 4, demonstrate that SARM1 LoF/GoF and NMNAT2 LoF variant alleles present in the human genome translate to altered protein enzymatic activities and axon vulnerability *in vitro*. Together with other data, this adds to a growing body of evidence linking altered NMNAT2 and SARM1 protein function in humans to susceptibility to axonal disease [5, 9–11]. All of this supports the hypothesis of an intrinsic axon vulnerability spectrum in the human population which is based on expression and activity of SARM1 and its axonal regulator NMNAT2, as illustrated in Figure 5.1 [5]. A potential link between PAD genome variants and other rare axonopathies or even more common neurodegenerative disorders remains unexplored. This chapter presents a small set of newly identified SARM1 alleles. For this purpose, genebass (UK Biobank) and 100,000 Genomes, two UK-based genomic databases, were screened for SARM1 coding variation. SARM1 variants are more common than NMNAT2 variants and were, thus, prioritised. Allele frequencies of predicted and confirmed SARM1 LoF alleles (chapter 3 and [12]), as well as known SARM1 GoF variants were compared between disease and control groups. It is acknowledged that the limited size of the cohorts in combination

with the low frequencies of the PAD variants are not sufficient to perform statistical tests and this represents a major limitation. Rather, this chapter is of an exploratory nature and the purpose was to help generate hypotheses for follow-up experimental work in the future.

5.2 Introduction

Genetic variation can result in, or increase the susceptibility to, neurological disorders. While rare genetic diseases often follow a Mendelian inheritance pattern where a single gene mutation is directly linked to a disease phenotype, more common neurological conditions, in particular neurodegenerative disorders, are less well understood [260]. Their heterogeneous nature determined by multiple genes and by the environment results in a complex aetiology. This makes it difficult to understand why the rate of disease progression, clinical presentation and severity of neurodegeneration vary from one patient to another [261]. One such clinically relevant example is variable susceptibility to chemotherapy-induced peripheral neuropathy (CIPN), an adverse effect caused by a spectrum of widely-used anticancer therapeutics [262]. Substantial inter-individual differences in the susceptibility, symptom severity, and onset of the peripheral neuropathy support an underlying genetic vulnerability [263]. Similar variability is observed in other conditions, such as diabetic peripheral neuropathy and it is likely that programmed axon death (PAD) genes - proposed to have widespread molecular involvement in human disease - may be underlying some of this observed variation [5].

5.2.1 The axon vulnerability spectrum

A body of evidence is pointing towards the existence of an axon vulnerability spectrum, as shown in Figure 5.1, amongst humans caused by both coding and gene expression variation of PAD genes [5, 7–11, 202, 234, 249]. What makes the proposed model clinically appealing is the fact that patients at the vulnerable end of the spectrum are most likely to benefit from interventions targeting the PAD pathway and disorders associated to these variants are promising indications in which to apply them [5]. These vulnerable individuals are hypothesised to carry SARM1 GoF and/or biallelic NMNAT2 LoF variants leading to high expression levels and/or enzymatic activity of the respective protein, putting their axons at highest risk for PAD-induced neurodegeneration. *In vivo* data from rodents strongly support this hypothesis where mouse phenotypes range from death at birth to rodents with highly resistant axons surviving ten times longer than axons in wild-type animals after injury [30, 82, 83, 99, 100, 103, 195, 217]. Two PAD proteins whose sequence and expression

are known to profoundly influence axonal health and NAD metabolism are NMNAT2 and SARM1 the role of which is extensively reviewed in previous sections (chapter 1, chapter 3, as well as chapter 4). Individuals with impaired NMNAT2 protein function and/or expression (therefore initiating PAD leading to activation of the pro-degenerative SARM1) together with those expressing high levels and/or hyperactive SARM1 are those considered most susceptible to axonopathy through this pathway [7–11]. Interestingly, a great variability in human NMNAT2 expression levels has been reported in post-mortem human brain and spinal cord tissue [202, 249]. This is likely to be the case for SARM1 and other PAD genes too. The previous sections, chapter 3 and chapter 4, demonstrate that some of the predicted LoF and GoF variant alleles present in the human genome translate to altered SARM1 and NMNAT2 enzymatic activity and axon susceptibility *in vitro*. Consequently, it is important to determine empirically what effect other genomic variation has on axonal health and whether these effects extend to chronic disease (for SARM1 GoF and/or NMNAT2 LoF mutants) or protection (in SARM1 LoF mutants and/or NMNAT2 GoF mutants). The human population database gnomAD lists several gene constraint metrics to aid gene and variant interpretation, one of which is the pLI, probability of loss of function intolerance score. This value is obtained by comparing observed and expected frequencies of nonsense, frameshift and splicing mutations for a protein of this size and likely reflects the evolutionary selection against the propagation of deleterious alleles. NMNAT2 and STMN2, a protein which resembles NMNAT2 in several properties [91], have a 0.99 and 0.98 probability of loss-of-function intolerance respectively, suggesting that a heterozygous LoF state by itself or in combination with other genes and/or environmental cues may compromise axonal health [226].

5.2.2 NMNAT2 & SARM1 variation associated with disease

At the start of this PhD, our knowledge on human variation within PAD genes was very limited. Work from myself (chapter 3 [12], chapter 4) and other members of the Coleman group together with others have slowly begun to close this gap in the past three years [7–12]. Previously, two separate genome-wide association studies (GWAS) had shown significant association of the chromosomal *SARM1* locus to sporadic ALS [204, 205]. In line with this, *Sarm1* deletion is protective in several, but not all, mouse models of ALS [193, 194]. The SARM1 activation mechanism most directly related to ALS are rare *SARM1* variants that disrupt its autoinhibitory ARM domain and, in consequence, hyperactivate SARM1 NADase basal activity, similarly - though much stronger - to the effect of E399K SARM1 discussed in chapter 3. These SARM1 GoF mutations are associated with sporadic ALS and other motor nerve disorders [9, 10].

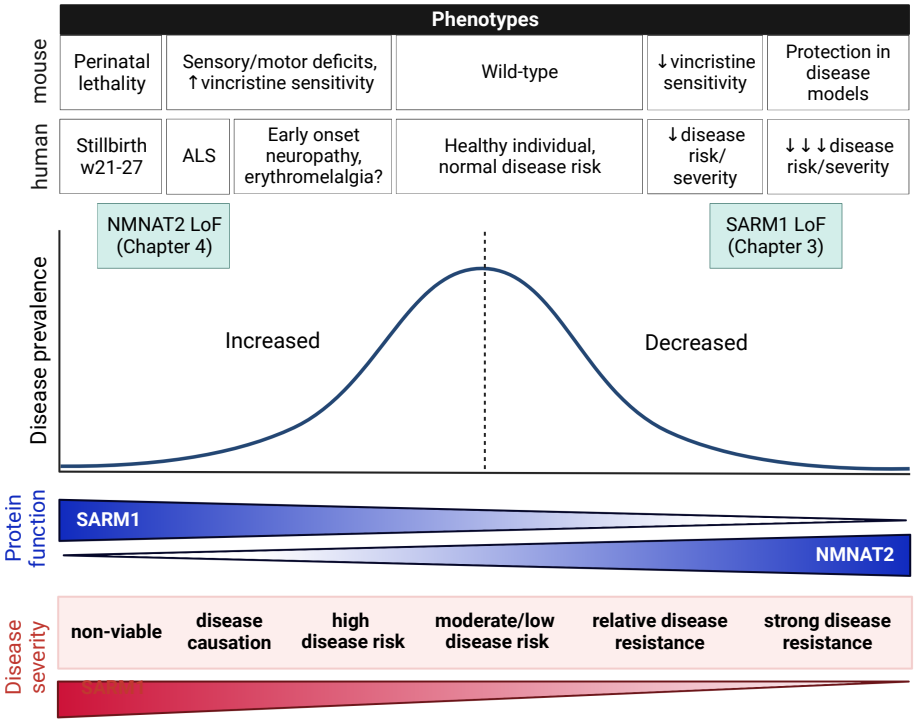


Figure 5.1: **The emergence of an axon vulnerability spectrum.** Illustration of the range of axon phenotypes observed and predicted in mice and humans and how these fit into a hypothesised axon vulnerability spectrum. The line graph represents a proposed prevalence of diseased axons in the human population. Protein expression/ enzymatic activity levels of the pro-survival NMNAT2 and pro-death SARM1 are shown as gradients underneath. The white boxes at the top show distinct phenotypes in humans and mice described in literature. Data from chapter 3 (SARM1 LoF coding variation) and chapter 4 (NMNAT2 LoF coding variation) provide further supporting evidence and their proposed position is indicated in the form of green boxes. Lower axon vulnerability, corresponding to the right side of the graph, may be likely a result of SARM1 LoF alleles present in the gnomAD or dbSNP databases disrupting SARM1 function and/or expression together with NMNAT2 GoF resulting in significantly higher protein expression levels/stability/activity. Conversely, higher axon vulnerability, corresponding to the left side of the graph, may likely result from SARM1 GoF alleles and/or NMNAT2 LoF. While this illustration is limited to what we know about how SARM1 and NMNAT2 variants and how they can contribute to axon vulnerability, other PAD genes are likely to play a role too. Adapted from Coleman and Höke [5]. This graph was generated using BioRender.com.

Another PAD gene which has been linked to ALS is *STMN2* [127, 234]. Its protein shares several properties with NMNAT2, including being short-lived and transported along the axon [71]. STMN2 levels are regulated by TDP-43 and were found to be significantly decreased in ALS patients [129, 130]. TDP-43 is a predominantly nuclear DNA/RNA-binding protein which has several functions, including transcriptional regulation and splicing [264]. When TDP-43 decreases, the *STMN2* transcript is truncated and results in a nonfunctional protein [129, 130]. Though unexplored, loss of STMN2, with or without TDP-43 pathology, may represent a common pathway in neurodegenerative disorders [127]. Moreover, a polymorphic intronic CA repeat in *STMN2* has been proposed as a risk factor for sporadic ALS. The authors report disease modifying effects, such as earlier age-of-onset and shorter survival duration [265]. In addition, human post mortem brain of patients with FTLD-tau show reduced levels of full-length *STMN2* mRNA but in the absence of the truncation [265]. Interestingly, other groups have found no such association between longer *STMN2* CA repeats and an ALS phenotype [266, 267]. While STMN2 depletion in sporadic ALS was hypothesised to be via SARM1 activation, recent data show that motor neuropathy with loss of distal neuromuscular junctions in *Stmn2* knockout mice is not Sarm1 dependent [131].

Current evidence support the idea that human variation in the form of SARM1 GoF mutants act as an additional disease risk factor rather than being directly causative in ALS (see Figure 5.1) [5, 9, 10, 12, 234]. Other pre-clinical studies strongly implicate that axon degeneration mechanisms controlled by SARM1 play a role in a wider range of neurodegenerative disorders, including e.g. Alzheimer's and Parkinson's disease [5, 234]. Complete NMNAT2 LoF, on the other hand, is incompatible with life in both mice and humans [8, 99, 100]. Milder LoF variants likely results in a spectrum of neuropathy phenotypes [7, 11], also discussed in chapter 4. Furthermore, NMNAT2 mRNA and protein levels are significantly reduced in the spinal cord of ALS patients, as well as brain tissue of AD patients [202, 249]. Moreover, the discontinued environmental toxin Vacor, an inhibitor of NMNAT2 enzyme activity [268], activates SARM1 via its metabolite VMN [76] and is associated to peripheral neuropathy in humans [269]. In fact, VMN shares structural similarity to the physiological SARM1 activator NMN and is the most potent activator of SARM1 reported so far [76].

In mice gene expression levels significantly impact axon vulnerability as a 70% NMNAT2 knockdown results in a sub-clinical effect. These mice show increased susceptibility to axonal stress, as well as early and age-dependent peripheral nerve axon defects [103]. It is, therefore, surprising that even though NMNAT2 coding variants can have profound effects no association with more common axonopathies has been found yet. Up to this point, we know of six patient cases where biallelic NMNAT2 mutations are associated to a detrimental

phenotype resembling the one observed in *Nmnat2*-null mice [7, 8, 99, 100], two of which are described in detail in chapter 4 [11]. As highlighted in chapter 1, pre-clinical data support an association of PAD with other disorders, apart from peripheral neuropathies and sporadic ALS [5].

5.2.3 The potential of WGS in PAD research

Genome wide association studies (GWAS) have been a particularly useful way of identifying specific genetic variations linked to common and complex disease. To date, however, known susceptibility loci identified by GWAS can only explain a subset of the heritability in neurological disease. Undetected rare and low-frequency variants likely contribute to this missing genetic component. The development of next generation sequencing tools accompanied by progressive cost reductions, especially whole-genome sequencing (WGS), enables further exploration and plays a crucial role in further elucidating pathogenic mechanism underlying neurodegeneration. With it comes the identification of countless rare variants of unknown significance which comes with several challenges, including reported statistical power limitation in assessing the burden of low-frequency variants.

In addition, most association studies focus on disease-promoting genetic variation while there is only limited reports focusing on variants protective against a disease. However, uncovering protective variants against neurodegeneration is equally important. This protective signal would be expected to be more prevalent in healthy individuals in comparison to diseased probands, suggestive of a protection against axonal insults. This idea resonates with the identification of SARM1 LoF variants [12] discussed in chapter 3. Moreover, several published studies show existing protective variants in protein-coding regions in Alzheimer's disease [270–273], as well as ALS [274]. A more recent collapsing genetic analysis using ProjectMine and the NYGC ALS consortium, for instance, identified rare variants in the IL18RAP 3'UTR which are protective against motor neuron disease reducing the risk by fivefold [275]. Limitations in the statistical power may be overcome with larger disease and control cohorts which are not currently available.

5.2.4 Aims and limitations of this chapter

Previously, chapter 3 and chapter 4 explored the functional consequences of naturally-occurring coding variation present in the human population. In contrast, this chapter uses large patient cohorts, including genomic data from diseased and healthy participants, as an appropriate starting point to generate hypotheses about how PAD is involved in human disease. The aim of this chapter was to screen genomic databases for SARM1 variants,

and assess their potential for GoF or LoF. Analysis was limited to SARM1 only, as data regarding its structure, activation and functional characterization of natural and artificial coding variants are extensive. This helps the functional prediction of newly-identified coding variants. It is acknowledged that the nature of the work presented is exploratory. The results serve hypotheses generation for future experimental work which was outside the scope of the timeline of my PhD. With the recruitment of bigger patient cohorts and the identification and functional characterization of additional variants, statistical power will increase in the future and facilitate moving forward in further elucidating how and which PAD gene variants influence human axon health.

Questions addressed:

- Are SARM1 variants present in the human databases UK Biobank and 100,000 Genomes Project? If so, do these coincide with other known variants that result in altered protein function?
- Are known SARM1 GoF variants over-represented in these disease cohorts?
- What is the frequency of total SARM1 LoF variants (predicted plus those confirmed in chapter 3) in control vs. disease groups?

5.3 Results

5.3.1 The use of the UK Biobank cohort to screen for human SARM1 coding missense variants

In the first part of this chapter, I explored sequencing data reported in the UK Biobank (UKB) which contains genomic information from 394,841 individuals of European ancestry (available on GeneBass: https://genebass.org/). Of note, UKB is a population-based cohort which recruited participants aged between 40-69 years during 2006-2010 from across the UK. It was designed as a large-scale prospective epidemiological resource which is not just confined to genetic data (genotyping, whole-exome and whole-genome) but also includes lifestyle and health information from half a million UK participants [276]. UKB is (in contrast to the 100,000 Genomes Project) not a disease-based source for genomic data and there is also evidence of a "healthy volunteer" selection bias [277] which is important to be kept in mind when interpreting the results of this chapter.

GeneBass is a platform that makes UKB sequencing data accessible and was used for the analysis performed here. The aim of GeneBass is to evaluate the impact of rare coding variation measured through whole exome sequencing, in particular their effects on human phenotypes. The dataset encompasses 4,529 phenotypes with gene-based and single-variant testing obtained from whole-exome sequencing across 394,841 individuals [278]. For the purpose of screening for SARM1 missense variants, I selected those phenotypes most relevant to neurodegenerative disorders and other human axonopathies. Inclusion criteria were disease prevalence (to increase statistical power) and an established involvement of SARM1 in corresponding animal model/s (see section 1.4.2) [5, 6]. In detail, the examined phenotypes were: Alzheimer's disease (AD), dementia, vascular dementia, Parkinson's disease (PD), ALS, facial nerve palsy, glaucoma, hereditary and idiopathic neuropathy, mononeuropathy, mononeuropathies of the upper limbs and mononeuropathies of the lower limbs. The findings are summarised in Table 5.1 - Table 5.11.

5.3.2 SARM1 CODING MISSENSE VARIATION PRESENT IN NEUROLOGICAL PHENOTYPES OF UK BIOBANK PARTICIPANTS

SARM1 domain	Coding variant[a]	rsID	Genomic location and change[b]	MAF[c]	Carriers		Known functional consequence
					Cases (1901)	Controls (392940)	
ARM	G109S	-	17:28372357 G>A	0	1	0	-
ARM	R121L	rs1289442893	17:28372394 G>T	0.0000147	1	11	-
ARM	**T218M***	rs371692238	17:28381385 C>T	0.0000147	1	30	-
ARM	L222V	rs782546001	17:28381396 C>G	0.0000294	1	45	-
ARM	R267W	rs11658194	17:28381531 C>T	0.0000147	1	130	strong GoF [9, 10]
ARM	**A294V****	rs372349604	17:28381613 C>T	0.0000147	1	77	-
ARM	N337D	rs375690432	17:28381741 A>G	0.0003822	1	270	partial LoF [9]
ARM	A341V	rs373458416	17:28381754 C>T	0.0001176	2	125	WT-like [9, 10]
SAM	Y501H	rs144613221	17:28385146 T>C	0.0029100	15	2795	-
TIR	R569C	rs571724138	17:28388248 C>T	0.0000294	2	95	LoF [12]
TIR	D637Y	rs1451417529	17:28388525 G>T	0	1	18	WT-like [10]
TIR	A719V	rs146812537	17:28396267 C>T	0.0004998	5	498	-

[a] Numbering in this and all following tables according to the canonical 724 amino acid long human SARM1.
[b] Numbering in this and all following tables according to the GRCh38 genome build.
[c] Minor allele frequency for European (non-Finnish) population in gnomAD v3.1.1 as the best ethnicity match in this and all other tables.

Table 5.1: **SARM1 coding variants in Parkinson's disease patients from UK Biobank, extracted from genebass.org.** *Variant also present in patient with hereditary motor and sensory neuropathy (HMSN) in UCL cohort. **Variant also found in patient in database GENESIS.

SARM1 domain	Coding variant	rsID	Genomic location and change	MAF	Carriers		Known functional consequence
					Cases (357)	Controls (394484)	
SAM	Y501H	rs144613221	17:28385146 T>C	0.0029100	2	2808	-

Table 5.2: **Single SARM1 coding variant found in both amyotrophic lateral sclerosis (ALS) (Phenotype ALS custom) and hereditary ataxia patients from UK Biobank, extracted from genebass.org.**

SARM1 domain	Coding variant	rsID	Genomic location and change	MAF	Carriers		Known functional consequence
					Cases (856)	Controls (393985)	
ARM	R267W	rs11658194	17:28381531 C>T	0.0000147	1	130	strong GoF [9, 10]
ARM	A309V	rs995788726	17:28381658 C>T	0.0000588	1	48	-
ARM	V331E	rs1555585331	17:28381724 T>A	0	1	19	strong GoF [9, 10]
ARM	A341V	rs373458416	17:28381754 C>T	0.0001176	1	126	WT-like [9, 10]
SAM	Q500R	rs1555585828	17:28385144 A>G	0	1	1	-
SAM	Y501H	rs144613221	17:28385146 T>C	0.0029100	12	2798	-
SAM	S558R	rs938798379	17:28388217 T>G	0.0000147	1	10	WT-like [10]

Table 5.3: **SARM1 coding variants in Alzheimer's disease patients from UK Biobank, extracted from genebass.org.**

SARM1 domain	Coding variant	rsID	Genomic location and change	MAF	Carriers		Known functional consequence
					Cases (1091)	Controls (392940)	
ARM	L138V	rs1555584211	17:28372444 T>G	0	1	21	-
ARM	R162G	-	17:28381216 C>G	0	1	0	-
ARM	A275V	rs376587698	17:28381556 C>T	0.0000294	1	228	WT-like [9, 10]
ARM	A309V	rs995788726	17:28381658 C>T	0.0000588	1	48	-
ARM	R310H	rs369186722	17:28381661 G>A	0.0001617	1	261	partial LoF [9]
ARM	A341V	rs373458416	17:28381754 C>T	0.0001176	1	126	WT-like [9, 10]
SAM	Q500R	rs1555585828	17:28385144 A>G	0	1	1	-
SAM	Y501H	rs144613221	17:28385146 T>C	0.0029100	11	2799	-
SAM	Y503C	rs1555585833	17:28385153 A>G	0	1	21	-
SAM	S558R	rs938798379	17:28388217 T>G	0.0000147	1	10	WT-like [10]
TIR	R697G	rs372946021	17:28396200 C>G	0	1	55	R697C is WT-like [10]
TIR	A719V	rs146812537	17:28396267 C>T	0.0004998	1	502	-
TIR	T724I	rs567632194	17:28396282 C>T	0.0000441	1	12	-

Table 5.4: **SARM1 coding variants in patients with unspecified dementia from UK Biobank, extracted from genebass.org.**

SARM1 domain	Coding variant	rsID	Genomic location and change	MAF	Carriers		Known functional consequence
					Cases (538)	Controls (394303)	
ARM	R121L	rs1289442893	17:28372394 G>T	0.0000147	2	10	-
ARM	V246I	-	17:28381468 G>A	0	1	6	-
SAM	Y501H	rs144613221	17:28385146 T>C	0.0029100	5	2805	-
SAM	Y503C	rs1555585833	17:28385153 A>G	0	1	21	-
TIR	D637Y	rs1451417529	17:28388525 G>T	0	1	18	WT-like

Table 5.5: **SARM1 coding variants in patients with vascular dementia from UK Biobank, extracted from genebass.org.**

SARM1 domain	Coding variant	rsID	Genomic location and change	MAF	Carriers		Known functional consequence
					Cases (351)	Controls (394490)	
ARM	R267W	rs11658194	17:28381531 C>T	0.0000147	1	130	strong GoF [9, 10]
SAM	D483E	rs377210302	17:28385094 C>A	0.0000147	1	37	WT-like [10]
SAM	A488E	rs782228906	17:28385108 C>A	0.0001176	1	89	WT-like [10]
SAM	Y501H	rs144613221	17:28385146 T>C	0.0029100	3	2807	-
TIR	A719V	rs146812537	17:28396267 C>T	0.0004998	1	502	-

Table 5.6: **SARM1 coding variants in patients with hereditary and idiopathic neuropathy from UK Biobank, extracted from genebass.org**

SARM1 domain	Coding variant	rsID	Genomic location and change	MAF	Carriers		Known functional consequence
					Cases (233)	Controls (394608)	
ARM	R267W	rs11658194	17:28381531 C>T	0.0000147	3	128	GoF [9, 10]
SAM	R463L	-	17:28384924 G>T	0	1	3	-
TIR	A719V	rs146812537	17:28396267 C>T	0.0004998	2	501	-

Table 5.7: **SARM1 coding variants in patients with "mononeuropathy in diseases classified" elsewhere from UK Biobank, extracted from genebass.org**

SARM1 domain	Coding variant	rsID	Genomic location and change	MAF	Carriers		Known functional consequence
					Cases (18076)	Controls (376765)	
MTS	A17P	rs782269124	17:28372081 G>C	0.0002353	6	69	-
MTS	P23A	-	17:28372099 C>G	0	1	16	-
MTS	W42R	rs913719958	17:28372156 T>C	0.0000294	1	19	-
MTS	P50L	-	17:28372181 C>T	0	1	3	-
MTS	E52K	-	17:28372186 G>A	0	1	6	-
ARM	E101K	-	17:28372333 G>A	0	1	3	
ARM	V112I	rs1032963037	17:28372366 G>A	0.0000147	2	28	weak GoF [9]
ARM	R131G	-	17:28372423 C>G	0.0000147	1	10	WT-like [9]
ARM	L138V	rs1555584211	17:28372444 T>G	0	1	21	-
ARM	V178I	-	17:28381264 G>A	0	1	2	-
ARM	A181T	-	17:28381273 G>A	0	2	3	-
ARM	M191L	-	17:28381303 A>T	0	1	1	-
ARM	E197D	-	17:28381323 G>T	0	1	6	-
ARM	T198A	-	17:28381324 A>G	0.0000147	1	13	-
ARM	R201K	rs138813409	17:28381334 G>A	0.0000147	1	0	-
ARM	L222V	rs782546001	17:28381396 C>G	0.0000294	5	41	-
ARM	Δ229-235	rs782325355	28381417_37del	0.000059	1	24	strong GoF [9]
ARM	R267W	rs11658194	17:28381531 C>T	0.0000147	7	124	strong GoF [9, 10]
ARM	A275V	rs376587698	17:28381556 C>T	0.0000294	11	218	WT-like [9, 10]
ARM	K281R	rs782032148	17:28381574 A>G	0.0000588	6	83	-
ARM	V283M	rs1555585276	17:28381579 G>A	0	1	32	-
ARM	A294V	rs372349604	17:28381613 C>T	0.0000147	4	74	-
ARM	L299P	-	17:28381628 T>C	0.0000147	1	3	-
ARM	A309V	rs995788726	17:28381658 C>T	0.0000588	1	48	-
ARM	R310H	rs369186722	17:28381661 G>A	0.0001617	11	251	partial LoF [9]
ARM	L312Q	-	17:28381667 T>A	0	1	6	-
ARM	V331E	rs1555585331	17:28381724 T>A	0	2	18	strong GoF [9, 10]
ARM	N337D	rs375690432	17:28381741 A>G	0.0003822	14	257	partial LoF [9]
ARM	E340L	rs781854217	17:28381750 G>A	0.0000588	8	49	E340K strong GoF [9, 10]
ARM	A341V	rs373458416	17:28381754 C>T	0.0001176	6	121	WT-like [9, 10]
ARM	Y348C	rs530896320	17:28381775 A>G	0.0000294	2	20	-
ARM	I355M	rs782487571	17:28381797 C>G	0.0000588	2	22	-
ARM	L358R	rs1555585352	17:28381805 T>G	0.0000147	3	8	-
ARM	S366G	rs782804317	17:28384363 A>G	0	2	11	-
ARM	T385A	-	17:28384420 A>G	0	1	4	GoF [9, 10]
ARM	A403G	rs782706244	17:28384475 G>A	0.0000147	1	7	-
SAM	E431G	rs1555585662	17:28384559 A>G	0	1	12	-
SAM	D439G	-	17:28384852 A>G	0	1	10	-
SAM	L442P	-	17:28384861 T>C	0	1	2	LoF [110]
SAM	N478S	-	17:28385078 A>G	0	1	4	-
SAM	D483E	rs377210302	17:28385094 C>A	0.0000147	1	37	WT-like [10]
SAM	A488E	rs782228906	17:28385108 C>A	0.0001176	2	88	WT-like [10]
SAM	A488V	rs782228906	17:28385108 C>T	0.0000147	2	16	WT-like [10]
SAM	Y501H	rs144613221	17:28385146 T>C	0.00291	125	2685	-
SAM	T502P	rs782421919	17:28385149 A>C	0.0000735	1	52	strong GoF [10]
SAM	H547Q	rs1555586323	17:28388184 C>A	0	1	10	-
SAM	S558N	-	17:28388216 G>A	0	1	2	WT-like [10]
TIR	R569C	rs571724138	17:28388248 C>T	0.0000294	5	92	LoF [12]
TIR	R570Q	rs539229444	17:28388252 G>A	0.0001029	1	22	LoF [12]
TIR	S590G	-	17:28388384 A>G	0	1	6	-
TIR	S590I	rs782491086	17:28388385 G>T	0	1	3	-
TIR	A600V	-	17:28388415 C>T	0	1	18	A600H is LoF [110]
TIR	K602N	rs35201495	17:28388422 G>C	0.0000147	1	11	WT-like [12]
TIR	R615H	rs782753946	17:28388460 G>A	0.0000441	3	14	WT-like [10]
TIR	D637Y	rs1451417529	17:28388525 G>T	0	1	18	WT-like [10]
TIR	V654M	rs782225125	17:28395941 G>A	0	4	44	WT-like [10]
TIR	E664K	rs543954200	17:28395971 G>A	0.0000294	2	26	E664Q is WT-like [279]
TIR	N679D	-	17:28396016 A>G	0	1	1	-
TIR	S684F	rs782256561	17:28396162 C>T	0.0000441	1	14	LoF [12]
TIR	E693D	-	17:28396190 G>C	0	1	9	weak GoF [10]
TIR	I696V	-	17:28396197 A>G	0	1	11	-
TIR	R697C	rs372946020	17:28396200 C>T	0.0000441	1	27	WT-like [10]
TIR	R697G	rs372946021	17:28396200 C>G	0	4	52	R697C is WT-like [10]
TIR	R702S	-	17:28396215 C>A	0	1	0	-
TIR	R705W	rs782438923	17:28396224 C>T	0.0000294	3	14	-
TIR	D706V	rs1027658221	17:28396228 A>T	0	1	5	-
TIR	A719V	rs146812537	17:28396267 C>T	0.0000941	22	481	-
TIR	P720T	-	17:28396269 C>A	0	1	4	-
TIR	A719V	rs146812537	17:28396267 C>T	0.0004998	1	12	-

Table 5.8: **SARM1 coding variants in patients with upper limb mononeuropathy from UK Biobank**

SARM1 domain	Coding variant	rsID	Genomic location and change	MAF	Carriers		Known functional consequence
					Cases (3923)	Controls (390918)	
MTS	A17P	rs782269124	17:28372081 G>C	0.0002353	1	74	-
ARM	L138V	rs1555584211	17:28372444 T>G	0	1	21	-
ARM	A145G	rs970546135	17:28372466 C>G	0.0000294	1	8	-
ARM	R267W	rs11658194	17:28381531 C>T	0.0000147	3	128	strong GoF [9, 10]
ARM	A275V	rs376587698	17:28381556 C>T	0.0000294	3	226	WT-like [9, 10]
ARM	K281R	rs782032148	17:28381574 A>G	0.0000588	2	87	-
ARM	**A294V***	rs372349604	17:28381613 C>T	0.0000147	2	76	-
ARM	R307P	rs1016678586	17-28381652 G>C	0.0000147	1	13	-
ARM	A309V	rs995788726	17:28381658 C>T	0.0000588	3	46	-
ARM	R310H	rs369186722	17:28381661 G>A	0.0001617	3	259	partial LoF [9]
ARM	L312Q	-	17:28381667 T>A	0	1	6	-
ARM	N337D	rs375690432	17:28381741 A>G	0.0003822	4	267	partial LoF [9]
ARM	A341V	rs373458416	17:28381754 C>T	0.0001176	2	125	WT-like [9]
ARM	Y348C	rs530896320	17:28381775 A>G	0.0000294	1	21	-
SAM	A488E	rs782228906	17:28385108 C>A	0.0001176	2	88	WT-like [10]
SAM	Y501H	rs144613221	17:28385146 T>C	0.00291	34	2776	-
SAM	G509V	rs1307126718	17:28385171 G>T	0	1	24	-
SAM	R535G	-	17:28385248 C>G	0	1	1	-
SAM	H547Q	rs1555586323	17:28388184 C>A	0	1	10	-
TIR	R615H	rs782753946	17:28388460 G>A	0.0000441	1	16	WT-like [10]
TIR	G650S	rs557710063	17-28395929 G>A	0.0000294	2	18	-
TIR	S684F	rs782256561	17:28396162 C>T	0.0000441	1	14	LoF [12]
TIR	R697G	rs372946021	17:28396200 C>G	0	1	55	WT-like [10]
TIR	R705W	rs782438923	17:28396224 C>T	0.0000294	1	16	-
TIR	A719V	rs146812537	17:28396267 C>T	0.0004998	7	496	-

Table 5.9: **SARM1 coding variants in patients with a mononeuropathy of the lower limb from UK Biobank, extracted from genebass.org.** *Variant also found in patient in database GENESIS.

SARM1 domain	Coding variant	rsID	Genomic location and change	MAF	Carriers		Known functional consequence
					Cases (538)	Controls (394303)	
MTS	P23A	-	17:28372099 C>G	0	1	16	-
ARM	V112I	rs1032963037	17:28372366 G>A	0.000015	1	29	weak GoF for basal NADase activity [9]
ARM	R159C	-	17:28381207 C>T	0	1	0	-
ARM	D209G	rs1555585201	17:28381358 A>G	0	1	7	-
ARM	T218M	rs371692238	17:28381385 C>T	0.000015	1	30	-
ARM	G237W	rs782357936	17:28381441 G>T	0	1	2	-
ARM	R267W	rs11658194	17:28381531 C>T	0.000015	1	130	strong GoF [9, 10]
ARM	A275V	rs376587698	17:28381556 C>T	0.000029	3	226	WT-like [9, 10]
ARM	K281R	rs782032148	17:28381574 A>G	0.000059	1	88	-
ARM	S290W	rs782769243	17:28381601 C>G	0.000073	1	40	-
ARM	R307P	rs1016678586	17:28381652 G>C	0.000015	1	13	-
ARM	A309V	rs995788726	17:28381658 C>T	0.000059	1	48	-
ARM	R310H	rs369186722	17:28381661 G>A	0.000162	3	259	partial LoF [9]
ARM	A315T	rs951188002	17:28381675 G>A	0	1	0	-
ARM	N337D	rs375690432	17:28381741 A>G	0.000382	1	270	partial LoF [9]
ARM	E340L	rs781854217	17:28381750 G>A	0.000059	2	55	strong GoF [9]
ARM	A341V	rs373458416	17:28381754 C>T	0.000118	3	124	WT-like [9, 10]
ARM	G360D	rs1427817559	17:28381811 G>A	0	1	1	-
SAM	Y501H	rs144613221	17:28385146 T>C	0.002910	13	2797	-
SAM	T540S	-	17:28385263 A>T	0	1	0	-
TIR	V667D	rs781912512	17:28395981 T>A	0	1	5	-
TIR	I696V	-	17:28396197 A>G	0	1	11	-
TIR	A719V	rs146812537	17:28396267 C>T	0.000500	4	499	-

Table 5.10: **SARM1 coding variants in patients with facial nerve palsy from UK Biobank, extracted from genebass.org.**

SARM1 domain	Coding variant	rsID	Genomic location and change	MAF	Carriers		Known functional consequence
					Cases (3923)	Controls (390918)	
MTS	A17P	rs782269124	17:28372081 G>C	0.0002353	2	73	-
ARM	R67S	-	17:28372231 C>A	0	1	0	-
ARM	A75D	rs1555584155	17:28372256 C>A	0	2	14	-
ARM	L92V	rs1171817944	17:28372306 C>G	0	2	4	-
ARM	R110C	rs782798088	17:28372360 C>T	0	1	16	-
ARM	V112I	rs1032963037	17:28372366 G>A	0.0000147	1	29	weak GoF
ARM	R121L	rs1289442893	17:28372394 G>T	0.0000147	1	11	-
ARM	L138V	rs1555584211	17:28372444 T>G	0	1	21	-
ARM	V178I	-	17:28381264 G>A	0	1	2	-
ARM	M191L	-	17:28381303 A>T	0	1	1	-
ARM	K193T	-	17:28381310 A>C	0	1	0	-
ARM	E196G	-	17:28381319 A>G	0	1	9	-
ARM	G207S	-	17:28381351 G>A	0	1	9	-
ARM	L222V	rs782546001	17:28381396 C>G	0.0000294	3	43	-
ARM	V241M	rs1333588274	17:28381453 G>A	0	1	11	-
ARM	R267W	rs11658194	17:28381531 C>T	0.0000147	2	129	strong GoF
ARM	A275V	rs376587698	17:28381556 C>T	0.0000294	8	221	WT-like
ARM	K281R	rs782032148	17:28381574 A>G	0.0000588	1	88	-
ARM	V283M	rs1555585276	17:28381579 G>A	0	2	31	-
ARM	A294V	rs372349604	17:28381613 C>T	0.0000147	1	77	-
ARM	L299P	-	17:28381628 T>C	0.0000147	1	3	-
ARM	R307P	rs1016678586	17:28381652 G>C	0.0000147	1	13	-
ARM	A309V	rs995788726	17:28381658 C>T	0.0000588	1	48	-
ARM	R310H	rs369186722	17:28381661 G>A	0.0001617	10	252	partial LoF
ARM	A315T	rs951188002	17:28381675 G>A	0	1	0	-
ARM	N337D	rs375690432	17:28381741 A>G	0.0003822	9	262	partial LoF
ARM	E340L	rs781854217	17:28381750 G>A	0.0000588	1	56	strong GoF
ARM	A341V	rs373458416	17:28381754 C>T	0.0001176	2	125	WT-like
ARM	G360D	rs1427817559	17:28381811 G>A	0	1	1	-
ARM	V364M	rs1555585623	17:28384357 G>A	0	1	0	-
ARM	T385A	-	17:28384420 A>G	0	1	4	GoF
ARM	A403G	rs782706244	17:28384475 G>A	0.0000147	1	7	WT-like [10]
SAM	V417G	-	17:28384517 T>G	0	1	1	-
SAM	D483E	rs377210302	17:28385094 C>A	0.0000147	1	37	WT-like [10]
SAM	A488E	rs782228906	17:28385108 C>A	0.0001176	3	87	WT-like [10]
SAM	A488V	rs782228906	17:28385108 C>T	0.0000147	1	17	WT-like [10]
SAM	P496A	-	17:28385132 C>G	0	1	10	-
SAM	Y501H	rs144613221	17:28385146 T>C	0.00291	72	2738	-
SAM	T502P	rs782421919	17:28385149 A>C	0.0000735	3	50	GoF [10]
SAM	G509V	rs1307126718	17:28385171 G>T	0	1	24	-
SAM	R535G	-	17:28385248 C>G	0	1	1	-
SAM	P549L	rs1241475032	17:28388189 C>T	0.0000147	1	4	WT-like [12]
TIR	S590G	-	17:28388384 A>G	0	1	6	-
TIR	E596Q	rs1555586409	17:28388402 G>C	0	1	2	WT-like [279]
TIR	L602N	rs35201495	17:28388422 G>C	0.0000147	1	11	WT-like [12]
TIR	R615H	rs782753946	17:28388460 G>A	0.0000441	1	16	WT-like [10]
TIR	L626P	rs368394015	17:28388493T>C	0	2	14	-
TIR	M630L	-	17:28388504 A>T	0	2	1	WT-like [120]
TIR	D637Y	rs1451417529	17:28388525 G>T	0	1	18	WT-like [10]
TIR	G650D	rs782196355	17:28395930 G>A	0	1	2	-
TIR	V654M	rs782225125	17>28395941 G>A	0	3	45	WT-like [10]
TIR	I657V	rs558864070	17:28395950 A>G	0	1	8	-
TIR	I696V	rs782022324	17:28396197 A>G	0	1	11	-
TIR	R697C	rs372946020	17:28396200 C>T	0.0000441	1	27	WT-like [10]
TIR	R697G	rs372946021	17:28396200 C>G	0	1	55	WT-like [10]
TIR	R697H	rs544071937	17:28396201 G>A	0	1	6	WT-like [10]
TIR	A702C	rs781850558	17:28396215 C>T	0	1	15	WT-like [10]
TIR	R705Q	rs782584686	17:28396225 G>A	0.0000294	1	16	-
TIR	D706V	rs1027658221	17:28396228 A>T	0	2	4	-
TIR	A719V	rs146812537	17:28396267 C>T	0.0000941	18	485	-
TIR	T724I	rs567632194	17:28396282 C>T	0.0000441	2	11	-

Table 5.11: **SARM1 coding variants in patients with glaucoma (Phenotype: H40 Glaucoma) from UK Biobank, extracted from genebass.org.** *Variant also found in patient in database GENESIS.

5.3.3 SARM1 LoF variant frequencies in axonopathy cohorts within the UK Biobank

Chapter 3 provides a full *in vitro* characterization of a selected group of SARM1 variants, the majority of which resulted in clear LoF where many of them influence SARM1 NADase activity and axon survival, likely reflecting protective effects in disease, while two confer dominant loss-of-function effects suggesting even stronger effects on disease risk [227]. In support of these proposed effects in disease, axons of Sarm1 hemizygous mice are partially protected in a range of disease models [217].

Consequently, the question occurred whether SARM1 LoF variants are present in disease and control cohorts within UKB. If so, do the observed frequencies match those reported in the population database gnomAD? [226]. To address this question, both confirmed SARM1 LoF alleles characterised in chapter 3, as well as predicted LoF variants (stop gained, start lost, splice donor, splice acceptor or frameshift) were taken into consideration in order to increase statistical power (see Table 5.12). Of note, SARM1 missense variants predicted to result in LoF by *in silico* prediction tools (e.g. SIFT, PolyPhen2) were not taken into consideration. While one could reason that SARM1 LoF variants may be over-represented/enriched within control groups, this is highly unlikely. Lack of a specific disease will not be due to the presence of SARM1 LoF variation but rather because another key genetic risk factors is missing [280]. As a result, the marginal increase in SARM1 LoF alleles within a control group may not be detectable. In contrast, "missing" LoF cases among a disease group may well be. This served as a rationale for the LoF screen.

I therefore asked the question whether carriers of SARM1 LoF variants have a lower risk of a neurological phenotype than individuals who are in the respective control groups. The findings are summarised in Table 5.12. Interestingly, the risk for predicted SARM1 LoF within the ADES dataset (Alzheimer's disease-specific, not part of the UK Biobank) is 3x lower than the general risk in the control group. Predicted LoF variants in Project MinE, a platform with genomic data from ALS patients, are 7x under-represented compared to the control cohort. These differences are even more pronounced when comparing Total LoF frequencies. Total LoF variants in Parkinson's disease are 2x under-represented compared to the control cohort. While these numbers are too small to make a firm conclusion, these findings support the hypothesis that naturally occurring SARM1 LoF variants could be associated with a decreased risk for neurodegeneration.

	Disease cohort	Numbers	Stop gained	Start lost	Splice acceptor	splice donor	Frameshift	Total Predicted LoF	Total LoF	**Expected frequency (Predicted LoF)**	**Expected frequency (Total LoF)**
Cases	Parkinson's disease	1901	0	0	0	0	0	0	1	0	0.00053
	ALS	357	0	0	0	0	0	0	0	0	0
	ALS (ProjectMine)	4366	1	0	0	0	0	1	1	0.00023	0.00023
	Hereditary ataxia	245	0	0	0	0	0	0	0	0	0
	Alzheimer's disease	900	1	0	0	0	0	1	1	0.00111	0.00111
	Unspecified dementia	1091	0	0	0	0	0	0	0	0	0
	Dementia associated to Alzheimer's disease	472	0	0	0	0	0	0	0	0	0
	Vascular dementia	538	0	0	0	0	0	0	0	0	0
	Alzheimer's disease (ADES)	8717	1	0	1	0	0	2	2	0.00023	0.00023
	Hereditary and idiopathic neuropathy	351	0	0	0	0	0	0	0	0	0
	Mononeuropathy classified elsewhere	233	0	0	0	0	0	0	0	0	0
	Other mononeuropathies	657	0	0	0	0	0	0	0	0	0
	Mononeuropathy of upper limb	18076	3	3	3	3	0	12	14	0.00066	0.00077
	Mononeuropathy of lower limb	3923	2	0	0	4	0	6	7	0.00153	0.00178
	Facial nerve disorders	2486	0	0	0	0	0	0	0	0	0
	Glaucoma	11588	7	1	1	2	0	11	11	0.00095	0.00095
	Total	57957	17	4	5	9	0	35	39		
Con-trols	Parkinson's disease	392940	122	30	43	61	22	278	422	0.00071	0.00107
	ALS	394484	122	30	43	61	22	278	424	0.00070	0.00107
	ALS (ProjectMine)	1832	1	0	0	1	1	3	-	0.00164	-
	Hereditary ataxia	394596	122	30	43	61	22	278	424	0.00070	0.00107
	Alzheimer's disease	393941	121	30	43	61	22	277	423	0.00070	0.00107
	Unspecified dementia	393750	122	30	43	61	22	278	424	0.00071	0.00108
	Dementia associated to Alzheimer's disease	394369	122	30	43	61	22	278	424	0.00070	0.00108
	Vascular dementia	394303	122	30	43	61	22	278	424	0.00071	0.00108
	Alzheimer's disease (ADES)	8942	1	0	1	0	4	6	-	0.00067	-
	Hereditary and idiopathic neuropathy	394490	122	30	43	61	22	278	424	0.00070	0.00107
	Mononeuropathy classified elsewhere	394608	122	30	43	61	22	278	424	0.00070	0.00107
	Other mononeuropathies	394184	122	30	43	61	22	278	424	0.00071	0.00108
	Mononeuropathy of upper limb	376765	119	27	40	58	22	266	303	0.00071	0.00080
	Mononeuropathy of lower limb	390918	120	30	43	57	22	272	417	0.00070	0.00107
	Facial nerve disorders	392355	122	30	43	61	22	278	406	0.00071	0.00103
	Glaucoma	383253	115	29	42	59	22	267	411	0.00070	0.00107
	Total	-	1855	454	653	925	342	4229	6393		

Table 5.12: **Occurrences of *SARM1* alleles encoding predicted and confirmed LoF variants in disease cohorts in the UK Biobank summarised.** Expected frequencies of Predicted LoF and Total LoF are calculated by dividing the number of Total Predicted LoF or Total LoF by the size of the respective disease cohort (Numbers). These frequencies are compared between cases and controls, respectively. Of note, disease cohorts where frequencies are 0 cannot be compared to controls.

5.3.4 The use of the 100,000 Genomes Project to screen for human SARM1 coding missense variants

Most patients with rare diseases remain without a molecular diagnosis after standard diagnostic testing [281–283]. To address this lack of diagnosis, the 100,000 Genomes Project (GEL) was launched in 2013 to apply whole-genome sequencing to the study and diagnosis of rare diseases and cancer patients [284]. In the second part of this chapter, I analysed sequencing data from a total of 3,998 patients with a suspected neurological condition that were recruited into the GEL programme between 2015 and 2018.

Sequencing data (main programme data release V11 2021-09-30) was analysed from probands recruited under the following neurological disease categories (Table 5.13 and Table 5.13): motor and sensory disorders of the PNS (n = 812), motor disorders of the CNS (n = 2,138) and neurodegenerative disorders (n = 1,048) (Figure 5.2). All analysis related to the GEL datasets were performed within a secure workspace named 'Research Environment'. Participants' sequencing data were analysed using the 'LabKey' data management software and the interactive variant analysis (IVA) platform. Data of participants with diseases belonging to either of the three sub groups (Figure 5.2) were filtered for missense SARM1 variants. Of note, (1) common variants with a gnomAD MAF > 0.01, unaffected relatives and participant cases marked as "solved" with variants in alternative genes were excluded. The findings are summarised in Table 5.14 - Table 5.21.

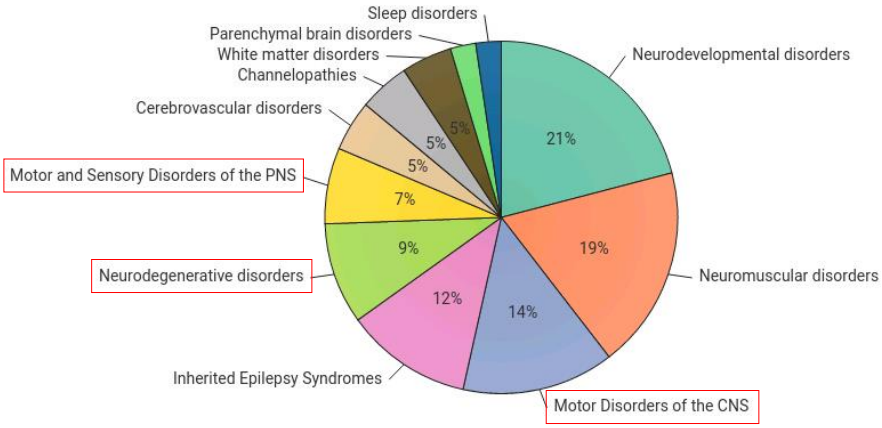


Figure 5.2: **Pie chart of neurological disease sub groups analysed within 100,000 Genomes Project.** Analysed sub groups are highlighted by a red box.

Disease sub group	Normalised specific disease	Participants
Motor disorders of the CNS	Early onset dystonia	404
	Hereditary ataxia	1143
	Herediatary spastic paraplegia	591
Motor and Sensory disorders of the PNS	CMT disease	701
	Paediatric motor neuronopathies	111
Neurodegenerative disorders	ALS or motor neuron disease	100
	Complex Parkinsonism (includes pallido-pyramidal syndromes)	208
	Early onset and familial Parkinson's Disease	568
	Early onset dementia	172
Total		3998

Table 5.13: **100,000 Genomes selected for rare SARM1 coding variant analysis.**

5.3.5 SARM1 coding missense variation present in rare diseases within the 100,000 Genomes Project

SARM1 domain	Coding variant	rsID	Genomic location and change	MAF	Cases (568)	Known functional consequence
MTS	A17P	rs782269124	17:28372081 G>C	0.0002353	1	-
MTS	A45T	rs782593684	17:28372165 G>A	0	1	-
ARM	A181T	rs1467944039	17:28381273 G>C	0.0000147	1	-
ARM	I187M	-	17:28381292 T>A	-	1	-
ARM	A275V	rs376587698	17:28381556 C>T	0.0000290	1	WT-like [9, 10]
ARM	S290W	rs782769243	17:28381601 C>G	0.0000735	1	-
ARM	A309V	rs995788726	17:28381658 C>T	0.0000588	1	-
ARM	R310H	rs369186722	17:28381661 G>A	0.0001617	1	partial LoF [9]
ARM	Y348C	rs530896320	17:28381775 A>G	0.0000294	2	-
ARM	K375T	rs782437027	17:28384391 A>C	0	2	-
ARM	T385N	rs147409181	17:28384421 C>A	0	1	T385A is GoF [9, 10]
SAM	S408P	rs113535815	17:28384489 T>C	0	1	-
SAM	E416K	rs147156050	17:28384513 G>A	0	1	partial LoF [12]
SAM	Y501H	rs144613221	17:28385146 T>C	0.00291	1	-
TIR	K602N	rs35201495	17:28388422 G>T	0.0000147	1	WT-like [12]

Table 5.14: **SARM1 missense variants patients with EO and familial Parkinson's disease in the 100k Genomes database.**

SARM1 domain	Coding variant	rsID	Genomic location and change	MAF	Cases (1143)	Known functional consequence
MTS	R48H	-	17:28372081 G>C	0	1	-
ARM	A275V	rs376587698	17:28381556 C>T	0.0000290	1	WT-like [9, 10]
ARM	K281R	rs782032148	17:28381574 A>G	0.0000588	1	-
ARM	A309V	rs995788726	17:28381658 C>T	0.0000588	1	-
ARM	R310H	rs369186722	17:28381661 G>A	0.0001617	1	partial LoF [9]
ARM	N337D	rs375690432	17:28381741 A>G	0.0003820	2	partial LoF [9]
TIR	A719V	rs146812537	17:28396267 C>T	0.0004998	1	-

Table 5.15: **SARM1 missense variants patients with hereditary ataxia in the 100k Genomes database.**

SARM1 domain	Coding variant	rsID	Genomic location and change	MAF	Cases (591)	Known functional consequence
ARM	E196G	-	17:28381319 A>G	0	1	-
ARM	A275V	rs376587698	17:28381556 C>T	0.0000290	1	WT-like [9, 10]
ARM	V283M	rs1555585276	17:28381579 G>A	0	1	-
ARM	R310H	rs369186722	17:28381661 G>A	0.0001617	1	partial LoF [9]
ARM	A346T	rs781882550	17:28381768 G>A	0.0000147	1	-
SAM	T475S	-	17:28385069 C>A	0	1	-
TIR	R569C	rs571724138	17:28388248 C>T	0.0000294	1	LoF [12]
TIR	K651R	rs1555587730	17:28395933 A>G	0.0000147	2	-
TIR	R697C	rs372946020	17:28396200 C>T	0.0000441	1	WT-like [10]

Table 5.16: **SARM1 missense variants patients with hereditary spastic paraplegia in the 100k Genomes database.**

SARM1 domain	Coding variant	rsID	Genomic location and change	MAF	Cases (701)	Known functional consequence
ARM	A301S	rs782606059	17:28381633 G>T	0.000117561	72	WT-like [9]
ARM	N337D	rs375690432	17:28381741 A>G	0.0003820	64	partial LoF [9]
SAM	C430ter	rs781927743	17:28384557 C>A	0	57	
TIR	L626P	rs368394015	17:28388493T>C	0	45	-
TIR	R697C	rs372946020	17:28396200 C>T	0.0000441	72	

Table 5.17: **SARM1 missense variants patients with Charcot-Marie-Tooth disease in the 100k Genomes database.**

SARM1 domain	Coding variant	rsID	Genomic location and change	MAF	Cases (404)	Known functional consequence
MTS	A9P	rs1224579416	17:28372057 G>C	0.0000294	1	-
ARM	A341V	rs373458416	17:28381754 C>T	0.0001176	1	WT-like [9, 10]
TIR	A719V	rs146812537	17:28396267 C>T	0.0000941	1	-

Table 5.18: **SARM1 missense variants patients with early-onset dystonia in the 100k Genomes database.**

SARM1 domain	Coding variant	rsID	Genomic location and change	MAF	Cases (111)	Known functional consequence
SAM	S408P	rs113535815	17:28384489 T>C	0	1	-
SAM	V582L	-	17:28388399 G>A	0.0000000	1 -	

Table 5.19: **SARM1 missense variants patients with paediatric motor neuronopathies in the 100k Genomes database.**

SARM1 domain	Coding variant	rsID	Genomic location and change	MAF	Cases (100)	Known functional consequence
ARM	S316R	rs782362670	17:28381680 C>A	0	1	-
SAM	S408P	rs113535815	17:28384489 T>C	0	1	-

Table 5.20: **SARM1 missense variants patients with ALS and other motor neuron disease in the 100k Genomes database.**

SARM1 domain	Coding variant	rsID	Genomic location and change	MAF	Cases (172)	Known functional consequence
ARM	A181T	rs1467944039	17:28381273 G>C	0.0000147	1	-

Table 5.21: **SARM1 missense variants patients with early-onset dementia in the 100k Genomes database.**

5.4 Discussion

5.4.1 Limitations of this chapter

In summary, large patient cohorts, including WGS data from diseased and healthy participants, were screened for rare SARM1 coding variants, and the identified missense mutations compared to the location of known SARM1 GoF and LoF variants. It is acknowledged that the nature of the work in this chapter is an exploratory one. The results serve hypotheses generation for future experimental work. With the recruitment of bigger patient cohorts and the identification and functional characterisation of additional SARM1 variants, statistical power will increase over time and facilitate moving forward in further elucidating how and which PAD gene variants influence human axon health.

5.4.2 Suggested future experimental work

Some of the identified variants can be prioritised for future experimental studies, excluding those which are too common in gnomAD and those present in cases with other identifiable causes. Variants of unknown significance occurring more than once across different disease groups together with variants altering conserved amino acids or important protein regions (e.g., SARM1 catalytic TIR site or autoinhibitory ARM domain) should be prioritised. Functional tests will include previously described assays (chapter 3) in mouse primary neurons and testing of protein stability and enzyme activity. These methods would have a higher throughput and lower cost than follow-up iPSC and knock-in mouse studies. In addition, other databases could be screened to increase statistical significance of any disease association discovered. These could include the following patient databases: The GENESIS Project (mostly CMT-related) [285], Project MINE (ALS research) [286], ClinVar (published relationships among human variations and phenotypes) [287], RD-Connect [288], DECIPHER [289] and MyGene2 (all rare diseases).

5.4.3 The role of SARM1 LoF in disease

While the observed reduced numbers of SARM1 LoF variants in ALS and AD cohorts are too small to make a firm conclusion, they are promising if the ratios hold up. A relative paucity of carriers of SARM1 alleles encoding LoF variants is predicted among individuals with axon pathologies compared to control groups [12]. Underrepresentation of LoF variants in AD patients would, for instance, further support the hypothesis that SARM1 contributes to the disease. If SARM1 LoF variants were to be underrepresented in disease cohorts, this would suggest that lowering SARM1 activity is a useful therapeutic

strategy in AD and related disorders [234]. Confirmation of this was not possible due to the low frequency of the confirmed LoF alleles and the restricted size of the UKB and GEL patient cohorts used. Nevertheless, this will become possible in the future as more SARM1 LoF variants are identified, and as disease cohorts increase. As such, it is predicted that carriers of SARM1 LoF alleles could have varying degrees of reduced susceptibility to different neurological conditions. It is also likely that any protective effect would only be detectable in a population where disease is expected, for example by modifying age-of-onset in carriers of pathogenic mutations. Such scenarios could be:

- Long-term diabetes mellitus without occurrence of neuropathy
- Traumatic brain injury with 'good' outcome
- ApoE4 genotype without AD, especially if beyond average age of onset with this genotyp
- PIB positive, elderly but cognitively normal
- Recurring multiple sclerosis relapses without entering progressive phase

Of note, additional functional analysis will be required in the future.

6

Discussion

6.1 Summary of findings

The results presented in this thesis show that:

- SARM1 LoF variants are present in the human population and influence axonal health *in vitro*. Those showing strong LoF in all assays used are located within the catalytic SARM1 TIR domain. They fail to deplete NAD in transfected HEK 293T cells, they lack basal and NMN-inducible NADase activity and fail to restore degeneration in transected primary neuronal cultures.
- Of the identified SARM1 LoF variants, two are dominant negative, and they are the first to be described in humans [12].
- Of the tested SARM1 variants, E399K SARM1 results in GoF and is predominantly found in Latino/Admixed Americans. Its increase of basal (constitutive) NADase activity is weaker than the one observed in hyperactive SARM1 GoF variants associated with sporadic ALS and other motor neuron diseases [9, 10]. Importantly, while all gnomAD participants had reached healthy adulthood at the time of recruitment it is unknown whether these carriers are neurologically healthy now.
- Known and predicted SARM1 LoF variants are more prevalent in control groups than disease cohorts. Since the amount of data, in combination with the low frequency of the variants, was insufficient to determine statistical significance, this finding rather serves as a hypothesis for future research.

- Carriers of biallelic NMNAT2 LoF variants develop rare axonopathies in a dose-dependent manner. These are perhaps accompanied by SCN9A-independent erythromelalgia which requires further investigation.
- The NMNAT2 region W92-H102aa appears to be functionally important. Of these mutated NMNAT2 residues, W92R, T95A, and the patient variant V98M NMNAT2 lead to a LoF of NAD synthesis activity and, as a result, fail to protect injured WT primary neuronal cultures when overexpressed. Other variants appear to be LoF due to lower expression levels. Whether this is due to protein instability remains to be addressed in future experiments.
- Publicly available datasets (e.g. gnomAD, 100,000 Genomes Project or UK Biobank) enable testing of disease association, especially regarding rare function- or/and expression-altering variants.

These findings have the following wider implications:

While existing data had already supported the idea of an intrinsic axon vulnerability spectrum in the human population influenced by PAD genes [5], the results of this thesis provide further evidence that axon health is influenced by the expression and enzymatic activities of the pro-degenerative SARM1 [12] and pro-survival NMNAT2 (see Figure 6.1). The data I gathered show that SARM1 LoF coding variation can be protective (chapter 3 and chapter 5) [12], whereas NMNAT2 LoF coding variation results in higher axon vulnerability (chapter 4). It is likely that other PAD proteins contribute to this spectrum, though perhaps to a lesser extent.

The acquired information on the characterised SARM1 and NMNAT2 variants together with findings from structural data and artificial mutants published elsewhere [110, 112, 113, 115, 120, 208] can help to delineate the extent to which PAD plays a role in human diseases [7–11] and to determine which pathologies are the most promising to target [5, 234]. The results can, for instance, also impact pre-clinical research in animal models that aim to develop and optimise PAD-targeting therapies, most promising of which are those targeting SARM1. This emphasises the importance of further researching the effects of decreasing SARM1 levels both in disease models and humans testing the efficacy of SARM1-targeting strategies, particularly for the use of antisense oligonucleotides.

The data suggest that SARM1 NADase LoF may be a protective factor against diseases associated to axonal impairment. Heterozygosity for SARM1 LoF variants, especially in the case of dominant negative allele carriers, could confer a protective phenotype making

axons less susceptible to PAD triggers (e.g. toxins, virus, or environmental factors) similar to observations made in mice [75, 217]. However, direct evidence that SARM1 LoF is protective against axon degeneration *in vivo* along with the exploration of additional, larger human cohorts (population-based and disease-focused) is indispensable to increase statistical significance for low-frequency PAD variants. The existence of dominant negative SARM1 variants in gnomAD is the best evidence yet that greatly lowering SARM1 activity in humans is not harmful. This is of great importance for drug discovery.

It will be important to understand whether the chronic high SARM1 NADase activity of E399K SARM1 is indeed compatible with a healthy life or whether the carriers' health is affected at a cellular level. Furthermore, it remains puzzling how other much stronger SARM1 GoF associated with sporadic ALS, for instance, are compatible with life [9, 10]. Do compensatory mechanism exist that differ to what happens when SARM1 is acutely activated?

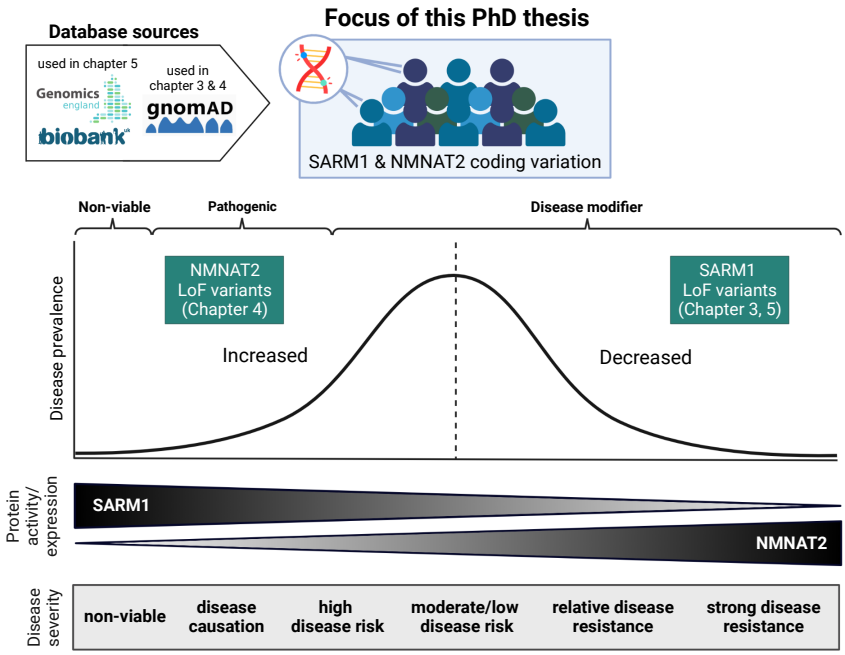


Figure 6.1: **PhD results support the idea of an axon vulnerability spectrum.** The results of this thesis demonstrate that SARM1 and NMNAT2 coding variants found in healthy (chapter 3 and 4) and diseased individuals (chapter 4 and 5) influence axonal health *in vitro*. Database sources used were gnomAD (population database), UK Biobank (prospective cohort study), and 100,000 Genomes Project (rare disease database). Parts of the graph adapted from Coleman and Höke 2020.

6.2 Future directions

Results in this thesis strongly support the postulated existence of an axon vulnerability spectrum [5]. To this date, the most promising link between PAD genes and human disease is SARM1 GoF associated with motor neuron disease [9, 10], as well as biallelic NMNAT2 LoF independently reported in six cases of rare human axonopathies [7, 8, 11], both of which need further expansion. Whether such a spectrum influences axon degeneration in other axonopathies, including complex neurodegenerative disorders, remains to be addressed by future studies.

6.2.1 Proof-of-concept in humans or knock-in mice

While axotomy assays using mouse primary neuronal cultures provides a convenient method at limited costs to test the functionality of PAD variants, it does not model mutations of the endogenous gene, nor is the expression at a physiological level that would be corresponding to that found in humans. Thus, proof-of-concept in e.g. iPSC-derived motor neurons is necessary. One also has to bear in mind interspecies differences that are likely to influence the outcome, such as in protein sequence, post-translational modifications, or protein expression. Another aspect important to bear in mind is the fact that human neurons have much longer axons. In addition, another significant aspect that remains to be observed is what outcome GoF or LoF SARM1 variants have in mouse models *in vivo*.

6.2.2 Expansion of patient databases is necessary

There is need for identifying additional affected individuals with similarly rare NMNAT2 LoF and SARM1 GoF variants. This could be addressed by creating databases, such as the 100,000 Genomes Project, to collect genomic (exome or targeted sequencing to limit costs) and clinical information of patients with rare clinical conditions. The following phenotypes should attract most attention: unsolved cases of rare chronic neuropathy, cases of unexplained erythromelalgia where SCN9A mutations have been excluded, cases of foetal loss, stillbirth, perinatal lethality associated to respiratory failure, early-onset muscular weakness and the failure to thrive. Carefully phenotyped patient populations are vital to firmly link neurological disease to a specific risk factor, such as genetic variation in a PAD gene, but cohort sizes need further expansion to increase statistical power. The low allele frequency of the identified variants, even after their enrichment in specific disease cohorts, means there is insufficient power to show genome-wide significance. This problem, however, may be overcome as larger disease cohorts become available. While a hypothesis-driven approach is not unbiased in the way GWAS studies are, it is a combination of

different approaches which will eventually provide most insight into how PAD genes play a role in influencing axonal health. After all, genome-wide significance for rare variants may not be achievable.

6.2.3 Peripheral neuropathy: a promising PAD target

A clinical setting where blocking PAD appears particularly promising and is strongly backed up by *in vitro* and *in vivo* data is peripheral neuropathy [151, 152, 177–179, 182, 197]. Two prevalent examples of peripheral neuropathy are chemotherapy-induced peripheral neuropathy (CIPN) and diabetes induced peripheral neuropathy (DIPN) [290]. They show a classic 'glove and stocking' distribution reflecting length-dependent axon degeneration which is likely to be influenced by PAD genes [5, 291]. In fact, CIPN is the most frequent cause of discontinuation, dose reduction and/or limitation during chemotherapeutic treatment and is a major unmet medical need in oncology [292]. It is interesting that patients affected by peripheral neuropathy show unexplained variability in axon degeneration which is independent of the primary cause. An intrinsic susceptibility to PAD could perhaps contribute to this variability. In fact, one of my proposed PhD projects considered examining this question. The plan was to test a cohort of severe CIPN cases, samples of which were provided by the PNRR (Peripheral Neuropathy Research Registry) with a customised PAD targeted sequencing panel encompassing coding regions for the genes *NMNAT2*, *SARM1* and *STMN2*. Initial progress was made in designing the panel but executing this plan was delayed by the pandemic and when it became possible to restart it the new data on SARM1 variants had altered the priorities [9, 10, 227]. There is compelling reason to argue that individuals whose genotypes suggest high susceptibility to PAD (those with functionally-confirmed GoF for SARM1, DLK1, MYCBP2; LoF for NMNAT1-3) will have significantly higher rates of neuropathy and/or more severe outcome than those whose genotypes suggest normal, or decreased susceptibility (functionally-confirmed LoF for SARM1, DLK1, MYCBP2; GoF for NMNAT1-3) to axonal damage. Of note, recently published data show that axon degeneration secondary to STMN2 depletion is independent of the SARM1 prodegenerative pathway [131, 293]. Interestingly, it has also been hypothesised that SARM1 deficiency could protect against diabetic cardiomyopathy too [294].

6.2.4 How PAD could contribute to complex disease

SARM1 activation through the loss of NMNAT2 is axon-specific. Nonetheless, there are other scenarios where SARM1 can cause cell death directly too. This is not just achieved

by hyperactivated SARM1 [9, 10] and SAM-TIR mutants lacking the autoinhibitory ARM domain. In fact, SARM1 can be activated by toxic metabolites of nicotinamide analogues, including the disused rodenticide vacor and 3-acetyl pyridine both of which directly activate SARM1 [76, 295]. It is therefore plausible that environmental toxins activating SARM1 could combine with other risk factors contributing to the pathophysiology of more complex neurological diseases [234]. While the existing data are still limited, another possible contribution to neurodegenerative disorders is axon death induced by endemic viruses. This includes infection with West Nile Virus, rabies, and more recently an association with Zika virus [296–298]. Interestingly, at least in the case of Zika virus, the pro-degenerative role of SARM1 appeared to be independent of its NADase activity which further raises questions regarding the proposed importance of NAD consumption for the prodegenerative function of the protein.

6.2.5 Rare peripheral neuropathies

SARM1 GoF likely acts as an additional risk factor for axon degeneration rather than being directly causative [5, 234]. In contrast, biallelic loss of NMNAT2 appears to be directly pathogenic, although this has so far only been seen in three families [7, 8, 11] and in mice [30, 99, 100]. NMNAT2 LoF leads to human axonopathies, the severity of which appears to be dose-dependent [5]. This can range from one extreme where a complete LoF is irreconcilable with life [8] to a less severe phenotype as in the German siblings suffering from a temperature-sensitive neuropathy accompanied by erythromelalgia [7]. The clinical case report discussed in chapter 4 represents an intermediate stage. In all three cases, it is believed that biallelic NMNAT2 LoF is causative of the phenotype strongly supported by *in vitro* and *in vivo* data [7, 8, 11]. The phenotypic heterogeneity in the clinical presentation of the associated ALS cases published by Gilley et al. raises interesting questions about the pathogenicity of SARM1 GoF variants and why they are not lethal [9]. Similarly, heterozygosity for NMNAT2 LoF, as is the case for all parents in the affected neuropathy cases [7, 8, 11], does not lead to any obvious consequences or symptoms in the parents. Experimental data from primary neuronal cultures show that both high SARM1 NADase activity, and low levels of NMNAT2 enzymatic activity are detrimental to axonal health [30, 119]. It is therefore surprising to observe that chronic expression of constitutive SARM1 NADase activity (as in the case of E399K SARM1 and the ALS-associated SARM1 GoF variants [9, 10]) is tolerated in humans. So are chronically low NMNAT2 levels during development in mice [103]. Whether this could be explained by an as of yet unexplored common compensatory mechanism activated under chronic conditions remains to be explored.

6.2.6 Insights from structural biology of SARM1

The past five years of PAD research have been dominated by a substantial progress in understanding SARM1 protein structure, its mechanism of auto-inhibition, and activation of NADase activity. The structures of individual SARM1 domains, truncated versions and the full-length protein have been determined through cryogenic electron microscopy (cryo-EM) and x-ray crystallography [110–115] with a specific focus on the ARM-TIR lock which keeps SARM1 in an autoinhibited state [115, 222]. Recently, our group and Bloom et al identified rare *SARM1* alleles that result in a disruption of the autoinhibitory ARM domain. Mutations within this region lead to increased constitutive (basal) NADase activity, much higher enzymatic activity than NMN-activated WT SARM1, and are associated to sporadic ALS and other motor disease. These enhance vulnerability to stresses, such as medium change, in primary neuronal cultures [9, 10].

6.2.7 NAD and related supplements

NAD/NMN ratios are crucial to the activity of SARM1 in axons. With this knowledge in mind, combined therapeutic strategies boosting NAD alongside low NMN levels may be effective. NAD loss is a known side effect of aging and countering NAD decline through supplementation with precursor molecules such as NR or NMN is a promising endeavour for many diseases [299]. Daily NMN supplementation, for instance, has shown to have positive metabolic and insulin-sensitizing in humans [300]. Several data support the translational value of NAD precursors in models of ageing and neurodegenerative disorders [301–305]. While these strategies have proven to be effective, findings from the PAD field suggest caution should be taken in the following cases: individuals with naturally-occurring reduced NMNAT2 levels or activity and those where NMNAT2 is depleted secondary to injury or impairment of axonal transport. Under healthy conditions NMN levels remain low as they feed into NAD production. In a diseased state where NMNAT2 is depleted, however, NMN rapidly accumulates and this would further be enhanced by supplementation of NMN or NR. While direct NAD administration would be the ideal way to bypass this problem, NAD itself is cell impermeable and therefore not suited as a therapeutic agent. Furthermore, neither of the above mentioned interventions represents a long-lasting avenue of protection, especially, when taking into account that SARM1 activation rapidly degrades NAD. Therefore, any of these steps could be taken as a supportive, but not causal treatment for neurodegenerative diseases anyway.

6.3 PAD-targeting therapies and their limitations

Targeting PAD by pharmaceutical intervention is currently being pursued [197, 206–208]. Of the different intervention methods, SARM1-blocking therapies have received most attention due to the promise of the lifelong protection SARM1 deletion offers, at least in mice. These SARM1 targeting therapies could be applied to various diseases where insufficient NMNAT2 levels, caused by impaired gene expression or protein function, kill axons. These include direct inhibition [207], the use of ASOs [217], or disrupting SARM1 activation [115]. Understanding the regulation of NMNAT2 stability and which residues are important for its enzymatic activity is also important. It is interesting how a molecule with such a short half life (40 min in HEK 293T cells and less than 4h in mouse primary neuronal cultures) manages to reach the furthest axons in humans before being degraded.

6.4 Other outstanding questions

The past three decades of PAD research have contributed greatly to our understanding of how axons die. With this increase in knowledge, there are still many questions that remain to be addressed especially regarding the downstream mechanisms of SARM1 activation. The current simplified stepwise model of WD is that transection causes NMNAT2 depletion in detached axons which in turn results in lower NAD levels due to lack of its synthesis. Sarm1 signalling is then activated, by a rise in the NMN/NAD ratio to then cause NAD depletion until a minimum threshold is reached initiating a downstream cascade which is yet to be fully deciphered. Several questions regarding this pro-death cascade in axons remain to be addressed:

NAD depletion (and consequently that of ATP) is widely thought to drive SARM1-dependent axon death [5, 81, 119]. However, whether it is the decline of this metabolite or other changes that cause axon death directly remains to be understood. In fact, SARM1 has other enzyme functions apart from NAD(P) degradation which include cyclisation of products and base exchange [75, 117, 219, 221]. Base exchange activity can dominate in some circumstances, and the full spectrum of base exchange products has not been fully understood [220]. While the removal of cADPR is not protective, it is unknown whether NaADP and ADPR, two calcium modulating molecules, have any contributing effect on axon degeneration [220, 306]. Furthermore, ROS accumulation (reflecting NADP(H) loss) is another likely consequence of SARM1 activation.

How active SARM1 TIR domains ultimately assemble within the full-length protein remains unclear. Activation upon NMN-binding leads to a conformational change and disruption

of the ARM:TIR lock, resulting in the formation of a double-layered TIR domain assembly followed by active site inhibition [112–116, 222]. It is also unclear whether SARM1 forms higher-order oligomers with other proteins, resulting in the formation of a large TIR-mediated death complex.

6.5 Conclusion

In summary, the work in this thesis demonstrates that the outcome of programmed axon degeneration *in vitro* can be influenced by coding variation in the genes *SARM1* and *NMNAT2*. I have characterised novel, function-altering variants of each gene, demonstrating the viability of SARM1 LoF and dominant negative alleles in humans for the first time. This will give future disease association studies greater statistical power. Future studies need to explore the effects of other human SARM1 and NMNAT2 mutations and their potential relevance to disease risk. It will also be important to understand whether PAD-blocking drugs will be limited to rare, inherited disorders (e.g. peripheral neuropathies associated with biallelic NMNAT2 LoF mutations) or whether they will find a wider application, including more common neurological disorders, such as ALS.

Bibliography

References

[1] Augustus Volney Waller. Xx. experiments on the section of the glossopharyngeal and hypoglossal nerves of the frog, and observations of the alterations produced thereby in the structure of their primitive fibres. *Philosophical Transactions of the Royal Society of London*, (140):423–429, 1850.

[2] John W Griffin. Augustus waller and the case of the disappearing axon. *Nature Clinical Practice Neurology*, 3(7):355–355, 2007.

[3] Michael P Coleman and Marc R Freeman. Wallerian degeneration, wlds, and nmnat. *Annual review of neuroscience*, 33:245, 2010.

[4] Cajal, S. Ramón. *Degeneration & regeneration of the nervous system.* Oxford University Press.

[5] Michael P Coleman and Ahmet Höke. Programmed axon degeneration: from mouse to mechanism to medicine. *Nature Reviews Neuroscience*, 21(4):183–196, 2020.

[6] Laura Conforti, Jonathan Gilley, and Michael P Coleman. Wallerian degeneration: an emerging axon death pathway linking injury and disease. *Nature Reviews Neuroscience*, 15(6):394–409, 2014.

[7] Peter Huppke, Eike Wegener, Jonathan Gilley, Carlo Angeletti, Ingo Kurth, Joost PH Drenth, Christine Stadelmann, Alonso Barrantes-Freer, Wolfgang Brück, Holger Thiele, et al. Homozygous nmnat2 mutation in sisters with polyneuropathy and erythromelalgia. *Experimental Neurology*, 320:112958, 2019.

[8] Marshall Lukacs, Jonathan Gilley, Yi Zhu, Giuseppe Orsomando, Carlo Angeletti, Jiaqi Liu, Xiuna Yang, Joun Park, Robert J Hopkin, Michael P Coleman, et al. Severe biallelic loss-of-function mutations in nicotinamide mononucleotide adenylyltransferase 2 (nmnat2) in two fetuses with fetal akinesia deformation sequence. *Experimental neurology*, 320:112961, 2019.

[9] Jonathan Gilley, Oscar Jackson, Menelaos Pipis, Mehrdad A Estiar, Ammar Al-Chalabi, Matt C Danzi, Kristel R van Eijk, Stephen A Goutman, Matthew B Harms, Henry Houlden, et al. Enrichment of sarm1 alleles encoding variants with constitutively hyperactive nadase in patients with als and other motor nerve disorders. *Elife*, 10:e70905, 2021.

[10] A Joseph Bloom, Xianrong Mao, Amy Strickland, Yo Sasaki, Jeffrey Milbrandt, and Aaron DiAntonio. Constitutively active sarm1 variants that induce neuropathy are enriched in als patients. *Molecular neurodegeneration*, 17(1):1–15, 2022.

[11] Caitlin B Dingwall, Amy Strickland, Sabrina W Yum, Aldrin Kay-Yuen Yim, Jian Zhu, Peter L Wang, Yurie Yamada, Robert E Schmidt, Yo Sasaki, A Joseph Bloom, et al. Macrophage depletion blocks congenital sarm1-dependent neuropathy. *The Journal of Clinical Investigation*, 2022.

[12] Mirlinda Ademi, Xiuna Yang, Michael P Coleman, and Jonathan Gilley. Natural variants of human sarm1 cause both intrinsic and dominant loss-of-function influencing axon survival. *Scientific reports*, 12(1):1–14, 2022.

[13] Elisa Merlini, Michael P Coleman, and Andrea Loreto. Mitochondrial dysfunction as a trigger of programmed axon death. *Trends in Neurosciences*, 45(1):53–63, 2022.

[14] Michael Coleman. Axon degeneration mechanisms: commonality amid diversity. 6(11):889–898.

[15] Valery L Feigin, Benjamin A Stark, Catherine Owens Johnson, Gregory A Roth, Catherine Bisignano, Gdiom Gebreheat Abady, Mitra Abbasifard, Mohsen Abbasi-Kangevari, Foad Abd-Allah, Vida Abedi, et al. Global, regional, and national burden of stroke and its risk factors, 1990–2019: A systematic analysis for the global burden of disease study 2019. *The Lancet Neurology*, 20(10):795–820, 2021.

[16] Ping Li, Yaling Nie, and Jingkai Yu. An effective method to identify shared pathways and common factors among neurodegenerative diseases. *PLoS One*, 10(11):e0143045, 2015.

[17] Yves Sagot, Michel Dubois-Dauphin, SA Tan, F De Bilbao, P Aebischer, JC Martinou, and AC Kato. Bcl-2 overexpression prevents motoneuron cell body loss but not axonal degeneration in a mouse model of a neurodegenerative disease. *Journal of Neuroscience*, 15(11):7727–7733, 1995.

[18] Megan K Houseweart and Don W Cleveland. Bcl-2 overexpression does not protect neurons from mutant neurofilament-mediated motor neuron degeneration. *Journal of Neuroscience*, 19(15):6446–6456, 1999.

[19] Cheng Qian and Feng-Quan Zhou. Updates and challenges of axon regeneration in the mammalian central nervous system. *Journal of molecular cell biology*, 12(10):798–806, 2020.

[20] R Adalbert and MP Coleman. Axon pathology in age-related neurodegenerative disorders. *Neuropathology and applied neurobiology*, 39(2):90–108, 2013.

[21] Raul Krauss, Todd Bosanac, Rajesh Devraj, Thomas Engber, and Robert O. Hughes. Axons matter: The promise of treating neurodegenerative disorders by targeting SARM1-mediated axonal degeneration. 41(4):281–293. Publisher: Elsevier Ltd.

[22] Timothy G Buchman. The community of the self. *Nature*, 420(6912):246–251, 2002.

[23] Raj Chovatiya and Ruslan Medzhitov. Stress, inflammation, and defense of homeostasis. *Molecular cell*, 54(2):281–288, 2014.

[24] Sabina Tahirovic and Frank Bradke. Neuronal polarity. *Cold Spring Harbor perspectives in biology*, 1(3):a001644, 2009.

[25] Reinhard L Friede. The relationship of body size, nerve cell size, axon length, and glial density in the cerebellum. *Proceedings of the National Academy of Sciences*, 49(2):187–193, 1963.

[26] Emily L Spaulding and Robert W Burgess. Accumulating evidence for axonal translation in neuronal homeostasis. *Frontiers in neuroscience*, 11:312, 2017.

[27] James N Sleigh, Alexander M Rossor, Alexander D Fellows, Andrew P Tosolini, and Giampietro Schiavo. Axonal transport and neurological disease. *Nature Reviews Neurology*, 15(12):691–703, 2019.

[28] Sandra Maday, Alison E Twelvetrees, Armen J Moughamian, and Erika LF Holzbaur. Axonal transport: cargo-specific mechanisms of motility and regulation. *Neuron*, 84(2):292–309, 2014.

[29] James C. Vickers, Anna E. King, Adele Woodhouse, Matthew T. Kirkcaldie, Jerome A. Staal, Graeme H. McCormack, Catherine A. Blizzard, Ruth E.J. Musgrove, Stanislaw Mitew, Yao Liu, Jyoti A. Chuckowree, Olivier Bibari, and Tracey C. Dickson. Axonopathy and cytoskeletal disruption in degenerative diseases of the central nervous system. 80(4):217–223. Publisher: Elsevier.

[30] Jonathan Gilley and Michael P Coleman. Endogenous nmnat2 is an essential survival factor for maintenance of healthy axons. *PLoS biology*, 8(1):e1000300, 2010.

[31] Liliana Lubińska. Early course of wallerian degeneration in myelinated fibres of the rat phrenic nerve. *Brain research*, 130(1):47–63, 1977.

[32] J B Cavanagh. The significance of the "dying back" process in experimental and human neurological disease. 3:219–67.

[33] John W. Griffin, Edwin B. George, Sung-Tsang Hsieh, and Jonathan D. Glass. Axonal degeneration and disorders of the axonal cytoskeleton. In *The Axon*, pages 375–390. Oxford University Press.

[34] E B George, J D Glass, and J W Griffin. Axotomy-induced axonal degeneration is mediated by calcium influx through ion-specific channels. 15(10):6445–52. Publisher: Society for Neuroscience.

[35] Marek Ma, Toby A Ferguson, Kathleen M Schoch, Jian Li, Yaping Qian, Frances S Shofer, Kathryn E Saatman, and Robert W Neumar. Calpains mediate axonal cytoskeleton disintegration during wallerian degeneration. *Neurobiology of disease*, 56:34–46, 2013.

[36] Jing Yang, Robby M. Weimer, Dara Kallop, Olav Olsen, Zhuhao Wu, Nicolas Renier, Kunihiro Uryu, and Marc Tessier-Lavigne. Regulation of axon degeneration after injury and in development by the endogenous calpain inhibitor calpastatin. 80(5):1175–1189. Publisher: Cell Press.

[37] S. K. Gupta, J. F. Poduslo, and C. Mezei. Temporal changes in PO and MBP gene expression after crush-injury of the adult peripheral nerve. 464(2):133–141.

[38] Bruce D Trapp, Peter Hauer, and G Lemke. Axonal regulation of myelin protein mrna levels in actively myelinating schwann cells. *Journal of Neuroscience*, 8(9):3515–3521, 1988.

[39] Augustus Waller. Experiments on the section of the glosso-pharyngeal and hypoglossal nerves of the frog, and observations of the alterations produced thereby in the structure of their primitive fibres. 76(189):369–376.

[40] V H Perry, M C Brown, E R Lunn, P Tree, and S Gordon. Evidence that very slow wallerian degeneration in c57bl/ola mice is an intrinsic property of the peripheral nerve. 2(9):802–8.

[41] J. D. Glass, T. M. Brushart, E. B. George, and J. W. Griffin. Prolonged survival of transected nerve fibres in c57bl/ola mice is an intrinsic characteristic of the axon. 22(5):311–321.

[42] E. R. Lunn, V. H. Perry, M. C. Brown, H. Rosen, and S. Gordon. Absence of wallerian degeneration does not hinder regeneration in peripheral nerve. 1(1):27–33.

[43] V. H. Perry, M. C. Brown, and E. R. Lunn. Very slow retrograde and wallerian degeneration in the CNS of c57bl/ola mice. 3(1):102–105.

[44] Michael P. Coleman, Laura Conforti, E. Anne Buckmaster, Andrea Tarlton, Robert M. Ewing, Michael C. Brown, Mary F. Lyon, and V. Hugh Perry. An 85-kb tandem triplication in the slow wallerian degeneration (wlds) mouse. 95(17):9985–9990.

[45] T. G. Mack, M. Reiner, B. Beirowski, W. Mi, M. Emanuelli, D. Wagner, D. Thomson, T. Gillingwater, F. Court, L. Conforti, F. S. Fernando, A. Tarlton, C. Andressen, K. Addicks, G. Magni, R. R. Ribchester, V. H. Perry, and M. P. Coleman. Wallerian degeneration of injured axons and synapses is delayed by a ube4b/nmnat chimeric gene. 4(12):1199–1206.

[46] Bogdan Beirowski, Elisabetta Babetto, Jon Gilley, Francesca Mazzola, Laura Conforti, Lucie Janeckova, Giulio Magni, Richard R. Ribchester, and Michael P. Coleman. Non-nuclear WldS determines its neuroprotective efficacy for axons and synapses in vivo. 29(3):653–668. Publisher: Society for Neuroscience Section: Articles.

[47] Elisabetta Babetto, Bogdan Beirowski, Lucie Janeckova, Rosalind Brown, Jonathan Gilley, Derek Thomson, Richard R Ribchester, and Michael P Coleman. Targeting NMNAT1 to axons and synapses transforms its neuroprotective potency in vivo. 30(40):13291–304. Publisher: Society for Neuroscience.

[48] Bogdan Beirowski, Elisabetta Babetto, Michael P Coleman, and Keith R Martin. The wlds gene delays axonal but not somatic degeneration in a rat glaucoma model. *European Journal of Neuroscience*, 28(6):1166–1179, 2008.

[49] Y. Sasaki, B. P. S. Vohra, F. E. Lund, and J. Milbrandt. Nicotinamide mononucleotide adenylyl transferase-mediated axonal protection requires enzymatic activity but not increased levels of neuronal nicotinamide adenine dinucleotide. 29(17):5525–5535.

[50] L. Conforti, G. Fang, B. Beirowski, M. S. Wang, L. Sorci, S. Asress, R. Adalbert, A. Silva, K. Bridge, X. P. Huang, G. Magni, J. D. Glass, and M. P. Coleman. NAD+ and

axon degeneration revisited: Nmnat1 cannot substitute for WldS to delay wallerian degeneration. 14(1):116–127. Number: 1 Publisher: Nature Publishing Group.

[51] Laura Conforti, Anna Wilbrey, Giacomo Morreale, Lucie Janeckova, Bogdan Beirowski, Robert Adalbert, Francesca Mazzola, Michele Di Stefano, Robert Hartley, Elisabetta Babetto, Trevor Smith, Jonathan Gilley, Richard A. Billington, Armando A. Genazzani, Richard R. Ribchester, Giulio Magni, and Michael Coleman. Wld ^{s} protein requires nmnat activity and a short n-terminal sequence to protect axons in mice. 184(4):491–500.

[52] Michael S. Cohen, Ananda K. Ghosh, Hyung Joon Kim, Noo Li Jeon, and Samie R. Jaffrey. Chemical genetic-mediated spatial regulation of protein expression in neurons reveals an axonal function for WldS. 19(2):179–187.

[53] Jack T. Wang, Zachary A. Medress, Mauricio E. Vargas, and Ben A. Barres. Local axonal protection by WldS as revealed by conditional regulation of protein stability. 112(33):10093–10100. Publisher: Proceedings of the National Academy of Sciences.

[54] Thomas H Gillingwater, Derek Thomson, Till G A Mack, Ellen M Soffin, Richard J Mattison, Michael P Coleman, and Richard R Ribchester. Age-dependent synapse withdrawal at axotomised neuromuscular junctions in wld(s) mutant and ube4b/nmnat transgenic mice. 543:739–755.

[55] Michelle A Avery, Amy E Sheehan, Kimberly S Kerr, Jing Wang, and Marc R Freeman. Wlds requires nmnat1 enzymatic activity and n16–vcp interactions to suppress wallerian degeneration. *Journal of Cell Biology*, 184(4):501–513, 2009.

[56] Felicitas Berger, Corinna Lau, Mathias Dahlmann, and Mathias Ziegler. Subcellular compartmentation and differential catalytic properties of the three human nicotinamide mononucleotide adenylyltransferase isoforms. *Journal of Biological Chemistry*, 280(43):36334–36341, 2005.

[57] Nadia Raffaelli, Leonardo Sorci, Adolfo Amici, Monica Emanuelli, Francesca Mazzola, and Giulio Magni. Identification of a novel human nicotinamide mononucleotide adenylyltransferase. 297(4):835–840.

[58] Jennifer M. MacDonald, Margaret G. Beach, Ermelinda Porpiglia, Amy E. Sheehan, Ryan J. Watts, and Marc R. Freeman. The drosophila cell corpse engulfment receptor draper mediates glial clearance of severed axons. 50(6):869–881.

[59] Seanna M Martin, Georgeann S O'Brien, Carlos Portera-Cailliau, and Alvaro Sagasti. Wallerian degeneration of zebrafish trigeminal axons in the skin is required for regeneration and developmental pruning. *Development*, 137(23):3985–3994, 2010.

[60] Robert Adalbert, Thomas H. Gillingwater, Jane E. Haley, Katherine Bridge, Bogdan Beirowski, Livia Berek, Diana Wagner, Daniela Grumme, Derek Thomson, Arzu Celik, Klaus Addicks, Richard R. Ribchester, and Michael P. Coleman. A rat model of slow wallerian degeneration (*Wld* ^{s}) with improved preservation of neuromuscular synapses. 21(1):271–277.

[61] Brandon M. Kitay, Ryan McCormack, Yunfang Wang, Pantelis Tsoulfas, and R. Grace Zhai. Mislocalization of neuronal mitochondria reveals regulation of wallerian degeneration and NMNAT/WLDS-mediated axon protection independent of axonal mitochondria. 22(8):1601–1614.

[62] Thomas L. Deckwerth and Eugene M. Johnson. Neurites can remain viable after destruction of the neuronal soma by programmed cell death (apoptosis). 165(1):63–72.

[63] Robert Adalbert, Antal Nógrádi, András Szabó, and Michael P. Coleman. The slow wallerian degeneration gene in vivo protects motor axons but not their cell bodies after avulsion and neonatal axotomy. 24(8):2163–2168.

[64] J T Finn, M Weil, F Archer, R Siman, A Srinivasan, and M C Raff. Evidence that wallerian degeneration and localized axon degeneration induced by local neurotrophin deprivation do not involve caspases. 20(4):1333–41.

[65] Eric D. Hoopfer, Todd McLaughlin, Ryan J. Watts, Oren Schuldiner, Dennis D.M. O'Leary, and Liqun Luo. Wlds protection distinguishes axon degeneration following injury from naturally occurring developmental pruning. 50(6):883–895. Publisher: Cell Press.

[66] Caroline Sievers, Nick Platt, V. Hugh Perry, Michael P. Coleman, and Laura Conforti. Neurites undergoing wallerian degeneration show an apoptotic-like process with annexin v positive staining and loss of mitochondrial membrane potential. 46(2):161–169.

[67] Alan V. Whitmore, Tullia Lindsten, Martin C. Raff, and Craig B. Thompson. The proapoptotic proteins bax and bak are not involved in wallerian degeneration. 10(2):260–261. Number: 2 Publisher: Nature Publishing Group.

[68] J. F. Burne, J. K. Staple, and M. C. Raff. Glial cells are increased proportionally in transgenic optic nerves with increased numbers of axons. 16(6):2064–2073.

[69] Kimberly A Fernandes, Katherine L Mitchell, Amit Patel, Olivia J Marola, Peter Shrager, Donald J Zack, Richard T Libby, and Derek S Welsbie. Role of sarm1 and dr6 in retinal ganglion cell axonal and somal degeneration following axonal injury. *Experimental eye research*, 171:54–61, 2018.

[70] Kwang Woo Ko, Jeffrey Milbrandt, and Aaron DiAntonio. SARM1 acts downstream of neuroinflammatory and necroptotic signaling to induce axon degeneration. 219(8):e201912047.

[71] Jung Eun Shin, Bradley R Miller, Elisabetta Babetto, Yongcheol Cho, Yo Sasaki, Shehzad Qayum, Emilie V Russler, Valeria Cavalli, Jeffrey Milbrandt, and Aaron DiAntonio. Scg10 is a jnk target in the axonal degeneration pathway. *Proceedings of the National Academy of Sciences*, 109(52):E3696–E3705, 2012.

[72] Jing Yang, Zhuhao Wu, Nicolas Renier, David J Simon, Kunihiro Uryu, David S Park, Peter A Greer, Cathy Tournier, Roger J Davis, and Marc Tessier-Lavigne. Pathological axonal death through a MAPK cascade that triggers a local energy deficit. 160(1):161–76. Publisher: NIH Public Access.

[73] Macarena S. Arrázola, Cristian Saquel, Romina J. Catalán, Sebastián A. Barrientos, Diego E. Hernandez, Nicolás W. Martínez, Alejandra Catenaccio, and Felipe A. Court. Axonal degeneration is mediated by necroptosis activation. 39(20):3832–3844. Publisher: Society for Neuroscience Section: Research Articles.

[74] Ema Ozaki, Luke Gibbons, Nuno GB Neto, Paul Kenna, Michael Carty, Marian Humphries, Pete Humphries, Matthew Campbell, Michael Monaghan, Andrew Bowie, and Sarah L Doyle. SARM1 deficiency promotes rod and cone photoreceptor cell survival in a model of retinal degeneration. 3(5):e201900618. Publisher: Life Science Alliance, LLC.

[75] Yo Sasaki, Thomas M. Engber, Robert O. Hughes, Matthew D. Figley, Tong Wu, Todd Bosanac, Rajesh Devraj, Jeffrey Milbrandt, Raul Krauss, and Aaron DiAntonio. cADPR is a gene dosage-sensitive biomarker of SARM1 activity in healthy, compromised, and degenerating axons. 329:113252. Publisher: Elsevier BV.

[76] Andrea Loreto, Carlo Angeletti, Weixi Gu, Andrew Osborne, Bart Nieuwenhuis, Jonathan Gilley, Elisa Merlini, Peter Arthur-Farraj, Adolfo Amici, Zhenyao Luo, et al.

Neurotoxin-mediated potent activation of the axon degeneration regulator sarm1. *ELife*, 10, 2021.

[77] Daniel W. Summers, Aaron DiAntonio, and Jeffrey Milbrandt. Mitochondrial dysfunction induces sarm1-dependent cell death in sensory neurons. 34(28):9338–9350. Publisher: Society for Neuroscience.

[78] S. S. Zhu, Y. Ren, M. Zhang, J. Q. Cao, Q. Yang, X. Y. Li, H. Bai, L. Jiang, Q. Jiang, Z. G. He, and Q. Chen. Wld(s) protects against peripheral neuropathy and retinopathy in an experimental model of diabetes in mice. 54(9):2440–2450.

[79] Aaron DiAntonio, Jeffrey Milbrandt, and Matthew D. Figley. The SARM1 TIR NADase: Mechanistic similarities to bacterial phage defense and toxin-antitoxin systems. 12:752898.

[80] Yue Sun, Qi Wang, Yi Wang, Wenran Ren, Ying Cao, Jiali Li, Xin Zhou, Wei Fu, and Jing Yang. Sarm1-mediated neurodegeneration within the enteric nervous system protects against local inflammation of the colon. 12(8):621–638.

[81] Josiah Gerdts, Daniel W. Summers, Jeffrey Milbrandt, and Aaron DiAntonio. Axon self-destruction: New links among SARM1, MAPKs, and NAD+ metabolism. 89(3):449–460. Publisher: Neuron.

[82] Josiah Gerdts, Daniel W Summers, Yo Sasaki, Aaron DiAntonio, and Jeffrey Milbrandt. Sarm1-mediated axon degeneration requires both sam and tir interactions. *Journal of Neuroscience*, 33(33):13569–13580, 2013.

[83] Jeannette M Osterloh, Jing Yang, Timothy M Rooney, A Nicole Fox, Robert Adalbert, Eric H Powell, Amy E Sheehan, Michelle A Avery, Rachel Hackett, Mary A Logan, et al. dsarm/sarm1 is required for activation of an injury-induced axon death pathway. *Science*, 337(6093):481–484, 2012.

[84] H N Jayaram, P Kusumanchi, and J A Yalowitz. NMNAT expression and its relation to NAD metabolism. 18(13):1962–72.

[85] Tingting Yan, Yan Feng, Jin Zheng, Xinjian Ge, Yi Zhang, Dongmei Wu, Jian Zhao, and Qiwei Zhai. Nmnat2 delays axon degeneration in superior cervical ganglia dependent on its nad synthesis activity. *Neurochemistry international*, 56(1):101–106, 2010.

[86] Stefan Milde, Jonathan Gilley, and Michael P Coleman. Axonal trafficking of NMNAT2 and its roles in axon growth and survival in vivo. 3(5):133–140.

[87] Yan Feng, Tingting Yan, Jin Zheng, Xinjian Ge, Yu Mu, Yi Zhang, Dongmei Wu, Jiu-lin Du, and Qiwei Zhai. Overexpression of wlds or nmnat2 in mauthner cells by single-cell electroporation delays axon degeneration in live zebrafish. 88(15):3319–3327. Eprint: https://onlinelibrary.wiley.com/doi/pdf/10.1002/jnr.22498.

[88] M. Cecilia Ljungberg, Yousuf O. Ali, Jie Zhu, Chia-Shan Wu, Kazuhiro Oka, R. Grace Zhai, and Hui-Chen Lu. CREB-activity and nmnat2 transcription are down-regulated prior to neurodegeneration, while NMNAT2 over-expression is neuroprotective, in a mouse model of human tauopathy. 21(2):251–267.

[89] Yanshan Fang, Lorena Soares, Xiuyin Teng, Melissa Geary, and Nancy M. Bonini. A novel drosophila model of nerve injury reveals an essential role of nmnat in maintaining axonal integrity. 22(7):590–595.

[90] Fang Fang, Pei Zhuang, Xue Feng, Pingting Liu, Dong Liu, Haoliang Huang, Liang Li, Wei Chen, Liang Liu, Yang Sun, Haowen Jiang, Jiangbin Ye, and Yang Hu. NMNAT2 is downregulated in glaucomatous RGCs, and RGC-specific gene therapy rescues neurodegeneration and visual function. 30(4):1421–1431.

[91] Stefan Milde, Jonathan Gilley, and Michael P Coleman. Subcellular localization determines the stability and axon protective capacity of axon survival factor nmnat2. *PLoS biology*, 11(4):e1001539, 2013.

[92] Paul R Mayer, Nian Huang, Colleen M Dewey, Daniel R Dries, Hong Zhang, and Gang Yu. Expression, localization, and biochemical characterization of nicotinamide mononucleotide adenylyltransferase 2. *Journal of Biological Chemistry*, 285(51):40387–40396, 2010.

[93] Corinna Lau, Christian Dölle, Toni I Gossmann, Line Agledal, Marc Niere, and Mathias Ziegler. Isoform-specific targeting and interaction domains in human nicotinamide mononucleotide adenylyltransferases. *Journal of Biological Chemistry*, 285(24):18868–18876, 2010.

[94] Xin Xiong, Yan Hao, Kan Sun, Jiaxing Li, Xia Li, Bibhudatta Mishra, Pushpanjali Soppina, Chunlai Wu, Richard I. Hume, and Catherine A. Collins. The highwire ubiquitin ligase promotes axonal degeneration by tuning levels of nmnat protein. 10(12):e1001440.

[95] Daniel W. Summers, Jeffrey Milbrandt, and Aaron DiAntonio. Palmitoylation enables MAPK-dependent proteostasis of axon survival factors. 115(37):E8746–E8754. Publisher: National Academy of Sciences.

[96] Elisabetta Babetto, Bogdan Beirowski, Emilie V Russler, Jeffrey Milbrandt, and Aaron DiAntonio. The phr1 ubiquitin ligase promotes injury-induced axon self-destruction. 3(5):1422–9. Publisher: NIH Public Access.

[97] Peter D. Mabbitt, Andrea Loreto, Marc-André Déry, Adam J. Fletcher, Mathew Stanley, Kuan-Chuan Pao, Nicola T. Wood, Michael P. Coleman, and Satpal Virdee. Structural basis for RING-cys-relay e3 ligase activity and its role in axon integrity. 16(11):1227–1236.

[98] Qiwei Zhai, Jing Wang, Anna Kim, Qing Liu, Ryan Watts, Eric Hoopfer, Timothy Mitchison, Liqun Luo, and Zhigang He. Involvement of the ubiquitin-proteasome system in the early stages of wallerian degeneration. 39(2):217–225.

[99] Amy N Hicks, Diego Lorenzetti, Jonathan Gilley, Baisong Lu, Karl-Erik Andersson, Carol Miligan, Paul A Overbeek, Ronald Oppenheim, and Colin E Bishop. Nicotinamide mononucleotide adenylyltransferase 2 (nmnat2) regulates axon integrity in the mouse embryo. 2012.

[100] Jonathan Gilley, Robert Adalbert, Gang Yu, and Michael P Coleman. Rescue of peripheral and cns axon defects in mice lacking nmnat2. *Journal of Neuroscience*, 33(33):13410–13424, 2013.

[101] Jonathan Gilley, Giuseppe Orsomando, Isabel Nascimento-Ferreira, and Michael P Coleman. Absence of sarm1 rescues development and survival of nmnat2-deficient axons. *Cell reports*, 10(12):1974–1981, 2015.

[102] Michele Di Stefano, Andrea Loreto, Giuseppe Orsomando, Valerio Mori, Federica Zamporlini, Richard P. Hulse, Jamie Webster, Lucy F. Donaldson, Martin Gering, Nadia Raffaelli, Michael P. Coleman, Jonathan Gilley, and Laura Conforti. NMN deamidase delays wallerian degeneration and rescues axonal defects caused by NMNAT2 deficiency in vivo. 27(6):784–794. Publisher: Elsevier.

[103] Jonathan Gilley, Paul R Mayer, Gang Yu, and Michael P Coleman. Low levels of nmnat2 compromise axon development and survival. *Human molecular genetics*, 28(3):448–458, 2019.

[104] Luke A. J. O'Neill and Andrew G. Bowie. The family of five: TIR-domain-containing adaptors in toll-like receptor signalling. 7(5):353–364. Publisher: Nature Publishing Group.

[105] Matyas Mink, Ben Fogelgren, Krzysztof Olszewski, Peter Maroy, and Katalin Csiszar. A novel human gene (SARM) at chromosome 17q11 encodes a protein with a SAM motif and structural similarity to armadillo/β-catenin that is conserved in mouse, drosophila, and caenorhabditis elegans. 74(2):234–244.

[106] Nicole T. Liberati, Katherine A. Fitzgerald, Dennis H. Kim, Rhonda Feinbaum, Douglas T. Golenbock, and Frederick M. Ausubel. Requirement for a conserved toll/interleukin-1 resistance domain protein in the caenorhabditis elegans immune response. 101(17):6593–6598. Publisher: National Academy of Sciences.

[107] Michael Carty, Rory Goodbody, Martina Schröder, Julianne Stack, Paul N. Moynagh, and Andrew G. Bowie. The human adaptor SARM negatively regulates adaptor protein TRIF–dependent toll-like receptor signaling. 7(10):1074–1081. Publisher: Nature Publishing Group.

[108] P. Panneerselvam, L. P. Singh, V. Selvarajan, W. J. Chng, S. B. Ng, N. S. Tan, B. Ho, J. Chen, and J. L. Ding. T-cell death following immune activation is mediated by mitochondria-localized SARM. 20(3):478. Publisher: Nature Publishing Group.

[109] Chiung-Ya Chen, Chia-Wen Lin, Chiung-Ying Chang, Si-Tse Jiang, and Yi-Ping Hsueh. Sarm1, a negative regulator of innate immunity, interacts with syndecan-2 and regulates neuronal morphology. *Journal of Cell Biology*, 193(4):769–784, 2011.

[110] Shane Horsefield, Hayden Burdett, Xiaoxiao Zhang, Mohammad K Manik, Yun Shi, Jian Chen, Tiancong Qi, Jonathan Gilley, Jhih-Siang Lai, Maxwell X Rank, et al. Nad+ cleavage activity by animal and plant tir domains in cell death pathways. *Science*, 365(6455):793–799, 2019.

[111] Michael Sporny, Julia Guez-Haddad, Mario Lebendiker, Valeria Ulisse, Allison Volf, Carsten Mim, Michail N Isupov, and Yarden Opatowsky. Structural evidence for an octameric ring arrangement of sarm1. *Journal of Molecular Biology*, 431(19):3591–3605, 2019.

[112] Matthew Bratkowski, Tian Xie, Desiree A Thayer, Shradha Lad, Prakhyat Mathur, Yu-San Yang, Gregory Danko, Thomas C Burdett, Jean Danao, Aaron Cantor, et al. Structural and mechanistic regulation of the pro-degenerative nad hydrolase sarm1. *Cell reports*, 32(5):107999, 2020.

[113] Yuefeng Jiang, Tingting Liu, Chia-Hsueh Lee, Qing Chang, Jing Yang, and Zhe Zhang. The nad+-mediated self-inhibition mechanism of pro-neurodegenerative sarm1. *Nature*, 588(7839):658–663, 2020.

[114] Michael Sporny, Julia Guez-Haddad, Tami Khazma, Avraham Yaron, Moshe Dessau, Yoel Shkolnisky, Carsten Mim, Michail N. Isupov, Ran Zalk, Michael Hons, and Yarden Opatowsky. Structural basis for sarm1 inhibition and activation under energetic stress. 9:1–25. Publisher: eLife Sciences Publications Ltd.

[115] Matthew D. Figley, Weixi Gu, Jeffrey D. Nanson, Yun Shi, Yo Sasaki, Katie Cunnea, Alpeshkumar K. Malde, Xinying Jia, Zhenyao Luo, Forhad K. Saikot, Tamim Mosaiab, Veronika Masic, Stephanie Holt, Lauren Hartley-Tassell, Helen Y. McGuinness, Mohammad K. Manik, Todd Bosanac, Michael J. Landsberg, Philip S. Kerry, Mehdi Mobli, Robert O. Hughes, Jeffrey Milbrandt, Bostjan Kobe, Aaron DiAntonio, and Thomas Ve. SARM1 is a metabolic sensor activated by an increased NMN/NAD+ ratio to trigger axon degeneration. 109(7):1118–1136.e11. Publisher: Cell Press.

[116] Yun Shi, Philip S Kerry, Jeffrey D Nanson, Todd Bosanac, Yo Sasaki, Raul Krauss, Forhad K Saikot, Sarah E Adams, Tamim Mosaiab, Veronika Masic, et al. Structural basis of sarm1 activation, substrate recognition, and inhibition by small molecules. *Molecular cell*, 82(9):1643–1659, 2022.

[117] Kow Essuman, Daniel W Summers, Yo Sasaki, Xianrong Mao, Aaron DiAntonio, and Jeffrey Milbrandt. The sarm1 toll/interleukin-1 receptor domain possesses intrinsic nad+ cleavage activity that promotes pathological axonal degeneration. *Neuron*, 93(6):1334–1343, 2017.

[118] Younghwa Kim, Ping Zhou, Liping Qian, Jen-Zen Chuang, Jessica Lee, Chenjian Li, Costantino Iadecola, Carl Nathan, and Aihao Ding. Myd88-5 links mitochondria, microtubules, and jnk3 in neurons and regulates neuronal survival. *The Journal of experimental medicine*, 204(9):2063–2074, 2007.

[119] Josiah Gerdts, EJ Brace, Yo Sasaki, Aaron DiAntonio, and Jeffrey Milbrandt. Sarm1 activation triggers axon degeneration locally via nad+ destruction. *Science*, 348(6233):453–457, 2015.

[120] Daniel W Summers, Daniel A Gibson, Aaron DiAntonio, and Jeffrey Milbrandt. Sarm1-specific motifs in the tir domain enable nad+ loss and regulate injury-induced sarm1 activation. *Proceedings of the National Academy of Sciences*, 113(41):E6271–E6280, 2016.

[121] Eleanor L. Hopkins, Weixi Gu, Bostjan Kobe, and Michael P. Coleman. A novel NAD signaling mechanism in axon degeneration and its relationship to innate immunity. 8:662. Publisher: Frontiers Media S.A.

[122] Piyali Mukherjee, Tyson A. Woods, Roger A. Moore, and Karin E. Peterson. Activation of the innate signaling molecule MAVS by bunyavirus infection upregulates the adaptor protein SARM1, leading to neuronal death. 38(4):705. Publisher: NIH Public Access.

[123] Mirian Galliote Morale, Walason da Silva Abjaude, Aline Montenegro Silva, Luisa Lina Villa, and Enrique Boccardo. HPV-transformed cells exhibit altered HMGB1-TLR4/MyD88-SARM1 signaling axis. 8:3476.

[124] Stefan Milde and Michael P. Coleman. Identification of palmitoyltransferase and thioesterase enzymes that control the subcellular localization of axon survival factor nicotinamide mononucleotide adenylyltransferase 2 (NMNAT2)*. 289(47):32858–32870.

[125] Ethan R. Graf, Heather M. Heerssen, Christina M. Wright, Graeme W. Davis, and Aaron di Antonio. Stathmin is required for stability of the drosophila neuromuscular junction. 31(42):15026–15034. Publisher: Society for Neuroscience.

[126] Qian Wang, Yuanxi Zhang, Minghui Wang, Won Min Song, Qi Shen, Andrew McKenzie, Insup Choi, Xianxiao Zhou, Ping Yue Pan, Zhenyu Yue, and Bin Zhang. The landscape of multiscale transcriptomic networks and key regulators in parkinson's disease. 10(1). Publisher: Nature Research.

[127] Jonathan D. Glass. Stathmin-2: adding another piece to the puzzle of TDP-43 proteinopathies and neurodegeneration. 130(11):5677–5680. Publisher: American Society for Clinical Investigation.

[128] Hansruedi Mathys, Jose Davila-Velderrain, Zhuyu Peng, Fan Gao, Shahin Mohammadi, Jennie Z Young, Madhvi Menon, Liang He, Fatema Abdurrob, Xueqiao Jiang, et al. Single-cell transcriptomic analysis of alzheimer's disease. *Nature*, 570(7761):332–337, 2019.

[129] Ze'ev Melamed, Jone López-Erauskin, Michael W Baughn, Ouyang Zhang, Kevin Drenner, Ying Sun, Fernande Freyermuth, Moira A McMahon, Melinda S Beccari, Jon W Artates, et al. Premature polyadenylation-mediated loss of stathmin-2 is a hallmark of tdp-43-dependent neurodegeneration. *Nature neuroscience*, 22(2):180–190, 2019.

[130] Joseph R Klim, Luis A Williams, Francesco Limone, Irune Guerra San Juan, Brandi N Davis-Dusenbery, Daniel A Mordes, Aaron Burberry, Michael J Steinbaugh, Kanchana K Gamage, Rory Kirchner, et al. Als-implicated protein tdp-43 sustains levels

of stmn2, a mediator of motor neuron growth and repair. *Nature neuroscience*, 22(2):167–179, 2019.

[131] Kelsey L Krus, Amy Strickland, Yurie Yamada, Laura Devault, Robert E Schmidt, A Joseph Bloom, Jeffrey Milbrandt, and Aaron DiAntonio. Loss of stathmin-2, a hallmark of tdp-43-associated als, causes motor neuropathy. *bioRxiv*, 2022.

[132] Yan-Jun Guo, Wei-Wei Pan, Sheng-Bing Liu, Zhong-Fei Shen, Ying Xu, and Ling-Ling Hu. ERK/MAPK signalling pathway and tumorigenesis (review). 19(3):1997–2007. Publisher: Spandidos Publications.

[133] Lauren J. Walker, Daniel W. Summers, Yo Sasaki, E. J. Brace, Jeffrey Milbrandt, and Aaron DiAntonio. MAPK signaling promotes axonal degeneration by speeding the turnover of the axonal maintenance factor NMNAT2. 6:e22540.

[134] Katsunori Nakata, Benjamin Abrams, Brock Grill, Alexandr Goncharov, Xun Huang, Andrew D. Chisholm, and Yishi Jin. Regulation of a DLK-1 and p38 MAP kinase pathway by the ubiquitin ligase RPM-1 is required for presynaptic development. 120(3):407–420.

[135] Syu-ichi Hirai, De Feng Cui, Takaki Miyata, Masaharu Ogawa, Hiroshi Kiyonari, Yoko Suda, Shinichi Aizawa, Yumi Banba, and Shigeo Ohno. The c-jun n-terminal kinase activator dual leucine zipper kinase regulates axon growth and neuronal migration in the developing cerebral cortex. 26(46):11992–12002. Publisher: Society for Neuroscience Section: Articles.

[136] Bradley R. Miller, Craig Press, Richard W. Daniels, Yo Sasaki, Jeffrey Milbrandt, and Aaron DiAntonio. A DLK-dependent axon self-destruction program promotes wallerian degeneration. 12(4):387–389.

[137] Xin Xiong, Xin Wang, Ronny Ewanek, Pavan Bhat, Aaron Diantonio, and Catherine A. Collins. Protein turnover of the wallenda/DLK kinase regulates a retrograde response to axonal injury. 191(1):211–223.

[138] Lukas J Neukomm, Thomas C Burdett, Andrew M Seeds, Stefanie Hampel, Jaeda C Coutinho-Budd, Jonathan E Farley, Jack Wong, Yonca B Karadeniz, Jeannette M Osterloh, Amy E Sheehan, and Marc R Freeman. Axon death pathways converge on axundead to promote functional and structural axon disassembly. 95(1):78–91.e5. Publisher: Elsevier.

[139] J. D. Vial. The early changes in the axoplasm during wallerian degeneration. 4(5):551–555.

[140] Andrea Loreto, Ciaran S. Hill, Victoria L. Hewitt, Giuseppe Orsomando, Carlo Angeletti, Jonathan Gilley, Cristiano Lucci, Alvaro Sanchez-Martinez, Alexander J. Whitworth, Laura Conforti, Federico Dajas-Bailador, and Michael P. Coleman. Mitochondrial impairment activates the wallerian pathway through depletion of NMNAT2 leading to SARM1-dependent axon degeneration. 134:104678.

[141] Ali Samii, John G. Nutt, and Bruce R. Ransom. Parkinson's disease. 363(9423):1783–1793.

[142] Khaled Radad, Wolf-Dieter Rausch, and Gabriele Gille. Rotenone induces cell death in primary dopaminergic culture by increasing ROS production and inhibiting mitochondrial respiration. 49(4):379–386.

[143] Angela Spivey. Rotenone and paraquat linked to parkinson's disease: Human exposure study supports years of animal studies. 119(6):A259.

[144] Andrea Loreto, Michele Di Stefano, Martin Gering, and Laura Conforti. Wallerian degeneration is executed by an NMN-SARM1-dependent late ca(2+) influx but only modestly influenced by mitochondria. 13(11):2539–2552.

[145] Darrel E. Goll, Valery F. Thompson, Hongqi Li, Wei Wei, and Jinyang Cong. The calpain system. 83(3):731–801. Publisher: American Physiological Society.

[146] Antoni Camins, Ester Verdaguer, Jaume Folch, and Mercè Pallàs. Involvement of calpain activation in neurodegenerative processes. 12(2):135–148. Eprint: https://onlinelibrary.wiley.com/doi/pdf/10.1111/j.1527-3458.2006.00135.x.

[147] Kathryn E. Saatman, Jennifer Creed, and Ramesh Raghupathi. Calpain as a therapeutic target in traumatic brain injury. 7(1):31–42.

[148] J W Griffin, E B George, and V Chaudhry. Wallerian degeneration in peripheral nerve disease. 5(1):65–75. Publisher: Bailliere Tindall Ltd.

[149] S. K. Ludwin and M. A. Bisby. Delayed wallerian degeneration in the central nervous system of ola mice: an ultrastructural study. 109(2):140–147.

[150] O. Steward and P. A. Trimmer. Genetic influences on cellular reactions to CNS injury: the reactive response of astrocytes in denervated neuropil regions in mice carrying a mutation (wld(s)) that causes delayed wallerian degeneration. 380(1):70–81.

[151] Min-Sheng Wang, Yue Wu, Deborah G. Culver, and Jonathan D. Glass. The gene for slow wallerian degeneration (wlds) is also protective against vincristine neuropathy. 8(1):155–161.

[152] Min Sheng Wang, Albert A. Davis, Deborah G. Culver, and Jonathan D. Glass. Wlds mice are resistant to paclitaxel (taxol) neuropathy. 52(4):442–447. Eprint: https://onlinelibrary.wiley.com/doi/pdf/10.1002/ana.10300.

[153] Min Sheng Wang, Guofu Fang, Deborah G. Culver, Albert A. Davis, Mark M. Rich, and Jonathan D. Glass. The WldS protein protects against axonal degeneration: A model of gene therapy for peripheral neuropathy. 50(6):773–779. Eprint: https://onlinelibrary.wiley.com/doi/pdf/10.1002/ana.10039.

[154] Gerd Meyer zu Horste, Timo A. Miesbach, Johanna I. Muller, Robert Fledrich, Ruth M. Stassart, Bernd C. Kieseier, Michael P. Coleman, and Michael W. Sereda. The wlds transgene reduces axon loss in a charcot-marie-tooth disease 1a rat model and nicotinamide delays post-traumatic axonal degeneration. 42(1):1–8.

[155] Mohtashem Samsam, Weiqian Mi, Carsten Wessig, Jürgen Zielasek, Klaus V. Toyka, Michael P. Coleman, and Rudolf Martini. The wlds mutation delays robust loss of motor and sensory axons in a genetic model for myelin-related axonopathy. 23(7):2833–2839.

[156] Morgane Stum, Heather M. McLaughlin, Erica L. Kleinbrink, Kathy E. Miers, Susan L. Ackerman, Kevin L. Seburn, Anthony Antonellis, and Robert W. Burgess. An assessment of mechanisms underlying peripheral axonal degeneration caused by aminoacyl-tRNA synthetase mutations. 46(2):432–443.

[157] R. R. Myers, H. M. Heckman, and M. Rodriguez. Reduced hyperalgesia in nerve-injured WLD mice: relationship to nerve fiber phagocytosis, axonal degeneration, and regeneration in normal mice. 141(1):94–101.

[158] Matt S Ramer, Gavin D French, and Mark A Bisby. Wallerian degeneration is required for both neuropathic pain and sympathetic sprouting into the drg. *Pain*, 72(1-2):71–78, 1997.

[159] C. Sommer and M. Schäfers. Painful mononeuropathy in c57bl/wld mice with delayed wallerian degeneration: differential effects of cytokine production and nerve regeneration on thermal and mechanical hypersensitivity. 784(1):154–162.

[160] Anna Ferri, Joshua R. Sanes, Michael P. Coleman, Jeanette M. Cunningham, and Ann C. Kato. Inhibiting axon degeneration and synapse loss attenuates apoptosis and disease progression in a mouse model of motoneuron disease. 13(8):669–673. Publisher: Elsevier.

[161] Antonella Sferra, Gilbert Baillat, Teresa Rizza, Sabina Barresi, Elisabetta Flex, Giorgio Tasca, Adele D'Amico, Emanuele Bellacchio, Andrea Ciolfi, Viviana Caputo, Serena Cecchetti, Annalaura Torella, Ginevra Zanni, Daria Diodato, Emanuela Piermarini, Marcello Niceta, Antonietta Coppola, Enrico Tedeschi, Diego Martinelli, Carlo Dionisi-Vici, Vincenzo Nigro, Bruno Dallapiccola, Claudia Compagnucci, Marco Tartaglia, Georg Haase, and Enrico Bertini. TBCE mutations cause early-onset progressive encephalopathy with distal spinal muscular atrophy. 99(4):974–983.

[162] Weiqian Mi, Bogdan Beirowski, Thomas H. Gillingwater, Robert Adalbert, Diana Wagner, Daniela Grumme, Hitoshi Osaka, Laura Conforti, Stefan Arnhold, Klaus Addicks, Keiji Wada, Richard R. Ribchester, and Michael P. Coleman. The slow wallerian degeneration gene, WldS, inhibits axonal spheroid pathology in gracile axonal dystrophy mice. 128(2):405–416.

[163] Thomas H. Gillingwater, Jane E. Haley, Richard R. Ribchester, and Karen Horsburgh. Neuroprotection after transient global cerebral ischemia in wld(s) mutant mice. 24(1):62–66.

[164] Terry C. Yin, Jaymie R. Voorhees, Rachel M. Genova, Kevin C. Davis, Ashley M. Madison, Jeremiah K. Britt, Coral J. Cintrón-Pérez, Latisha McDaniel, Matthew M. Harper, and Andrew A. Pieper. Acute axonal degeneration drives development of cognitive, motor, and visual deficits after blast-mediated traumatic brain injury in mice. 3(5):ENEURO.0220–16.2016.

[165] Ali Sajadi, Bernard L. Schneider, and Patrick Aebischer. Wlds-mediated protection of dopaminergic fibers in an animal model of parkinson disease. 14(4):326–330.

[166] Daphne M. Hasbani and Karen L. O'Malley. WldS mice are protected against the parkinsonian mimetic MPTP. 202(1):93–99.

[167] Hsiao-Chun Cheng and Robert E. Burke. The WldS mutation delays anterograde, but not retrograde, axonal degeneration of the dopaminergic nigro-striatal pathway in vivo. 113(3):683–691. Eprint: https://onlinelibrary.wiley.com/doi/pdf/10.1111/j.1471-4159.2010.06632.x.

[168] Jo Ann V. Antenor-Dorsey and Karen L. O'Malley. WldS but not nmnat1 protects dopaminergic neurites from MPP+ neurotoxicity. 7:5.

[169] Shinjiro Kaneko, Jing Wang, Marie Kaneko, Glenn Yiu, Joanna M Hurrell, Tanuja Chitnis, Samia J Khoury, and Zhigang He. Protecting axonal degeneration by increasing nicotinamide adenine dinucleotide levels in experimental autoimmune encephalomyelitis models. 26(38):9794–804. Publisher: Society for Neuroscience.

[170] Ikuo Tsunoda, Tomoko Tanaka, Emily Jane Terry, and Robert S. Fujinami. Contrasting roles for axonal degeneration in an autoimmune versus viral model of multiple sclerosis: When can axonal injury be beneficial? 170(1):214–226.

[171] Tanuja Chitnis, Jaime Imitola, Yue Wang, Wassim Elyaman, Prianka Chawla, Maia Sharuk, Khadir Raddassi, Roderick T. Bronson, and Samia J. Khoury. Elevated neuronal expression of CD200 protects wlds mice from inflammation-mediated neurodegeneration. 170(5):1695–1712.

[172] Lingting Jin, Jingjing Zhang, Xin Hua, Xingxing Xu, Jia Li, Jiaojiao Wang, Mianxian Wang, Huitao Liu, Haoyu Qiu, Man Chen, Xu Zhang, Ying Wang, and Zhihui Huang. Astrocytic SARM1 promotes neuroinflammation and axonal demyelination in experimental autoimmune encephalomyelitis through inhibiting GDNF signaling. 13(9):1–13. Number: 9 Publisher: Nature Publishing Group.

[173] Gareth R. Howell, Richard T. Libby, Tatjana C. Jakobs, Richard S. Smith, F. Campbell Phalan, Joseph W. Barter, Jessica M. Barbay, Jeffrey K. Marchant, Nagaraju Mahesh, Vittorio Porciatti, Alan V. Whitmore, Richard H. Masland, and Simon W. M. John. Axons of retinal ganglion cells are insulted in the optic nerve early in DBA/2j glaucoma. 179(7):1523–1537.

[174] Natalie D. Bull, Glyn Chidlow, John P. M. Wood, Keith R. Martin, and Robert J. Casson. The mechanism of axonal degeneration after perikaryal excitotoxic injury to the retina. 236(1):34–45.

[175] CHENG-HU WANG, BO WANG, RI-LE WENDU, HUI-E BI, GUO-FAN CAO, CHAO JI, QIN JIANG, and JIN YAO. Protective role of wallerian degeneration slow (wlds) gene against retinal ganglion cell body damage in a wallerian degeneration model. 5(2):621–625.

[176] Yanli Zhu, Lihong Zhang, Yo Sasaki, Jeffrey Milbrandt, and Jeffrey M. Gidday. Protection of mouse retinal ganglion cell axons and soma from glaucomatous and ischemic injury by cytoplasmic overexpression of nmnat1. 54(1):25–36.

[177] Elliot Turkiew, Debbie Falconer, Nicole Reed, and Ahmet Höke. Deletion of sarm1 gene is neuroprotective in two models of peripheral neuropathy. 22(3):162–171. Publisher: NIH Public Access.

[178] Stefanie Geisler, Ryan A. Doan, Amy Strickland, Xin Huang, Jeffrey Milbrandt, and Aaron DiAntonio. Prevention of vincristine-induced peripheral neuropathy by genetic deletion of SARM1 in mice. 139(12):3092–3108.

[179] Stefanie Geisler, Ryan A. Doan, Galen C. Cheng, Aysel Cetinkaya-Fisgin, Shay X. Huang, Ahmet Höke, Jeffrey Milbrandt, and Aaron DiAntonio. Vincristine and bortezomib use distinct upstream mechanisms to activate a common SARM1-dependent axon degeneration program. 4(17). Publisher: American Society for Clinical Investigation.

[180] Kaili Liu, Lu Yang, Gang Wang, Jiaqi Liu, Xuan Zhao, Yi Wang, Jiali Li, and Jing Yang. Metabolic stress drives sympathetic neuropathy within the liver. 33(3):666–675.e4.

[181] Yurie Sato-Yamada, Amy Strickland, Yo Sasaki, Joseph Bloom, Aaron DiAntonio, and Jeffrey Milbrandt. SARM1 promotes axonal, synaptic, and mitochondrial pathologies in charcot-marie-tooth disease type 2a. Pages: 2022.05.17.492364 Section: New Results.

[182] Yalan Cheng, Jun Liu, Yi Luan, Zhiyuan Liu, Hejin Lai, Wuling Zhong, Yale Yang, Huimin Yu, Ning Feng, Hui Wang, Rui Huang, Zhishui He, Menghong Yan, Fang Zhang, Yan Gang Sun, Hao Ying, Feifan Guo, and Qiwei Zhai. SARM1 gene deficiency attenuates diabetic peripheral neuropathy in mice. 68(11):2120–2130. Publisher: American Diabetes Association Inc.

[183] Nils Henninger, James Bouley, Elif M. Sikoglu, Jiyan An, Constance M. Moore, Jean A. King, Robert Bowser, Marc R. Freeman, and Robert H. Brown. Attenuated traumatic axonal injury and improved functional outcome after traumatic brain injury in mice lacking *Sarm1*. 139(4):1094–1105.

[184] Nikolaos K. Ziogas and Vassilis E. Koliatsos. Primary traumatic axonopathy in mice subjected to impact acceleration: A reappraisal of pathology and mechanisms with high-resolution anatomical methods. 38(16):4031–4047. Publisher: J Neurosci.

[185] Christina M. Marion, Dennis P. McDaniel, and Regina C. Armstrong. Sarm1 deletion reduces axon damage, demyelination, and white matter atrophy after experimental traumatic brain injury. 321:113040. Publisher: Academic Press.

[186] Donald V. Bradshaw, Andrew K. Knutsen, Alexandru Korotcov, Genevieve M. Sullivan, Kryslaine L. Radomski, Bernard J. Dardzinski, Xiaomei Zi, Dennis P. McDaniel, and Regina C. Armstrong. Genetic inactivation of SARM1 axon degeneration pathway improves outcome trajectory after experimental traumatic brain injury based on pathological, radiological, and functional measures. 9(1):89.

[187] Younghwa Kim, Ping Zhou, Liping Qian, Jen Zen Chuang, Jessica Lee, Chenjian Li, Costantino Iadecola, Carl Nathan, and Aihao Ding. MyD88-5 links mitochondria, microtubules, and JNK3 in neurons and regulates neuronal survival. 204(9):2063. Publisher: The Rockefeller University Press.

[188] Malinki Sur, Puja Dey, Ankita Sarkar, Sudipta Bar, Dipanjana Banerjee, Swati Bhat, and Piyali Mukherjee. Sarm1 induction and accompanying inflammatory response mediates age-dependent susceptibility to rotenone-induced neurotoxicity. 4(1):1–13. Number: 1 Publisher: Nature Publishing Group.

[189] Charlotte Massoll, Wasym Mando, and Shravan K. Chintala. Excitotoxicity upregulates SARM1 protein expression and promotes wallerian-like degeneration of retinal ganglion cells and their axons. 54(4):2771–2780.

[190] Luke Gibbons, Ema Ozaki, Chris Greene, Anne Trappe, Michael Carty, Judith A. Coppinger, Andrew G. Bowie, Matthew Campbell, and Sarah L. Doyle. SARM1 promotes photoreceptor degeneration in an oxidative stress model of retinal degeneration. 16:852114.

[191] Christine Vande Velde, Michael L. Garcia, Xinghua Yin, Bruce D. Trapp, and Don W. Cleveland. The neuroprotective factor wlds does not attenuate mutant SOD1-mediated motor neuron disease. 5(3):193–203.

[192] Lindsey R. Fischer, Deborah G. Culver, Albert A. Davis, Philip Tennant, Minsheng Wang, Michael Coleman, Seneshaw Asress, Robert Adalbert, Guillermo M. Alexander, and Jonathan D. Glass. The WldS gene modestly prolongs survival in the SOD1g93a fALS mouse. 19(1):293–300.

[193] Owen M Peters, Elizabeth A Lewis, Jeannette M Osterloh, Alexandra Weiss, Johnny S Salameh, Jake Metterville, Robert H Brown, and Marc R Freeman. Loss of sarm1 does not suppress motor neuron degeneration in the SOD1g93a mouse model of amyotrophic lateral sclerosis. 27(21):3761–3771.

[194] Matthew A. White, Ziqiang Lin, Eugene Kim, Christopher M. Henstridge, Emiliano Pena Altamira, Camille K. Hunt, Ella Burchill, Isobel Callaghan, Andrea Loreto,

Heledd Brown-Wright, Richard Mead, Camilla Simmons, Diana Cash, Michael P. Coleman, and Jemeen Sreedharan. Sarm1 deletion suppresses TDP-43-linked motor neuron degeneration and cortical spine loss. 7(1):166.

[195] Jonathan Gilley, Richard R Ribchester, and Michael P Coleman. Sarm1 deletion, but not wlds, confers lifelong rescue in a mouse model of severe axonopathy. *Cell reports*, 21(1):10–16, 2017.

[196] Kanchana K. Gamage, Irene Cheng, Rachel E. Park, Mardeen S. Karim, Kazusa Edamura, Christopher Hughes, Anthony J. Spano, Alev Erisir, and Christopher D. Deppmann. Death receptor 6 promotes wallerian degeneration in peripheral axons. 27(6):890–896.

[197] Stefanie Geisler, Shay X Huang, Amy Strickland, Ryan A Doan, Daniel W Summers, Xianrong Mao, Jiwoong Park, Aaron DiAntonio, and Jeffrey Milbrandt. Gene therapy targeting sarm1 blocks pathological axon degeneration in mice. *Journal of Experimental Medicine*, 216(2):294–303, 2019.

[198] Craig Press and Jeffrey Milbrandt. Nmnat delays axonal degeneration caused by mitochondrial and oxidative stress. 28(19):4861–4871. Publisher: Society for Neuroscience Section: Articles.

[199] M Di Stefano, I Nascimento-Ferreira, G Orsomando, V Mori, J Gilley, R Brown, L Janeckova, M E Vargas, L A Worrell, A Loreto, J Tickle, J Patrick, J R M Webster, M Marangoni, F M Carpi, S Pucciarelli, F Rossi, W Meng, A Sagasti, R R Ribchester, G Magni, M P Coleman, and L Conforti. A rise in NAD precursor nicotinamide mononucleotide (NMN) after injury promotes axon degeneration. 22(5):731–742. Publisher: Nature Publishing Group.

[200] Hua Shen, Krzysztof L. Hyrc, and Mark P. Goldberg. Maintaining energy homeostasis is an essential component of WldS-mediated axon protection. 59:69–79.

[201] Alexander Schulz, Franziska Wagner, Martin Ungelenk, Ingo Kurth, and Christoph Redecker. Stroke-like onset of brain stem degeneration presents with unique MRI sign and heterozygous NMNAT2 variant: a case report. 5(1):23.

[202] Yousuf O Ali, Hunter M Allen, Lei Yu, David Li-Kroeger, Dena Bakhshizadehmahmoudi, Asante Hatcher, Cristin McCabe, Jishu Xu, Nicole Bjorklund, Giulio Taglialatela, et al. Nmnat2: Hsp90 complex mediates proteostasis in proteinopathies. *PLoS biology*, 14(6):e1002472, 2016.

[203] Stefan Milde, Robert Adalbert, M. Handan Elaman, and Michael P. Coleman. Axonal transport declines with age in two distinct phases separated by a period of relative stability. 36(2):971–981.

[204] Isabella Fogh, Antonia Ratti, Cinzia Gellera, Kuang Lin, Cinzia Tiloca, Valentina Moskvina, Lucia Corrado, Gianni Sorarù, Cristina Cereda, Stefania Corti, et al. A genome-wide association meta-analysis identifies a novel locus at 17q11. 2 associated with sporadic amyotrophic lateral sclerosis. *Human molecular genetics*, 23(8):2220–2231, 2014.

[205] Wouter Van Rheenen, Aleksey Shatunov, Annelot M Dekker, Russell L McLaughlin, Frank P Diekstra, Sara L Pulit, Rick AA Van Der Spek, Urmo Võsa, Simone De Jong, Matthew R Robinson, et al. Genome-wide association analyses identify new risk variants and the genetic architecture of amyotrophic lateral sclerosis. *Nature genetics*, 48(9):1043–1048, 2016.

[206] Robert O. Hughes, Todd Bosanac, Xianrong Mao, Thomas M. Engber, Aaron DiAntonio, Jeffrey Milbrandt, Rajesh Devraj, and Raul Krauss. Small molecule SARM1 inhibitors recapitulate the SARM1-/- phenotype and allow recovery of a metastable pool of axons fated to degenerate. 34(1):108588.

[207] Todd Bosanac, Robert O Hughes, Thomas Engber, Rajesh Devraj, Andrew Brearley, Kerstin Danker, Kenneth Young, Jens Kopatz, Melanie Hermann, Antoine Berthemy, Susan Boyce, Jonathan Bentley, and Raul Krauss. Pharmacological SARM1 inhibition protects axon structure and function in paclitaxel-induced peripheral neuropathy. 144(10):3226–3238. Publisher: Oxford University Press (OUP).

[208] Matthew Bratkowski, Thomas C. Burdett, Jean Danao, Xidao Wang, Prakhyat Mathur, Weijing Gu, Jennifer A. Beckstead, Santosh Talreja, Yu-San Yang, Gregory Danko, Jae Hong Park, Mary Walton, Sean P. Brown, Christopher M. Tegley, Prem Raj B. Joseph, Charles H. Reynolds, and Shilpa Sambashivan. Uncompetitive, adduct-forming SARM1 inhibitors are neuroprotective in preclinical models of nerve injury and disease.

[209] Stephen T Sherry, M-H Ward, M Kholodov, J Baker, Lon Phan, Elizabeth M Smigielski, and Karl Sirotkin. dbsnp: the ncbi database of genetic variation. *Nucleic acids research*, 29(1):308–311, 2001.

[210] Tim Hubbard, Daniel Barker, Ewan Birney, Graham Cameron, Yuan Chen, L Clark, Tony Cox, J Cuff, Val Curwen, Thomas Down, et al. The ensembl genome database project. *Nucleic acids research*, 30(1):38–41, 2002.

[211] Fabian Sievers, Andreas Wilm, David Dineen, Toby J Gibson, Kevin Karplus, Weizhong Li, Rodrigo Lopez, Hamish McWilliam, Michael Remmert, Johannes Söding, et al. Fast, scalable generation of high-quality protein multiple sequence alignments using clustal omega. *Molecular systems biology*, 7(1):539, 2011.

[212] Pauline C Ng and Steven Henikoff. Predicting deleterious amino acid substitutions. *Genome research*, 11(5):863–874, 2001.

[213] Vasily Ramensky, Peer Bork, and Shamil Sunyaev. Human non-synonymous snps: server and survey. *Nucleic acids research*, 30(17):3894–3900, 2002.

[214] Jonathan Gilley and Andrea Loreto. Microinjection of superior cervical ganglion neurons for studying axon degeneration. In *Axon Degeneration*, pages 25–39. Springer, 2020.

[215] John Jumper and Demis Hassabis. Protein structure predictions to atomic accuracy with alphafold. *Nature Methods*, 19(1):11–12, 2022.

[216] Thomas D Goddard, Conrad C Huang, Elaine C Meng, Eric F Pettersen, Gregory S Couch, John H Morris, and Thomas E Ferrin. Ucsf chimerax: Meeting modern challenges in visualization and analysis. *Protein Science*, 27(1):14–25, 2018.

[217] Stacey Anne Gould, Jonathan Gilley, Karen Ling, Paymaan Jafar-Nejad, Frank Rigo, and Michael Coleman. Sarm1 haploinsufficiency or low expression levels after antisense oligonucleotides delay programmed axon degeneration. *Cell reports*, 37(11):110108, 2021.

[218] Bogdan Beirowski. Emerging evidence for compromised axonal bioenergetics and axoglial metabolic coupling as drivers of neurodegeneration. *Neurobiology of Disease*, page 105751, 2022.

[219] Zhi Ying Zhao, Xu Jie Xie, Wan Hua Li, Jun Liu, Zhe Chen, Ben Zhang, Ting Li, Song Lu Li, Jun Gang Lu, Liangren Zhang, Li-he Zhang, Zhengshuang Xu, Hon Cheung Lee, and Yong Juan Zhao. A cell-permeant mimetic of NMN activates SARM1 to produce cyclic ADP-ribose and induce non-apoptotic cell death. 15:452–466. Publisher: Elsevier.

[220] Carlo Angeletti, Adolfo Amici, Jonathan Gilley, Andrea Loreto, Antonio G. Trapanotto, Christina Antoniou, Elisa Merlini, Michael P. Coleman, and Giuseppe Orsomando. SARM1 is a multi-functional NAD(p)ase with prominent base exchange activity, all regulated bymultiple physiologically relevant NAD metabolites. 25(2):103812.

[221] Wan Hua Li, Ke Huang, Yang Cai, Qian Wen Wang, Wen Jie Zhu, Yun Nan Hou, Sujing Wang, Sheng Cao, Zhi Ying Zhao, Xu Jie Xie, et al. Permeant fluorescent probes visualize the activation of sarm1 and uncover an anti-neurodegenerative drug candidate. *Elife*, 10:e67381, 2021.

[222] Chen Shen, Mihir Vohra, Pengfei Zhang, Xianrong Mao, Matthew D. Figley, Jian Zhu, Yo Sasaki, Hao Wu, Aaron DiAntonio, and Jeffrey Milbrandt. Multiple domain interfaces mediate SARM1 autoinhibition. 118(4). Publisher: National Academy of Sciences.

[223] Yo Sasaki, Hiroki Kakita, Shunsuke Kubota, Abdoulaye Sene, Tae Jun Lee, Norimitsu Ban, Zhenyu Dong, Joseph B. Lin, Sanford L. Boye, Aaron Di Antonio, Shannon E. Boye, Rajendra S. Apte, and Jeffrey Milbrandt. SARM1 depletion rescues NMNAT1-dependent photoreceptor cell death and retinal degeneration. 9:1–19. Publisher: Elife.

[224] Pete A Williams, Jeffrey M Harder, Nicole E Foxworth, Brynn H Cardozo, Kelly E Cochran, and Simon WM John. Nicotinamide and wlds act together to prevent neurodegeneration in glaucoma. *Frontiers in Neuroscience*, 11:232, 2017.

[225] Elizabeth M Smigielski, Karl Sirotkin, Minghong Ward, and Stephen T Sherry. dbsnp: a database of single nucleotide polymorphisms. *Nucleic acids research*, 28(1):352–355, 2000.

[226] Konrad J Karczewski, Laurent C Francioli, Grace Tiao, Beryl B Cummings, Jessica Alföldi, Qingbo Wang, Ryan L Collins, Kristen M Laricchia, Andrea Ganna, Daniel P Birnbaum, et al. The mutational constraint spectrum quantified from variation in 141,456 humans. *Nature*, 581(7809):434–443, 2020.

[227] Mirlinda Ademi, Xiuna Yang, Michael P. Coleman, and Jonathan Gilley. Natural variants of human SARM1 cause both intrinsic and dominant loss-of-function influencing axon survival. 12(1):13846. Number: 1 Publisher: Nature Publishing Group.

[228] Kow Essuman, Daniel W. Summers, Yo Sasaki, Xianrong Mao, Aldrin Kay Yuen Yim, Aaron DiAntonio, and Jeffrey Milbrandt. TIR domain proteins are an ancient family of NAD+-consuming enzymes. 28(3):421–430.e4. Publisher: Cell Press.

[229] Li Wan, Kow Essuman, Ryan G Anderson, Yo Sasaki, Freddy Monteiro, Eui-Hwan Chung, Erin Osborne Nishimura, Aaron DiAntonio, Jeffrey Milbrandt, Jeffery L Dangl, et al. Tir domains of plant immune receptors are nad+-cleaving enzymes that promote cell death. *Science*, 365(6455):799–803, 2019.

[230] Azadeh Izadifar, Julien Courchet, Daniel M. Virga, Tine Verreet, Stevie Hamilton, Derya Ayaz, Anke Misbaer, Sofie Vandenbogaerde, Laloe Monteiro, Milan Petrovic, Sonja Sachse, Bing Yan, Maria-Luise Erfurth, Dan Dascenco, Yoshiaki Kise, Jiekun Yan, Gabriela Edwards-Faret, Tommy Lewis, Franck Polleux, and Dietmar Schmucker. Axon morphogenesis and maintenance require an evolutionary conserved safeguard function of wnk kinases antagonizing sarm and axed. 109(18):2864–2883.e8. Publisher: Elsevier.

[231] Christopher Del Nagro, Yang Xiao, Linda Rangell, Mike Reichelt, and Thomas O'Brien. Depletion of the central metabolite NAD leads to oncosismediated cell death. 289(51):35182–35192. Publisher: American Society for Biochemistry and Molecular Biology Inc.

[232] Porkodi Panneerselvam, Laishram Pradeepkumar Singh, Bow Ho, Jianzhu Chen, and Jeak Ling Ding. Targeting of pro-apoptotic TLR adaptor SARM to mitochondria: Definition of the critical region and residues in the signal sequence. 442(2):263–271. Publisher: Portland Press.

[233] Heather S Loring, Janneke D Icso, Venkatesh V Nemmara, and Paul R Thompson. Initial kinetic characterization of sterile alpha and toll/interleukin receptor motif-containing protein 1. *Biochemistry*, 59(8):933–942, 2020.

[234] Michael P Coleman. Axon biology in als: mechanisms of axon degeneration and prospects for therapy. *Neurotherapeutics*, pages 1–12, 2022.

[235] Ankita Sarkar, Nripa Kumari, and Piyali Mukherjee. The curious case of SARM1: Dr. jekyll and mr. hyde in cell death and immunity? Publisher: John Wiley and Sons Inc.

[236] R. Grace Zhai, Yu Cao, P. Robin Hiesinger, Yi Zhou, Sunil Q. Mehta, Karen L. Schulze, Patrik Verstreken, and Hugo J. Bellen. Drosophila NMNAT maintains neural integrity independent of its NAD synthesis activity. 4(12):e416. Publisher: Public Library of Science.

[237] R. Grace Zhai, Fan Zhang, P. Robin Hiesinger, Yu Cao, Claire M. Haueter, and Hugo J. Bellen. NAD synthase NMNAT acts as a chaperone to protect against neurodegeneration. 452(7189):887–891. Number: 7189 Publisher: Nature Publishing Group.

[238] Pei-Wen Chiang, Juan Wang, Yang Chen, Quan Fu, Jing Zhong, Yanhua Chen, Xin Yi, Renhua Wu, Haixue Gan, Yong Shi, et al. Exome sequencing identifies nmnat1 mutations as a cause of leber congenital amaurosis. *Nature genetics*, 44(9):972–974, 2012.

[239] Robert K Koenekoop, Hui Wang, Jacek Majewski, Xia Wang, Irma Lopez, Huanan Ren, Yiyun Chen, Yumei Li, Gerald A Fishman, Mohammed Genead, et al. Mutations in nmnat1 cause leber congenital amaurosis and identify a new disease pathway for retinal degeneration. *Nature genetics*, 44(9):1035–1039, 2012.

[240] Isabelle Perrault, Sylvain Hanein, Xavier Zanlonghi, Valérie Serre, Michael Nicouleau, Sabine Defoort-Delhemmes, Nathalie Delphin, Lucas Fares-Taie, Sylvie Gerber, Olivia Xerri, et al. Mutations in nmnat1 cause leber congenital amaurosis with early-onset severe macular and optic atrophy. *Nature genetics*, 44(9):975–977, 2012.

[241] Marni J Falk, Qi Zhang, Eiko Nakamaru-Ogiso, Chitra Kannabiran, Zoe Fonseca-Kelly, Christina Chakarova, Isabelle Audo, Donna S Mackay, Christina Zeitz, Arundhati Dev Borman, et al. Nmnat1 mutations cause leber congenital amaurosis. *Nature genetics*, 44(9):1040–1045, 2012.

[242] Richard A. Slivicki, Yousuf O. Ali, Hui-Chen Lu, and Andrea G. Hohmann. Impact of genetic reduction of NMNAT2 on chemotherapy-induced losses in cell viability in vitro and peripheral neuropathy in vivo. 11(1):e0147620.

[243] Winnie S Liang, Travis Dunckley, Thomas G Beach, Andrew Grover, Diego Mastroeni, Douglas G Walker, Richard J Caselli, Walter A Kukull, Daniel McKeel, John C Morris, et al. Gene expression profiles in anatomically and functionally distinct regions of the normal aged human brain. *Physiological genomics*, 28(3):311–322, 2007.

[244] Winnie S Liang, Eric M Reiman, Jon Valla, Travis Dunckley, Thomas G Beach, Andrew Grover, Tracey L Niedzielko, Lonnie E Schneider, Diego Mastroeni, Richard Caselli, et al. Alzheimer's disease is associated with reduced expression of energy metabolism genes in posterior cingulate neurons. *Proceedings of the National Academy of Sciences*, 105(11):4441–4446, 2008.

[245] Vivianna M Van Deerlin, Patrick Sleiman, Maria Martinez-Lage, Alice Chen-Plotkin, Li-San Wang, Neill R Graff-Radford, Dennis W Dickson, Rosa Rademakers, Bradley F Boeve, Murray Grossman, et al. Common variants at 7p21 are associated with frontotemporal lobar degeneration with tdp-43 inclusions. *Nature genetics*, 42(3):234–239, 2010.

[246] Timothy G Lesnick, Spiridon Papapetropoulos, Deborah C Mash, Jarlath Ffrench-Mullen, Lina Shehadeh, Mariza De Andrade, John R Henley, Walter A Rocca, J Eric Ahlskog, and Demetrius M Maraganore. A genomic pathway approach to a complex disease: axon guidance and parkinson disease. *PLoS genetics*, 3(6):e98, 2007.

[247] Linda B Moran, DC Duke, Manuel Deprez, DT Dexter, RKB Pearce, and MB Graeber. Whole genome expression profiling of the medial and lateral substantia nigra in parkinson's disease. *Neurogenetics*, 7(1):1–11, 2006.

[248] Angela Hodges, Andrew D Strand, Aaron K Aragaki, Alexandre Kuhn, Thierry Sengstag, Gareth Hughes, Lyn A Elliston, Cathy Hartog, Darlene R Goldstein, Doris Thu, et al. Regional and cellular gene expression changes in human huntington's disease brain. *Human molecular genetics*, 15(6):965–977, 2006.

[249] Benjamin A Harlan, Kelby M Killoy, Mariana Pehar, Liping Liu, Johan Auwerx, and Marcelo R Vargas. Evaluation of the nad+ biosynthetic pathway in als patients and effect of modulating nad+ levels in hsod1-linked als mouse models. *Experimental neurology*, 327:113219, 2020.

[250] Pascal Röderer, Lara Klatt, Felix John, Verena Theis, Konstanze F. Winklhofer, Carsten Theiss, and Veronika Matschke. Increased ROS level in spinal cord of wobbler mice due to nmnat2 downregulation. 55(11):8414–8424.

[251] Nara Sobreira, François Schiettecatte, David Valle, and Ada Hamosh. Genematcher: a matching tool for connecting investigators with an interest in the same gene. *Human mutation*, 36(10):928–930, 2015.

[252] Irina A Rodionova, Harmon J Zuccola, Leonardo Sorci, Alexander E Aleshin, Marat D Kazanov, Chen-Ting Ma, Eduard Sergienko, Eric J Rubin, Christopher P Locher, and Andrei L Osterman. Mycobacterial nicotinate mononucleotide adenylyltransferase: structure, mechanism, and implications for drug discovery. *Journal of Biological Chemistry*, 290(12):7693–7706, 2015.

[253] Tianjun Zhou, Oleg Kurnasov, Diana R Tomchick, Derk D Binns, Nick V Grishin, Victor E Marquez, Andrei L Osterman, and Hong Zhang. Structure of human

nicotinamide/nicotinic acid mononucleotide adenylyltransferase: Basis for the dual substrate specificity and activation of the oncolytic agent tiazofurinast. *Journal of Biological Chemistry*, 277(15):13148–13154, 2002.

[254] Joel A Yalowitz, Suhong Xiao, Mangatt P Biju, Aśok C Antony, Oscar W Cummings, Mark A Deeg, and Hiremagalur N Jayaram. Characterization of human brain nicotinamide 5′-mononucleotide adenylyltransferase-2 and expression in human pancreas. *Biochemical Journal*, 377(2):317–326, 2004.

[255] Gavin E Crooks, Gary Hon, John-Marc Chandonia, and Steven E Brenner. Weblogo: a sequence logo generator. *Genome research*, 14(6):1188–1190, 2004.

[256] John Jumper, Richard Evans, Alexander Pritzel, Tim Green, Michael Figurnov, Olaf Ronneberger, Kathryn Tunyasuvunakool, Russ Bates, Augustin Žídek, Anna Potapenko, et al. Highly accurate protein structure prediction with alphafold. *Nature*, 596(7873):583–589, 2021.

[257] Mihaly Varadi, Stephen Anyango, Mandar Deshpande, Sreenath Nair, Cindy Natassia, Galabina Yordanova, David Yuan, Oana Stroe, Gemma Wood, Agata Laydon, et al. Alphafold protein structure database: massively expanding the structural coverage of protein-sequence space with high-accuracy models. *Nucleic acids research*, 50(D1):D439–D444, 2022.

[258] Eric F Pettersen, Thomas D Goddard, Conrad C Huang, Elaine C Meng, Gregory S Couch, Tristan I Croll, John H Morris, and Thomas E Ferrin. Ucsf chimerax: Structure visualization for researchers, educators, and developers. *Protein Science*, 30(1):70–82, 2021.

[259] Pawel Bieganowski and Charles Brenner. Discoveries of nicotinamide riboside as a nutrient and conserved nrk genes establish a preiss-handler independent route to nad+ in fungi and humans. *Cell*, 117(4):495–502, 2004.

[260] Angeliki Vgontzas and William Renthal. Introduction to neurogenetics. *The American Journal of Medicine*, 132(2):142–152, 2019.

[261] Yiru Anning Wang, Jan Edward Kammenga, and Simon Crawford Harvey. Genetic variation in neurodegenerative diseases and its accessibility in the model organism caenorhabditis elegans. *Human genomics*, 11(1):1–10, 2017.

[262] Sandy Eldridge, Liang Guo, and John Hamre III. A comparative review of chemotherapy-induced peripheral neuropathy in in vivo and in vitro models. *Toxicologic pathology*, 48(1):190–201, 2020.

[263] R Michael Baldwin, Kouros Owzar, Hitoshi Zembutsu, Aparna Chhibber, Michiaki Kubo, Chen Jiang, Dorothy Watson, Rachel J Eclov, Joel Mefford, Howard L McLeod, et al. A genome-wide association study identifies novel loci for paclitaxel-induced sensory peripheral neuropathy in calgb 40101novel genetic loci for paclitaxel-induced peripheral neuropathy. *Clinical Cancer Research*, 18(18):5099–5109, 2012.

[264] Edward B Lee, Virginia M-Y Lee, and John Q Trojanowski. Gains or losses: molecular mechanisms of tdp43-mediated neurodegeneration. *Nature Reviews Neuroscience*, 13(1):38–50, 2012.

[265] Mercedes Prudencio, Jack Humphrey, Sarah Pickles, Anna-Leigh Brown, Sarah E Hill, Jennifer M Kachergus, Ji Shi, Michael G Heckman, Matthew R Spiegel, Casey Cook, et al. Truncated stathmin-2 is a marker of tdp-43 pathology in frontotemporal dementia. *The Journal of clinical investigation*, 130(11), 2020.

[266] Jay P Ross, Fulya Akcimen, Calwing Liao, Dan Spiegelman, Ben Weisburd, Nicolas Dupre, Patrick A Dion, Guy Rouleau, and Sali MK Farhan. Questioning the association of the stmn2 dinucleotide repeat with als. *medRxiv*, 2022.

[267] Paolo Niccolò Doronzio, Serena Lattante, Giuseppe Marangi, Francesco Martello, Amelia Conte, Giulia Bisogni, Daniela Bernardo, Agata Katia Patanella, Emiliana Meleo, Marcella Zollino, et al. Analysis of stmn2 ca repeats in italian als patients shows no association. *Amyotrophic Lateral Sclerosis and Frontotemporal Degeneration*, pages 1–3, 2022.

[268] Daniela Buonvicino, Francesca Mazzola, Federica Zamporlini, Francesco Resta, Giuseppe Ranieri, Emidio Camaioni, Mirko Muzzi, Riccardo Zecchi, Giuseppe Pieraccini, Christian Dölle, et al. Identification of the nicotinamide salvage pathway as a new toxification route for antimetabolites. *Cell chemical biology*, 25(4):471–482, 2018.

[269] Peter A LeWitt. The neurotoxicity of the rat poison vacor: a clinical study of 12 cases. *New England Journal of Medicine*, 302(2):73–77, 1980.

[270] Kristin L Ayers, Uyenlinh L Mirshahi, Amr H Wardeh, Michael F Murray, Ke Hao, Benjamin S Glicksberg, Shuyu Li, David J Carey, and Rong Chen. A loss of function variant in casp7 protects against alzheimer's disease in homozygous apoe undefined allele carriers. *BMC genomics*, 17(2):229–237, 2016.

[271] Bruno A Benitez, Sheng Chih Jin, Rita Guerreiro, Rob Graham, Jenny Lord, Denise Harold, Rebecca Sims, Jean-Charles Lambert, J Raphael Gibbs, Jose Bras, et al. Missense variant in treml2 protects against alzheimer's disease. *Neurobiology of aging*, 35(6):1510–e19, 2014.

[272] Rebecca Sims, Sven J Van Der Lee, Adam C Naj, Céline Bellenguez, Nandini Badarinarayan, Johanna Jakobsdottir, Brian W Kunkle, Anne Boland, Rachel Raybould, Joshua C Bis, et al. Rare coding variants in plcg2, abi3, and trem2 implicate microglial-mediated innate immunity in alzheimer's disease. *Nature genetics*, 49(9):1373–1384, 2017.

[273] Thorlakur Jonsson, Jasvinder K Atwal, Stacy Steinberg, Jon Snaedal, Palmi V Jonsson, Sigurbjorn Bjornsson, Hreinn Stefansson, Patrick Sulem, Daniel Gudbjartsson, Janice Maloney, et al. A mutation in app protects against alzheimer's disease and age-related cognitive decline. *Nature*, 488(7409):96–99, 2012.

[274] John E Landers, Judith Melki, Vincent Meininger, Jonathan D Glass, Leonard H Van Den Berg, Michael A Van Es, Peter C Sapp, Paul WJ Van Vught, Diane M McKenna-Yasek, Hylke M Blauw, et al. Reduced expression of the kinesin-associated protein 3 (kifap3) gene increases survival in sporadic amyotrophic lateral sclerosis. *Proceedings of the National Academy of Sciences*, 106(22):9004–9009, 2009.

[275] Chen Eitan, Aviad Siany, Elad Barkan, Tsviya Olender, Kristel R van Eijk, Matthieu Moisse, Sali MK Farhan, Yehuda M Danino, Eran Yanowski, Hagai Marmor-Kollet, et al. Whole-genome sequencing reveals that variants in the interleukin 18 receptor accessory protein 3′ utr protect against als. *Nature neuroscience*, 25(4):433–445, 2022.

[276] Cathie Sudlow, John Gallacher, Naomi Allen, Valerie Beral, Paul Burton, John Danesh, Paul Downey, Paul Elliott, Jane Green, Martin Landray, et al. Uk biobank: an open access resource for identifying the causes of a wide range of complex diseases of middle and old age. *PLoS medicine*, 12(3):e1001779, 2015.

[277] Anna Fry, Thomas J Littlejohns, Cathie Sudlow, Nicola Doherty, Ligia Adamska, Tim Sprosen, Rory Collins, and Naomi E Allen. Comparison of sociodemographic and health-related characteristics of uk biobank participants with those of the general population. *American journal of epidemiology*, 186(9):1026–1034, 2017.

[278] Konrad J Karczewski, Matthew Solomonson, Katherine R Chao, Julia K Goodrich, Grace Tiao, Wenhan Lu, Bridget M Riley-Gillis, Ellen A Tsai, Hye In Kim, Xiuwen

Zheng, et al. Systematic single-variant and gene-based association testing of thousands of phenotypes in 394,841 uk biobank exomes. *Cell Genomics*, 2(9):100168, 2022.

[279] Yong Juan Zhao, Wei Ming He, Zhi Ying Zhao, Wan Hua Li, Qian Wen Wang, Yun Nan Hou, Yongjun Tan, and Dapeng Zhang. Acidic ph irreversibly activates the signaling enzyme sarm1. *The FEBS Journal*, 288(23):6783–6794, 2021.

[280] Federica Perrone, Rita Cacace, Julie van der Zee, and Christine Van Broeckhoven. Emerging genetic complexity and rare genetic variants in neurodegenerative brain diseases. *Genome medicine*, 13(1):1–13, 2021.

[281] Kym M Boycott, Ana Rath, Jessica X Chong, Taila Hartley, Fowzan S Alkuraya, Gareth Baynam, Anthony J Brookes, Michael Brudno, Angel Carracedo, Johan T den Dunnen, et al. International cooperation to enable the diagnosis of all rare genetic diseases. *The American Journal of Human Genetics*, 100(5):695–705, 2017.

[282] Kimberly Splinter, David R Adams, Carlos A Bacino, Hugo J Bellen, Jonathan A Bernstein, Alys M Cheatle-Jarvela, Christine M Eng, Cecilia Esteves, William A Gahl, Rizwan Hamid, et al. Effect of genetic diagnosis on patients with previously undiagnosed disease. *New england journal of medicine*, 379(22):2131–2139, 2018.

[283] Jenny C Taylor, Hilary C Martin, Stefano Lise, John Broxholme, Jean-Baptiste Cazier, Andy Rimmer, Alexander Kanapin, Gerton Lunter, Simon Fiddy, Chris Allan, et al. Factors influencing success of clinical genome sequencing across a broad spectrum of disorders. *Nature genetics*, 47(7):717–726, 2015.

[284] M Caulfield, J Davies, M Dennys, L Elbahy, T Fowler, S Hill, and KL Woods. The 100,000 genomes project protocol. *Genomics Engl. P*, 3:1–112, 2017.

[285] Michael Gonzalez, Marni J Falk, Xiaowu Gai, Richard Postrel, Rebecca Schüle, and Stephan Zuchner. Innovative genomic collaboration using the genesis (gem. app) platform. *Human mutation*, 36(10):950–956, 2015.

[286] Project mine: study design and pilot analyses of a large-scale whole-genome sequencing study in amyotrophic lateral sclerosis. *European Journal of Human Genetics*, 26(10):1537–1546, 2018.

[287] Melissa J Landrum, Jennifer M Lee, George R Riley, Wonhee Jang, Wendy S Rubinstein, Deanna M Church, and Donna R Maglott. Clinvar: public archive of relationships among sequence variation and human phenotype. *Nucleic acids research*, 42(D1):D980–D985, 2014.

[288] Sabina Gainotti, Paola Torreri, Chiuhui Mary Wang, Robert Reihs, Heimo Mueller, Emma Heslop, Marco Roos, Dorota Mazena Badowska, Federico De Paulis, Yllka Kodra, et al. The rd-connect registry & biobank finder: a tool for sharing aggregated data and metadata among rare disease researchers. *European Journal of Human Genetics*, 26(5):631–643, 2018.

[289] Eugene Bragin, Eleni A Chatzimichali, Caroline F Wright, Matthew E Hurles, Helen V Firth, A Paul Bevan, and G Jawahar Swaminathan. Decipher: database for the interpretation of phenotype-linked plausibly pathogenic sequence and copy-number variation. *Nucleic acids research*, 42(D1):D993–D1000, 2014.

[290] Robert Prior, Lawrence Van Helleputte, Veronick Benoy, and Ludo Van Den Bosch. Defective axonal transport: a common pathological mechanism in inherited and acquired peripheral neuropathies. *Neurobiology of disease*, 105:300–320, 2017.

[291] Jamie Burgess, Maryam Ferdousi, David Gosal, Cheng Boon, Kohei Matsumoto, Anne Marshall, Tony Mak, Andrew Marshall, Bernhard Frank, Rayaz A Malik, et al. Chemotherapy-induced peripheral neuropathy: epidemiology, pathomechanisms and treatment. *Oncology and therapy*, 9(2):385–450, 2021.

[292] Andreas A Argyriou, Athanasios P Kyritsis, Thomas Makatsoris, and Haralabos P Kalofonos. Chemotherapy-induced peripheral neuropathy in adults: a comprehensive update of the literature. *Cancer management and research*, 6:135, 2014.

[293] Jone Lopez-Erauskin, Mariana Bravo-Hernandez, Maximiliano Presa, Michael W Baughn, Ze'ev Melamed, Melinda S Beccari, Ana Rita Agra de Almeida Quadros, Aamir Zuberi, Karen Ling, Oleksandr Platoshyn, et al. Stathmin-2 loss leads to neurofilament-dependent axonal collapse driving motor and sensory denervation. *bioRxiv*, 2022.

[294] Chi Fung Lee, Hina Nizami, Haiwei Gu, and Christine Light. Sarm1 nad hydrolase deficiency normalizes fibrosis and ameliorates cardiac dysfunction in diabetic hearts. *The FASEB Journal*, 36, 2022.

[295] Tong Wu, Jian Zhu, Amy Strickland, Kwang Woo Ko, Yo Sasaki, Caitlin B Dingwall, Yurie Yamada, Matthew D Figley, Xianrong Mao, Alicia Neiner, et al. Neurotoxins subvert the allosteric activation mechanism of sarm1 to induce neuronal loss. *Cell reports*, 37(3):109872, 2021.

[296] Kristy J Szretter, Melanie A Samuel, Susan Gilfillan, Anja Fuchs, Marco Colonna, and Michael S Diamond. The immune adaptor molecule sarm modulates tumor necrosis

factor alpha production and microglia activation in the brainstem and restricts west nile virus pathogenesis. *Journal of virology*, 83(18):9329–9338, 2009.

[297] Vinod Sundaramoorthy, Diane Green, Kelly Locke, Carmel M O'Brien, Megan Dearnley, and John Bingham. Novel role of sarm1 mediated axonal degeneration in the pathogenesis of rabies. *PLoS pathogens*, 16(2):e1008343, 2020.

[298] Colin L Crawford, Christina Antoniou, Lina Komarek, Verena Schultz, Claire L Donald, Paul Montague, Susan C Barnett, Christopher Linington, Hugh J Willison, Alain Kohl, et al. Sarm1 depletion slows axon degeneration in a cns model of neurotropic viral infection. *Frontiers in Molecular Neuroscience*, 15, 2022.

[299] Michael S. Bonkowski and David A. Sinclair. Slowing ageing by design: the rise of NAD+ and sirtuin-activating compounds. 17(11):679–690.

[300] Mihoko Yoshino, Jun Yoshino, Brandon D. Kayser, Gary J. Patti, Michael P. Franczyk, Kathryn F. Mills, Miriam Sindelar, Terri Pietka, Bruce W. Patterson, Shin-Ichiro Imai, and Samuel Klein. Nicotinamide mononucleotide increases muscle insulin sensitivity in prediabetic women. 372(6547):1224–1229. Publisher: American Association for the Advancement of Science.

[301] Kevin D. Brown, Sadia Maqsood, Jing-Yi Huang, Yong Pan, William Harkcom, Wei Li, Anthony Sauve, Eric Verdin, and Samie R. Jaffrey. Activation of SIRT3 by the NAD precursor nicotinamide riboside protects from noise-induced hearing loss. 20(6):1059–1068.

[302] Bing Gong, Yong Pan, Prashant Vempati, Wei Zhao, Lindsay Knable, Lap Ho, Jun Wang, Magdalena Sastre, Kenjiro Ono, Anthony A. Sauve, and Giulio M. Pasinetti. Nicotinamide riboside restores cognition through an upregulation of proliferator-activated receptor-γ coactivator 1α regulated β-secretase 1 degradation and mitochondrial gene expression in alzheimer's mouse models. 34(6):1581–1588.

[303] Kathryn F. Mills, Shohei Yoshida, Liana R. Stein, Alessia Grozio, Shunsuke Kubota, Yo Sasaki, Philip Redpath, Marie E. Migaud, Rajendra S. Apte, Koji Uchida, Jun Yoshino, and Shin-Ichiro Imai. Long-term administration of nicotinamide mononucleotide mitigates age-associated physiological decline in mice. 24(6):795–806.

[304] Natalie E. de Picciotto, Lindsey B. Gano, Lawrence C. Johnson, Christopher R. Martens, Amy L. Sindler, Kathryn F. Mills, Shin-Ichiro Imai, and Douglas R. Seals. Nicotinamide mononucleotide supplementation reverses vascular dysfunction and oxidative stress with aging in mice. 15(3):522–530.

[305] Ji H. Park, Aaron Long, Katrina Owens, and Tibor Kristian. Nicotinamide mononucleotide inhibits post-ischemic NAD(+) degradation and dramatically ameliorates brain damage following global cerebral ischemia. 95:102–110.

[306] Frank JP Kühn and Andreas Lückhoff. Sites of the nudt9-h domain critical for adp-ribose activation of the cation channel trpm2. *Journal of Biological Chemistry*, 279(45):46431–46437, 2004.